UNIVERSITAT DE BARCELONA

Physico-chemical aspects on molecular motor

Aleix Ciudad Álvarez

ADVERTIMENT. La consulta d'aquesta tesi queda condicionada a l'acceptació de les següents condicions d'ús: La difusió d'aquesta tesi per mitjà del servei TDX (**www.tdx.cat**) i a través del Dipòsit Digital de la UB (**diposit.ub.edu**) ha estat autoritzada pels titulars dels drets de propietat intel·lectual únicament per a usos privats emmarcats en activitats d'investigació i docència. No s'autoritza la seva reproducció amb finalitats de lucre ni la seva difusió i posada a disposició des d'un lloc aliè al servei TDX ni al Dipòsit Digital de la UB. No s'autoritza la presentació del seu contingut en una finestra o marc aliè a TDX o al Dipòsit Digital de la UB (framing). Aquesta reserva de drets afecta tant al resum de presentació de la tesi com als seus continguts. En la utilització o cita de parts de la tesi és obligat indicar el nom de la persona autora.

ADVERTENCIA. La consulta de esta tesis queda condicionada a la aceptación de las siguientes condiciones de uso: La difusión de esta tesis por medio del servicio TDR (**www.tdx.cat**) y a través del Repositorio Digital de la UB (**diposit.ub.edu**) ha sido autorizada por los titulares de los derechos de propiedad intelectual únicamente para usos privados enmarcados en actividades de investigación y docencia. No se autoriza su reproducción con finalidades de lucro ni su difusión y puesta a disposición desde un sitio ajeno al servicio TDR o al Repositorio Digital de la UB. No se autoriza la presentación de su contenido en una ventana o marco ajeno a TDR o al Repositorio Digital de la UB (framing). Esta reserva de derechos afecta tanto al resumen de presentación de la tesis como a sus contenidos. En la utilización o cita de partes de la tesis es obligado indicar el nombre de la persona autora.

WARNING. On having consulted this thesis you're accepting the following use conditions: Spreading this thesis by the TDX (**www.tdx.cat**) service and by the UB Digital Repository (**diposit.ub.edu**) has been authorized by the titular of the intellectual property rights only for private uses placed in investigation and teaching activities. Reproduction with lucrative aims is not authorized nor its spreading and availability from a site foreign to the TDX service or to the UB Digital Repository. Introducing its content in a window or frame foreign to the TDX service or to the UB Digital Repository is not authorized (framing). Those rights affect to the presentation summary of the thesis as well as to its contents. In the using or citation of parts of the thesis it's obliged to indicate the name of the author.

Physico-chemical aspects on molecular motors

Ph.D. thesis

February 2008

Programa de doctorado de Física Avançada
Bienio 2003-2005
Departamento de Estructura i Constituents de la Matèria
Universitat de Barcelona

Aleix Ciudad Álvarez

Ph.D. advisor
José María Sancho Herrero

UNIVERSITAT DE BARCELONA

Contents

Acknowledgments

This work was funded by the Ministerio de Educación y Ciencia (Spain) under Project No. FIS2006-11452-C03-01 and Grant No. BES-2004-3208. I would like to thank my supervisor, J.M. Sancho. I'm also grateful to A.M. Lacasta and G.P. Tsironis, which have participated in the elaboration of Parts I and III, respectively.

1

Introduction: motor systems at the nanoscale

The discovery of molecular motors was not a single and isolated event but a set of gradual approaches from microscopic to nanoscopic systems. For example, the knowledge of the activity of muscle cells is pretty old, and even though the first myosin was identified about a century ago, it was not until 1986 when actin filaments were visualized under a microscope [1]. But until 1995 [2] the first single molecule measurement was not performed. Among other technical problems, to deal with such small objects implied thermal noise detection, that couldn't be distinguished from the desired signal. Microscopic techniques were developed in order to decrease the background noise allowing a progressive improving in image resolution. However, some years before, optical trapping techniques allowed measurement of individual kinesin motion [3]. In this text we will not cover a rigorous survey on the history of single molecule experiments. For a general survey on this topic we recommend Ref. [4].

Here we will introduce some of the most studied motor nano-systems. We will emphasize only some general features that are well established and that will be important for our theoretical work as experimental input. A more detailed survey can be found in Ref.[5]. We will introduce motor systems, not just motor proteins, because we assume that a linear motor and its track (or a rotor and its stator) are intimately related. However, sometimes a track can hold more than one protein type motion, as it is the case of the microtubule, which can hold kinesin

and dynein stepping. Then, we will introduce linear motors and their tracks as separated subsections but they shouldn't be considered separately when trying to understand their behaviour. Now we will proceed to the biochemical description of several molecular motor systems.

1.1 Microtubule based motion

1.1.1 Microtubules

Microtubules are a set of cylindrical structures that constitute the first type of the cytoskeleton filaments. The other two types are actin filaments and intermediate filaments. While the functions of the latter remain unclear, the two first types have both structural and regulating functions. Structurally, they form the skeleton that provides consistency to the cell, while at the same time they are the network that makes possible all the intracellular traffic. We will focus on this latter property, which is related to the activity of motor proteins.

Structurally, a microtubule is a polymer of tubulin dimers, also called $\alpha\beta$ heterodimers as they are built by two monomers α and β. The dimer has a length of $\simeq 8.2nm$ [6] and it is able to bind other dimers to form different arrays. The most stable is the A-lattice, which is the standard arrangement of the microtubule, see Fig.1.1. It consists on 13 linear polymers (protofilaments) of tubulin dimers which are laterally bound in such a way that they form a closed cylinder of $\sim 24nm$ diameter. However, in a protofilament each tubulin does not match exactly with their neighbours in adjacent protofilaments but there is an axial shift of $\sim 0.92nm$. According to this, the microtubule has supertwisting properties with a period of $\sim 12nm$, which is 1.5 times the size of the dimer. Thus, after the whole supertwist an α monomer supertwist is followed by a β monomer supertwist and viceversa.

Microtubules are polar structures, i.e. their ends can be distinguished. Based on the rate of polymerization we say that there is a plus-end or fast growing end (the $\alpha \rightarrow \beta$ arrow) and a minus-end or slow growing end ($\beta \rightarrow \alpha$). This is a consequence of the asymmetric properties of the tubulin dimers. The lateral

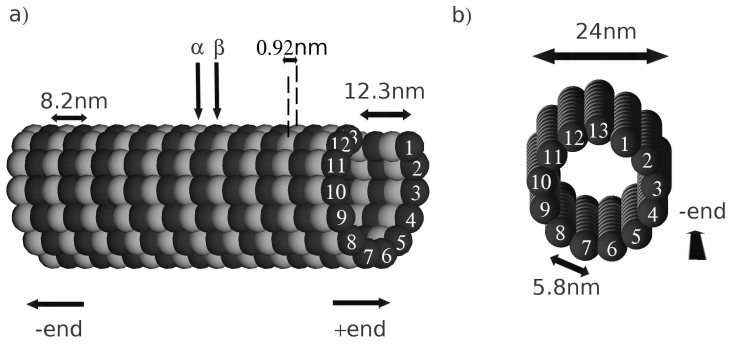

Figure 1.1: **Three dimensional scheme of a microtubule.** a) Lateral view with the fast growing end pointing to the right and the slow growing end pointing to the left. We can appreciate every tubulin dimer as composed of a gray sphere (α subunit) and a dark sphere (β subunit). The $\alpha-\alpha$ or $\beta-\beta$ distance is $8.2nm$. In this array there are 13 parallel protofilaments which have a lateral shit of $0.92nm$ which induces a supertwist that is patent at the edges of the microtubule. A complete turn of the supertwist produces $12.3nm$ along the symmetry axis, which corresponds to a length of three tubulin subunits. b) The microtubule seen from the plus end to the minus end with a small tilt on the vertical axis. Protofilaments are numbered clockwise. We can appreciate that the diameter is about $24nm$ and that the approximate distance between two consecutive protofilaments is about $5.8nm$.

distance between two consecutive protofilaments can be extracted by dividing the perimeter of the microtubule's surface by 13, which gives $5.8nm$. In Figure 1.1 we can see all these parameters.

1.1.2 Kinesins

Kinesin motors actually constitute a numerous superfamily of motile proteins. However all of them share some common properties. They are essentially proteins that are able to generate motion and force while they interact with a microtubule. The conventional kinesin, the first that was identified and that will be one of the main targets of this thesis, consists of two 120-kDa heavy chains and two 64-kDa light chains [5]. It has on one edge two globular heads of 10nm of diameter, connected by a neck, which is connected to the stalk, of about $80nm$ long. At the end of the stalk there is a fan-like end where a cargo, like a vesicle or a small organelle is attached. Essentially, kinesin uses both heads as if they

were a bipedal, so maybe they should be called feet instead. We will keep calling them heads only not to be confusing. Kinesin-1, the family at which conventional kinesin belongs, walk along a microtubule following a path which is parallel to a protofilament [6]. Moreover, the motion of the two heads is coordinated in an asymmetric hand-over-hand fashion [7]. A single kinesin-1 can walk processively along $\sim 100nm$ [8], although the run length, i.e. the covered distance without detaching from the microtubule, is variable and mutations on the neck region can modify this value significantly [8].
Kinesin performs $8.2nm$ steps and it consumes a single ATP per step [9] reaching a maximum velocity of about $800nm/s$. Each of the heads is able to catalyze an ATP molecule and the role of them is exchanged after every whole cycle. The size of the step is not by chance, as it coincides with the tubulin periodicity of the microtubule. Experimentally, the maximum forces that a kinesin-1 can produce are of the order of $5 - 7pN$.

There are, however, other type of kinesins that are not processive, i.e. they are able to produce only a single step and after this they detach from the microtubule. In such cases there is need for cooperation between a certain quantity of these proteins in order to achieve an effective transport of a cargo. In the N-2 family, kinesin have four heads divided in two motor domains. Then they are able to bind two microtubules simultaneously, one at each edge of the stalk. They are essential in mitotic process, as they contribute to the formation and the dynamic evolution of the mitotic spindle.

A key feature of kinesins is that they are able to read the polarity of the microtubule in order to walk only to the plus-end (conventional kinesin) or towards the minus end (NCD kinesin). This is called the directionality of kinesin, and it seems to be directly related with the neck region [10]. In figure 1.2 we show two versions of a crystal structure in order to illustrate the main parts of the motor core and some typical distances.

1.1.3 Dyneins

Dyneins are minus-end directed motors that are involved not only on transport and mitosis processes but also in the assembly and motility of cilia and flagella [5].

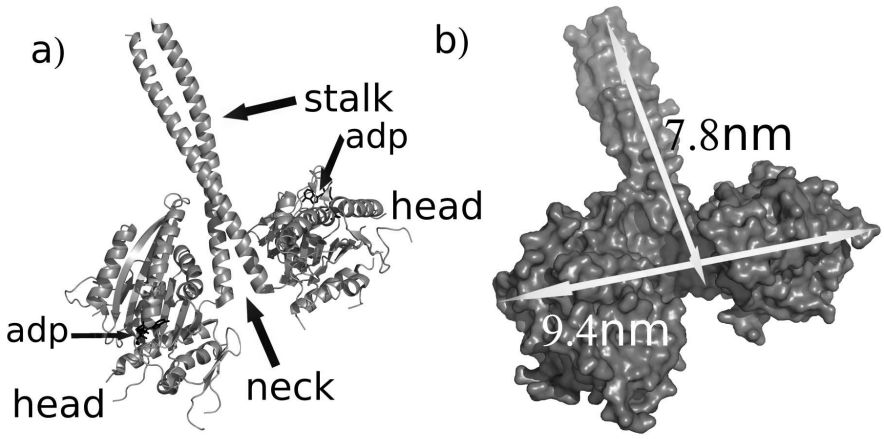

Figure 1.2: **Pymol renderings of a NCD kinesin from 1N6M file of the Protein Data Bank.** a) Cartoon representation. We can see the two head domains connected by the neck. The stalk begins at the neck linker, even if does not appear complete in the figure. In black there is a bound ADP on each head, illustrating the enzymatic character of these domains. b) A surface representation where a head to head distance and a neck-stalk scale is shown.

They have from one to three heavy chains (HC) that exhibit motor and ATP-ase activity. The rest of the structure is composed of several intermediate and light chains see Fig.1.3. We can distinguish between flagellar/ciliar and cytoplasmic dynein. While the former can have from 1 to 3 HC, the latter has two. In comparison with kinesin, the size of a dynein is much larger. Only the heavy chain is composed of three distinguishable regions that exceed the size of a whole kinesin. The heavy chain is attached to the other domains through the N-terminus, which is followed by a ring of seven domains, $AAA-i$ with $i \in [1,6]$ and a C-domain. Only $AAA-1$ has ATPase activity, but is the one which is furthest from the microtubule, which is connected to the ring through a flexible stalk and a MT-binding domain [11, 5].

Concerning the ATP-dependent dynamics, we can say that ATP binding at $AAA-1$ induces microtubule releasing. Then, ADP and P_i releases from the pocket are highly accelerated in the presence of MT. Both facts indicate a direct communication between microtubules and $AAA-1$, which are more than $20nm$ distant.

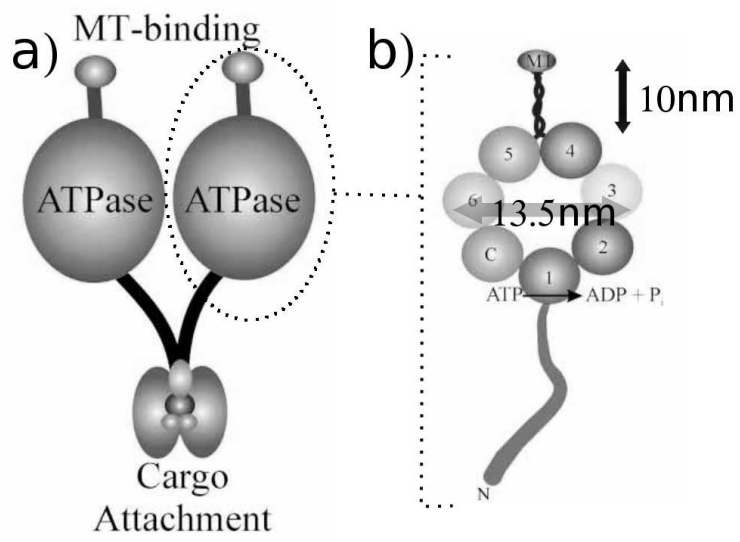

Figure 1.3: **Illustration of cytoplasmic dynein (modified from Ref.[11]).** a) Illustration of the whole structure. At the bottom we can see the light chains and the intermediate chains. There they bind the cargo that has to be transported. The light chains connect with the N-term (amino terminal, labelled as N in the figure) of the heavy chains, which are two in the case of cytoplasmic dynein but can be from 1 to 3 in other type of flagellar/ciliar dynein. HC have ATP-ase activity, which is the mechanism to obtain the energy in order to achieve motor activity. The C-term (up, attached to the MT) of each HC is composed of a stalk ($\sim 10nm$, the region from the 4-5 AAA sites to the MT domain region) and a microtubule binding domain. b) A heavy chain domain in more detail. We can appreciate the seven globular subdomains, forming a ring of AAA sites of $\sim 13.5nm$ (labelled with numbers from 1 to 6 and an additional C). AAA-1 is the only domain with ATPase activity.

Dyneins generate forces of about $\sim 5pN$ and move along MT's with a step size equal to the tubulin periodicity $\simeq 8nm$. There is evidence for processive motion and consequently for coordination between different heavy chains. However, dyneins don't seem to follow paths that are parallel to protofilament direction but they move across the microtubule surface [12].

Dyneins are directly related with male fertility and the development of the left-right axis of the embryo, as they are responsible for the motion of cilia and flagella [13, 14].

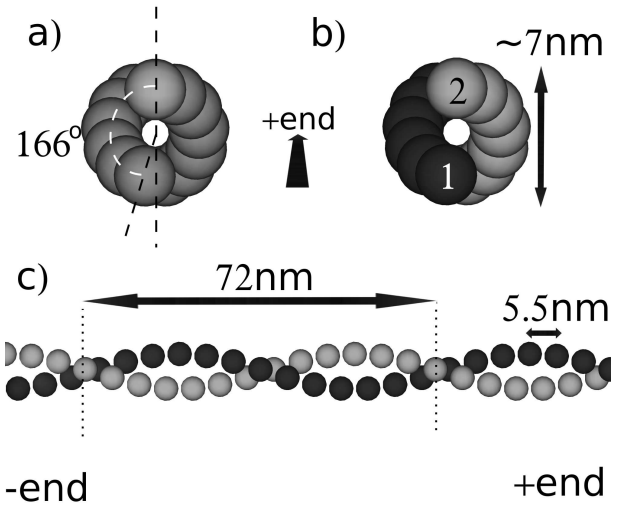

Figure 1.4: **Scheme of an actin filament.** a) Actin filament seen from the minus to the plus-end. Following the left-handed interpretation, each monomer is located at a place which is rotated $\simeq 166^o$ with respect to the previous monomer. b) With the right handed interpretation we can consider two protofilaments, marked with numbers 1 and 2. The maximum diameter of the filament at a given axial position is about $7nm$. c) A lateral view where we can appreciate the $72nm$ period length and the $5.5nm$ distance between consecutive monomers in a given protofilament.

1.2 Actin based motion

1.2.1 Actin filaments

Actin is a globular $\sim 45kDa$ protein that polymerizes into actin filaments, which are mainly involved in two functions. On the one hand they serve as part of the cytoskeleton and on the other hand they act as contractile structure when crosslinked with myosin fibers. The former property is common to all eukaryotic cells, while the latter belongs to muscle cells. Actin filaments participate also in cell motility, cell division, cytokinesis, cell signaling and vesicle-organelle transport among others. Concerning motor activity they are the tracks for myosin motors, which we will introduce now. These filaments are polar, like microtubules. The plus-end is distinguished because it polymerizes faster than the minus or slow-growing-end.

1.2.2 Myosins

Even though myosins are classically known to be responsible of muscle contraction, they are also involved in many biological processes, like motility, adhesion, endocytosis, cytoplasmic streaming, neuron growth, structural maintenance and polarization [5]. They also transport organelles and other cellular components. They normally use ATP as the energy carrier, like kinesin and dynein. Structurally, they have 1 or 2 heavy chains and 1 or 2 light chains. Myosin V, for example, has two heavy chains and walks processively along an actin filament in a hand-over-hand fashion, recalling kinesin's motion. Other types, like muscle Myosin II, have one heavy chain and have a non processive action. In any case, myosin motor domains are reasonably greater than the corresponding motor domains in kinesins. Actually, they are more than double in size.

There are 14 families of myosins. Family I is related with cell motility, vesicle transport, endocytosis among other functions. Family II is where the conventional muscle myosin belongs to. They are also related with cytokinesis or morphogenesis. Family III is basically related to cell structure and signal transduction. More details can be found at [5]. Our focus of attention is towards family V and VI, where myosins are dimeric and processive. Family IXb is processive but monomeric. Myosins I and V move towards the plus end of actin filaments. Other myosins like VI and IX move towards the minus-end. This is important concerning cellular transport since actin filament usually have their plus end oriented towards the cell periphery. Then, plus ended myosins transport materials to the periphery while minus ended do the opposite. Processive V myosins perform $36nm$ steps, which corresponds to the pseudo periodicity of actin filaments, i.e. the periodicity obtained when projecting the actin structure into a 2D plane. They stall at forces of $\sim$ 2pN.

In Figure 1.5 we can see a crystal structure of one of the two heavy chains of a V myosin and part of a light chain. We can notice the localization of the ADP nucleotide and that the size of the domain is considerably bigger than the corresponding for kinesin. In Figure 1.6 we can see 14 images of a V myosin in different conformations [15]. They suggest a mechanical cycle based in hand-over-hand motion. We can appreciate the two motor domains, that seem to be quite flexible. The rising action seems quite vertical as well, which doesn't allow to

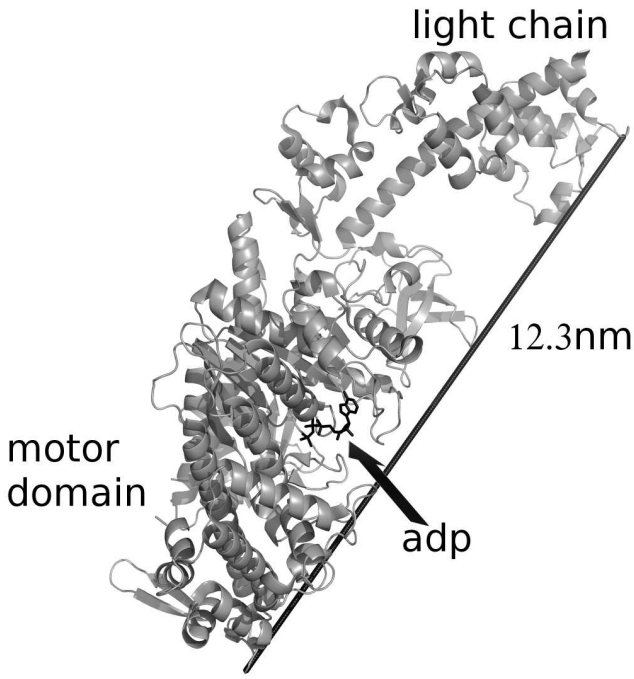

Figure 1.5: **Pymol representation of a V-myosin from 1W7J.pdb** We can appreciate a single heavy chain and part of a light chain of a V-myosin crystal structure. The rod accounts for a size measurement of $12.3nm$, which is considerably larger than kinesin's motor domain. In black there is an bound ADP nucleotide.

differentiate between symmetric and asymmetric hand-over-hand motion.

1.3 DNA-RNA based motion

1.3.1 DNA and RNA

DNA and RNA are nucleotide polymers that are related with genetic information. However, from the motile point of view, they are the tracks that some enzymes as DNA and RNA polymerases (DNAp and RNAp) or ribosomes use to walk along DNA and RNA, respectively. The internal structure of DNA and RNA is very similar, as they are polymers of four nucleotides. Of these four different bases, three of them are shared by DNA and RNA and they are Cytosine (C), Guanine

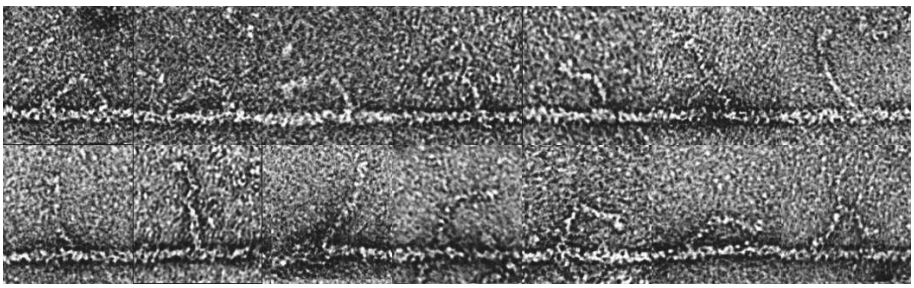

Figure 1.6: **Images from different V-myosin conformations, adapted from Ref.[15].** We can see 14 averaged stained images from a V-myosin in different conformations. The resolution is $2nm$. The order of the images is built upon considering a hand-over-hand motion, even though there is no direct observation of the dynamics.

(G) and Adenine (A). However, the fourth base is different in the two tracks. While we have Thymine (T) for DNA, we have Uracile (U) for RNA. In any case, we can forget the differences between bases for now as the motors we will introduce are able to walk along all the bases, although not indifferently.
DNA tracks are normally folded in a two stranded double helix, in the B-DNA conformation, but when a DNAp motor is walking along, during replication, for example, only one strand is used as a track. RNAp, however, use both strands as support for motion. The periodicity of these polymers is characterized by a very small period compared to the periods in the tracks introduced before. We know that a base pair (bp) is $\simeq 0.33nm$ long. The width of the double helix is between 2.2 and $2.6nm$, but this is not a static value as the motor action exerts bending effect on the polymer. Concerning polarity, DNA and RNA are polar tracks, as they are differentiated by the two different terminus. One terminus is 5' corresponding to the free phosphate group while the 3' terminus corresponds to the free sugar end. In a double helix conformation, the strands are oriented in an antiparallel way.

In Figure 1.7 we can see a crystal structure of a B-DNA. We can appreciate the antiparallel orientations of the strands, marked in black and white. In general, these polymers can adopt very different 3D structures, specially in the case of RNA chains. However the motor that walks along it has to temporarily unfold the local structure in order to slide along the chain. Unlike microtubule or actin

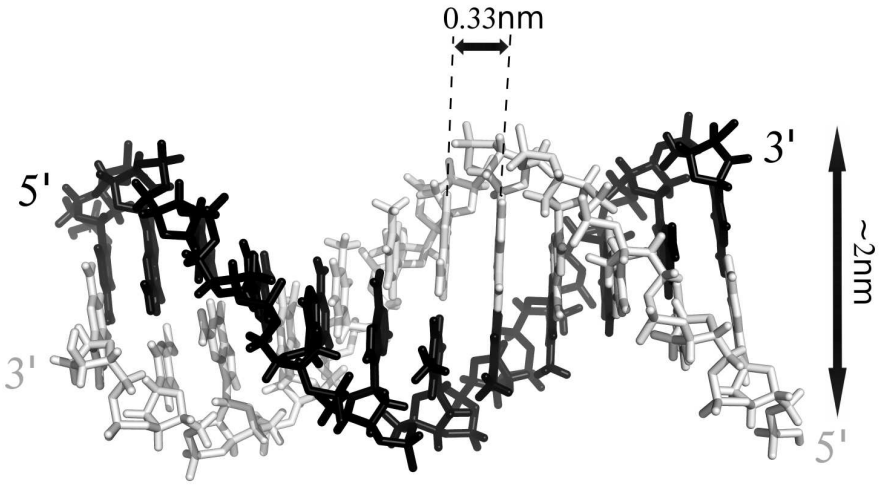

Figure 1.7: **Pymol representation of a B-DNA from Ref.[17]** In black we see the 5'-3' strand while 3'-5' is shown in light gray. We can see the base pair distance ($\simeq 0.33nm$) and the approximated width of the helix ($\sim 2nm$).

based motion, the tracks of DNA and RNA have encoded information. There is, however, a proposal of quantum information on microtubules [16] but it is still a very open question and it does not necessary imply that motors read this information, while DNAp and RNAp read it.

1.3.2 RNA and DNA polymerases

DNA polymerases are molecular motors that use a single strand of DNA in order to replicate it. They walk along DNA in the 3'-5' direction performing $0.34nm$ steps and generating forces up to $35pN$. As the process can be continued by another DNAp, the processivity of this motor is not high. On the other hand, RNAp are motors that use *both strands* of DNA as tracks, even though they read from 3'-5' strand to perform the transcription process, which produces RNA strands in the order 5'-3'. They perform steps of the size as DNAp, i.e. bp steps, but they generate forces that don't overcome $25pN$. The energy source is not only

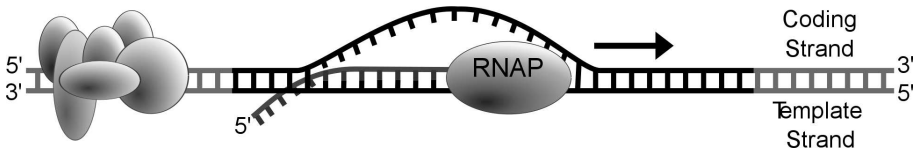

Figure 1.8: **Scheme of transcription** We can see a RNA polymerase sliding along a double helix DNA in the direction marked by the arrow. Even though the RNAp uses both strands as tracks, it reads 3'-5' information, i.e. the information from the template strand. (Image from public domain).

ATP but also the other four nucleotides: UTP, TTP, CTP and GTP, abbreviated under the general term NTP. UTP is specific of RNAp and TTP is specific of DNAp, being CTP, GTP and ATP common to both type of devices.

These motors do not only walk along their tracks but also they recognize track sequences and synthesize polymers that will be tracks of other motors. They are motors that *transcribe and replicate the tracks.* After all, a kind of this action is needed in order to preserve the track molecules. On the other hand, the constituents of the track are the *residues* of the energetic fuel. In Figure 1.8 we can see a scheme of transcription performed by a RNAp. We can see how the motor reads the 3'-5' DNA while building a 5'-3' RNA.

1.3.3 Ribosomes

Ribosomes are big and complex structures made of ribosomal RNA (65%) and ribosomal proteins (35%). Their main function is to read the mRNA and attach the matching tRNA for every messenger triplet. The aminoacids of the transfer RNA are bound by the ribosome and they constitute the protein that mRNA was encoding. We are not concerned on the complex details of this machine but on the properties related with motor activity. Ribosomes walk along mRNA in the 5'-3' direction, even though the huge volume and subsequent friction may produce a motion of the track in the laboratory frame.

These $20nm-$diameter machines are the last piece of a self sustained motor system: they walk along tracks in order to *produce*, among other things, molecular motors. As tracks were synthesized by DNAp and RNAp, motors are synthesized

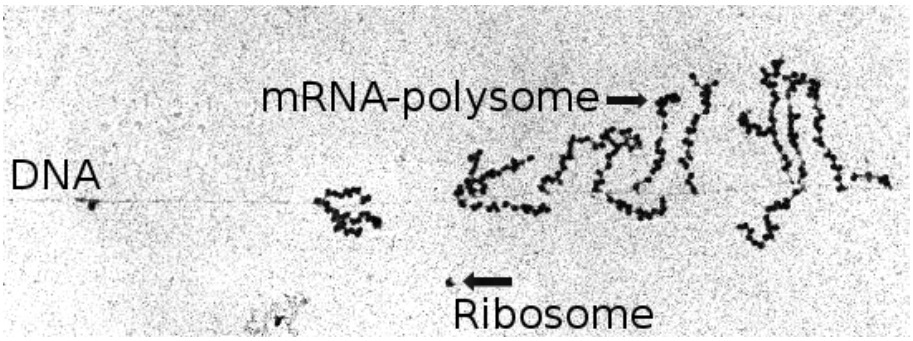

Figure 1.9: **Polysomes** A stretched DNA of *E. coli* read by RNA polymerases that produce mRNA. The messenger RNA strands are read by Polysomes, i.e. by more than one ribosome at the same time. (Adapted from Ref.[18])

by ribosomes. These machines allow the biological motor systems to be self-reproduced and maintained.

In Figure 1.9 we can see how different ribosomes can simultaneously walk along mRNA which is simultaneously being produced from a DNA by a RNAp. This picture reflects that the biological steps are not strictly disjunctive.

1.4 Rotatory systems

1.4.1 Bacterial Flagellar Motor

Most bacteria swim thanks to the rotation of bacterial flagella coated on their external surface. This motion is passive, as bacterial flagella are rigid helices that are propelled by a rotatory machine which is embedded in the cytoplasmic membrane. We call to this machine Bacterial Flagellar Motor (BFM) [19]. They are devices that use the electrochemical potential due to different ionic concentration at both sides of the membrane. Specifically, it uses the ion flux from one side of the membrane to the other to extract the energy used for the rotation. The crossing ions define two types of BFM: one of them uses proton flux and we call to the force that they produce *proton motive force* (pmf) while there are Na^+ powered BFM which produce sodium motive force (smf). Usually the flux is directed from the exterior to the interior of the bacteria, as the internal ion concentration is

lower. Typically there is a $150mV$ effective potential with respect to the exterior. Under normal conditions BFM can rotate with a frequency up to $1000Hz$.

Structurally, the Bacterial Flagellar Motor is divided into the rotor and the stator. In Figure 1.10 we can see an electron cryotomography image of a BFM [20]. We can appreciate the stator and the rotor as well as the C-ring. The stator has a diameter of $\sim 60nm$ [20]. The rotor has a variable number of torque generating units, from 8 to 16, and it is bound to the flagella via a hook. These torque generating units work independently as they can be activated or inhibited as the total frequency seems to be enhanced or decreased an increment of velocity that corresponds to the quotient between the total velocity and the number of torque generating units [21, 22]. In each of the torque generating units there is an independent flux of ions, and the interaction between the stator and the rotor, which has to produce the torque, seems to be of electrostatic nature [23].

The rotational steps have been measured in Ref.[24] and kinetic measurements are available in [25, 26]. In [24] they measure steps of 13.7^o, which corresponds to 26 steps per revolution. This is in agreement with the structural periodicity of the FliG protein in the rotor place where the torque is generated. However, there is evidence that ~ 1000 Na^+ ions [25] or ~ 1200 protons [24] are required to complete a revolution. This indicates that more than one single ion is involved in the production of a single step. On the other hand, the periodicity of ~ 10 torque generating units is not fitting the step size in a direct way. Much work is needed to clarify the stechiometry of this motor.

Eventually, a BFM can reverse its direction [27]. It is known that in *E. coli*, even if almost all the flagella rotate counter-clockwise, it is found that it can appear a flagella that starts to rotate clockwise. This helps to change the swimming direction. There are also BFM that are able to switch between action and rest in order to allow the bacteria to optimize its search for food.

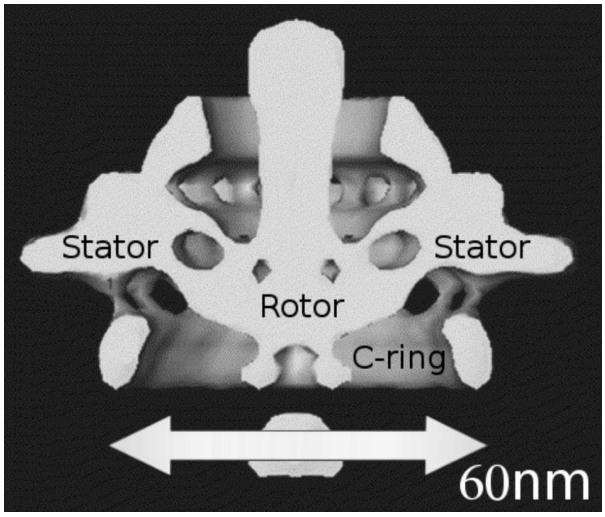

Figure 1.10: **Bacterial Flagellar Motor stator-rotor structure adapted from Ref.[20]** Electron cryotomography of a BFM where the rotor and the stator can be differentiated except in the interaction domains, where they appear as the same structure. The diameter of the C-ring, $\simeq 60nm$, gives the scale to the figure.

1.4.2 $F_O - F_1$ ATP synthethase

The $F_O - F_1$ ATP synthase is a device that is found at the inner membrane of the mitochondria, at the thylakoid membrane of chloroplasts and at the plasma membrane of bacteria [5]. It is in fact a set of two motors which operate in competition. The F_O part rotates embedded in the membrane while F_1 is located outside the membrane and connected to the F_O by a shaft, called the γ domain. The stator also connects both parts (see Figure 1.11).

The F_O part is a rotatory motor that uses the ion gradient at both sides of the membrane to obtain the energy required for the rotation. It can remind the Bacterial Flagellar Motor, but some differences arise. In the BFM there were several torque generating units working in parallel, while in the F_O there is only one. In any case, the torque seems generated, as in BFM, by electrostatic interactions between the rotor and the stator [28]. The F_O is divided into a variable number of sections, which goes from 10 to 14. Each of these cavities is negatively charged and when an ion enters the cavity the whole charge is compensated and

then the cavity can move inside the membrane, which is hydrophobic. We have to imagine all the cavities neutralized except the one passing through the stator region, which releases the ion and is affected by the stator charge. Then, in this motor, an ion is tightly coupled to a discrete rotation of the F_O unit.

When looking from the F_O to the F_1 perspective, the natural, non-forced motion of the F_O is clockwise, while the natural motion of F_1 is counterclockwise. They are generating opposing torques and under physiological conditions it is the F_O which is winning. The connection between both units is the γ shaft, which acts as a mechanical axis. This means that F_O is forced to rotate against its natural direction. This leads to the main feature of the ATP synthase. While an isolated F_1 hydrolyzes ATP as a mechanoenzyme, when forced, it is able to synthesize it. Thus we are in front of a reversible machine. In fact, almost all the ATP in the cell is produced due to the action of this enzyme.

Structurally, F_1 can be divided into six domains, three α and three β regions, which are alternated forming a ring. The β domains have catalytic and synthezising properties. The rest state of the system is when we have an empty β, an ADP-P_i-bound β and an ATP-bound β. Depending on the resulting global torque, the ATP is hydrolyzed or the $ADP - P_i$ is converted into ATP. As there are three active sites, the measured angle steps are of 120^o, even if each step is divided into 90^o and 30^o substeps, thought to be related with ATP binding and $ADP - P_i$ release, respectively [**?**]. When free from the F_O forcing, F_1 can rotate from 0.2 to $10Hz$, depending on the ATP concentration.

From the theoretical point of view, the ATP synthase is probably the most challenging device, as it is composed of two very different subdevices that are forcing to each other being both reversible and mechanically coupled. In Figures 1.11 and 1.12 we see some representations of the ATP synthase with the different domains marked and with some typical distances.

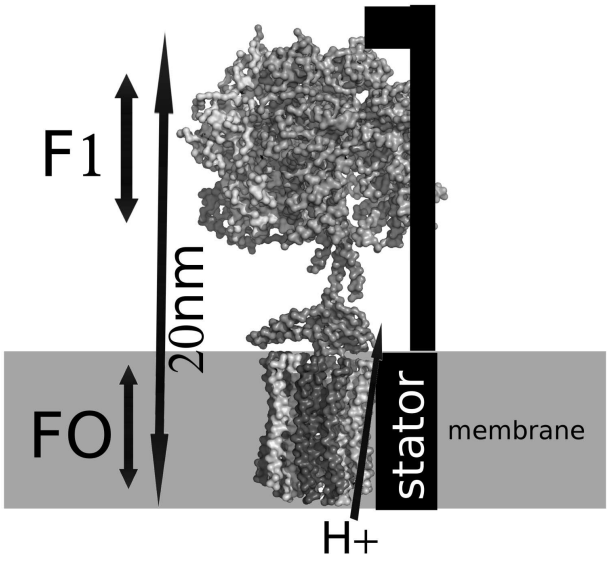

Figure 1.11: **Pymol representation of an ATP-synthase from 1QO1.pdb.** In this lateral view we can see the $20nm$ height of the whole device. We can appreciate the γ shaft as the connecting part between the two rotating structures. We have sketched the stator domain, which serves as ion crossing region and also connects both rotating machines. In grey, there is the membrane-hydrophobic zone so ions can only cross through the stator channel.

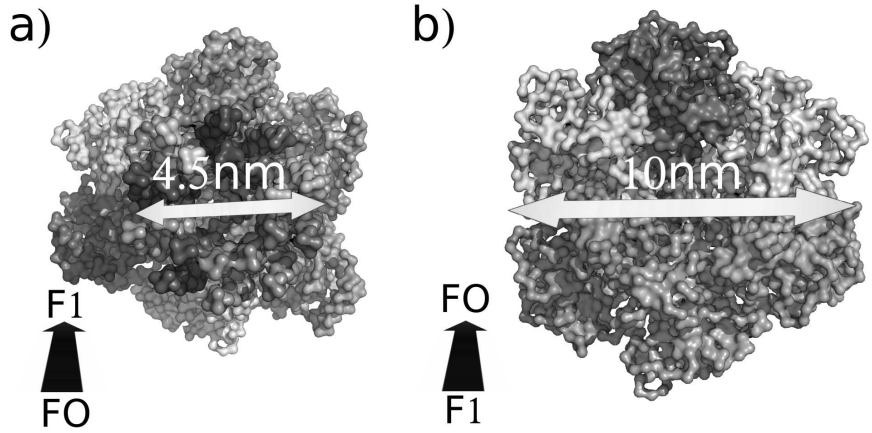

Figure 1.12: **Pymol representation of an ATP-synthase from 1QO1.pdb.** a) Seen from F_O to F_1 we can appreciate the $4.5nm$ diameter of the F_O ring with ten subunits. b) Seen from F_1 to F_O we can see the top of the F_1 unit, which is a ring of three α and three β units. The diameter is about $10nm$.

1.5 Summary

In this introduction we have presented the most typical motor systems. Some of them will be the objects of our further analysis. But among all the examples, it is the kinesin-microtubule system the main target of this thesis. First of all, we will proceed with a collection of ratchet-based models that will allow us to introduce kinetic and energetic aspects. After this, a more detailed chemical kinetic description is provided in order to understand how the mechanical forces affect the chemical rates. Finally, and focusing on kinesin motors, we will present, on the one hand, an electrostatic model for tubulin and kinesin. On the other hand, we will introduce a phenomenological model for the interactions between tubulin heterodimers and the different nucleotide states of kinesin heavy domains, which have been studied in recent experiments.

Part I

Ratchet-based models

2

Introduction

2.1 Brownian motion and Langevin equations

In 1827, Robert Brown observed at his microscope how a pollen particle suspended on water exhibited an irregular motion [29]. He thought that maybe such a motion could be related with the basis of life, but he proved that it wasn't. Almost a century passed until A. Einstein, in 1905, was able to provide an explanation for this phenomena and used it to proof the atomic nature of matter. In a few words, brownian motion can be understood as the trace of a particle which is small enough to be affected by the smallest particle impacts and big enough to be tracked by a microscope. The irregular motion is a reflection of the local fluctuations of momentum in the bath. Einstein related brownian motion with temperature and diffusion, fact that took the attention of physicists and chemists, as these were magnitudes that were macroscopic and then could be used to measure microscopic properties and specially the bridge quantity between the macroscopic and microscopic worlds: the Avogadro number N_A.

In the last years of the XXth century, experimental techniques were already able to track particles small enough to be visibly affected by thermal fluctuations. With the arrival of single molecule techniques, the relevance of brownian motion in biological molecules has been put out of question. As long as the behavior of a protein is to be understood, the presence of brownian motion cannot be

neglected. Sometimes, a proposed mechanism may be robust under thermal fluctuations, while other models use these fluctuations as a part of the mechanism. Thus such an erratic motion needs to be mathematically described. In this section we will provide an intuitive view of the quantitative properties of brownian motion and other aspects related with it.

We will make use of the two main results due to Einstein [30]. First of all, the displacement vector $\vec{r}$ that the big particle performs after every Δt can be decomposed into cartesian coordinates and then each coordinate can be treated as a one dimensional brownian motion. The key point is that the motion has zero mean and a mean square displacement equal to $\langle \Delta r^2 \rangle \sim 2dDt$, where d is the dimensionality of the system and D is the diffusion coefficient, which can be interpreted as $D = \frac{k_B T}{\lambda}$ where λ is the translational drag coefficient . This is a fluctuation-dissipation relation and it establishes the connection between microscopic fluctuations and macroscopic diffusion. The relation for the mean square displacement and the connection of the diffusion coefficient with the drag coefficient together with temperature are the two main results found by Einstein.

Thus a brownian particle is an erratic object wandering through the media with zero neat displacement but with a finite and growing-with-time variance that is proportional to temperature and inversely proportional to friction. These properties are very important in nanometric systems because even if on average these motions are compensated, the brownian jiggling affects appreciably the state of every nano particle like a protein. This means that every state which is not bound with an energy larger than several times the thermal energy cannot be stable.

We can calculate how effective is diffusion for intracellular transport by introducing biological numbers in the fluctuation-dissipation relation. Let's use the Stokes formula for the friction of a spherical object

$$\lambda = 6\pi\eta R, \tag{2.1}$$

where η is the viscosity of water $\eta \simeq 10^{-9} pN \cdot s/nm^2$. We apply to a nanoparticle

of radius $\sim 25nm$. Thermal energy is expressed as $k_BT = 4.1pN \cdot nm$ so then

$$D = \frac{k_BT}{\lambda} = \frac{k_BT}{6\pi\eta R} \simeq 9 \cdot 10^6 nm^2/s. \tag{2.2}$$

Then, this brownian particle will explore a radius a given by $\sqrt{6Dt}$ in three dimensions. If we consider a cell of being $5\mu m$ long, the 25nm particle will last a time $t = a^2/6D \simeq 0.1s$ in order to explore the whole cell. For a $1mm$-long bacteria, this time is greater than 5 hours. For more examples, see [14]. The time to explore a certain distance by diffusion grows proportionally to the square of this distance. This means that even if for low distances the time can be relatively short, for greater distances it increases parabolically. Moreover, this exploration time grows linearly with the size of the brownian particle. It is interesting to note that small particles can rapidly be spread along the whole cell, while other bigger structures may need an active transport. Surprisingly, a kinesin can pull a $25nm$-radius-vesicle at a velocity of about $1\mu m/s$, which means that such an active transport is more than 50 times slower than the passive diffusion! In fact, the active and passive times do not equal until we evaluate distances of $54\mu m$. This is a point where we have to remark the importance of directionality. Some substances are not needed everywhere in the cell but in some specific locations, so then, active transport is more effective even if sometimes is slower. It is worth mentioning that the viscosity in the cytoplasm may be considerably higher than the corresponding to the water, and that sometimes the distances needed to travel can reach a whole meter in the case of some nerve cells. In this latter case the active transport is much rapid than passive diffusion. We can also notice that sometimes the cargo of a motor protein is not so tiny as having a 25-nm radius but a $5\mu m$ radius in the case of some big mitochondria. With such a size, the diffusing time is incredibly long, while a kinesin can still carry it at $\sim 1\mu m/s$. See more details in Fig.2.1.

Mathematically, there are several ways to deal with brownian motion, but maybe the most direct and intuitive is the use of Langevin equations, which are no more than Newton's dynamical equation where a stochastic force is added.

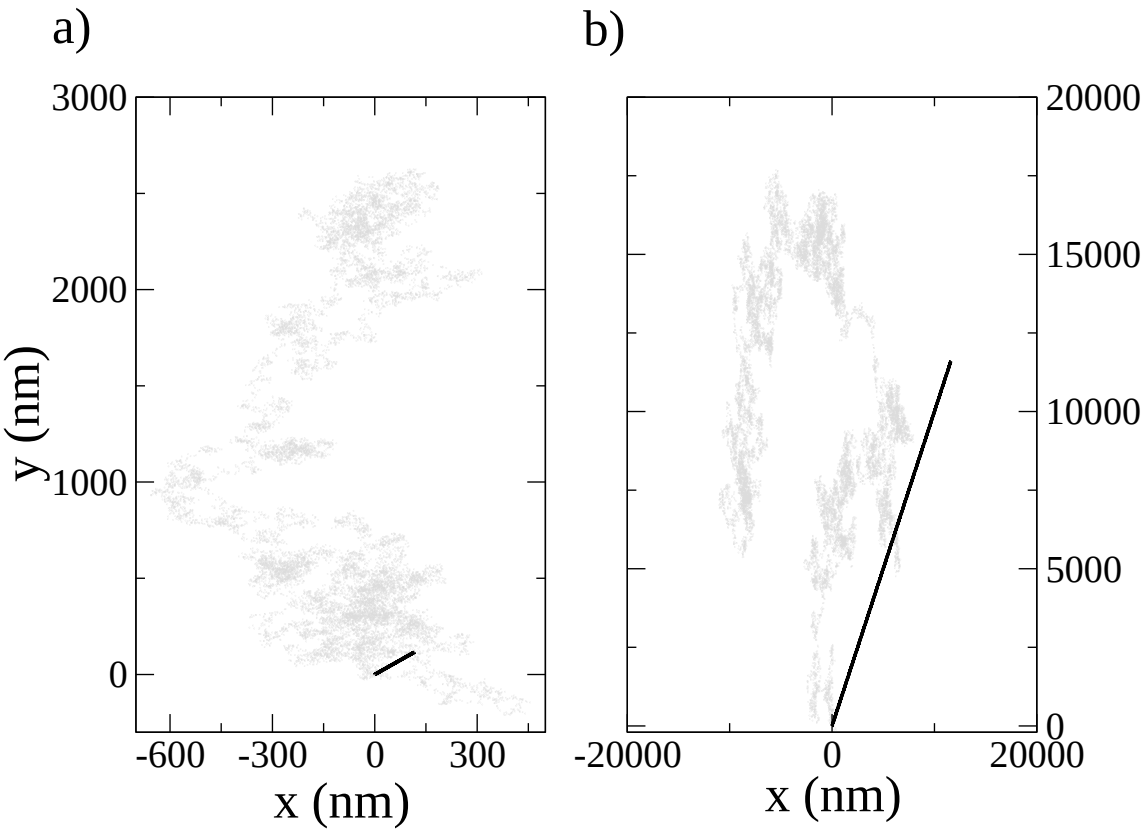

Figure 2.1: **Passive and active transport.** In a) we can see $0.16s$ of a brownian particle simulation in 2D where grey indicates brownian motion and black a motor trajectory. The parameters are $k_BT = 4.1pN \cdot nm$, $\lambda = 10^{-6}pNs/nm$. The mean velocity for the motor is $v = 1\mu/s$ in the direction $y = x$. It is clear that at this time diffusion has explored further places. However, if the desired target would be at negative y, a directed motion would have been more effective since the erratic exploration has been poor on this zone. In b) we can see a critical situation where $t = 16.4s$. This value comes from the consideration that the exploration radius (mean square displacement) is equal to the net displacement of the motor. Then $t = 4k_BT/\lambda v^2 = 16.4s$. In the figure it is clear that active transport explores a similar distance from the origin than thermal diffusion. And what's more important: at larger times, active transport goes beyond than diffusion.

We have Newton's second law for a particle

$$m\ddot{x} = \sum_i f_i. \tag{2.3}$$

Now we can split the force terms into four characteristic forces that will constantly appear in the formalism: the drag $-\lambda\dot{x}$, the potential gradient $-dV(x,t)/dx$, the external $f_{ext}(t)$ and the stochastic force $\xi(t)$, leading to

$$m\ddot{x} = -\lambda\dot{x} - \frac{dV(x,t)}{dx} + f_{ext}(t) + \xi(t), \tag{2.4}$$

where possible time dependences are indicated. We can show now that the second derivative can be neglected in a nanoscopic environment as Reynolds number Re[1] is extremely low, $\sim 10^{-5}$ for a $1\mu m$-long vesicle. For all the purposes, inertia can be neglected, then, and we can reduce our dynamical equation to what we is usually called an overdamped equation, with the general form

$$\lambda\dot{x} = -\frac{dV(x,t)}{dx} + f_{ext}(t) + \xi(t). \tag{2.5}$$

It is remarkable how, in the absence of thermal noise or in cases where the observable magnitude is not affected by a zero-mean-value noise, the velocity of the particle is proportional to the force, as Aristotle already stated. It is worth mentioning that Aristotle took his conclusion from an experiment where damping produced a terminal velocity. Thus we will deal with Aristotle dynamics where a stochastic force is added by hand. Such a force, in order to reproduce the fluctuations due to temperature, must hold some statistical properties. Specifically, $\xi(t)$ is a thermal force [31] if

$$\langle\xi(t)\rangle = 0 \tag{2.6}$$

and

$$\langle\xi(t)\xi(t')\rangle = 2\lambda k_B T\delta(t-t'), \tag{2.7}$$

which means that the noise has zero mean and is delta-correlated in time. Such a correlation relates the thermal force with the specific drag coefficient and the temperature. This is called a fluctuation-dissipation theorem.

[1] $Re = \frac{\rho L v}{\eta}$, where ρ is the density of the liquid, L the characteristic length of the system, v the velocity and η the viscosity.

In order to implement the thermal force in an algorithm, there is a subtlety relying the integration of motion. The non-stochastic forces can be integrated at first order following simple Euler's rule,

$$x = x_0 + \frac{\Delta t}{\lambda} \sum_i \vec{f}_i. \tag{2.8}$$

However, the thermal force obeys a different integration rule. From eq (2.7) one can agree with, for a finite time step,

$$\langle \xi(t)\xi(t+\Delta t)\rangle = \frac{2\lambda k_B T}{\Delta t} \tag{2.9}$$

where we have used that

$$\lim_{\Delta t \to 0} \frac{1}{\Delta t} = \delta(\Delta t). \tag{2.10}$$

Then we can write in the limit of very small Δt

$$\langle \xi^2(t)\rangle = \frac{2\lambda k_B T}{\Delta t}. \tag{2.11}$$

If we want to integrate the thermal force in an equation like $\lambda \dot{x} = \xi(t)$, we will use

$$x = x_0 + \frac{\Delta t}{\lambda} \sqrt{\langle \xi^2(t)\rangle} N(0;1) \tag{2.12}$$

where $N(0;1)$ is a gaussian random number with zero average and variance equal to unity. This random number guarantees the statistical properties of the thermal force. Then

$$x = x_0 + \sqrt{\frac{2k_B T \Delta t}{\lambda}} N(0;1). \tag{2.13}$$

We can see how, while other forces are integrated with a direct proportionality to Δt, the thermal force is proportional to the square root of this increment. Thus with the equation $\lambda \dot{x} = \xi(t)$ we simply obtain a pure brownian motion, which can be applied to free diffusing molecules in the environment. We can use Langevin dynamics to describe the effects of a potential or an external force. It is of special importance the case of a brownian particle trapped in an harmonic potential $V(x) = \frac{1}{2}kx^2$, where k is the harmonic stiffness. The corresponding

Langevin equation is

$$\lambda \dot{x} = -kx + \xi(t). \tag{2.14}$$

It can be shown that the mean value $\langle x \rangle = 0$ while

$$\langle x^2 \rangle = \frac{k_B T}{k}, \tag{2.15}$$

according with the Energy Equipartition Theorem. The latter expression compares the elastic energy with the thermal energy,

$$\frac{1}{2} k \langle x^2 \rangle \sim \frac{k_B T}{2}. \tag{2.16}$$

This is a useful expression, since whenever we have a noisy signal from, for example, an optical tweezer, we can calculate the variance of the signal and obtain the stiffness of the trap, see Fig.2.2 and 2.3. Notice, however, that if the signal is already filtered to improve a step-finder accuracy or a similar trajectory analysis, then the information concerning thermal fluctuations is already lost.

2.2 Energetic considerations on overdamped motors

In this section we will discuss some general aspects concerning overdamped motors, like work, heat, first and second law of thermodynamics, dissipated heat, efficiencies, etc. A motor performs a useful work only if there is a force that is opposing the motion. This force can be conservative, as in the case of an electric field or an harmonic potential (as it is the case when we use optical tweezers), or it can be non-conservative, as in the case of friction. If we only have friction and the motive force f_m of the motor we can write

$$\lambda \dot{x} = f_m. \tag{2.17}$$

We have to notice that in such overdamped systems we are always at mechanical equilibrium, as friction compensates any other forces in the system. In this case, the work performed by the motor W along a one-dimensional path $x : 0 \to L$ is 0 because there are no conservative external forces. However, there is a non-

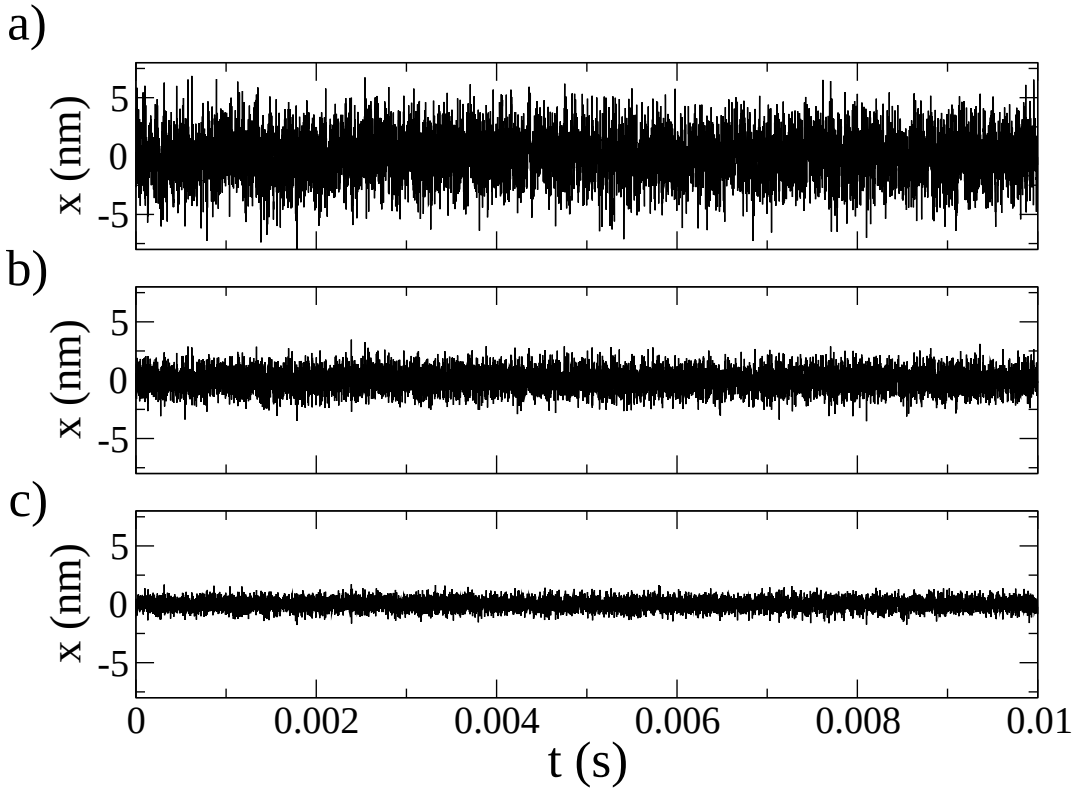

Figure 2.2: **Thermal fluctuations of a nano-particle under an harmonic potential.** Langevin simulations of a brownian particle under an harmonic potential of stiffness k in a one-dimensional space. We perform the simulation with three different k. In a) $k = 1pN/nm$, in b) $k = 5pN/nm$ and in c) $k = 20pN/nm$. If they were experimental trajectories from an optical tweezer or other single molecule technique, we could guess the stiffness of the potential from the standard deviation of the trajectory. From the simulation we can perform the mean and standard deviation computation obtaining $\sigma_x^a = 2.040; \sigma_x^b = 0.920; \sigma_x^c = 0.478nm$, where the upper-case index accounts for the three different realizations. Knowing that $\sigma_x \simeq \sqrt{\frac{k_B T}{k}}$ we obtain $k^a = 0.985; k^b = 4.844; k^c = 17.944pN/nm$ which are in a reasonable good agreement with the real values.

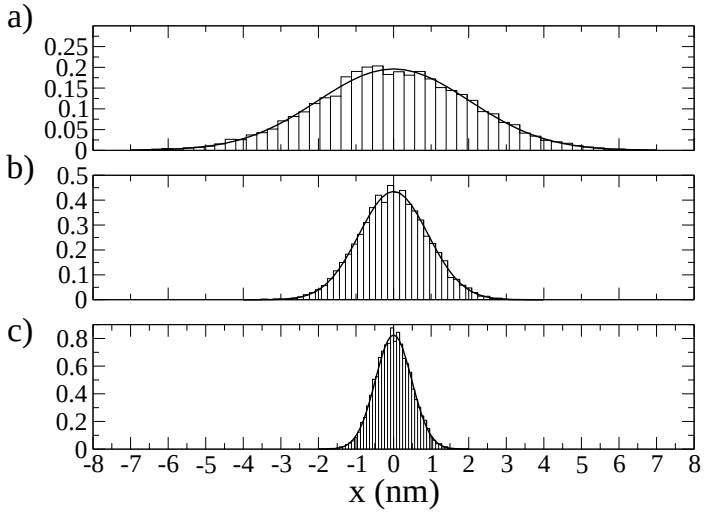

Figure 2.3: **Distribution of the thermal fluctuations under an harmonic potential** On the three figures we show normalized histograms of the realizations shown in 2.2. As we can see, the distribution is clearly gaussian with zero mean and $\sigma = 2.028; 0.914; 0.483nm$ for a), b) and c), respectively.

conservative force applied to the motor: friction. The dissipated heat Q is the work performed by the drag force $-\lambda\dot{x}$,

$$Q = \int_0^L \lambda\dot{x}dx. \tag{2.18}$$

It is defined positive because it is the heat produced from the motor. But the force produced by the motor cannot come from nowhere. Thus there is the need for an external force f_{ext} which produces a useful work W. Then, the first law of thermodynamics states for the energy generated by the motor E,

$$E = W + Q, \tag{2.19}$$

where Q is the heat release. The efficiency η can be defined as

$$\eta = \frac{W}{E} = \frac{W}{W + Q}, \tag{2.20}$$

where

$$W = -\int_0^L f_{ext} dx \qquad E = \int_0^L f_m dx. \tag{2.21}$$

In general, it is clear that $\eta < 1$ as $Q > 0$. In an overdamped system, the limit $\eta \to 1$ can only be reached when $\dot{x} \to 0$. The energy conservation in (2.19) can be reformulated in terms of a dynamical equation,

$$\lambda \dot{x} = f_m + f_{ext} \tag{2.22}$$

where f_{ext} must be ≤ 0. Otherwise it would be an assisting force. It is interesting to consider the case where both f_m and f_{ext} are constants because the heat is simply $Q = \lambda v L$ and we can write

$$\eta = \frac{-f_{ext} L}{-f_{ext} L + \lambda v L} = \frac{-f_{ext}}{-fext + \lambda v} = \frac{1}{1 - \frac{\lambda v}{f_{ext}}}. \tag{2.23}$$

Now, using the dynamical equation, we know that

$$\dot{x} \equiv v = \frac{1}{\lambda}(f_m + f_{ext}), \tag{2.24}$$

so then

$$\eta = \frac{-f_{ext}}{f_m}. \tag{2.25}$$

It is clear that η goes to zero if f_{ext} is null. It is also evident that $\eta \to 1$ if $f_{ext}/f_m \to -1$ or in other words, $f_{ext} + f_m \to 0$. This means that if we pull the motor with exactly the same force as the motive force but opposing to the motion, then we reach the maximum efficiency... even if there is no motion! The reason is clear, because if there is no motion there is no dissipation and consequently there are no heat losses.

At this point we have not discussed the role of the thermal noise in these expressions yet. Thermal fluctuations can be considered, from the point of view of the motor, as an external force. Sometimes this force can be opposing and sometimes assisting, with the condition that the probability of these two cases has to be equal. As the thermal noise is essentially the thermal bath, we include its work

as interchange of heat with the bath, so the definition of the heat is modified as

$$Q = \int_0^L [\lambda v - \xi(t)]dx. \tag{2.26}$$

Another interesting quantity to analyze in overdamped motors is the power P, defined as the negative time derivative of useful work,

$$P \equiv \frac{-dW}{dt}. \tag{2.27}$$

As the motor is moving with an average velocity v, we can write

$$P = -f_{ext}\frac{dx}{dt} = -f_{ext}v. \tag{2.28}$$

This is in fact a definition for the average power, but it is still a useful quantity as it can provide a characteristic power curve P vs f_{ext}. The external force is increased and the response is a decay in the velocity, so we will encounter an external force that produces a maximum power in the motor. But before going into a quantitative expression we need a force-velocity relation for a motor. As it is too soon in this thesis to write a proper and accurate expression, we can take from (2.24) that the velocity can be written as

$$v = v_{max}\frac{f_m + f_{ext}}{f_m}, \tag{2.29}$$

with $v_{max} = \frac{f_m}{\lambda}$.

We can check that at $f_{ext} = 0$ the motor moves at its maximum velocity. On the other limit, when $f_{ext} + f_m = 0$, the velocity vanishes, see Fig. 2.4. This specific value of f_{ext} is usually called the *stall force*. However, in this thesis we will call it the *mechanical* stall force, as we will show that there are other, not directly mechanical ways to stall the motor. Equation (2.29) is a linear relation that even if it's not the most accurate, it is still useful for many levels of description. We will go back to this topic many times, as the force-velocity curve is one of the most crucial characterizations of a motor. Substituting (2.29) into (2.28) we obtain the power output,

$$P = -f_{ext}v_{max}\frac{f_m + f_{ext}}{f_m} \tag{2.30}$$

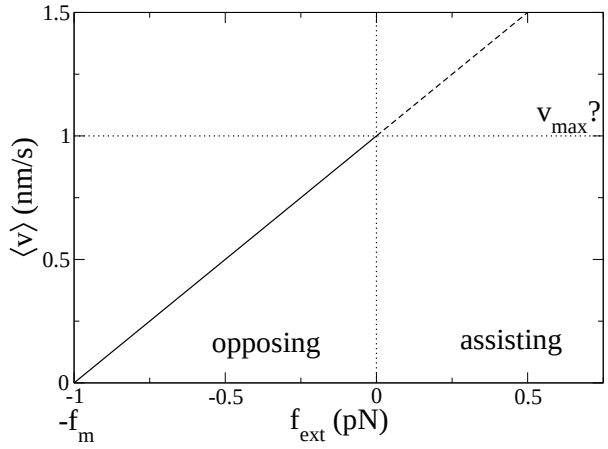

Figure 2.4: **Linear approximation of a force-velocity curve.** Plot of the relation (2.29) with $f_m = 1pN$ and $v_{max} = 1nm/s$. We can distinguish two regions: the region of positive f_{ext} where the force is assisting the motion and the region of negative f_{ext} where the load is extracting useful work from the motor. The concept of v_{max} here is the velocity at $f_{ext} = 0$, because at assisting loads the velocity can increase in some cases and then the parameter does not reflect the real maximum velocity.

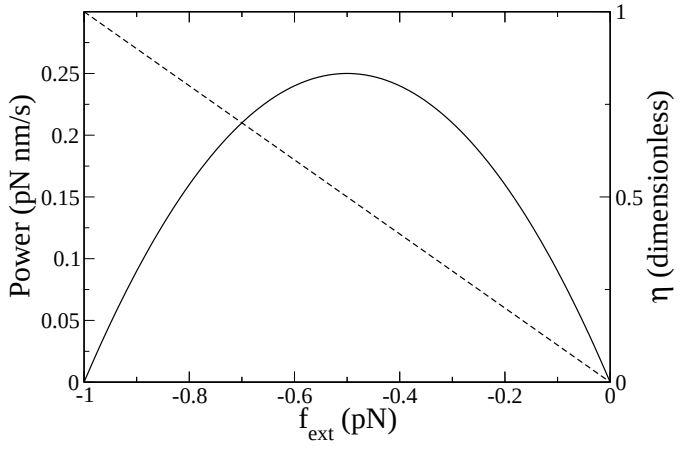

Figure 2.5: **Power and efficiency as a function of f_{ext}.** We show, only for opposing forces, the power (solid line) and the efficiency (dashed line). We can see the parabolic behavior of P with its maximum at $f_{ext} = -f_m/2$. The efficiency increases linearly as the modulus of the external force grows.

which can be arranged as

$$P = -f_{ext}^2 \frac{v_{max}}{f_m} - f_{ext} v_{max}. \tag{2.31}$$

As the second derivative $d^2P/df_{ext}^2 0$ is negative and constant, we can notice that the parabolic power reaches a maximum at $f_{max} = -f_m/2$, see Fig.2.5.

3

A first mechanical model

Now it is time to start modelling some general aspects of a motor protein. We start with kinesin-1, which was measured with optical traps in [9] with enough accuracy to clearly observe individual steps as well as to obtain curves for the mean velocity as a function of the two main control variables: the ATP concentration, [ATP], and the external force f_{ext}. It was not the first time that these magnitudes were measured, but completeness of the data and its precision promoted the appearing of the first theoretical and quantitative models. The analysis we will present now is mainly inspired by a previous work of M. Bier [32]. The main goal of the section is to give an introductory survey on the mechanical aspects of kinesin and its relation with the chemical ATP hydrolysis that is tightly coupled with the mechanical cycle. It also provides a framework from which next models can be an improvement.

3.1 The simplest model

The most remarkable thing that several experimental groups [3, 33, 34] observed in their optical tweezers experiments was that kinesin performs discrete steps. Four years later, the group of S. M. Block observed that such steps were coupled with the process of ATP hydrolysis [35]. Today we now that every kinesin performs a $\sim 8nm$ step per ATP hydrolysis. That is, the mechanics is directly, tightly coupled with chemistry. With this simple but crucial experimental fact we

can relate the rate of ATP hydrolysis, r_{ATP} with the mean velocity of the motor $\langle v \rangle$ by simply multiplying the distance covered by the motor every step,

$$\langle v \rangle = L r_{ATP}, \tag{3.1}$$

where for kinesin, $L \simeq 8nm$. Under this strong coupling, we only need a chemical model for the rate of catalysis of the nucleotide and then the mechanics is straightforwardly obtained. And even though this simple assumption is not generally accurate, the amount of useful information that can provide is remarkable.

Let's consider, as in the experiments, that at constant load conditions, the motor mean velocity is constant. This would mean that the rate of ATP hydrolysis is constant as well. We call ΔG_{ATP} to the energy provided by a single nucleotide (we suppose for now that all the energy is used). As this energy is spent after a L forward step, we can write

$$\Delta G_{ATP} = \int_0^L f_m(x) dx, \tag{3.2}$$

where we recall that f_m is the motive force of the motor. The simplest assumption that can be made is that f_m is constant during the step. Then we can write

$$f_m(x) = f_m = \frac{-dV(x)}{dx} \tag{3.3}$$

and then

$$V(x) = -f_m x = \frac{-\Delta G_{ATP}}{L} x, \tag{3.4}$$

where $V(x)$ is the tilted potential associated to the motive force. This potential must satisfy the condition

$$\Delta G_{ATP} = V(x = 0) - V(x = L). \tag{3.5}$$

Now we can write the corresponding Langevin equation for this oversimplified model of a kinesin motor,

$$\lambda \dot{x} = \frac{-dV(x)}{dx} + \xi(t) = f_m + f_{ext} + \xi(t), \tag{3.6}$$

where λ is the drag coefficient and $\xi(t)$ the thermal gaussian-white noise as usual. The reduction to a 1-dimensional model is justified experimentally, because kinesin walks along microtubules parallel to the protofilament's axis direction [6]. Moreover, we can calculate the mean square displacement in order to obtain information about the fluctuations. We define the randomness parameter r (dimensionless) as

$$r \equiv \lim_{t\to\infty} \frac{\langle \Delta x(t)^2 \rangle}{L\langle x(t) \rangle} \tag{3.7}$$

where L is the step size of the motor. $\langle x \rangle$ is the average position for N different motor runs, $\langle x \rangle = \frac{1}{N}\sum_i x_i$. On the other hand,

$$\langle \Delta x(t)^2 \rangle = \langle (x(t) - x(0))^2 \rangle - \langle x(t) \rangle^2. \tag{3.8}$$

In order to calculate this quantity from the different realizations or trajectories we sum

$$\langle \Delta x(t)^2 \rangle = \frac{1}{N}\sum_i (x_i(t) - x_i(0))^2 - (\frac{1}{N}\sum_i x_i(t))^2. \tag{3.9}$$

The mean value $\langle x(t) \rangle$ is easily obtained by integrating the Langevin equation,

$$x(t) = x(0) + \frac{f_m + f_{ext}}{\lambda} t + \int_0^t \xi(\tau) d\tau, \tag{3.10}$$

where we set now $x(0) = 0$. Averaging, we obtain

$$\langle x(t) \rangle = \frac{f_m + f_{ext}}{\lambda} t \Rightarrow \langle v \rangle = \frac{f_m + f_{ext}}{\lambda}, \tag{3.11}$$

where $\langle \int_0^t \xi(\tau) d\tau \rangle = \int_0^t \langle \xi(\tau) \rangle d\tau = 0$, see Fig.3.1. Now we can calculate the mean square displacement by performing $x(t)x(t')$. Averaging and subtracting $\langle x(t) \rangle^2$ we obtain that

$$\langle x(t)^2 \rangle - \langle x(t) \rangle^2 = \frac{2k_B T}{\lambda} t. \tag{3.12}$$

Then, substituting (3.11) and (3.12) into (3.7) we can write for the randomness

$$r = \frac{2k_B T}{L(f_m + f_{ext})}. \tag{3.13}$$

We can notice that the randomness parameter does not depend on the drag coefficient, which makes this parameter very useful as the friction coefficient is

not easy to obtain from experiments. Note also that r diverges (see Fig.3.1) as $f_{ext} + f_m \to 0$, which is a theoretical prediction that is reasonably confirmed by experiments [9, 36], although near the stall force value measurements are highly subjected to statistical errors and whether the randomness diverges or not at this point is not very clear yet.

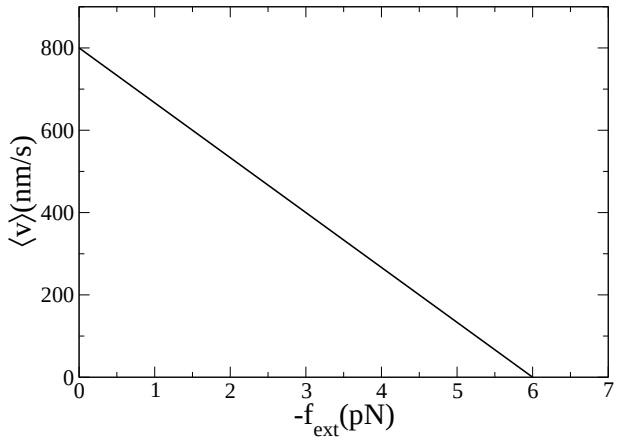

Figure 3.1: Mean velocity versus the external force. As the motion is continuous, the decay of the velocity with the force is linear.

The efficiency η can be computed by assuming that for each L increment along x we spend an energy ΔG_{ATP}. Then

$$\eta = \frac{-f_{ext} L}{\Delta G_{ATP}}. \tag{3.14}$$

This efficiency is maximum at stalling conditions, but not because at these conditions the motor is doing the most useful job but because the dissipation is minimized. Again such an efficiency does not provide an intuitive description of how effective the motor is acting. In order to improve this concept we can think of the efficiency after some steps instead on focusing on a single step. To achieve this we have to introduce a new and crucial quantity: the coupling ratio c, which is the ratio of the useful events (steps) respect to the total number of consumed ATP molecules. From [35] we know that a kinesin has a coupling ratio equal to unity, at least far from the stall force values. However, other motors may have

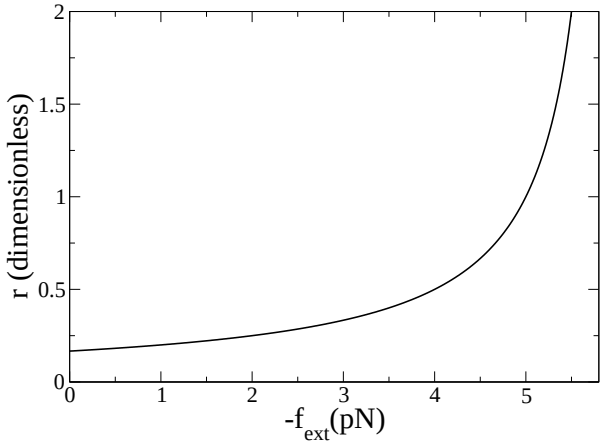

Figure 3.2: Randomness versus the external force. At low loads the randomness is within a reasonably constant regime, while it diverges near the stall force. Experiments show, in contrast with this figure, that the stable value of the randomness at low loads and high [ATP] is approximately 0.5.

other type of coupling ratio values and it is worth introducing this concept into the efficiency. If, after N ATP molecules are hydrolyzed, only a fraction of this, cN is converted into steps, the efficiency becomes

$$\eta_g = \frac{-Lf_{ext}cN}{N\Delta G_{ATP}} = \frac{-cLf_{ext}}{\Delta G_{ATP}}. \tag{3.15}$$

We can see how the global perception of the efficiency becomes more intuitive as it is now multiplied by the coupling ratio. The question now is: what's the value of c and what are their dependencies? The answer is that it depends very much on the specific properties of each model. In this simple model we are introducing the coupling ratio is intrinsically equal to one as the energy consumption is tightly coupled to motion through the linear potential. However, we can add this concept by hand with simple and reasonable assumptions. We can accept that the coupling ratio is equal to one when there is no external load, $c \to 1$ when $f_{ext} \to 0$. On the other hand, near to the stall force value, even if the motor does not move, it can still *trying* to perform steps and wasting ATP. Then we can suppose that $c \to 0$

as $f_{ext} \to -f_m$. We then obtain

$$c(f_{ext}) = 1 + \frac{f_{ext}}{f_m}. \tag{3.16}$$

With this oversimplified version of the load dependence of the coupling ratio, which has no other purpose that introducing the concept at first order, we can write for the global efficiency

$$\eta_g = (1 + \frac{f_{ext}}{f_m})\frac{Lf_{ext}}{\Delta G_{ATP}}. \tag{3.17}$$

Now the efficiency has a parabolic shape similar to the corresponding for the power (see Fig.3.3) and it also reaches a maximum at $-fm/2$, and not the linear dependence of Figure 2.5, see Fig.3.1.

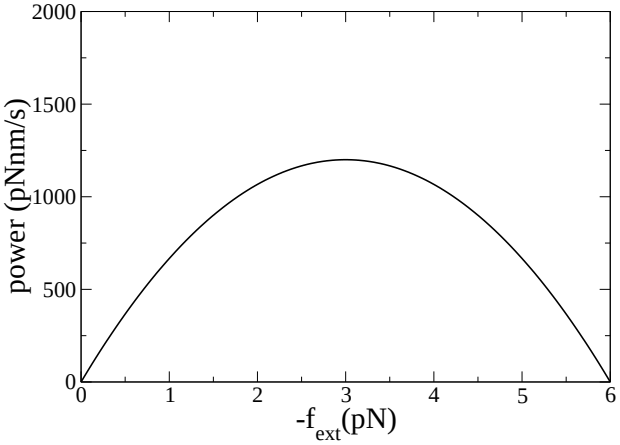

Figure 3.3: Power output versus the external force. The parabolic shape reminds the power-force curves of mesoscopic motors.

Now there is another useful concept that we can introduce with this oversimplified version of the tilted potential model. We know that the drag force for a $0.5\mu m$-radius silica bead in water is about $\lambda \simeq 10^{-6} pNs/nm$. However, we can recall that the maximum velocity of kinesin-1 is about $800nm/s$ [9]. Using our model we know that

$$\langle v \rangle = \frac{f_m + f_{ext}}{\lambda}, \tag{3.18}$$

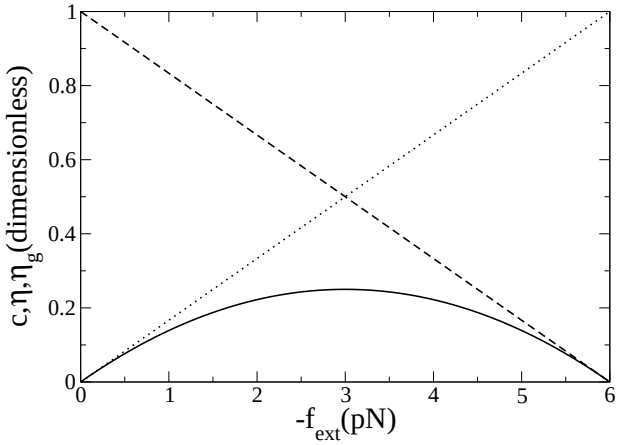

Figure 3.4: Dotted line shows the efficiency as defined in (3.15). It is maximum when the motor does not move and the dissipation rate is null. The dashed line represents a simple version of the coupling ratio which decays linearly with the load. This ratio allows the plot, in solid line, of the global efficiency of eq.(3.17). This redefinition of the efficiency is more intuitive and accounts not only for dissipation but also for ATP wasting.

so then, supposing that $\langle v \rangle_{max}$ is acquired when $f_{ext} = 0$, we can write

$$\langle v \rangle_{max} = \frac{f_m}{\lambda}. \tag{3.19}$$

Using $\langle v \rangle_{max} \simeq 800nm/s$ and $f_m \simeq= 6pN$, we obtain that $\lambda_{eff} \simeq 7.5 \cdot 10^{-3} pNs/nm$, which is a value 7500 times bigger than the expected for the drag coefficient in water. How can we explain such a discrepancy? First of all, let's recall the *effective* drag

$$\lambda_{eff} \equiv \frac{f_m}{\langle v \rangle_{max}}, \tag{3.20}$$

from in eq(3.19). This effective value is consistent with a brownian particle which is undergoing thermal fluctuations and is subjected to the potential $V(x) = -f_m x$. In such a picture, the motion of the motor-particle is *smooth*, as long as thermal fluctuations can be considered smooth. In other words, if we look at the trajectory $x - t$ of the particle we would see a straight line with slope f_m/λ when there is no load. In this context, the motor moves *continuously* along its track with a constant velocity and constant motive force. Under this simplified picture,

the effective friction appears to be extremely larger than what is expected from Stokes friction coefficient. The explanation of this effect comes when one tries to zoom in into a motor trajectory and realizes that the motion of the motor is not smooth at all, but it has a step-like form, like a staircase, see Fig.3.5. The motor *steps and rests*. During some time, it produces a motive force and advances a distance L, but then it stops during a certain *dwell* or *waiting* time until the next step is produced. Such behaviour may seem weird at first sight, but since it was measured experimentally [3] the frequency at which staircase trajectories appear, not only at the molecular motors field but at many others, is astonishing. The appearing of what we will call steps from now on establishes the limitation of this very simple model and motivates the introduction of more sophistication.

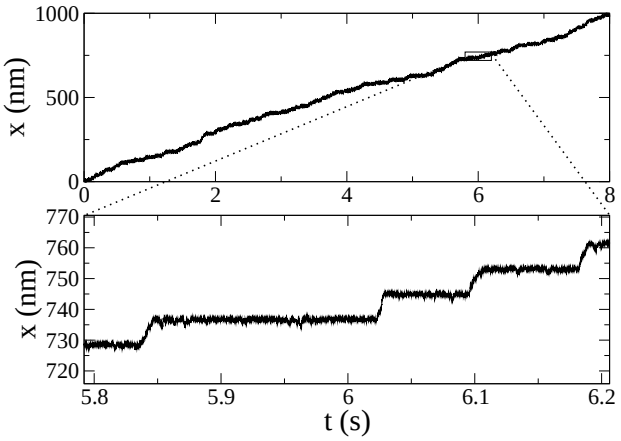

Figure 3.5: Simulated trajectory of the model with the values used in [37]. In the upper figure we can see a longer range of distance and notice that the stepping appearance is hardly visible. In the lower figure there is an magnification where the steps are clearly visible. The upper figure suggests that a high friction model with no steps can predict the mean velocity properties, which is the virtue and the defect of this model.

3.2 [ATP] and load dependent barriers: a stepping model

A first model introducing steps that are coupled with the energy consumption [32] was based on a tilted potential like the one introduced in the previous sections but with a peculiarity: the potential contained periodically flat zones with no potential gradient. This was added with the intention of modeling the dwell times where the motor is not advancing but waiting for the next step. The simulated brownian particle simply falls slope down and then diffuses until the next slope zone is found. With this potential, the resulting trajectories are already step-like as in the experimental results. It is quite simple to estimate the resulting mean velocity of the model. We know that each cycle has a length L, and α is the fraction of this length that is occupied by the flat zone. Then, the motor falls down along $(1-\alpha)L$ and diffuses along a segment of length αL. The falling time is

$$t_1 = (1-\alpha)L/b \tag{3.21}$$

where b is the slope in absolute value.
On the other hand, the time to explore the whole flat segment is [32]

$$t_2 \sim \frac{\lambda\alpha^2 L^2}{2k_B T}, \tag{3.22}$$

where Einstein's fluctuation-dissipation relation has been used. The total length L divided by total time of the cycle gives the mean velocity,

$$\langle v\rangle = \frac{L}{t_1+t_2} = \frac{1}{\frac{(1-\alpha)}{b} + \frac{\lambda\alpha^2 L}{2k_B T}}. \tag{3.23}$$

We can interpret now the slope b to be equal to f_m/λ, and then

$$\langle v\rangle = \frac{1/\lambda}{\frac{(1-\alpha)}{f_m} + \frac{\alpha^2 L}{2k_B T}}. \tag{3.24}$$

This model is quite appealing as it is able to describe the stepping phenomenology without entering into mathematical complications. However, it is not enough. The first and main objection against the model comes from the

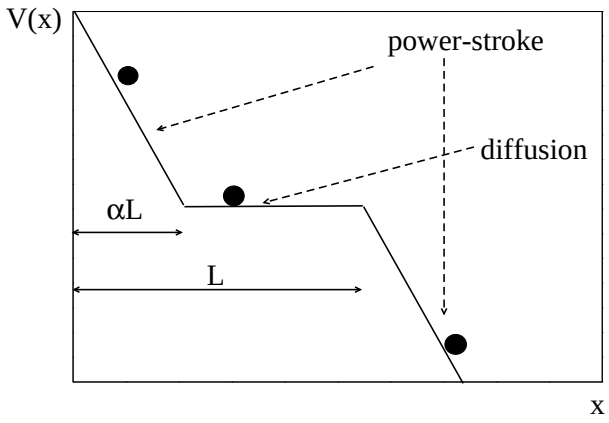

Figure 3.6: Scheme of the potential used in [32]. There are power stroke regions followed by free diffusing plateaus, which modulate the dwell times.

following calculation. From Eq.(3.24) we can substitute realistic values in the zero-load case and expect to obtain a velocity of around $800nm/s$. This has to be accomplished within the boundaries for the α parameter: $\alpha \in [0, 1]$. When doing this, we see that there is no solution for α from which the global time can be $0.01s$, which is the value for $\langle v \rangle = 800nm/s$ and $L = 8nm$. In fact, one obtains $\alpha \sim 35.5$, which indicates that in the model there is a need for more obstacles than a simple plateau to diffuse along.

This is the main reason to introduce a *potential barrier* instead of the plateau region. This potential barrier will have an activation energy E_A and we will study how this energy has to depend on the two main-experimental control variables: the external load and the ATP concentration. Now the two pieces of every potential cycle will be distinguished as the activation region (positive slope) and power-stroke region (negative slope, Figure 3.7). The mathematical details are expressed as

$$V(x) = \begin{cases} \frac{E_A}{L(1-\alpha)}x, & 0 < x \leq L(1-\alpha) \\ -\frac{(\Delta G_u + E)}{\alpha L}x + \frac{E_A + (1-\alpha)\Delta G_u}{\alpha}, & L(1-\alpha) < x \leq L, \end{cases} \tag{3.25}$$

where ΔG_u is the used free energy in the ATP hydrolysis. This potential is a

tilted ratchet potential. The reason not to write the whole-available free energy from a single nucleotide is discussed later.

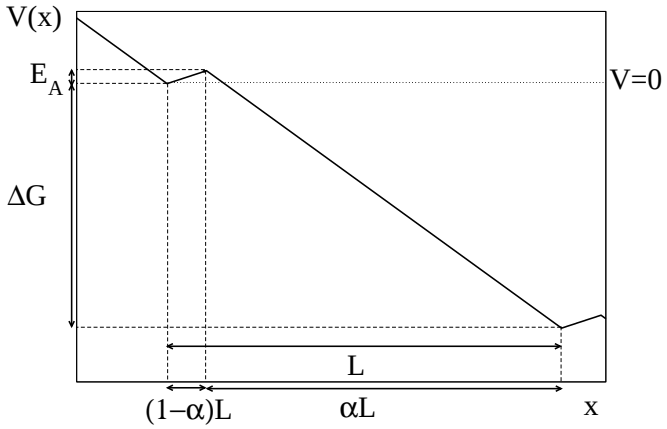

Figure 3.7: Scheme of the potential used in the complete model. The barrier is affected by the two control variables, [ATP] and f_{ext}.

Before entering into more technical details we can perform the same analysis as before in order to see how the total global time of the cycle is splitted into two times, one to cross the barrier and the other to perform the power-stroke. The total time is again $0.01s$ as before, so then

$$0.01s = t_0 e^{E_A/k_B T} + \frac{\lambda \alpha L}{f_m}, \tag{3.26}$$

where we have used a Kramers-like crossing barrier time, which we will discuss right now. What is important in this previous equation is that, even setting the greatest possible value to α, which is the case of $\alpha \to 1$, we obtain that the second term is $\sim 1.3 \cdot 10{-}6s$, which is $\sim 0.1\%$ of the total time. With this simple estimation we can guess that the time to cross the barrier has to be predominant over the power stroke time. In other words, the motor spends most if its time resting, and performs the steps so quickly that the contribution of the step time is not very relevant concerning the mean velocity. This is one of the first strong conclusions of our analysis: the mean velocity of a molecular motor, and in particular kinesin-1, is mainly governed by the dwell times, and not by the time used

to perform the L-displacement.

So then we are interested in the time for a brownian particle to cross an activation barrier. For energy walls which are considerably higher than the thermal energy k_BT, the Kramers approximation states that the crossing time obeys

$$t = t_0 e^{E_A/k_BT}, \tag{3.27}$$

where t_0 is a prefactor which specific dependencies on the drag coefficient and the shape of the potential. However, once t_0 is fixed, the total time is changed only by the height of the potential in an exponential way. This is what we are going to do. We will have an activation energy that will depend on the control variables in a way that a change on these variables will produce a change in the barrier and by extension to the waiting time.

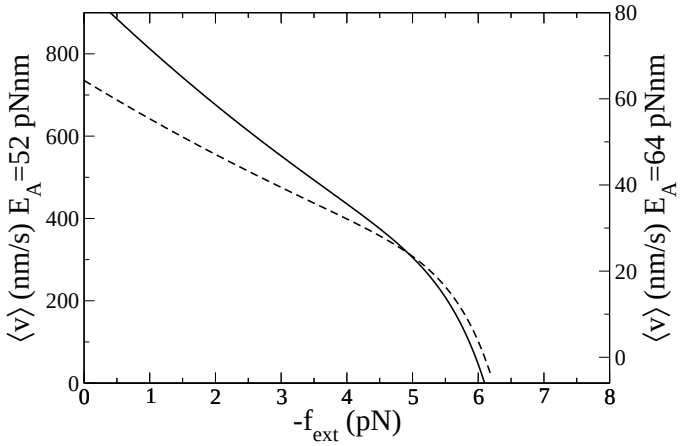

Figure 3.8: Plots of (3.28) for two different values of $E_A = 52, 64$ which approximately emulate the two different [ATP] values of [9], $[ATP] = 2mM$ and $5\mu M$, respectively. The experimental data is not shown explicitly, but it is clear that the agreement is not quantitatively good but qualitatively reasonable.

In the Appendix A1 we see how using Smoluchowski's equation and our poten-

tial we can arrive to an analytical expression for the mean velocity (see Fig.3.8),

$$\langle v \rangle = \frac{(E_A + \Delta G_u + f_{ext}L)^2}{\lambda L k_B T} e^{-\frac{E_A}{k_B T}} (1 - e^{\frac{-(\Delta G_u + f_{ext}L)}{k_B T}}). \tag{3.28}$$

Additionally it is very interesting to perform the ratio of the two velocities v_1 and v_2. We can define r_r as the ratio of the backward/forward rates, and

$$r_r = e^{\frac{-\Delta G_u}{k_B T}}, \tag{3.29}$$

or

$$r_r(f_{ext}) = e^{\frac{-(\Delta G_u + f_{ext}L)}{k_B T}} \tag{3.30}$$

for load-dependent situations.

This is a fundamental property of the kinetic processes where backward transitions occurs with an appreciable frequency, as is the case in molecular motors. Moreover, this result does not depend on the specific shape of the potential as long as the energetic gaps are maintained. The ratio r_r can be used to obtain measurements of free energy differences. If we are able to measure r_r from a model we can directly obtain the free energy associated to the process.

It is worth calculating the randomness parameter r for the value of the mean velocity of eq.(3.28),

$$r = \frac{2(k_B T)^2}{(E_A + \Delta G_u + f_{ext}L)^2} \frac{e^{E_A/k_B T}}{1 - e^{-(\Delta G + f_{ext}L)/k_B T}}. \tag{3.31}$$

We know that for kinesin-1 the randomness at zero load is approximately 0.5, which suggests that the value for E_A is close to $17pNnm$ when $\Delta_G \simeq 50pNnm$. For stalling values of the force the randomness diverges as it was predicted also by the previous approximation.

Even though we have provided algebraic expressions for the mean velocity, there are certainly approximations and not exact results. For faithful quantities of the mean velocity of brownian particles under a periodic potential we can use

the following quadratures, taken from Ref.[38, 39],

$$\langle v\rangle = \frac{Lk_BT}{\lambda}\frac{\left(1-e^{-(\Delta G_u+f_{ext}L)/k_BT}\right)}{\int_0^L dxI_+(x)}, \tag{3.32}$$

$$D = \frac{k_BTL^2}{\lambda}\frac{\int_0^L dxI_+^2(x)I_-(x)}{\left[\int_0^L dxI_+(x)\right]^3}, \tag{3.33}$$

where

$$I_\pm(x) = \pm\frac{\lambda e^{\mp U(x)/k_BT}}{k_BT}\int_x^{x\pm L} dye^{\pm U(y)/k_BT}, \tag{3.34}$$

and

$$U(x) = V(x) - f_{ext}x. \tag{3.35}$$

Before going into a quantitative comparison with experimental data we finish our theoretical description with the influence of the substrate concentration, $[ATP]$ for the case of kinesin-1. Even though the enzymatic kinetics is a topic that belongs essentially to the next chapter in this thesis and there we will analyze with detail the Michaelis-Menten systems, we need to introduce now the Michaelis-Menten equation, written as

$$\langle v\rangle = v_{max}\frac{[ATP]}{k_M+[ATP]}, \tag{3.36}$$

where v_{max} is the velocity when the substrate concentration is very large and k_M, the Michaelis constant, is a quantity inversely related with the affinity of the substrate to the motor, i.e. the greater k_M the lower affinity of ATP for kinesin-1. If we relate this expression with eq.(3.28) we can write

$$v_{max}\frac{[ATP]}{k_M+[ATP]} = \frac{(E_A+\Delta G_u+f_{ext}L)^2}{\lambda Lk_BT}e^{-\frac{E_A}{k_BT}}(1-e^{\frac{-(\Delta G_u+f_{ext}L)}{k_BT}}), \tag{3.37}$$

as plotted in Fig.3.9. The idea is to give an effective value of E_A as a function of the external force and the substrate concentration. However, as this equation does not allow to isolate E_A we cannot write this dependence explicitly.

Parameter	$f_{ext} = 1.05pN$	$f_{ext} = 3.59pN$	$f_{ext} = 5.63pN$
$v_{max}(nm/s)$	813 ± 28	715 ± 19	404 ± 32
$k_M(\mu M)$	88 ± 7	140 ± 6	312 ± 49

Table 3.1: Values of the michaelian parameters obtained in [9].

3.3 Results and discussion

We can simulate a brownian particle travelling through one dimension under the influence of the tilted ratchet potential (3.25). Some trajectories are shown in Fig.3.10.

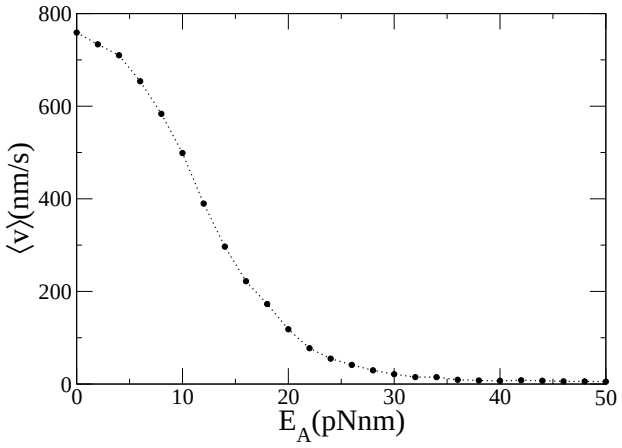

Figure 3.9: Mean velocity as a function of the activation barrier. The values are obtained by simulating the model at the values of the parameters shown in Table 3.2.

For this analysis we focus our attention to the experimental data of Ref.[9]. There are three velocity-[ATP] sets of data (see Fig.3.11), each one for a different load. All these curves fit Michaelis-Menten equation but the two kinetic parameters v_{max} and k_M differ from one case to the other. It may be intuitive that v_{max} decays with the load, but it is more unexpected the fact that k_M grows with the load, which means that at high loading the affinity of the ATP for the kinesin heads is lower than at zero load conditions. The different values for v_{max}, k_M are written in Table 3.1.

We also have two force-velocity curves, one at high $[ATP](= 2mM)$ and

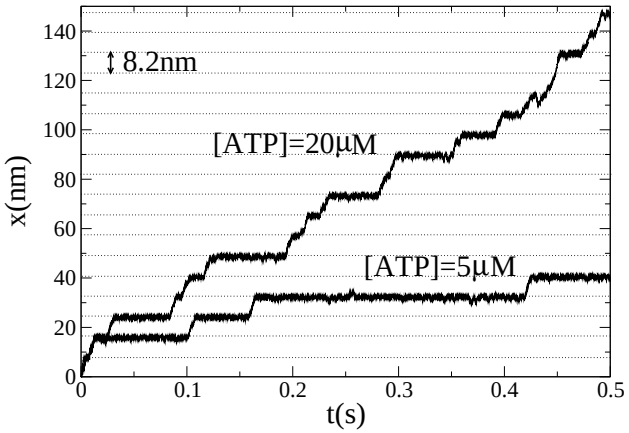

Figure 3.10: Two numerical trajectories at different [ATP] in order to illustrate how the waiting times grow with the nucleotide concentration. Notice as well the size of the steps, which always correspond to $8.2nm$.

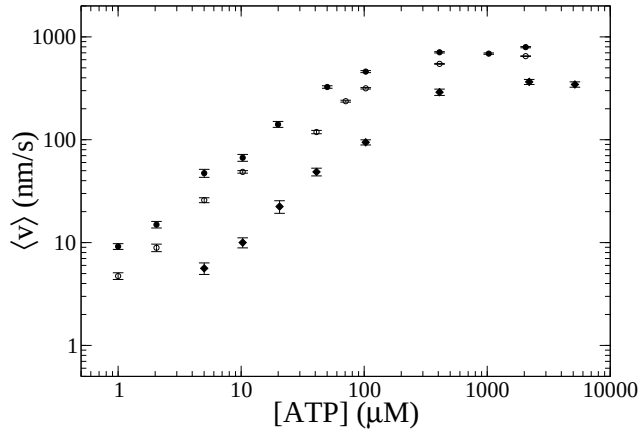

Figure 3.11: Experimental data [9] for the mean velocity as a function of the ATP concentration. There are three curves at different load conditions, $f_{ext} = 1.05$, 3.59 and 5.63 pN for filled circles, open circles and diamonds, respectively. All the three curves fit Michaelis Menten equation with different values for the kinetic parameters, shown in Table 3.1.

the other at low $[ATP](= 5\mu M)$. It can be seen that the maximum velocity is $\sim 800nm/s$, while the maximum or stall force is at an absolute value of $\sim 6.5pN$. There are also measurements of the stall force at different values of [ATP] (see Fig.3.12) showing, with considerable dispersion, that the stall force increases with increasing loads. In any case, if we estimate a mean value of stall force around 6pN, which other and more modern experiments seem to confirm with no [ATP]-dependence [40], we can do the following consideration. If the energy of an ATP molecule is taken as $25k_BT$ [41], then, 6pN of force along 8.2nm implies a total amount of work equal to $12k_BT$, which is about the half of the available energy. We don't have to worry about the energy dissipated by friction, as it does not reach 1pNnm if we consider the step to be performed in $\sim 100\mu s$. For a better estimation of the free energy available in an ATP molecule we have to write

$$\Delta G = \Delta G^0 + k_BT \ln\left(\frac{[ATP]}{[ADP][P_i]}\right), \tag{3.38}$$

where ADP and P_i are the products of the reaction. ΔG^0 is the equilibrium value and at standard conditions is $\simeq 55pNnm$. The product concentrations are $\sim 10nM$ [7], so then

$$\Delta G = (55 + 4.1 \ln[10^4[ATP]])pNnm, \tag{3.39}$$

where $k_BT \simeq 4.1pNnm$ and the [ATP] is measured in μM. For the low [ATP] case, $[ATP] = 5\mu M$, $\Delta G \simeq 100pNnm$, and for the high $[ATP] \simeq 2mM$, $\Delta G \simeq 120pNnm$. These two values of the free energy divided by the step size give an interval of $[12, 15]$ pN, which are forces considerably higher than the stall forces of kinesin. Curiosly, experiments show that the stall force is about the half of these values. One possible interpretation of this fact comes from the entropic term of the free energy. Once the ATP molecule has entered into the pocket, the nucleotide is isolated from the rest of the solution and the entropic barriers become strongly reduced. The relative orientation of the ATP with the molecule of water of the hydrolysis is not random anymore but specific to optimize the reactivity. Moreover, inside the pocket, the definition of a temperature may be put into question. As a global effect, the entropic energy is lowered by the enzyme while the enthalpic part is still $50pNnm$. If we only consider this enthalpic contribution we obtain a force of $6pN$ with no $[ATP]$-dependence. This is in good

Parameter	Value
λ	$0.008pNs/nm$
E_0	$1pNnm$
k_M	$1020\mu M$
α	$0.97(dimensionless)$

Table 3.2: Values of the parameters used in [37].

agreement with last experimental data [40], but in the context of this model we simply will take the used free energy

$$\Delta G_u = \frac{1}{2}\Delta G, \tag{3.40}$$

which gives a good approximation and keeps an [ATP]-dependence of the stall force, which at least is consistent with the data of [9].

Once the model is well defined it is time to search for a set of parameters that can be in a reasonable agreement with the experimental data. In order to do this, we first consider the case $f_{ext} = 0$. Then, we make the assumption that in eq.(3.37) both sides have the same prefactor, which means that the prefactor on the right side does not depend on E_A, i.e.

$$\frac{E_A + \Delta G_u}{\lambda L k_B T} \to v_{max}. \tag{3.41}$$

Furthermore, if $\Delta G_u \gg k_B T$,

$$e^{\frac{-(\Delta G_u)}{k_B T}} \to 0, \tag{3.42}$$

so we obtain

$$E_A = E_0 + E([ATP]) = k_B T \ln\left(1 + \frac{k_M}{[ATP]}\right). \tag{3.43}$$

E_0 is the remaining barrier when $[ATP]$ is infinite.

In Table 3.2 we show a set of values of the parameters for which there is a reasonable agreement between the theoretical predictions and the experimental data. We can see how $\lambda \sim 10^{-2}$ pNs/nm is much greater than the corresponding drag coefficient for the bead in water. We already know that this discrepancy is due to the fact that here λ is an effective friction that reduces the overall mean velocity when in fact the velocity is decreased due to long waiting times. The

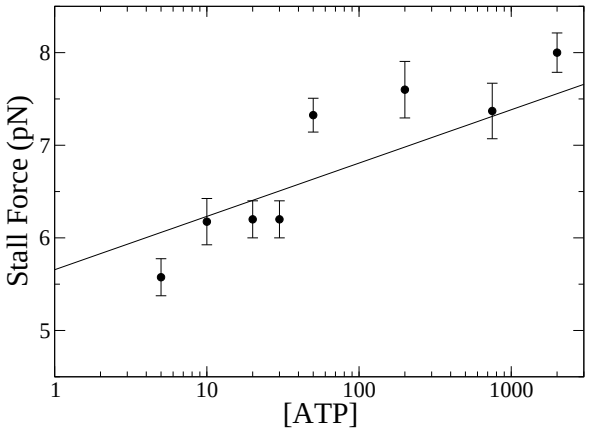

Figure 3.12: Stall force versus ATP concentration. We can see how the stall force increases with [ATP] although a saturation at high concentrations could be interpreted as well. In any case, the error of the data is too big to analyze this magnitude accurately. Solid line is the theoretical plot of (3.39), divided by L.

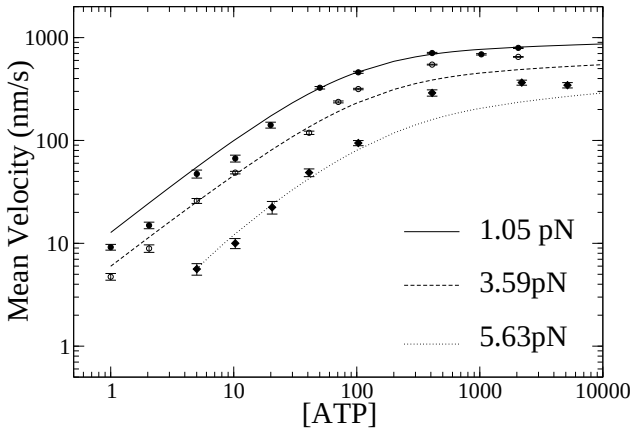

Figure 3.13: Mean velocity versus [ATP] with the same experimental points as in 3.11. Lines are predictions of the model, solid, dashed and dotted for $f_{ext} = 1.05$, 3.59 and 5.63 pN respectively . The agreement is qualitatively good, although not very accurate.

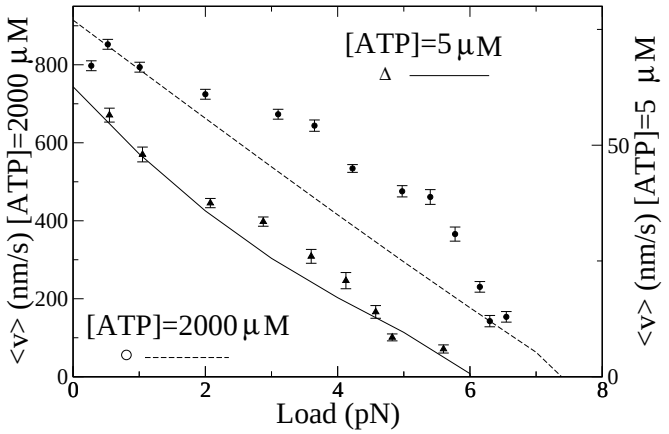

Figure 3.14: Mean velocity versus the external force for two different $[ATP] = 5\mu$M and $2mM$ for solid, dashed (theoretical predictions) and triangles, circles for experimental points, respectively. Again, the agreement is qualitatively appealing, although the curvature at high ATP concentration is lacking in the model prediction.

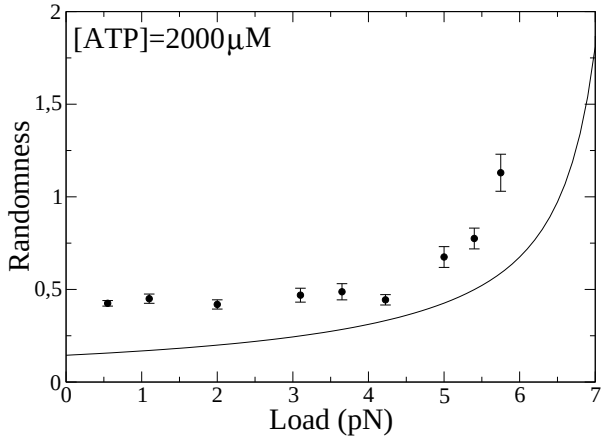

Figure 3.15: Randomness versus load for $[ATP] = 2mM$. We can see how the model (solid line) systematically underestimates the experimental values (points).

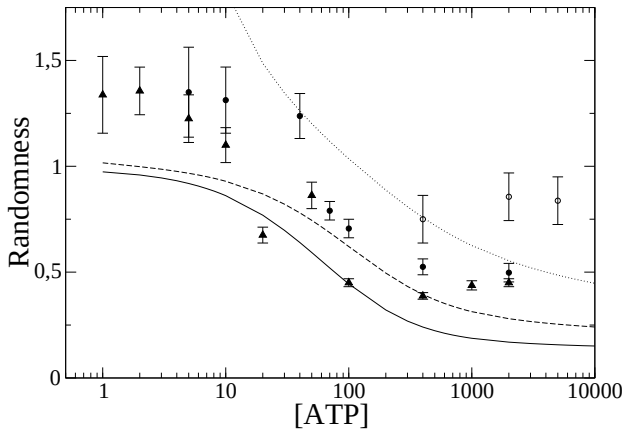

Figure 3.16: Randomness versus $[ATP]$ for the three different values of the load given in 3.13.

other parameters, $E_0 = 1$ pNnm, $k_M = 1020\mu$M and $\alpha = 0.97$ do not need to be realistic as they have a strong effective character. It is interesting to notice that in fact the barrier E_0 becomes useless, as the results do not differ very much if we set $E_0 = 0$. The reason for this is that friction is estimated in such a way that under saturating ATP concentration and under no load, it provides a good agreement with the experimental velocity. In other words, this model consider the ATP saturating and zero load trajectories as straight lines with no stepping, i.e. a continuous motion, and then, we have fixed the correspondent friction to such a non-stopping motion. In the limit of $\alpha \to 1$ and $E_0 \to 0$ we recover the ideal case of a straight single tilted line. This has sense as long as we do not decrease appreciably the [ATP] or increase the external force, as these factors would imply the appearance of an effective barrier. We conclude that, for $[ATP] \to \infty$ and/or $f_{ext} \to 0$, the ideal case is the most practical approach.

In Figure 3.12 we can see the predictions for the stall force as a function of [ATP]. The [ATP]-dependence of this stall force is, as we already mentioned, controversial. First, because the data of the figure [9] has a reasonable variance. But most of all because more recent measurements [40] seem to conclude the opposite, i.e. that the stall force does not depend on the ATP concentration. In

the context of this approach, we have considered a simple assumption: if the stall force depends on the available free energy and this free energy depends on [ATP] concentration (it grows with it), then it is natural, mathematically speaking, to think that the stall force grows with [ATP]. However, in a single kinesin, there is a single ATP molecule, not an ensemble, and the canonical way of calculating the Gibbs energy may not be applicable to a single enzyme. Under our point of view, neither the experiments nor the theory is very clear on the nucleotide-concentration dependence of the stall force and the available energy.

In Figure 3.13 we can see the theoretical predictions for the mean velocity-[ATP] curves once the parameters have been fitted. Although the agreement is reasonably good, one has to admit that separated Michaelis-Menten fits for every curve give better agreement, and we will take advantage of this fact in the next chapter. In Figure 3.14 we can see the predictions and experimental data for the force-velocity curves. It is clear that the agreement is not optimal but qualitatively consistent. The force-velocity curves don't have the proper curvature. Furthermore, in Figure 3.15, where we show the load dependence of the randomness at high [ATP], we can see how the randomness is systematically underestimated. As the proposed value for the friction is considerably higher than the physical drag coefficient derived from Stokes we know we are working in a situation where the physical steps are not performed very quickly. Finally, in Figure 3.16 we can see theoretical predictions for the randomness as a function of ATP concentration. Neither quantitatively nor qualitatively these results agree with experimental data. Clearly, the randomness variable discerns the limits of our model.

The main results of this work are published in Ref.[37]. Even though it is a first approach and there are some assumptions that have to be refined, it is interesting to see how the need for a formalism combining mechanics and chemistry becomes patent. Our approach is essentially mechanical, and we have added chemical information by modulating the activation barrier. Perhaps we should have introduced a load dependence on the barrier as well, because it is experimentally shown that dwell times are strongly affected by the load. In any case, our model represents a significant step forward after the work of M. Bier [32]

and it provides interesting clues for future models. Retrospectively, we could be more severe in our criticism. The experimental data that is used in the model is essentially kinetic, though load-dependent. Thus it is better to begin with a more kinetic-type model and introduce the load afterwards, as it will be seen in next chapter. Mechanical models are very interesting for kinesin, but they are focused on other non kinetic aspects as directionality or the mechanism of the step itself.

4

The inchworm model

In the previous section, the molecular motor itself was coarse-grained as it was considered a point brownian particle under the influence of the potential induced by the motor-track interaction. In this next modelling we will focus on the motor with deeper detail. Specifically, we will model a *conformational change*, which is an internal morphological motion that a motor performs every cycle. The idea is that such a change in its conformation drives the motion of the motor when it is coupled with the track. In the previous tilted-potential model the force produced by the motor was introduced by hand through the potential, but the question of how the motor decides its directionality arises. We know that the tracks are polar structures, but for every track different motors have different directionalities, i.e. some of them move towards one end of the track and others move in the opposite direction. In this next way of modelling we will discuss these aspects in an explicit way.

Another important aspect of the conformational changes in a molecular motor is related with the energetics. As the energy provided by an ATP molecule is finite, not all the conformational changes are allowed but only those that require less energy than ΔG_{ATP}. Controlling and analyzing the energy input and output is one of the main goals of this model. We will also measure through numerical simulations quantities like the coupling ratio.

4.1 Motivation and previous modelling.

The inchworm mechanism was originally introduced in the context of molecular motors in [42]. This way of motion was one of the three classical candidates when speculating about the true mechanism used by processive kinesin-1 walking along the microtubule. In fact, this discussion appears when trying to describe the choreography performed by a dimer walking along a linear track. Apart from the inchworm, the other two mechanisms were symmetric and asymmetric hand-over-hand. While an inchworm motor moves, as its name indicates, as a succession of stretching and contracting movements, in a way that the leading head is always leading and the trailing head is systematically behind. On the other hand, a hand-over-hand motion alternates the role of the two heads of the dimer. At every cycle their roles permutate. The feet of a walking man are considered to move in a hand-over-hand fashion. The distinction between the symmetric and the asymmetric cases comes from a second order detail. A hand-over-hand mechanism implies a rotation around a certain axis. In the case of a walking man, there is a rotation of the hip in every step. We say that the mechanism is asymmetric if every cycle implies a change in the sense of the rotation in a way that the axis of rotation does not accumulate a net angle of rotation. In the symmetric case the rotation is always clockwise or counter-clockwise, and if we would walk in this fashion we'd become easily queasy. It's not common to find examples of symmetric hand-over-hand motion, however. An interesting remark is that both symmetric and asymmetric are not distinguishable when the rotation is around the axis that defines the lateral direction of the motion. In this case a reversal in rotation would imply a reversal in the direction of motion, and that is why the distinction is referred to the rotation around the vertical direction. Graphical details of these mechanisms are sketched in Fig.4.1

For some years the actual mechanism of kinesin-1 was discussed and there seemed to be experimental support for all the possibilities. However, in [7] the true mechanism was found to be the asymmetric hand-over-hand, even though the existence of symmetric events cannot be discarded. Such a discovery may decrease the interest in inchworms mechanisms, but it cannot be discarded to find examples, natural o synthetic, of inchworm-like molecular devices. In further

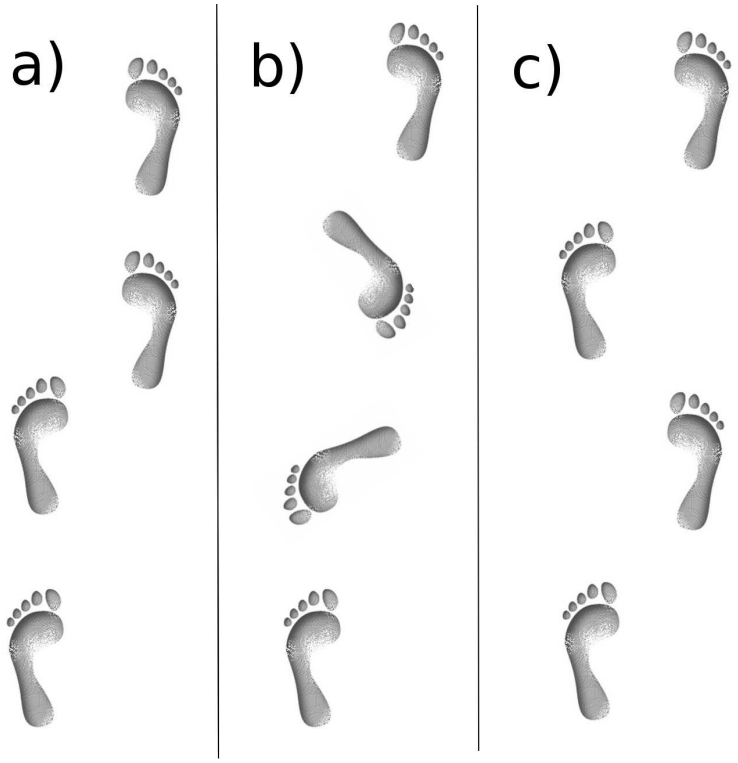

Figure 4.1: The three classical stepping mechanisms proposed for processive conventional kinesins in a footprint scheme. a) The inchworm mechanism consists in a cycle of stretching-contracting regimes. The leading and trailing feet don't exchange their roles. b) In the symmetric hand-over-hand mechanism there is an alternation of the leading and trailing roles, accompanied by a rotation of the whole body. c) The asymmetric hand-over-hand mechanism alternates leading and trailing roles and also alternate the direction of rotation. If one step is clockwise, next is counter-clockwise.

sections we will analyze with deep detail some realistic scenarios for kinesin and inchworm proposals will be ruled out. However, it is still a very interesting mechanism which can help us to understand many features of molecular motors.

In [42] a dimer composed of two brownian particles coupled by an harmonic linear spring was introduced as a modelling of a molecular motor, see Fig. 4.2 The spring represented the internal degree of freedom that allowed to perform conformational changes. It is the extreme reduction of a protein, but still is a powerful tool. This object is not still a motor until we consider the track where it has to move along. This track is simply a ratchet potential with no tilting. Such a track introduces polarity, periodicity and directional motion

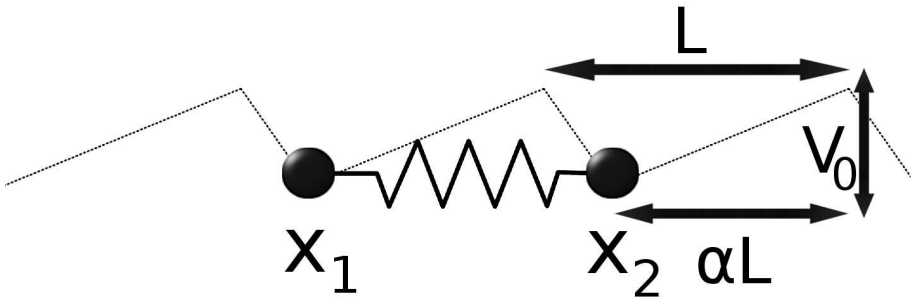

Figure 4.2: A dimer composed of two equal particles connected by a linear spring and subjected to a ratchet potential.

We can define the parameters of the model in the following way, see Figure 4.2. We call k to the stiffness of the spring, l to the equilibrium length of the spring. x_1, x_2 are the positions of the trailing and leading heads, respectively. The track is characterized by a period L, a barrier V_0 and an asymmetry factor α that splits the potential into regions $\alpha L, (1-\alpha)L$ with positive and negative slope, respectively. It is important to distinguish between l, the rest length of the spring, and L, the period of the track.

The dynamics of the model consists on the following: We will suppose that $l = n(t)L$, where $n(t)$ switches from 1 to 2 and viceversa. The mechanism is then quite simple. We have the dimer with the heads resting at consecutive minimums. Suddenly, l switches from L to $2L$. Then, the spring will relax to its new rest state and the dimer will be elongated. As the ratchet potential is asymmetric the response of the to heads will be different. We can distinguish two cases:

Forward motion: If the stiffness of the spring is relatively low, the elastic force in response to the change in l is not very high. In this case, the forces produced by the potential are of the order or higher than the elastic force. This implies that during the elongating relaxation, the head pushing along the softest wall, with slope $V_0/\alpha L$ as α is supposed to be greater than 1/2, can move forward and overcome the barrier more rapidly than the other head, which is under a harder slope, $V_0/(1-\alpha)L$. After some relaxation, the rest state will be the following. The leading head is on the minimum next to the one that occupied before the conformational change. However, the trailing head is exactly at the same location as before. This is the first part of the mechanism, see Fig. 4.3b). Now the second part needs another change in l, which turns back from $2L$ to L. Now the leading head, during the shortening relaxation, cannot overcome the hard slope while the trailing head can move forward very easily and overcome the barrier V_0. Once the relaxation is complete, the whole dimer is displaced exactly a period L, see Fig. 4.3c). There is a coupling between the conformational cycle of the motor with the performance of a single step, as it is the case in many real molecular motors. This aspect is only one of the many appealing features of this model. It provides a simple but very clear idea of how a conformational change which has no polarity preference can be rectified by a polar track in order to produce a step. The whole cycle is shown if Fig. 4.3.

Backward motion: As it shown in Fig. 4.4, we discuss now the case where the stiffness is so high that the elastic forces in response to the changes in the equilibrium length are much higher than the forces induced by the ratchet potential. In this case, when the dimer is elongating, the trailing head overcomes the barrier first, as it is closer, $(1-\alpha)L$ to the minimum than in the case of the leading head, αL. When the first relaxation is completed, is the trailing head the one that has promoted a period while the leading head has stayed, see Fig.4.4b). Then the second transition occurs and it is clear that now the leading head will perform a transition in a way that the whole dimer will be displaced a period in the opposite direction than in the previous case, see Fig. 4.4c). We have seen, then, how the stiffness k is a parameter that can reverse the motion of the motor. This fact, added to the experimental knowledge that conventional kinesin and

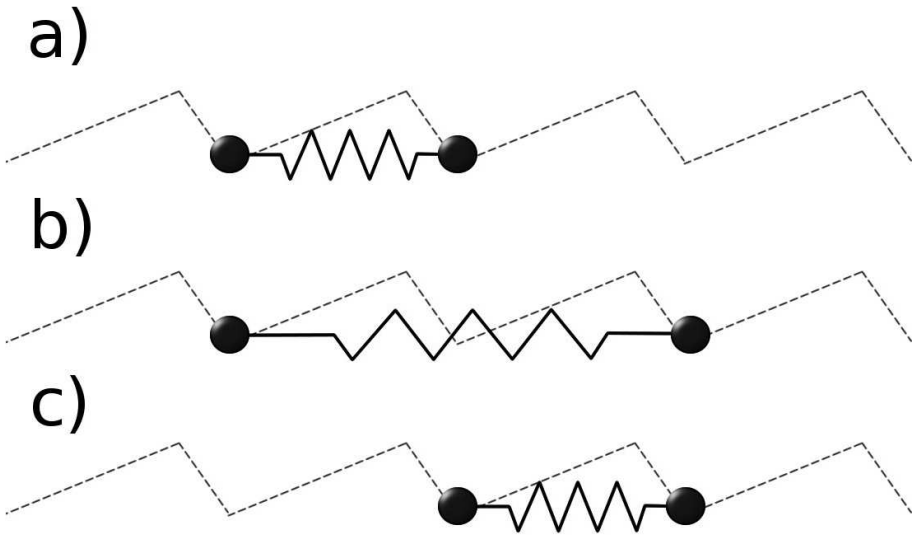

Figure 4.3: The first mechanism (forward motion). The dimer has a low stiffness and the elastic forces are smaller or comparable with the ratchet induced forces. Then , after a dwell time in its rest state (a) there is a stretching stage where the right-head can overcome the barrier before than the left-head, even if this barrier is located further from its initial position (b). At the relaxing stage, the left-head can overcome the barrier and complete a step (c).

ncd move to the plus-end and minus-end of the microtubule, respectively and that they seem to have different properties on their necks give support to the hypothesis that the neck, or the properties of the connecting parts between the two heads, can actually be responsible of the directionality of the motor.

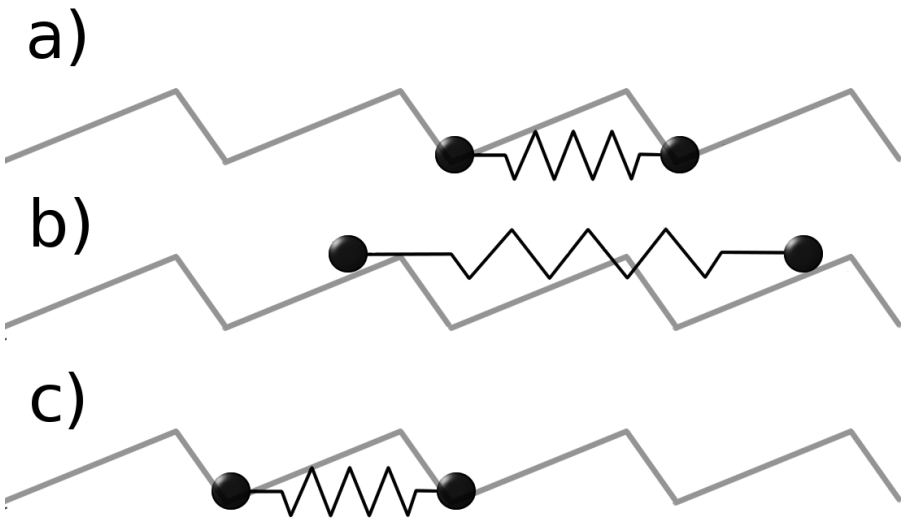

Figure 4.4: The second mechanism. The dimer has a high stiffness and the elastic forces are greater than the ratchet induced forces. Then, after a dwell time in its rest state (a) there is a stretching stage where the left-head can overcome the barrier before than the right-head, because this barrier is located further from its initial position (b). At the relaxing stage, the right-head can overcome the barrier and complete a step (c).

As it surely has been noticed, the proposed mechanism in [42] that we are now reproducing does not need thermal noise in order to work. It is a perfectly newtonian device that contrasts the wide noise-inspired literature in the molecular motors field. In the presence of noise, however, the mechanism can still work with no substantial changes, which makes the system quite robust under fluctuations. However there are some properties that are not so well defined and that can be improved. Here we expose some criticism to the model with the aim to improve it.

One can calculate the energy required to perform the two transitions of the mechanical cycle. After the transition $l : L \to 2L$, there is a contribution of elastic

energy ΔE_{el}

$$\Delta E_{el} = \frac{1}{2} k L^2. \tag{4.1}$$

During the second transition, $l : 2L \rightarrow L$, there is another input of energy of the same value, so then we need a free energy input

$$\Delta G = 2\Delta E_{el} = kL^2. \tag{4.2}$$

In the case of kinesin, $L \simeq 8nm$, so then $\Delta G \simeq 64k$ pNnm. We know that the available free energy of ATP is approximately $100pNnm$, which means that the maximum stiffness we can achieve is $\sim 1.6pN/nm$. In [42] we enter into the backward motion regime when $k \sim 8pN/nm$, but this would imply huge free energy inputs, so we cannot accept this regime at this quantitative level. Nevertheless, the model can be generalized to a compass model where the conformational change is magnified by an arm level, as in Fig. 4.5. We can imagine a compass with arms of length C. By Pythagoras' theorem, the height of the compass H is

$$H = \sqrt{C^2 - (\frac{x_2 - x_1}{2})^2}. \tag{4.3}$$

If we now locate the conformational change at a vertical distance h from the upper vertex of the compass where the spring follows

$$f_{el} = -k(\Delta s - s_0), \tag{4.4}$$

where

$$\Delta s = \frac{h}{H}\Delta x \qquad s_0 = \frac{h}{H} l_0, \tag{4.5}$$

so then it is equivalent to have the spring at any level of the compass than to have it at the level of the track if we redefine the effective stiffness as

$$k_{eff} = \frac{h}{H} k. \tag{4.6}$$

Thus with this lever arm assumption we can perform the whole cycle with a energy input of

$$\Delta G = kL^2(\frac{h}{H})^2. \tag{4.7}$$

In a kinesin-1, we can accept that $H \sim 3nm$ and if we suppose that the elongation

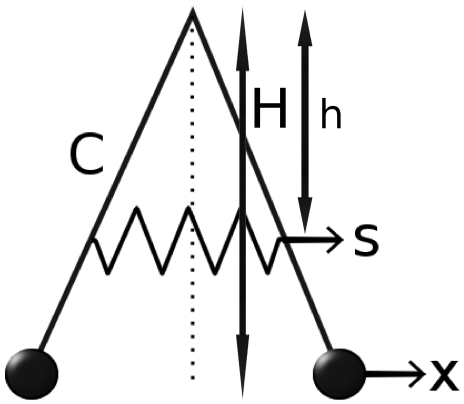

Figure 4.5: Due to lever arm effect, a small stretching on the spring can induce large conformational changes in the dimer. Notice, however, that the energy is applied away from the particles. In the figure, C is the length of the arm, H the vertical distance from the x-axis to the upper vertex that joins the two arms. The axis defined by the spring is written as the s-axis.

occurs at $\sim 1nm$ far from the neck linker, then we obtain

$$\Delta G \sim \frac{k}{9} 64 pN nm, \tag{4.8}$$

which allows to reach regimes until $k \sim 14 pN/nm$. However we have to comment that the heads are usually the enzymes of the motor and the energy is localized on them. The hypothesis of the compass would be in accordance with a motor that concentrates the energy near the point of rotation, as is the case in some myosins which are thought to work with arm lever power-stroke.

Other missing points of the model are the frequency of the energy arrival or the justification of a change in an elastic property. In [42] a constant frequency of conformational changes is used. It is known that the arrival of ATP to the motor is random following Poisson distributed times [7]. Furthermore, when the motor is working on a conformational change, it shouldn't be able to accept a new ATP molecule. Thus the way of introducing the hydrolysis rate should be improved in order to obtain substrate concentrations dependences. On the other hand, it is not clear whether the motor can exhibit spontaneous changes in its elastic properties. Instead of a change in the rest length of the spring it is more

convenient to introduce time dependent motive forces that allow the control of the energy input and to relate it with fuel consumption.

4.2 The improved inchworm model

In order to improve all the aspects commented in the previous section we will introduce the following dynamic scheme: The dimer is, as before, resting with $l = L$. When a fuel molecule is attached to the dimer, a stretching force f_s appears. This stretching force acts to produce an elongation to the spring until $x_2 - x_1 = 2L$. In this situation, where the elongation is $2L$, the stretching force disappears and the spring relaxes by itself until the initial configuration (with elongation L). Fuel binding is not allowed while stretching, but it is not forbidden at the relaxing stage. With this modification we can control the input of energy and then measure quantities like the global efficiency or the coupling ratio. The dynamic scheme is shown in Fig. 4.6,

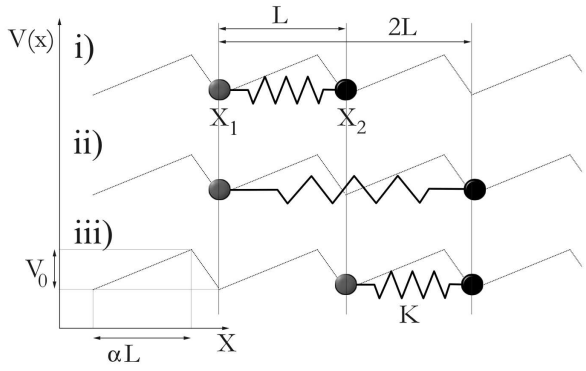

Figure 4.6: Scheme of the improved inchworm model. Two spring coupled particles are subjected to the periodic ratchet potential $V(x)$, which has height V_0, period L and asymmetry factor α. i) The spring is relaxed and each particle matches a potential minimum because the rest length of the spring is equal to the period of the potential. In ii) an stretching force appears in such a way that the leading head x_2 is pulled to the right and the trailing head x_1 is pulled to the left. The force disappears when the elongation doubles the rest length. Then, the spring relaxes and the step is completed with a L displacement, as shown in iii)

and the equations of motion are the following,

$$\lambda \dot{x_1} = -V'(x_1) - k(x_1 - x_2 - L) - f_s(t) - \frac{F}{2} + \xi_1(t), \tag{4.9}$$

$$\lambda \dot{x_2} = -V'(x_2) + k(x_1 - x_2 - L) + f_s(t) - \frac{F}{2} + \xi_2(t). \tag{4.10}$$

The positions x_1, x_2 correspond to the trailing and leading heads, respectively. λ is the drag coefficient, $F = -f_{ext}$ is the external force and $\xi_i(t)$ are the thermal noises.

First of all, we can perform some useful calculations in some limiting cases. When there is no temperature and the asymmetry factor α is equal to 1, we can calculate the time of the mechanical cycle in the two cases (low and high stiffness). The stretching process consists on the raising of the leading head, x_2 along the slope V_0/L and against the elastic force, giving

$$\frac{dx_2}{dt} = \frac{1}{\lambda}(\frac{E - V_0}{L} - kx_2), \tag{4.11}$$

where the stretching force is the energy of a fuel molecule, E, divided by the step size, L. In the limit of $t \to \infty$ gives

$$x_2 = \frac{E - V_0}{kL}. \tag{4.12}$$

This imposes a boundary for the parameters in order to work in a newtonian regime. As x_2 should be greater than L in order to overcome the barrier,

$$E - V_0 > kL^2, \tag{4.13}$$

which implies that $E - V_0$ should be greater than the energy input of the model of Ref.[42].

For the relaxation process, we can write the following equation for the trailing head,

$$\frac{dx_1}{dt} = \frac{1}{\lambda}(k(L - x_1) - \frac{V_0}{L}), \tag{4.14}$$

which at infinite times gives

$$x_1 = L - \frac{V_0}{kL}, \tag{4.15}$$

which imposes another boundary in order to achieve the total relaxation in the newtonian regime,

$$L - \frac{V_0}{kL} > L, \tag{4.16}$$

which is impossible to achieve as $V_0 > 0$. We see that in the total asymmetry limit, $\alpha = 1$, the newtonian regime cannot work as the spring by itself does not have the power to overcome the barrier. We can introduce now similar equations for $\alpha < 1$. Then, the equation for the condition of the leading head becomes,

$$\frac{dx_2}{dt} = \frac{1}{\lambda}(\frac{E - V_0/\alpha}{L} - kx_2), \tag{4.17}$$

which gives, in the steady state,

$$x_2 = \frac{E - V_0/\alpha}{kL}, \tag{4.18}$$

and gives the condition

$$E - \frac{V_0}{\alpha} > \alpha k L^2, \tag{4.19}$$

or, in other words,

$$k < \frac{E - V_0/\alpha}{\alpha L^2}. \tag{4.20}$$

For the trailing head we write

$$\frac{dx_1}{dt} = \frac{1}{\lambda}(k(L - x_1) - \frac{V_0}{\alpha L}), \tag{4.21}$$

which gives

$$x_1 = L - \frac{V_0}{\alpha k L}, \tag{4.22}$$

and imposing $x_1 > \alpha L$,

$$k > \frac{V_0}{\alpha(1-\alpha)L^2}. \tag{4.23}$$

This imposes strong conditions on the parameters. Joining eqs.(4.20) and (4.23) we arrive to

$$\frac{V_0}{\alpha(1-\alpha)L^2} < k < \frac{E - V_0/\alpha}{\alpha L^2}. \tag{4.24}$$

If we want to have a window of real k holding these conditions we must satisfy

$$\frac{V_0}{\alpha(1-\alpha)L^2} < \frac{E - V_0/\alpha}{\alpha L^2}, \tag{4.25}$$

or in other words

$$E > \frac{V_0}{\alpha(1-\alpha)}. \tag{4.26}$$

We can appreciate that this condition is quite restrictive. If $E \simeq 100pNnm$, corresponding to an ATP molecule, then V_0 must be always lower than $16pNnm$ for $\alpha = 0.8$.

The main conclusion of these calculations is that although the newtonian regime can be achieved, it is too restrictive for the values of the parameters. The presence of thermal noise helps to overcome the barriers and then relaxes the previous conditions. In the relaxation stage, the noise is particularly useful because when the spring is not stiff enough to overcome the barrier with its own elastic force, the thermal noise facilitates the transition with high efficiency.

The values of the parameters have been chosen in a nano scale to mimic some molecular motors such the kinesin, even if this model is purely theoretical. This choice is worthy since it allows quantitative comparison with a real motor. The periodicity of the potential L is taken to be the periodicity of microtubules, $8nm$. If we take the asymmetric factor $\alpha = 0.8$ and $V_0 = 50pNnm$ the efficiency of our model is optimized as it is checked numerically. $E = 100pNnm$ corresponds to good approximation of the accepted value for the energy of hydrolysis of an ATP. The thermal energy is $k_BT = 4.1pNnm$, corresponding to the environmental temperature. The stiffness of the motor is chosen $k = 1pN/nm$ in order to have stretching forces that perform works within the available energy. Finally, the drag force $\lambda = 2 \cdot 10^{-4} pNs/nm$. The reason to choose this parameter at the end is simple: we don't have precise information about it and since it defines a timescale in the problem, its value can help to tune the order of magnitude that we wish for the mean velocity. Using these values, and for very high ATP concentrations we obtain in numerical simulations a maximum velocity of $667nm/s$, which is already in the scale of kinesin-1.

4.3 The ATP hydrolysis

The dependence with ATP concentration is introduced in this model as a probability p of catching an ATP molecule. When the motor is free from ATP, $p \in (0, 1)$ is the uniform probability per time step Δt of binding one molecule. When it occurs, more ATP binding is forbidden and stretching takes place until the elongation is $2L$. Then, the stretching force disappears and the spring relaxes. When $x_2 - x_1$ is again L, one cycle is completed and ATP binding is allowed. In the absence of external load, this mechano-chemical cycle induces a L displacement of the motor towards one end of the potential. On the other hand, our approach controls how much energy E_T is applied to the system by simply multiplying E by the number n of ATP consumed: $E_T = nE$. The mean velocity of the motor, when the ATP concentration is saturating and $f_{ext} = 0$, is maximum and dependent only on the intrinsic properties of the motor and by E. Let t_{on} be the time spent to perform a single step, i.e. the stretching plus the relaxing time. Thus, $V_{max} = L/t_{on}$. Using the given values of the parameters, simulations show that $t_{on} \sim 0.012$s, which gives $V_{max} \sim 667$nm/s. However, the global speed $\langle v \rangle$ will be slowed down when the ATP concentration decreases. Typically, the $[ATP]$-dependence on $\langle v \rangle$ is given by the Michaelis-Menten relation [43]. In our model, we have previously defined p as the uniform probability to get an ATP per time step Δt and with $p = 0$ while the motor stretches and relaxes. It can be accepted that, as the reaction frequency is proportional to $[ATP]$, then $[ATP]$ is proportional to p.

Then, we have

$$\langle v \rangle = V_{max} \frac{p}{k_M + p}, \tag{4.27}$$

where k_M is the Michaelis constant for the probability. It is important to remark how p depends on the temporal increment Δt that we use. Specifically, p is the probability binding per time step. If Δt decreases we can achieve a greater rate of ATP binding. In the case of $p = 1$, every Δt a new nucleotide is bound. However, this does not mean that [ATP] is infinite. The time step defines a maximum concentration, which is $[ATP]_{max}$. Then,

$$p = \frac{[ATP]}{[ATP]_{max}}. \tag{4.28}$$

On the other hand we know that

$$k_{binding} = A[ATP], \tag{4.29}$$

where A is a constant of proportionality. If $[ATP] = [ATP]_{max}$, we have

$$k_{binding}^{max} = A[ATP]_{max} = \frac{1}{\Delta t}, \tag{4.30}$$

where it is clear that $1/\Delta t$ is the maximum available rate. We obtain

$$[ATP]_{max} = \frac{1}{A\Delta t} \tag{4.31}$$

and then

$$p = A\Delta t[ATP], \tag{4.32}$$

which is the most useful relation. When we substitute this expression into the Michaelis Menten equation we can have p instead of $[ATP]$, but we have to take into account that the Michaelis constant is not the real constant k_M^{real} that we would measure in an experiment, but

$$k_M^{real} = A\Delta t k_M. \tag{4.33}$$

From now on, we will deal with p and not with $[ATP]$. Fig.4.7 shows how the michaelian behavior fits well the simulated values of the mean velocity. However, for finite values of f_{ext}, both kinetic parameters V_{max} and K_M change. In Ref.[43] it is shown that the effect of the external load in kinesin can be interpreted as an inhibition process, and this is one of the main topics of the second chapter. For now it is enough to write the equations for the f_{ext}-dependence on the two kinetic parameters, and the justification will be clarified and developed in the next chapter. The expressions, which are introduced in (7.8) and (7.9) are

$$V_{max}(f_{ext}) = \frac{V_{max}(f_{ext} = 0)}{1 + \frac{1}{K_{iu}(1 - f_m/f_{ext})}} \tag{4.34}$$

and

$$k_M(f_{ext}) = k_M(f_{ext} = 0)\frac{1 + \frac{1}{K_{ic}(1 - f_m/f_{ext})}}{1 + \frac{1}{K_{iu}(1 - f_m/f_{ext})}}. \tag{4.35}$$

and they allow to express the velocity of the motor as a function of the two control variables p and f_{ext}.

4.4 Results and discussion[1]

There are five parameters to fit, which are $f_m, V_{max}(f_{ext}=0), k_M(f_{ext}=0), K_{ic}$ and K_{iu}. The methodology to obtain their numerical values is the following. First we need at least three $\langle v\rangle - p$ curves as in Fig.4.7 from the numerical simulations of Fig. 4.8 and extract the michaelian parameters of each of them.

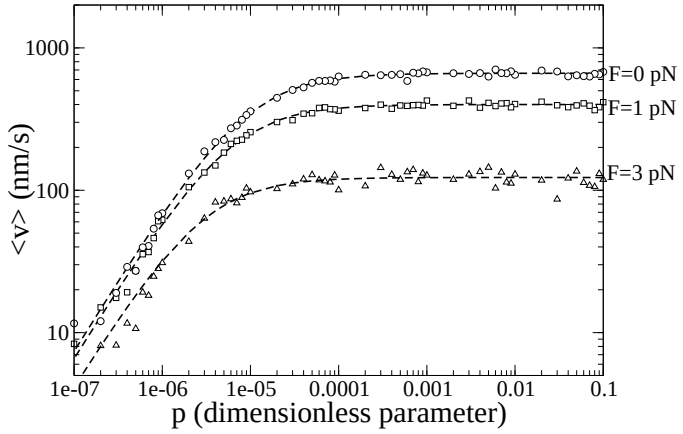

Figure 4.7: Mean velocity versus p for three different values of the load, where $F \equiv -f_{ext}$. The three curves are michaelian and two kinetic parameters are extracted from each of them. Lines are michaelian fits and points are simulation data. Circles, squares and triangles correspond to $f_{ext} = 0, -1, -4pN$, respectively.

Then we obtain three pairs of values for V_{max} and K_M which we show in Table 4.1.

Once we have these parameters we fit the three values for V_{max} following eq.(4.34) as shown in Fig. 4.9. This allows to obtain f_m, $V_{max}(f_{ext}=0)$ and K_{iu}. The next step is to fit eq.(4.35) and to obtain $k_M(f_{ext}=0)$ and K_{ic}.

In our simulations, $f_m \sim 5.25$pN. K_{iu} and K_{ic} are the uncompetitive and competitive inhibition constants, respectively, and are a quantitative measure of

[1]This section uses information derived in Part II

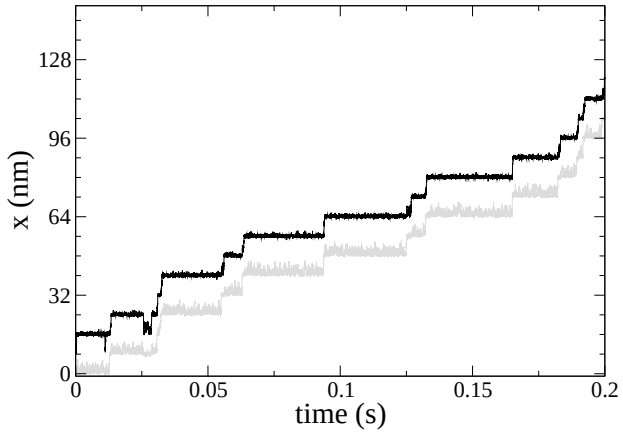

Figure 4.8: Simulated trajectory for the trailing (gray) and the leading (black) head. Note the stepping fashion of the motion.

$f_{ext}(pN)$	-0	-1	-3
$V_{max}(nm/s)$	663.5	400.3	122.9
$k_M/10^6(dimensionless)$	8.88	5.99	2.87

Table 4.1: Values of the michaelian parameters obtained in the simulations (see Fig.4.9).

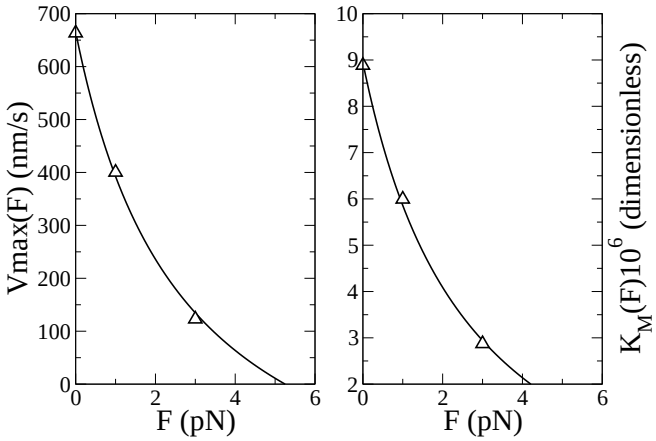

Figure 4.9: Left image: The three points are the values of V_{max} obtained from the fits of fig. 4.7. The curve is the fit of eq.(4.34). Right image: The same procedure for the Michaelis constant k_M. We fit the equation (4.35).

how F affects the motor when it is free from nucleotide (K_{ic}) or when it has an ATP (K_{iu})[2]. From values of Table 4.1 we have fitted the values of the inhibition constants obtaining $K_{iu} \sim 0.338 \cdot 10^{-6}$ and $K_{ic} \sim 2.131 \cdot 10^{-6}$. As they are dissociation constants, the effect of the load on the ATP-bound state is greater than in the ATP-free configuration. This means that the force acts as an uncompetitive mixed inhibitor, while in Ref.[43] it is shown that kinesin is also mixed but competitive. This difference is responsible of the curvature on $\langle v \rangle - f_{ext}$ curves at high ATP concentration. Figure 4.10 shows these curves with the simulation data and the predictions of the analytical expression with an excellent agreement.

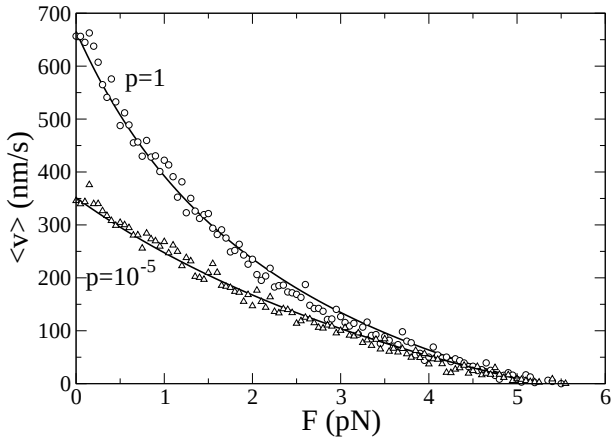

Figure 4.10: Mean velocity-force curves for $p = 1$ (circles) and 10^{-5}(triangles). The solid lines are plots of (4.27) where the load dependence on the kinetic parameters has been already introduced. The agreement is excellent.

It is interesting to use the definitions of efficiency shown in the previous section. The coupling ratio c can be written as

$$c = \frac{x_{CM}}{nL}, \tag{4.36}$$

where x_{CM} is the the position of the center of mass of the dimer,

$$x_{CM} = \frac{1}{2}(x_1 + x_2) \tag{4.37}$$

[2]See next chapter for a better description of the kinetic processes

(we consider both particles of equal mass and drag), and n is the number of consumed ATP's. The global efficiency can be written

$$\eta_G = \frac{W}{nE}, \tag{4.38}$$

where W is the useful work, that can be written also like $W = -f_{ext}x_{CM}$. We can then join the expressions for c and η_G and write

$$\eta = \frac{-cf_{ext}L}{E} \tag{4.39}$$

This means that the global efficiency is simply the efficiency in a single step multiplied by the coupling ratio. We can go further if we consider the fact that V_{max} is proportional to c, and then,

$$c = \frac{1}{1 + \frac{1}{K_{iu}(1-f_m/f_{ext})}} \qquad \eta = \frac{L}{E}\frac{-f_{ext}}{(1 + \frac{f_{ext}}{K_{iu}(f_m - f_{ext})})}. \tag{4.40}$$

Fig.4.11 shows the simulated data for $c(f_{ext})$ and $\eta(f_{ext})$ as well as the theoretical predictions. It is interesting to remark that the maximum efficiency is slightly below 0.15.

We have seen how a very simple theoretical device is able to exhibit a lot of features that are characteristic of a motor, like force-velocity curves or substrate concentration dependence. This model is an improvement of the one presented in [42], as it incorporates a control on the energetics of the process and allows to quantify useful work, efficiency, coupling ratio, etc. Moreover, a generic formalism is introduced to characterize the kinetics of the motor without considering microscopic details. Even though this type of formalism will be developed in the next chapter, we have seen how simple inhibition theory can be straightforwardly applied to molecular motors in order to obtain analytical expressions for the substrate concentration and load dependence of the mean velocity. So, summarizing, the work developed here is a useful example to show how to characterize a molecular motor and how some experimental features can be described by very simple mechanisms.

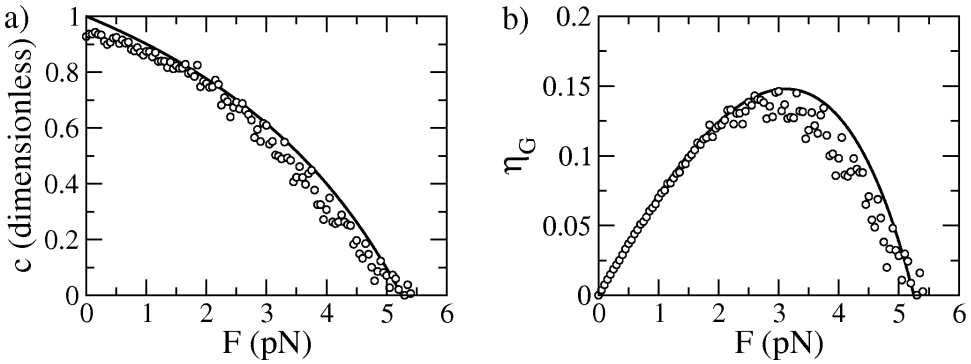

Figure 4.11: a) Coupling ratio versus the load. In the previous section we made a linear hypothesis of this magnitude and here we see that this motor exhibits a non-linear relation. Qualitatively, however, the discrepancy is not dramatic. We see how this coupling quotient decreases with the load. Notice that at zero load is never equal to one. Near the stall force, all the fuel is wasted. b) The global efficiency versus the load exhibits a maximum at $\sim 3pN$, with a value of ~ 0.15. It is interesting to note that both magnitudes suffer more fluctuations at high loads. This corresponds to an increase of the randomness.

5

Rotatory ratchet nano-devices

5.1 Generalities

Rotatory machines can also be studied under a mechanical way of modelling. Even if the true nature of these motors seem to be electrostatic, elastic deformations of the rotor can be used in order to emulate directed motion. The philosophy is exactly the same as in the previous linear inchworm model. Here we also have inchworm mechanism but in a closed-circular structure that is under the effect of a periodic ratchet potential. As we will point it out right now, there are some similarities and differences with respect to the linear case.

First, as we have already mentioned, the rotatory devices we are going to introduce are inchworm systems, i.e. a set of nano-particles coupled with nearest neighbours by linear springs. Whenever some energy is available it is transformed into a stretching work between two consecutive particles. This stretching elongates the spring until a value equal to the double of the equilibrium angular length of the spring. After this, the power stroke disappears and the system relaxes again. In such a cycle, the whole system advances, or rotates, one period of the potential, even if several times this process is in vain and the energy is wasted.

Even though these rotatory machines are also nano-devices, they are not diffusing on the cytoplasm but embedded into a membrane. Specifically, is the stator

what is embedded in the membrane, so the rotation can be done under a drag of the membrane with the stator and another drag of the stator with rotor or simply a drag of the rotor with the membrane, depending on how the stator surrounds the rotor. The viscosity of this membrane can be considered approximately a thousand times greater than the one for the cytoplasm (considered similar to the water). We need, however, a value for the drag force of each rotor-particle. Let r be the radius of the particles and R the radius of the rotor. If $\gamma_t = 6\pi\eta r$ is the translational drag coefficient and γ_r the rotational one, we can write

$$\gamma_t \frac{dl}{dt} = f_S, \tag{5.1}$$

where dl is the longitudinal displacement after a rotation $d\theta = dl/R$ and f_S is the stretching force, which is applied tangentially. We can also write

$$\gamma_r \frac{d\theta}{dt} = \tau_S, \tag{5.2}$$

where $\tau_S = Rf_S$ is the stretching torque. Changing l by θ in (5.1) and doing some algebra we arrive to

$$\gamma_t R^2 \frac{d\theta}{dt} = \tau_S, \tag{5.3}$$

which compared with (5.2) gives

$$\gamma_r = \gamma_t R^2 = 6\pi\eta r R^2. \tag{5.4}$$

This means that the drag coefficient that we will use in our rotational equations should be the same as in the previous model ($\sim 2 \cdot 10^{-4} pNs/nm$) but multiplied by the square of the rotor radius. This radius is of the order of $25nm$ in the two cases that we inspire our analysis: the FO of the ATP synthase and the Bacterial Flagellar Motor (BFM) [5]. This leads to a value of $\gamma_r \sim 0.1 pN \cdot nm \cdot s/rad$.

The properties of the ratchet potential are very similar to the linear case. The asymmetric factor α is chosen equal to 0.9, slightly greater than the 0.8 value of the linear case. The reason is simply that the closer α to unity the better the effectiveness of the mechanism, even though the minimum of the potential becomes more narrow and the simulation requires a lower time step. The height of the barrier is chosen with the following criterion: too high values of V_0 make very

improbable noise transitions and then the thermal fluctuations cannot help the mechanism. Very low values, on the other hand, produce too many noise induced transitions and what is more important: the forces induced by the potential are too low compared with the stretching and elastic ones, so the mechanism does not work. Summarizing, V_0 has to be at least more than 5 times k_BT and lower than Δ_G. The specific value is chosen to be that maximizing the value of the mean velocity.

The energy input is not ATP based this time. Most rotatory machines work with ion flux across the membrane where they are embedded. We have to write some typical values for the total membrane free energy and discuss the stechiometry if the system. First, is basic to say that a membrane potential has two main contributions: the gradient of ions $\Delta\mu$ and the electrostatic potential $\Delta\Psi$ and that is the reason why we called it an electrochemical potential. We write

$$\Delta G = \Delta\mu + \Delta\Psi. \tag{5.5}$$

The value of $\Delta\Psi$ is considered to be of the order of $150mV$, which in our usual units is

$$\Delta\Psi \simeq 24pNnm. \tag{5.6}$$

For the chemical contribution we write

$$\Delta\mu = k_BT \ln\left(\frac{[ion]_{ext}}{[ion]_{int}}\right), \tag{5.7}$$

where $[ion]_{int}$ and $[ion]_{ext}$ are the ionic concentrations inside and outside the membrane, respectively. Rotatory devices use proton or sodium ions, so $[ion]$ can be read as $[H^+]$ or $[Na^+]$ depending on the case. We know that the thermal energy is $k_BT = 4.1pNnm$ and the values of the specific ionic concentrations, even though depend on the lab conditions, will be taken from Ref.[25]. Then, $[ion]_{int} = 30mM$ and $[ion]_{ext}$ is a control variable that varies in a $[5, 100]mM$ range. This implies a $\Delta\mu$ contribution from -7 to $5pNnm$. Added to the electrostatic contribution (also called membrane potential), the spectrum of available free energy is $(17 - 29)pNnm$, depending on the value of $[ion]_{ext}$. This is the free energy available for every single crossing ion. In this point is relevant to discuss

the stechiometry of these motors. While ATP-driven motors seem to have a well defined stechiometry of one nucleotide for every step, in the case of ion driven machines this number is not so clear and even the integer nature of this number remains obscure. What is clear is that the motion of the FO of the ATP-synthase is the power that produces F_1 rotation and ATP synthesis. To add complication to this subject, the FO can be found with 10 to 14 subunits. The rotation of the FO produces a rotation of the F_1, which has three subunits. Everytime the F_1 rotates $2\pi/3rad$, an ATP is synthesized. This implies that the FO needs 3.33 to 4.67 rotation of their subunits in order to produce a single subunit step on the FO. From an energetic point of view, the energy required to synthesize an ATP is at least $120pNnm$. Then, a minimum of 4 ions are required to contribute to this amount of free energy.

While FO has a single torque generating unit, BFM has about 8-10, while it has 26 structural subunits. It is known [25] that about 1000 ions are required to a complete revolution of the motor. This means that every step of the subunit requires about 38 ions to be performed. However, there are 8 to 10 torque generating units and this means that every of these units should use about 4 ions per step, as in the previous case of FO.

We have to discuss how are we going to implement the energy input in this model. The Nerst equation tells us that the free energy has two contributions, i.e. the chemical and the membrane potential. While the latter can be considered as a constant, the former has more subtleties. This statistichal contribution comes from the fact that ions can cross in both directions and that the power stroke can eventually be applied backwards. However, in our modelling the polarity of the ratchet is fixed and does not change with the specific transition of the ion. Thus, even if the device can rotate clock and counterclockwise due to thermal noise, the power stroke can be applied only in one of the orientations. In a kinesin, there is some finite (and low) probability that an ADP and a P_i are joined in a single ATP in a catalytic site of a kinesin, but this would not imply a step backward of the protein. In the case of a BFM, the backward transition of an ion implies a backward motion of the motor, and that is why the entropic term has to be added to the free energy. However, our model is strongly limited to these features

and we will consider the case of a motor with no backward stroke. Thus, only $\Delta\Psi$ will contribute to the free energy that is used to perform the step. This latter assumption implies that the total free energy available is $\Delta\Psi \sim 24pNnm$. This will be the available energy for a single event in our F_O-like model while for our BFM inspired device we will use $100pNnm$, which is approximately four times $\Delta\Psi$, according with the approximation of 4 ions per event. This simplification, although unrealistic, allows to use independently the binding probability parameter p and the energy available for the power stroke E.

We have to distinguish between two limiting cases: the low and high coupling regimes. The coupling strength is determined by the stiffness. We don't have to confuse this coupling with the coupling ratio, which has another meaning. When the stiffness is low, the system is poorly coupled and we are close to the case of the linear dimer presented in the previous chapter. However, a single event in a single spring is supposed to rotate the whole system. When a dimer is stretched, the response of the rest of the system is not very high, so the current stretching dimer can move as if it were independent from the rest of the particles. As the next-consecutive spring will perform the same cycle later, it will move as well in a quasi-independent way, and so on. This case has double inchworm character, because each spring movement is followed by its consecutive partner. The second-highly coupled regime corresponds to high values of the stiffness. In this case, the response of the system under a stretching event is strong, so then the stretching dimer cannot advance if it does not perform its job with energy enough to force the whole system rotation. What we see is that this regime requires high stretching torques in order to be achieved. In next sections we apply all these ideas to some specific modellings and we will see how to avoid the low coupled regime for the case of FO and BFM, as both structures are relatively rigid and there are many reasons to expect that they perform a high coupled rotation.

5.2 A preliminary rotatory device model with a single torque generating unit.

Inspired from the FO unit of the ATP synthase we build a rotatory device model that performs a stretching event every time an ion crosses the membrane. As

there is only one single channel, the number of torque generating units is equal to one, as seen in Fig.5.1. In the simulation algorithm, the stretching events will occur successively in consecutive springs. Let θ_i be the coordinate for every particle and k the stiffness of the springs, which are all equal. Let $N = 10$ be the total number of particles, so then the angle difference between subunits is $\Delta\theta = 2\pi/N \simeq 0.63rad$.

The available free energy per event is, as we have already mentioned, $\sim 25pNnm$. With this energy and having 10 particles to surmount an energetic wall of $V_0 \simeq 25pNnm$ (this value optimizes the velocity of the motor), the system cannot have a high coupling in order to achieve some motion. We simulate the following equations:

$$\lambda_r\dot{\theta}_i = -V'(\theta_i) + \frac{\tau_{ext}}{N} + \tau_{elR}(\theta_i, \theta_{i-1}) + \tau_{elL}(\theta_i, \theta_{i+1}) + \tau_{sRi}(t) + \tau_{sLi}(t) + \xi_i(t), \quad (5.8)$$

where τ_{ext} is the external torque, $N = 10$ is the number of particles, τ_{elR}, τ_{elL} are the two elastic components of the torque (L accounts for a left-handed or counterclockwise torque and R for the opposite sense), τ_{sLi}, τ_{sRi} are the two components of the stretching torque and $\xi_i(t)$ are the thermal forces (gaussian white noise). The elastic torque is calculated following

$$\tau_{el}(\theta_i, \theta_{i+1}) = -k(\theta_{i+1} - \theta_i - \Delta\theta), \quad (5.9)$$

where

$$\Delta\theta = \frac{2\pi}{N}. \quad (5.10)$$

The stretching torque is simply the available energy E divided by $\Delta\theta$. The ratchet potential induces a torque

$$\tau_{V1} = \frac{V_0}{\Delta\theta\alpha} \qquad \theta \in (0, \alpha\Delta\theta) \quad (5.11)$$

and

$$\tau_{V2} = \frac{V_0}{\Delta\theta(1-\alpha)} \qquad \theta \in (\alpha\Delta\theta, \Delta\theta), \quad (5.12)$$

considering that moreover we have periodic boundary conditions $V(0) = V(2\pi)$.

The equations of motion are also the following index and boundary conditions,

$$i \in (1, N) \qquad \theta_0 = \theta_N \qquad \theta_{N+1} = \theta_1. \tag{5.13}$$

To compute the mean angular velocity $\langle \omega \rangle$ we calculate the mean value of θ,

$$\langle \theta \rangle \equiv \frac{1}{N} \sum_{i=1}^{N} \theta_i. \tag{5.14}$$

In Figure 5.2 we can see individual trajectories for each particle.

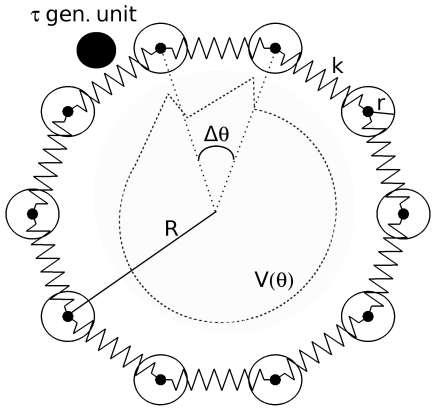

Figure 5.1: **Scheme of the rotating system:** The outer circle represents the stator with $N = 10$ coupled particles. Each particle is linearly coupled to their two neighbours by a spring of stiffness k. The black solid circle is the only torque generating unit if the system, i.e. only the spring beside this unit is able to stretch due to ion crossing. The inner circle shows the angular potential, which is flat except near the torque generating unit. Specifically, it is non-zero in the torque generating unit and the next unit beside, in order to rectify the motion when the spring stretches and shrinks. R is the radius of the rotor while r is the radius of the particles of this rotor.

In this model, the mechanism is very similar to the one presented in the previous chapter. The spring which is under the ratchet (non-zero) potential is stretched until it is elongated twice its natural angle. Then the stretching torque disappears and the spring relaxes. In our algorithm we forbid new stretching

events to occur until the spring has recovered its initial relaxed configuration. This allows the system not to begin the stretching of the neighboring spring, which reduces the efficiency of the whole mechanism. What we do is to wait until the cycle is completed, no matter if it has successfully produced a step or not. Then we allow the neighboring spring to wait for an event. This mechanism implies that the non-zero section of the potential is translated an angle $\Delta\theta$ after every event. However, since this angle is precisely the period of the potential and since the two particles connected by the spring are relaxed around the minima, we can be sure that we are not adding neither extracting energy to the system. If we would translate the potential just after stretching completion, we would be adding energy and our calculations should take this fact into account. In the trajectories, as most of the particles are under no potential, they don't exhibit step-like trajectories. However, there are some regions that sequentially appear to move in discrete steps, corresponding to the time when they are close to the torque generating unit.

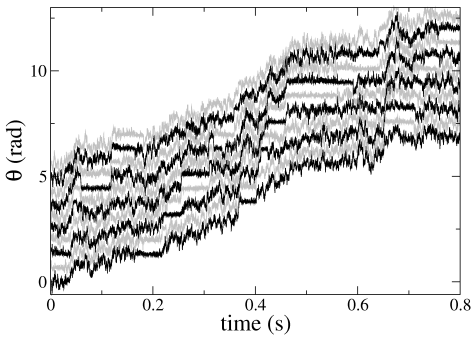

Figure 5.2: **Trajectories of the $N = 10$ units.** We can see the trajectories for each of the 10 particles of the rotor. As only the ones near the torque generating unit are under a non-zero potential, we can see the stepping appearance only at some given intervals of time in each particle. These step-like intervals jump from one pair of consecutive particles to the next in a sequential way, as it can be appreciated in the figure.

In the simulations, we are using a thermal energy of $k_BT = 4.1pNnm$, a time integration step $\Delta t = 10^{-6}s$, a stiffness $k = 10pN/nm$, $V_0 = 25pNnm$ and $\alpha = 0.9$. These values may seem quite arbitrary, but they can be justified with

$\tau_{ext}(pNnm)$	0	-5	-10
$\omega_{max}(rad/s)$	8.72	6.76	4.92
$k_M/10^{-}5(dimensionless)$	4.52	6.40	8.74

Table 5.1: Values of the michaelian parameters obtained in the simulations.

the following reasons. First of all, it is interesting to work with values that are reasonably within biological thresholds. Secondly, once some of the parameters are chosen, like the thermal energy or the available energies for the power stroke, the spectrum of values for the rest of the parameters is strongly reduced. Only a tedious set of simulation trials can give an idea of these narrow windows and furthermore it provides the set of values that are maximizing the angular velocity of the motor.

Once the simulation is completed, the two control variables, p and τ_{ext} can be moved in order to characterize the response of the motor under forcing and under lack of substrate. We will try to proceed with a similar analysis as in the previous section with the linear and dimeric case. First of all, we perform three sets of simulations, each with a different load. Specifically, we will work with the cases $\tau_{ext} = 0, -5, -10pNnm$. For each of these cases we will perform a scan for different values of the binding probability p. We can see the results in Figure 5.3. We can see how the curves are Michaelian, at least for $p > 10^{-5}$. Now we fit each of these curves following the M-M equation

$$\omega = \omega_{max}\frac{p}{p + k_M}, \tag{5.15}$$

where ω_{max} and k_M are load dependent kinetic parameters. We obtain the values shown in Table 5.1. Notice however how for very low p the agreement is not very good, specially for high loads, where it is quite difficult to have simulation data.

Once we have obtained these parameters we try to apply the same theory presented in the previous section. We can write now

$$\omega_{max} = \frac{\omega_{max}(0)}{1 - \frac{\tau_{ext}}{k_{iu}(\tau_m + \tau_{ext})}} \tag{5.16}$$

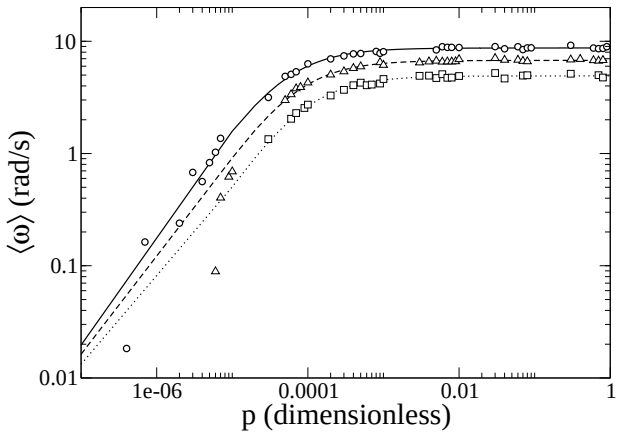

Figure 5.3: **Mean velocity $\langle\omega\rangle$ versus the binding probability p.** The points are simulation data from three different conditions: circles, triangles and squares correspond to $\tau_{ext} = 0, -5, -10 pNnm$, respectively. In the same order, solid, dashed and dotted lines correspond to the Michaelis-Menten fit for every set of points.

and

$$k_M = k_M(0)\frac{1 - \frac{\tau_{ext}}{k_{ic}(\tau_m+\tau_{ext})}}{1 - \frac{\tau_{ext}}{k_{iu}(\tau_m+\tau_{ext})}}, \tag{5.17}$$

where τ_m is the motive torque. Notice that we use τ_{ext} with negative values for the useful work regime, while in some figures we plot the load as a positive quantity. The reason is that sometimes it seems easier to think the load as a positive quantity and sometimes is more intuitive to think it as a negative torque opposing to the motion. In addition, we can find both criteria in literature, so we don't adopt a single convention as it should produce no confussion.

Once the fit process (see Fig.5.4) is completed we can summarize the values of the parameters, which are shown in Table 5.2. We can see how the maximum angular (zero load) velocity is $8.72 rad/s$ and $k_M(0) = 4.41 \cdot 10^{-5}$. Later we see that the motive torque τ_m is $\simeq 25 pNnm$, which is precisely the value of the free energy that is available in every event. On the other hand we can see how $k_{iu} = 0.86$, the uncompetitive inhibition constant, is greater than $k_{ic} = 0.27$, the competitive inhibition constant. This means that this motor acts as a competitive mixed inhibitor. However, both quantities are quite similar, and that is the reason

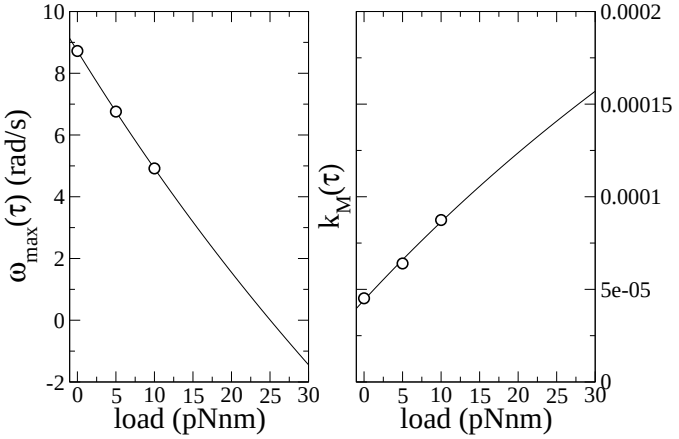

Figure 5.4: **Fit of the parameters.** On the left figure, the three different ω_{max} obtained from the curves of Fig.5.3 versus the corresponding load. The solid line is a fit of eq.(5.16). On the right side we have the three different values of k_M obtained from the fitting process and the curve is the fit from the eq.(5.17). The resulting parameters are shown in Table 5.2.

parameter	$\omega_{max}(0)$	$k_M(0)$	k_{iu}	k_{ic}	τ_m
value	$8.72 rad/s$	$4.41 \cdot 10^{-5}$	0.86	0.27	$25.04 pNnm$

Table 5.2: Values of the model parameters. The parameters without explicit given unit are dimensionless.

why the force-velocity curves are almost linear.

With the set of parameters given in Table 5.2 we can plot the mean angular velocity as a function of the load and see if it agrees with the simulation data. The results are shown in Figure 5.5. At high p, we see how the agreement is excellent (the solid line is in perfect agreement with the circles). However, at low values of the binding probability, the agreement is worse than poor (the dotted line with respect to the squares). There is no surprise in the plots as the theory applied considers that the motive torque must be independent of p. However, simulations show that the maximum torque does depend on the concentration (see Fig.5.5), *even if we have not taken into account the entropic term of the free energy.* In the figure, the dashed line is simply a linear regression of the data, giving

$$\langle \omega \rangle \simeq 1.76 + 0.21 \tau_{ext} pNnm, \tag{5.18}$$

which gives $\tau_m \simeq 8.5pNnm$. In principle, it seems counterintuitive to find this result, as we didn't include the entropic term of the free energy, which has the substrate concentration dependence in an explicit way. The reason has to be thought in terms of some kinetic considerations. In Appendix A2 we show some calculations that are devoted to analyze such a dependence.

Summarizing, we have analyzed a simple rotatory model with a single torque generating unit within a nano-biological scale. The available energies suggest that such an inchworm mechanism is not very efficient in this case. However, we have observed force-velocity curves and quasi Michaelian substrate-velocity dependences. We have also provided an interesting clue to the fact that different substrate concentrations can produce different stall torque values without taking into account entropic contributions in the free energy. This could be also applied to kinesin [ATP]-dependence on the stall force, but in this case the motor is tightly bound to the microtubule while there is no power stroke acting, so the applicability is not straightforward.

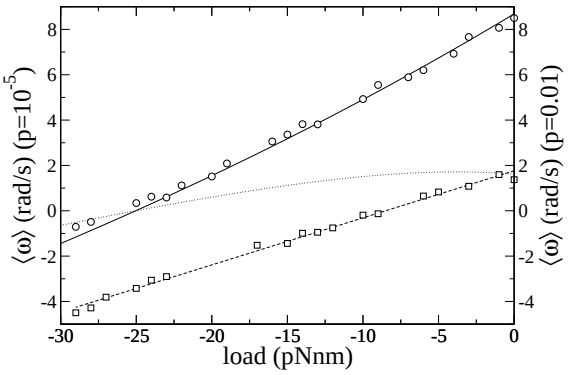

Figure 5.5: **Load-velocity curves for two different values of p.** Circles and squares correspond to simulation data for $p = 0.01$ and $p = 10^{-5}$, respectively. Solid line is the plot of the equation (5.15), so we see how the prediction agrees with the simulated data. However, dotted line is the prediction for the other, lower-p, case. We see how the disagreement is complete. While the prediction decays until a stalling value which is the same as in the high-p case, the simulations show that the decay occurs much faster. Dashed line is simply a linear regression fitting the simulation data.

In Figure 5.6 we can see the data for the global efficiency and the coupling ratio. What is most remarkable is that the efficiencies are extremely low. The maximum values achieved do not reach 10^{-2}, which contrasts with the claims that ATP synthase can be close to efficiency one. The reason for the low efficiency is directly measured through the coupling ratio, which is clearly away from a tight coupling mechanism. In this mechanism, most of the crossing ions are wasted, even at zero load conditions. We think that the available energy, $25pNnm$ for a single event is too low to satisfactorily move the whole system. There is also the possibility that we could have overestimated the value of the drag coefficient. We have used values for the friction that are 3 orders of magnitude higher than in the linear case.

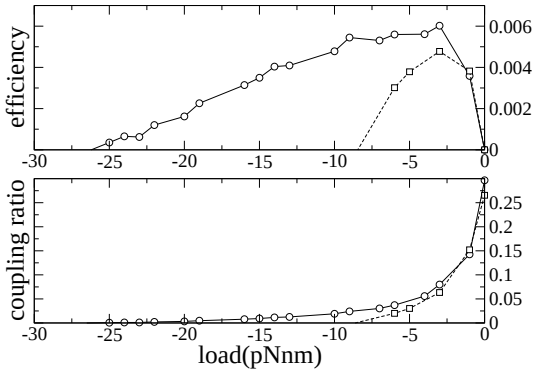

Figure 5.6: **Efficiency and coupling ratio versus the load.** In the upper figure we can see simulation data for the efficiency versus the external torque (here written as negative). Lines are only guides between points, while circles and squares correspond to $p = 0.01$ and $p = 10^{-5}$, respectively. We observe typical parabolic-like shapes even though they are not symmetric. Maximum efficiencies are really small as they rarely reach $5 \cdot 10^{-3}$. It is relevant that at low values of p the efficiency reaches negative values at lower loads. On the lower figure we plot the data for the coupling ratio, with the same correspondence of symbols with the simulation conditions. The coupling ratio decays from an initial value slightly above 0.25 and it reaches the zero in an equivalent way as the efficiency does.

Appendix A1

Let us perform the calculation of the Kramers formula for the overcoming of a barrier built with linear pieces. We begin with Smoluchowski's equation

$$\frac{\partial f(x,t)}{\partial t} = \frac{1}{\lambda}(\frac{\partial}{\partial x}(V'(x)) + \frac{k_B T \partial}{\partial x})f(x,t) \tag{5.19}$$

where $f(x,t)$ is the probability density function. An equivalent expression is

$$\frac{\partial f(x,t)}{\partial t} = -\frac{\partial}{\partial x} j(x,t), \tag{5.20}$$

where $j(x,t)$ is the probability current. Considering a stationary state, $\frac{\partial f(x,t)}{\partial t} = 0$, so $j(x,t)$ will be a constant. Then

$$j = -\frac{V'(x)f(X,T)}{\lambda} - \frac{k_B T}{\lambda}\frac{\partial f}{\partial x} \tag{5.21}$$

and, rearranging some terms, gives

$$\frac{\partial f(x)}{\partial x} + \frac{V'(x)f(x)}{k_B T} = -\frac{j\lambda}{k_B T} \tag{5.22}$$

We can rewrite last expression as

$$\frac{d}{dx}[f(x)e^{\frac{V(x)}{k_B T}}] = -\frac{j\lambda}{k_B T}e^{\frac{V(x)}{k_B T}} \tag{5.23}$$

where we have used

$$e^{\int \frac{V'(x)}{k_B T}dx} = e^{\frac{V(x)}{k_B T}} \tag{5.24}$$

We integrate from $x = 0$ (corresponding to a first potential minimum) to $x = B$ (corresponding to the second potential minimum, where $V = 0$). Here we derive

in general, for any potential. Later we will use the one presented before. Thus

$$[f(x)e^{\frac{V(x)}{k_BT}}]_0^B = -\frac{j\lambda}{k_BT}\int_0^B e^{\frac{V(x)}{k_BT}}dx. \tag{5.25}$$

It's reasonable to suppose $f(B) = 0$ (no particles at the maximum), so then we can solve j

$$j = \frac{k_BT}{\lambda}\frac{f(0)e^{\frac{V(0)}{k_BT}}}{\int_0^B dxe^{\frac{V(x)}{k_BT}}} \tag{5.26}$$

It's also reasonable to suppose that j is very small around $x = 0$, so, from (eq)5.22

$$\frac{\partial f}{\partial x} = -\frac{V'(x)}{k_BT}f(x) \tag{5.27}$$

Integrating between $x = 0$ and a point x of the 'bell', we obtain

$$f(x) = f(0)e^{\frac{-V(x)+V(0)}{k_BT}}. \tag{5.28}$$

Proceeding like this, the diffusive particles' population around the minimum is given by

$$n_a = \int_{x_1}^{x_2} f(x)dx \tag{5.29}$$

where x_1 and x_2 are two points around $x = 0$. We arrive at last to the expression for the frequency of escape k across the barrier, which is the ratio between the current crossing and the non-succeeding population.

$$k = \frac{j}{n_a}. \tag{5.30}$$

We obtain the expression we wanted to arrive, k as a function of $V(x)$

$$k = (\frac{k_BT}{\lambda})\frac{1}{\int_{-\infty}^{\infty} dxe^{\frac{V(x)}{k_BT}}\int_{-\infty}^{\infty} dxe^{-\frac{V(x)}{k_BT}}}, \tag{5.31}$$

where we have extended the integration limits to infinity because the integration is realized over a local expansion of the potential. We call I_1 to the left integral and I_2 to the right one. This is a well known result and from it one can arrive to Arrhenius' law taking expansions around the minimum and the maximum. We

will do it but without expanding it because with our potential the integral can be performed analytically, obtaining a theoretical expression for the rate of the reaction as a function of the parameters discussed before.

We will first call $V_1(x)$, $V_2(x)$, $V_3(x)$ to the three pieces , respectively, of the potential presented in eq.(3.25). We have to integrate

$$I_2 = \int_{-\infty}^{\infty} dx e^{-\frac{V(x)}{k_B T}}, \tag{5.32}$$

where $V(x)$ is the potential around the minimum at $x = 0$. So we can perform the integral in two parts,

$$\int_{-\infty}^{\infty} dx e^{-\frac{V(x)}{k_B T}} = \int_{-\infty}^{0} dx e^{-\frac{V_1(x)}{k_B T}} + \int_{0}^{\infty} dx e^{-\frac{V_2(x)}{k_B T}}. \tag{5.33}$$

We obtain an analytical result for the potential. The expression for $V(x)$ is

$$V(x) = \begin{cases} -\frac{(\Delta G_u + E_A)}{\alpha L} x & \text{if } -L\alpha < x < 0 \\ \frac{E_A}{L(1-\alpha)} x & \text{if } 0 < x < L(1-\alpha) \\ -\frac{(\Delta G_u + E_A)}{\alpha L} x + E_A + \frac{1-\alpha}{\alpha}(\Delta G_u + E_A) & \text{if } L(1-\alpha) < x < L \end{cases}$$

so then,

$$\int_{-\infty}^{\infty} dx e^{-\frac{V(x)}{k_B T}} = k_B T l_0 (\frac{\alpha}{\Delta G + E_A} + \frac{1-\alpha}{E_A}). \tag{5.34}$$

If we do the same around the maximum in

$$I_1 = \int_{-\infty}^{\infty} dx e^{\frac{V(x)}{k_B T}}, \tag{5.35}$$

where

$$\int_{-\infty}^{\infty} dx e^{\frac{V(x)}{k_B T}} = \int_{-\infty}^{0} dx e^{\frac{V_2(x)}{k_B T}} + \int_{0}^{\infty} dx e^{\frac{V_3(x)}{k_B T}}, \tag{5.36}$$

we obtain

$$\int_{-\infty}^{\infty} e^{\frac{V(x)}{k_B T}} = k_B T L e^{\frac{E_A}{k_B T}} (\frac{\alpha}{\Delta G_u + E_A} + \frac{1-\alpha}{E_A}). \tag{5.37}$$

Because

$$k = \frac{k_B T}{\lambda I_1 I_2}, \tag{5.38}$$

we can join the results and stay that

$$k = \frac{1}{\lambda L^2 k_B T \beta^2} e^{-\frac{E_A}{k_B T}} \tag{5.39}$$

where we have defined

$$\beta_0 = \frac{\alpha}{\Delta G_u + E_A} + \frac{1-\alpha}{E_A}. \tag{5.40}$$

Thus we obtain for the mean velocity

$$\langle v \rangle = \frac{1}{\lambda L k_B T \beta_0^2} e^{-\frac{E_A}{k_B T}}. \tag{5.41}$$

Let's perform an idealistic estimation of the magnitude of E_A. With the usual value for the kinesin parameters and setting the limit where $\alpha \to 1$ and $\Delta G_u \sim 50 pNnm$ (half of the typical ATP hydrolysis energy, as discussed in [41, 37]) we obtain, when setting $\langle v \rangle \simeq 800 nm/s$, that $E_A \sim 53 pNnm$, i.e. of the same order of magnitude that ΔG_u. When moving the asymmetry parameter α the value for E_A only decreases to $49 pNnm$ when $\alpha \to 0.5$. If we would use $\Delta G_u \simeq 100 pNnm$ the values for the activation barrier would only be increased by $\sim 5 pNnm$. With these clues we can obtain a first calibration to enter into the kinesin experimental scale of Ref.[9].

When the external force is applied, the total potential affecting the motor is modified in a way that an opposing load reduces the global slope of the effective potential. In the limit case of the stall force, the total potential has no net slope and then there is no directed motion. Nevertheless, we don't know yet how the external force is affecting the activation barrier. If we are able to calculate the f_{ext}-dependence of E_A we can obtain an estimation of the mean velocity by means of a Kramers rate. If we apply the external force f_{ext} the two energies E_A and ΔG_u are substituted by $E_A - f_{ext} L(1-\alpha)$ and $\Delta G_u + f_{ext} L$. With these substitutions we obtain a load-dependent velocity

$$\langle v \rangle = \frac{1}{\lambda L k_B T \beta_f^2} e^{-\frac{E_A - f_{ext} L(1-\alpha)}{k_B T}}, \tag{5.42}$$

with

$$\beta_f = \frac{\alpha}{\Delta G_u + f_{ext}L + E_A - f_{ext}(1-\alpha)} + \frac{1-\alpha}{E_A - f_{ext}L(1-\alpha)}. \tag{5.43}$$

If we analyze the limit of $f_{ext} \to \frac{-\Delta G_u}{L}$ then $\beta_f \to \frac{1}{E_A}$. We obtain the following velocity

$$\langle v \rangle = \frac{(E_A + \Delta G_u(1-\alpha))^2}{\lambda L k_B T} e^{-\frac{(E_A + \Delta G_u(1-\alpha)))}{k_B T}}. \tag{5.44}$$

We can work in the approximation $\alpha \to 1$ to write

$$\langle v \rangle = \frac{E_A^2}{\lambda L k_B T} e^{-\frac{E_A}{k_B T}}. \tag{5.45}$$

This is the velocity of the particles travelling from left to right. Now we can write a similar expression for the particles travelling backward, applying the same concepts derived in previous expressions. We call now to the left-to-right velocity v_1 and the right-to-left velocity v_2. Then, for $f_{ext} = 0$,

$$\langle v_1 \rangle = \frac{(E_A + \Delta G_u)^2}{\lambda L k_B T} e^{-\frac{E_A}{k_B T}} \tag{5.46}$$

and

$$\langle v_2 \rangle = \frac{(E_A + \Delta G_u)^2}{\lambda L k_B T} e^{-\frac{(E_A + \Delta G_u)}{k_B T}}. \tag{5.47}$$

In order to have a proper definition of total mean velocity is important to take into account the backward processes, and that is why we redefine $\langle v \rangle$ as

$$\langle v \rangle = \langle v_1 \rangle - \langle v_2 \rangle, \tag{5.48}$$

and then

$$\langle v \rangle = \frac{(E_A + \Delta G_u)^2}{\lambda L k_B T} e^{-\frac{E_A}{k_B T}} (1 - e^{\frac{-\Delta G_u}{k_B T}}). \tag{5.49}$$

The correction respect to the previous expression does not seem important at zero load, but it gains relevance as we increase the strength of the external forcing. Specifically, when $f_{ext} = -\Delta G_u / L$, $\langle v \rangle$ is strictly zero. We can write in general

$$\langle v \rangle = \frac{(E_A + \Delta G_u + f_{ext}L)^2}{\lambda L k_B T} e^{-\frac{E_A}{k_B T}} (1 - e^{\frac{-(\Delta G_u + f_{ext}L)}{k_B T}}). \tag{5.50}$$

Appendix A2

When there is no stretching event acting on the system, the potential barrier is V_0 and the load is τ_{ext}, if we consider a tightly coupled system. Then we have the following rate of forwards events

$$r_{\rightarrow} \propto e^{-\frac{V_0 - \tau_{ext}\alpha\Delta\theta}{k_B T}} \tag{5.51}$$

and the backwards rate

$$r_{\leftarrow} \propto e^{-\frac{V_0 + \tau_{ext}(1-\alpha)\Delta\theta}{k_B T}}. \tag{5.52}$$

In absence of power stroke events, the total backward/forward transition quotient is $r = r_{\leftarrow}/r_{\rightarrow}$,

$$r = e^{\frac{\tau_{ext}\Delta\theta(2\alpha-1)}{k_B T}}. \tag{5.53}$$

Now, when the free energy coming from the crossing ion is present, the energy profile is different. We will consider that there is a free energy difference E between two consecutive minima. Then, the modified rates r'_i are

$$r'_{\rightarrow} \propto e^{-\frac{V_0 - \tau_{ext}\alpha\Delta\theta - E}{k_B T}}, \tag{5.54}$$

$$r'_{\leftarrow} \propto e^{-\frac{V_0 + \tau_{ext}(1-\alpha)\Delta\theta + E}{k_B T}}, \tag{5.55}$$

and

$$r' = \frac{r'_{\leftarrow}}{r'_{\rightarrow}} = e^{\frac{2E + \tau_{ext}\Delta\theta(2\alpha-1)}{k_B T}}. \tag{5.56}$$

The point is now to consider that during a dwell or waiting time we have to consider r to be the current rate while during the power stroke event (during t_{on}), the rate has to be like r'. At a single event, $\langle t_{on}\rangle/\langle t_{ev}\rangle$ is the fraction of time that the motor is at the r' state. The free energy difference while there is no E

acting can be written as

$$\Delta G = \frac{\tau_{ext}\Delta\theta(2\alpha - 1)}{k_B T}, \tag{5.57}$$

while in the other case there is a free energy

$$\Delta G' = \frac{2E + \tau_{ext}\Delta\theta(2\alpha - 1)}{k_B T}. \tag{5.58}$$

In the whole process, the system is under these two values of free energy, so we can calculate the average value $\hat{\Delta G}$,

$$\hat{\Delta G} = \frac{p}{p + k_M}\Delta G' + (1 - \frac{p}{p + k_M})\Delta G, \tag{5.59}$$

where it is easy to show that

$$\frac{t_{on}}{t_{ev}} = \frac{p}{p + k_M}. \tag{5.60}$$

We obtain

$$\hat{\Delta G} = \frac{p}{p + k_M}\frac{2E + \tau_{ext}\Delta\theta(2\alpha - 1)}{k_B T} + (1 - \frac{p}{p + k_M})\frac{\tau_{ext}\Delta\theta(2\alpha - 1)}{k_B T}. \tag{5.61}$$

As we are interested in the stall torque value, we set $\hat{\Delta G} = 0$ and then

$$\tau_m = \frac{2E}{(2\alpha - 1)\Delta\theta}\frac{p}{p + k_M}. \tag{5.62}$$

This means that the stall torque value has a michaelian response with k_M. If $p = 0$, then the stall torque is zero as well as there are no power stroke events. However, k_M is extremely low, which makes this effect difficult to see if we are not measuring data on a regime $p < k_M$. In the rotatory model we have presented, $p = 10^{-5}$ is clearly under k_M, so then τ_m is strongly reduced.

We see then how the effective free energy is modified as a function of the substrate concentration without the need to introduce the entropic term in the free energy. As τ_m is supposed to be $\simeq \Delta G_T/\Delta\theta$, we have provided a reason of why the stall torque depends on the binding probability p. But maybe there

are other important factors contributing to this effect. The angular potential is zero everywhere except close to the torque generating unit. However, the external torque is applied everywhere, in each particle of the rotor. Then, for the particles which are not under a non-zero ratchet potential, is very easy to be dragged by the external torque. This produces a backward motion that the torque generating unit can hardly compensate when the rate of crossing ions is low. It is true that we have incorporated the external torque in a quite arbitrary way. The assumption that the whole load is shared by all the particles is not necessarily true neither realistic. Maybe the whole load should be applied to the stretching particles. From an experimental point of view, maybe a conservative load has no sense since what is usually used is a non-conservative load introduced through different rotation drags. But in this model we have been inspired by how the F_1 of the ATP synthase may transfer the torque to the F_O through the shaft. We think it is reasonable to think that the load is shared by all the rotor in F_O, although this question is far from being clarified.

Part II

Chemical kinetic models

6

Introduction

Even though every molecular motor exhibits different structural properties and probably different mechanical features, there is a realm where all the protein devices can be understood under general and well defined magnitudes. Chemical kinetics of molecular machines is a wide field well supported by experimental data, as almost all the measurements are based on the variables that this discipline imposes. Reaction rates, dwell times, binding affinities... are some of the most common parameters to characterize the chemical processes inside a motor protein. From the point of view of the modelling this level of description is essentially phenomenological as the whole motor is considered to be a black box with some specific features. This fact allows to establish quantitative comparison between very different machines, which sometimes can have similar kinetic properties. Thus in this chapter we are not going to analyze molecular motors in a very fundamental way, but to introduce chemical kinetic models that are in agreement with experimental data. These models are very useful to biochemical analysis and they are the basis to address more fundamental levels of description.

From now on, we will consider molecular motors as simple enzymes, and then the mechanical velocities will be obtained by multiplying the velocity of the reaction by the displacement that the motor performs every cycle. Additionally, it should be multiplied as well by the coupling ratio, since not all the chemical cycles are successfully converted into mechanical steps. But in some cases we will

find that the chemical equations can take the coupling ratio into account, so in principle we can deal with chemical enzymes and after this to obtain physical magnitudes. In this chapter we are not interested in more fundamental details, but this kinetic phenomenology cannot be enough without a parallel and more microscopic understanding of the underlying mechanism of the nano devices.

One of the main problems and at the same time one of the most interesting features of the molecular motors topic is the following: when building a mechanical model it is not clear how to introduce the chemical components; when describing the chemical scheme it is not clear how to introduce the mechanical part. But molecular motors are mechano-enzymes, so consequently we have to deal with these two disciplines simultaneously. In this chapter we are going to focus our attention into a chemical-based approach but incorporating the mechanical forces as virtual or effective substances that depend all the time on the actual value of the mechanical force. We will discuss a new way to incorporate such ingredient in a Michaelis Menten formalism obtaining good agreements with experimental data.

In order to begin, we have to recall the fundamental ingredient of any kinetic model: the law of mass action. Given a reaction like

$$A + B \xrightarrow{k_1} C + D \tag{6.1}$$

the law of mass action establishes that the rate of reaction is proportional to the product of concentrations of the reactants, i.e.

$$\frac{d[C]}{dt} = \frac{d[D]}{dt} \propto [A][B]. \tag{6.2}$$

In a more general form we can introduce the stechiometric coefficients λ_i as

$$\lambda_a A + \lambda_b B \xrightarrow{k_1} C + D\ , \tag{6.3}$$

where now

$$\frac{d[C]}{dt} = \frac{d[D]}{dt} \propto [A]^{\lambda_1}[B]^{\lambda_b}. \tag{6.4}$$

In the Appendix B1 of this chapter we provide some simple calculations to illus-

trate the basis of the proportionality between the reaction rate and the reactant concentration.

Nevertheless, the reaction are not usually unidirectional, but arrows in the two senses are allowed,

$$A \underset{k_{-1}}{\overset{k_1}{\rightleftharpoons}} B \,. \tag{6.5}$$

Then, following the law of mass action, we could write

$$\frac{d[B]}{dt} = \frac{-d[A]}{dt} = k_1[A] - k_{-1}[B]. \tag{6.6}$$

If we impose an equilibrium condition, then $d[B]/dt = 0$ and

$$\frac{k_{-1}}{k_1} = \frac{[A]_{eq}}{[B]_{eq}} \equiv k^0, \tag{6.7}$$

which defines the equilibrium concentrations $[A]_{eq}$ and $[B]_{eq}$, at which there is no net change in the population of the species A and B. We have also defined k^0 as the equilibrium constant of this reaction. From Kramers rate theory we can relate this rates to the free energy concepts. We can agree that the ratio of backwards/forwards rates gives

$$\frac{k_{-1}[B]}{k_1[A]} = e^{-\Delta G/k_B T}, \tag{6.8}$$

so then

$$\Delta G = -k_B T \ln\left(\frac{[B]}{[A]}\right) + k_B T \ln\left(k^0\right). \tag{6.9}$$

We define

$$\Delta G^0 \equiv k_B T \ln\left(k^0\right), \tag{6.10}$$

which is the equilibrium free energy, while the concentrations dependent term is the entropic free energy. It is clear, then, how to relate kinetic rates in the chemical equation with the free energies associated with them. This latter case is intimally related with the free energy across a membrane due to the concentration gradient, supposing there is no mediator of the reaction. The role of the mediator is, however, so common that is difficult to find biological reactions without intermediate molecules regulating the kinetics of the process. The paradigmatic

kinetic equations describing the effect of these mediators or *enzymes* are the so called Michaelis-Menten (M-M) equations.

6.1 Michaelis Menten formalism and Hill exponent

Let's consider the following reaction

$$S + E \underset{k_{-1}}{\overset{k_1}{\rightleftharpoons}} SE \xrightarrow{k_2} P + E \,, \tag{6.11}$$

where S is the substrate, E the enzyme, P the product and SE the complex enzyme-substrate. From now on we adopt the following notation:

$$s = [S] \qquad e = [E] \qquad p = [P] \qquad x = [SE]. \tag{6.12}$$

We can write then for the velocity of reaction r (the production of P)

$$r = k_2 x. \tag{6.13}$$

We can also assume the hypothesis of

$$\frac{dx}{dt} = 0, \tag{6.14}$$

which implies

$$k_1(e - x)s - k_{-1}x + k_2 x = 0. \tag{6.15}$$

This allows to write x as

$$x = \frac{es}{s + \frac{k_{-1}+k_2}{k1}}. \tag{6.16}$$

We now define the Michaelis constant k_M as

$$k_M \equiv \frac{k_{-1} + k_2}{k_1} \tag{6.17}$$

and the maximum velocity of reaction r_{max}

$$r_{max} = k_2 e. \tag{6.18}$$

It is clear that as e is the total enzyme concentration, $k_2 e$ represents the maximum possible rate, which corresponds to the case where all the enzymes are at work. On the other hand, k_M represents the affinity of the substrate for the enzyme. If $k_a \gg k_{-1}$ then k_M is big and the substrate has a high affinity for the enzyme. We can write then

$$r = r_{max} \frac{s}{s + k_M}, \tag{6.19}$$

which is the standard way of writing the M-M equation. These two parameters are the necessary numbers in order to characterize a simple enzyme which is acting with a single binding site and without external forcing. If the enzyme would have several binding sites, let's say n, the reaction could be written in the form

$$nS + E \underset{k_{-1}}{\overset{k_1}{\rightleftarrows}} S_n E \xrightarrow{k_2} nP + E\,, \tag{6.20}$$

and then

$$x = \frac{s^n e}{s^n + k_M}. \tag{6.21}$$

We can write then the generalized M-M equation, which now it is usually called Hill's equation,

$$r = n r_{max} \frac{s^n}{s^n + k_M}. \tag{6.22}$$

This equation can also be interpreted as the description of a system where there are several enzymes which can cooperate. If $n = 1$ we could say that the enzymes are independent and there is no cooperation. If $n > 1$ the cooperation is positive, and there is a synergy, while $n < 1$ produces a negative effect respect to the independent case. We call to n the Hill exponent, which is a useful quantity when we want to measure the degree of cooperativity of different enzymes.

6.2 Kinetic inhibition

An inhibitor is a factor that decreases the rate of the global reaction, while an activator has the opposite effect: it enhances the reaction velocity. However, there are many ways of activate or inhibit a reaction. These factors are so important that they can be considered the responsible of almost all the regulation processes in genetic networks. Furthermore, almost all the drugs are chemical inhibitors. Moreover, and in relation with the topic of this thesis, the mechanical forces applied to a motor can be considered as inhibitors of the reaction. This is the main reason to introduce here the inhibition formalism.

6.2.1 Classification

The inhibitors can be classified into two main groups: reversible and irreversible. Irreversible inhibition consists on inhibitors that after affecting the mechanism of the enzyme for the first time there is no chance for the enzyme to be free again from the inhibitor. They are also called inactivators. In the case of a covalently bound irreversible inhibitor we say that we have a suicide inhibitor.
On the other hand, a reversible inhibitor can bind or force the enzyme but eventually can unbind it or allow the enzyme free behaviour path. We will focus in this type of inhibitors, because when a mechanical forcing is stopped the motors are able to recover their initial velocity.
Another main classification is based on the total percentage that the inhibitor can reduce from the non-inhibited rate. If the inhibitor can completely stop the reaction we say is a full inhibitor. Otherwise is a partial inhibitor. In experiments with molecular motors it has been seen that an external forcing can completely stall the motor, so we are dealing with full inhibitors. Moreover, some motors can be reversed at superstall forces, but this will require a more complicated formalism that will be introduced later.

Once we have classified molecular motors as reversible and full inhibitors we can distinguish some subclassification depending on how the two kinetic parameters k_M and r_{max} are affected when the inhibitor concentration increases. We present now the canonical cases, which are the competitive, uncompetitive, mixed and non-competitive inhibitions.

6.2.2 Competitive inhibition

We can now enter into the discussion of the case where there is a second substrate in the system that is able to compete with S. Specifically, we are interested in the cases where this second substrate inhibits the reaction. For now, it is enough to consider this substrate as a substance, but we will see later how a mechanical force can be considered an inhibitor. First, we consider the case of a competitive inhibitor, with the scheme

$$\begin{array}{ccccc} E + S & \underset{k_{-1}}{\overset{k_1}{\rightleftarrows}} & ES & \xrightarrow{k_2} & E + P \\ {\scriptstyle k_{ic}}\uparrow\downarrow{\scriptstyle I} & & & & \\ EI & & & & \end{array} , \tag{6.23}$$

where we have simplified the reaction

$$E + I \underset{k_{-3}}{\overset{k_3}{\rightleftarrows}} EI \ , \tag{6.24}$$

with

$$k_{ic} = \frac{k_{-3}}{k_3}. \tag{6.25}$$

k_{ic} is the competitive inhibition constant, which is, furthermore, a dissociation constant as it increases when the dissociated state increases its relative strength. We adopt

$$y = [EI] \qquad i = [I] \ , \tag{6.26}$$

and we can still write

$$r = k_2 x, \tag{6.27}$$

but now we have to solve for x and y, for which we assume there are no variations in time,

$$\frac{dx}{dt} = \frac{dy}{dt} = 0. \tag{6.28}$$

We obtain the following equations

$$k_1 s(e - x - y) = (k_{-1} + k_2)x \tag{6.29}$$

and

$$k_{ic}y = (e - x - y)i. \tag{6.30}$$

We obtain for the EI complex

$$y = \frac{e - x}{1 + \frac{k_{ic}}{i}}, \tag{6.31}$$

and then, after a little tedious algebra, we find

$$x = \frac{es}{s + k_M(1 + \frac{i}{k_{ic}})}. \tag{6.32}$$

Finally,

$$r = r_{max}\frac{s}{s + k_M(1 + \frac{i}{k_{ic}})}. \tag{6.33}$$

What we find is that we obtain a Michaelian expression but redefining

$$k_M(i) = k_M(i = 0)(1 + \frac{i}{k_{ic}}). \tag{6.34}$$

Then, as the inhibitor concentration increases, k_M increases as well.

This is the response of a competitive inhibitor: whenever it competes with substrate binding, the Michaelis constant is affected and then the binding affinity is slowed down as $i > 0$. Note that r_{max} is not affected, and only for $i \to \infty$ the velocity of the reaction goes to zero, i.e. only when binding is forbidden. This type of inhibition can be also called an entropic or effusive inhibition as it enhances the entropic barrier that the substrate has to surmount in order to enter into the enzymatic cavity. In fact, we can write explicitly how the entropic barrier depends on the inhibitor concentration. If we have the simple scheme

$$E + S \underset{k_{-1}}{\overset{k_1}{\rightleftharpoons}} ES\,, \tag{6.35}$$

we can calculate the forward rate $r_{\rightarrow}$ as

$$r_{\rightarrow} = k_1 s(e - x) \tag{6.36}$$

and the backward rate $r \leftarrow$

$$r_{\leftarrow} = k_{-1}x. \tag{6.37}$$

Following Kramers kinetics already used in the previous chapter we can write

$$\frac{r \leftarrow}{r_{\rightarrow}} = e^{-\Delta G/k_B T}. \tag{6.38}$$

Then, the free energy can be written as

$$\Delta G = -k_B T \ln \left(\frac{k_{-1}x}{k_1 s(e-x)}\right). \tag{6.39}$$

If we add the inhibition as

$$\begin{array}{ccc} E + S & \underset{k_{-1}}{\overset{k_1}{\rightleftharpoons}} & ES\,, \\ {\scriptstyle k_{-2}}\uparrow\downarrow{\scriptstyle k_2} & & \\ EI & & \end{array} \tag{6.40}$$

we obtain for the backward/forward ratio

$$\frac{r \leftarrow}{r_{\rightarrow}} = \frac{k_{-1}x}{k_1 s(e-x)}\left(1 + \frac{i}{k_{ic}}\right). \tag{6.41}$$

Then

$$\Delta G = -k_B T \ln \left(\frac{k_{-1}x}{k_1 s(e-x)}\left(1 + \frac{i}{k_{ic}}\right)\right). \tag{6.42}$$

We can compare this expression with the non-inhibited case (6.39) and conclude that

$$\Delta G_I = -k_B T \ln \left(1 + \frac{i}{k_{ic}}\right) \tag{6.43}$$

is the inhibitor contribution to the entropic barrier.

6.2.3 Uncompetitive inhibition

Instead of binding the free enzyme, we can consider an inhibitor that binds the enzyme-substrate complex in the form

$$E + S \underset{k_{-1}}{\overset{k_1}{\rightleftarrows}} ES \xrightarrow{k_2} E + P\,, \qquad (6.44)$$

$$ES \underset{k_{iu}}{\overset{I}{\rightleftarrows}} ESI$$

Then we define

$$y \equiv [ESI] \qquad k_{iu} \equiv \tfrac{k_{-3}}{k_3}\,, \qquad (6.45)$$

and assume

$$\frac{dy}{dt} = 0. \qquad (6.46)$$

As a consequence we can write

$$y = \frac{i}{k_{iu}} x, \qquad (6.47)$$

and assuming again that x does not change in time,

$$k_1(e - x - y)s = (k_{-1} + k_2)x, \qquad (6.48)$$

we solve the system to obtain $r = k_2 x$,

$$r = r_{max} \frac{s}{s(1 + \frac{i}{k_{iu}}) + k_M}. \qquad (6.49)$$

This is equivalent to write

$$r = r_{max}(i) \frac{s}{s + k_M(i)}, \qquad (6.50)$$

where

$$r_{max}(i) = \frac{r_{max}(0)}{(1 + \frac{i}{k_{iu}})} \qquad (6.51)$$

and

$$k_M(i) = \frac{k_M(0)}{(1 + \frac{i}{k_{iu}})}. \qquad (6.52)$$

Thus for the uncompetitive cases both k_M and r_{max} change with i. Specifically, they both decrease when the inhibition increases. Again we can study how the inhibitor concentration distorts the reversible kinetics between e and $x = [ES]$. We remind that for $i = 0$

$$\frac{r_{\leftarrow}}{r_{\rightarrow}} = \frac{k_{-1}}{k_1}\frac{(e_0 - e)}{es}, \tag{6.53}$$

where now we have performed the following changes: If we had e for the total enzyme concentration now we write e_0, and by e here we mean the free enzyme, i.e. $e = e_0 - e - e_i$. Following this temporary conversion we can write for the inhibited case

$$\frac{r_{\leftarrow}}{r_{\rightarrow}} = \frac{k_{-1}}{k_1}\frac{(e_0 - e)}{es(1 + \frac{i}{k_{iu}})}, \tag{6.54}$$

which clearly produces the following free energy contribution

$$\Delta G_I = k_B T \ln (1 + \frac{i}{k_{iu}}). \tag{6.55}$$

6.2.4 Mixed inhibition

The most general of these canonical examples is the mixed scheme, which is the sum of the two previous cases. Now the inhibitor can bind the free enzyme with a constant k_{ic} and at the same time it can bind the complex enzyme-substrate with constant k_{iu}. We have the scheme

$$\begin{array}{ccccc} E + S & \underset{k_{-1}}{\overset{k_1}{\rightleftharpoons}} & ES & \xrightarrow{k_2} & E + P\,, \\ {\scriptstyle k_{ic}}\uparrow\downarrow{\scriptstyle I} & & {\scriptstyle k_{iu}}\uparrow\downarrow{\scriptstyle I} & & \\ EI & & ESI & & \end{array} \tag{6.56}$$

Considering that now

$$z \equiv [ESI] \qquad y \equiv [EI]\,, \tag{6.57}$$

and that the hypothesis here are the sum of the hypothesis of the two previous cases, we can write the equations

$$z = \frac{i}{k_{iu}}x, \tag{6.58}$$

$$e - x - y - z = \frac{k_{ic}}{i} y \Rightarrow y = \frac{e - x - y}{1 + \frac{k_{ic}}{i}} \tag{6.59}$$

and

$$k_1(e - x - y - z)s = (k_{-1} + k_2)x. \tag{6.60}$$

Again we have the global rate expressed as

$$r = k_2 x, \tag{6.61}$$

so we solve for x and after some algebra we can write

$$r = r_{max} \frac{s}{s(1 + \frac{i}{k_{iu}}) + k_M(1 + \frac{i}{k_{ic}})}, \tag{6.62}$$

which is clearly a superposition of the competitive and uncompetitive cases. In order to write the Michaelian equation we redefine

$$r_{max}(i) = \frac{r_{max}(0)}{(1 + \frac{i}{k_{iu}})} \tag{6.63}$$

and

$$k_M(i) = k_M(0) \frac{(1 + \frac{i}{k_{ic}})}{(1 + \frac{i}{k_{iu}})}, \tag{6.64}$$

so then we can write again

$$r = r_{max}(i) \frac{s}{s + k_M(i)} \tag{6.65}$$

and deal the system as a parameter-variable Michaelis-Menten equation.

Following the perspective of considering the mixed case as the superposition of the competitive and uncompetitive cases we can subdivide the mixed type into two subtypes depending on the relative substraction of the two inhibition constants. If the competitive inhibition constant k_{ic} is greater than the uncompetitive inhibition constant, k_{iu} we have a mixed uncompetitive case, while $k_{ic} < k_{iu}$ implies a mixed competitive cases. The reason to characterize the system with the lower inhibition constant is that they are dissociation constants and the lower the k_i the stronger the effect it has on the enzyme.

It is worth working again with the free energy contribution in order to evaluate how the mixed case modifies the free energy between e and x. We adopt the same variable convention of the latter uncompetitive case and defining

$$e_x \equiv [ES] \qquad e_y \equiv [EI] \qquad e_z \equiv [ESI]\,, \tag{6.66}$$

we can write

$$e_y = e\frac{i}{k_{ic}}, \tag{6.67}$$

and

$$k_3(e_0 - e - e_y - e_z)i = k_{-3}e_z \tag{6.68}$$

which can be expressed as

$$e_z = \frac{e_0 - e(1 + \frac{i}{k_{ic}})}{1 + \frac{k_{iu}}{i}}. \tag{6.69}$$

Then the forward/backward rates are

$$r_{\rightarrow} = k_1 es \tag{6.70}$$

and

$$r_{\leftarrow} = k_{-1}(e_0 - e - e_y - e_z). \tag{6.71}$$

The ratio between them becomes

$$\frac{r_{\leftarrow}}{r_{\rightarrow}} = \frac{k_{-1}}{k_1 es}\frac{(e_0 - e(1 + \frac{i}{k_{ic}}))}{(1 + \frac{i}{k_{iu}})}. \tag{6.72}$$

As the ratio for the $i = 0$ case is simply

$$\frac{r_{\leftarrow}}{r_{\rightarrow}} = \frac{k_{-1}(e - e_0)}{k_1 es}, \tag{6.73}$$

the contribution to the free energy of the inhibitor concentration is

$$\Delta G_I = -k_B T \ln\left(\frac{(e_0 - e(1 + \frac{i}{k_{ic}}))}{(e_0 - e)(1 + \frac{i}{k_{iu}})}\right). \tag{6.74}$$

In this case we cannot easily separate the free energy contribution from the en-

zyme concentration. We have to consider again the hypothesis $\frac{d(e_0-e-e_y-e_z)}{dt} = 0$ to obtain

$$k_1 es = (k_{-1} + k_2)(e_0 - e - e_y - e_z) \tag{6.75}$$

and consequently we isolate e/e_0 as

$$\frac{e}{e_0} = \frac{1}{(1 + \frac{i}{k_{iu}})(\frac{s}{k_M}) + (1 + \frac{i}{k_{ic}})}. \tag{6.76}$$

We can substitute rewrite eq.(6.74) as

$$\Delta G_I = -k_B T \ln \left(\frac{(1 - \frac{e}{e_0}(1 + \frac{i}{k_{ic}}))}{(1 - \frac{e}{e_0})(1 + \frac{i}{k_{iu}})}\right) \tag{6.77}$$

and arrange it into

$$\Delta G_I = -k_B T \ln \left(\frac{(\frac{e_0}{e} - (1 + \frac{i}{k_{ic}}))}{(\frac{e_0}{e} - 1)(1 + \frac{i}{k_{iu}})}\right). \tag{6.78}$$

Then we substitute eq.(6.76) obtaining, after some algebra,

$$\Delta G_I = k_B T \ln \left(1 + i(\frac{1}{k_{iu}} - \frac{k_M}{k_{ic} s})\right). \tag{6.79}$$

We can see how for $s \gg k_M$ or $s \to \infty$ we recover the uncompetitive case.

6.2.5 Non-competitive inhibition

The last canonical case is the non-competitive inhibition which is a particular case of mixed inhibition where both inhibition constants have the same value. Then, the inhibitor has the same affinity for the two states of the enzyme. The scheme is simply

$$\begin{array}{ccccc} E + S & \underset{k_{-1}}{\overset{k_1}{\rightleftharpoons}} & ES & \xrightarrow{k_2} & E + P\,, \\ {\scriptstyle k_i}\uparrow\downarrow{\scriptstyle I} & & {\scriptstyle k_i}\uparrow\downarrow{\scriptstyle I} & & \\ EI & & ESI & & \end{array} \tag{6.80}$$

where

$$k_i \equiv k_{ic} = k_{iu}\,. \tag{6.81}$$

It is easy to see that the kinetic M-M equation becomes

$$r = \frac{r_{max}}{(1 + \frac{i}{k_i})} \frac{s}{s + k_M}, \tag{6.82}$$

so in this case we have to consider a variable r_{max} while k_M is maintained as a constant. The contribution to the free energy is, using the general mixed case and using $k_i = k_{iu} = k_{ic}$,

$$\Delta G_I = k_B T \ln (1 + \frac{i}{k_i}(1 - \frac{k_M}{S})). \tag{6.83}$$

Interestingly, for $s = k_M$ the free energy contribution is equal to zero. As the Michaelis constant has the meaning of the concentration at which the enzyme is 50% occupied, it is reasonable to see that the inhibition affects exactly the same to the free and occupied enzyme so the balance between the two populations is unaffected.

7

The external load as an inhibitor in kinesin's motion

7.1 Introduction

In this section it is shown how the formalism of kinetic inhibition can be straightforwardly applied to the case of mechanical loading of molecular motors [43]. Even though in the previous chapter the formalism was already applied to describe the behaviour of a theoretical device, here we introduce all the detailed steps but applied to a real molecular motor: the kinesin-1 or conventional kinesin, using the experimental data from [9]. The main goal is to achieve an analytical expression for the mean velocity of the motor as a function of the two control variables: the ATP concentration, [ATP], and the external load F.

The usual way to introduce the mechanical force in chemical process is based on the mechanical work that the external force exerts along the two chemical states [44]. Let's suppose the reaction coordinate has a certain projection along the axis of motion in such a way that the whole reaction implies an $x-$displacement of $x_A \to x_B$. Then the force f_{ext} produces a work

$$W = f_{ext}(x_B - x_A). \tag{7.1}$$

The whole free energy can be written as [41]

$$\Delta G(f_{ext}) = \Delta G^0 + f_{ext}(x_B - x_A) + k_B T \ln \frac{[B]}{[A]}. \tag{7.2}$$

At equilibrium, $\Delta G = 0$,

$$\Delta G^0 + f_{ext}(x_B - x_A) = -k_B T \ln K_{eq}, \tag{7.3}$$

or, isolating K_{eq},

$$K_{eq}(f_{ext}) = e^{\frac{-\Delta G^0}{k_B T} - \frac{f_{ext}(x_B - x_A)}{k_B T}}. \tag{7.4}$$

In other words, the mechanical force alters the equilibrium constant with an exponential dependence. Now we could use the calculation of ΔG_I for the most general case, which is the mixed case. If the free energy of the inhibitor has to be equivalent to the work performed by the external force, then

$$\Delta G_I = f_{ext}(x_B - x_A), \tag{7.5}$$

so then, using 6.79 we obtain

$$i = \frac{e^{\frac{-f_{ext}(x_B - x_A)}{k_B T}} - 1}{\frac{1}{k_{iu}} - \frac{k_M}{s k_{ic}}}. \tag{7.6}$$

This rude identification leads to a strong-exponential increase of i with increasing loads. This implies that the reaction rate decays exponentially with this load, but this is not in agreement with the experimental data. From [9, 36] we know that the force-velocity curves do not decay in this exponential way but with the opposite curvature, i.e. at low loads the decrease of the velocity is not very strong, but near the stall force value the velocity decays very rapidly. One has to make use of a two or more states model in order to achieve this behaviour, like in Ref.[45]. In this work, the kinesin data is in agreement with a 2-state model where one barrier can be located at $x = 0$ and the other at $x = 1.8nm$. This is interesting as in Ref. [40] there seem to be a $\sim 2nm$ displacement and then another of $\sim 6nm$ long. However, the time spent at this stage is so small that cannot significantly contribute to the global mean velocity. What we want is to give a simple formalism that can be able to describe the mean velocity as a function of the load and

the ATP concentration without the need to introduce potential profiles that do not correspond to proper trajectories. For now we will focus on a more simple and chemically based way of describing the kinetics of kinesin. Our approach is based on inhibition theory and does not need to suppose a split of the step into two displacements.

7.2 Analysis and results

Following the classification of inhibitors described before, we can consider kinesin as a full-reversible-mixed-competitive inhibitor. Full because the load is able to completely stall the motor. Reversible because when the load is not applied anymore the velocity is recovered. Mixed because both v_{max} and k_M change with the load. Finally, it is competitive because the effect of k_{ic} is stronger that the effect of k_{iu}. In other words, $k_{ic} < k_{iu}$. The idea of relating inhibition theory with the effect of kinesin loading comes from a very simple fact. From experimental data of Ref.[9] we can see how the velocity$-[ATP]$ curves agree with Michaelis-Menten equation. Specifically there are three curves, loaded with $1.05, 3.58, 5.63pN$, respectively. In Figure 7.1 we can see these curves with their corresponding Michaelian fit. We already showed in the previous chapter in Table 3.1 the results of the M-M fit of the previous curves.

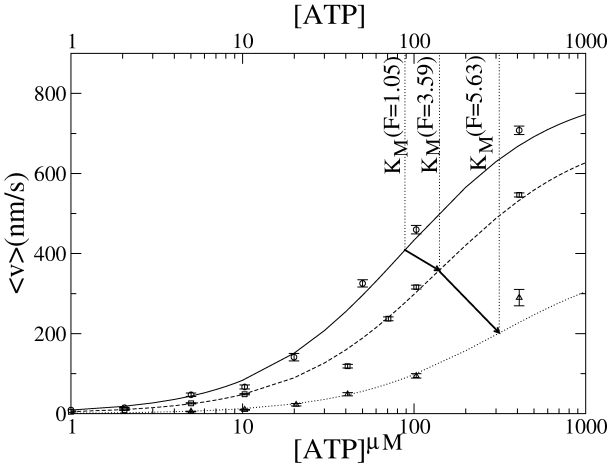

Figure 7.1: **Mean velocity versus ATP concentration.** We can see how k_M is increased with higher loads while v_{max} decreases.

Thus, having different and well defined M-M curves each having its corresponding set of kinetic parameters, it is a temptation to apply inhibition theory, which is classically developed to deal with variable k_M, v_{max} scenario but still within M-M schemes. The only point in order to establish a bridge between this well known chemical kinetic theory and kinesin loading is to connect the mechanical force, f_{ext} or simply $-F$ with the corresponding and in this case effective inhibitor concentration $i \equiv [I]$. We say it is an effective concentration because it is not a real substance diffusing in the media, but a mechanical variable. However, we can write an equation that relates F with i, and then the application of inhibition theory will be straightforward.

First, it is worth analyzing the limits of the desired $F - i$ relation. We shall agree that for $F = 0$ we should recover $i = 0$, i.e. if the motor is not loaded we have a null inhibitor concentration. On the other hand, the motor stalls at $F = F_S$, the stall force value. At this point, the velocity has to vanish, and the only way to achieve it through an inhibitor is strictly having an infinite inhibitor concentration. It is true that this implies an infinite ΔG_I as it can be seen from the expressions in the previous section. But there is a reasonable explanation to consider it as a valid assumption. In the scheme (6.56) we can see how the arrow marked with the constant k_2 has no returning partner as in the case of the arrows k_1, k_{-1}. This means that we are considering the process $ES \to E + P$ as irreversible. In other words, the free energy between these two states is considered as infinite. Naturally, it is an approximation, but a good one: the probability that an ADP molecule and a phosphate group P_i meet in a kinesin binding pocket and that they form an ATP is extremely low. So to consider this process as irreversible even when this implies an infinite free energy difference is reasonable. Consequently, in order to stop the motion it is reasonable as well to consider a infinite ΔG_I given by $i \to \infty$. The question now is how to explicitly write the $i - F$ relation. One can write the most simple equation that satisfies the two limiting cases as

$$i = \frac{1}{\frac{F_S}{F} - 1}. \tag{7.7}$$

We easily check that $i \to 0$ if $F \to 0$ and $i \to \infty$ if $F \to F_S$. Then, the application of inhibition is straightforward now. We only have to apply this relation in order to substitute i by F and then proceed with the analysis of the experimental data.

We will expose now a simple methodology to obtain the values of the parameters from the curves of Ref.[9]. This method was previously used in the first chapter in order to characterize the force-velocity curves in the theoretical inchworm model, but now it is the proper place to understand where all those formulae comes from. There are five parameters: first, the zero-load or natural k_M and v_{max}. Then, the two inhibition constants k_{ic} and k_{iu}. And finally, the stall force value, F_S. All of them are far from being meaningless numbers but significant quantities that are well defined and that provide useful information.

The first step of the analysis consists in fitting the different values of the apparent r_{max} as a function of F. We simply substitute (7.7) into

$$r_{max}(i) = \frac{r_{max}(0)}{(1 + \frac{i}{k_{iu}})} \tag{7.8}$$

and perform a nonlinear fit with the three data points. We show the results in Figure 7.2.

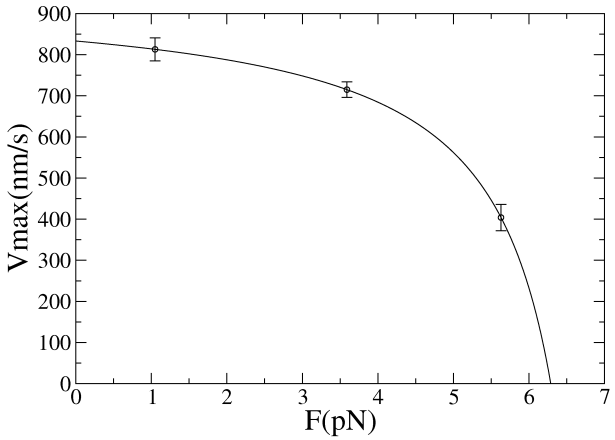

Figure 7.2: v_{max} versus the load. Points are experimental data and the line corresponds to the fit of the data following eqs(6.63) and (7.7).

The reason to begin with the fit of r_{max} data and not with k_M is simple: v_{max} depends only in one of the inhibition constants, the uncompetitive k_{iu}, while k_M depends on both k_{iu} and k_{ic}. Thus we fit the data and obtain that $k_{iu} \simeq 8.04\mu M$ and $F_S \simeq 6.3pN$. Furthermore, the zero-load v_{max} is $\simeq 833.26nm/s$.

Note that now we are using v_{max} instead of r_{max}. The reason is that we have

transformed the velocity of the reaction into a physical velocity. This can be done thanks to the tight coupling ([9]) between the mechanical step and the chemical cycle. We will discuss its validity further in this section.

The next step of the method is to proceed similarly with the data for k_M. Now we can use the values obtained in the previous step in order not to have so many parameters for a three point set of data. We use

$$k_M(i) = k_M(0)\frac{(1+\frac{i}{k_{ic}})}{(1+\frac{i}{k_{iu}})}, \tag{7.9}$$

obtaining the two remaining quantities: $k_M(F=0) = 76.10\mu M$ and $k_{ic} = 1.15\mu M$. As we already anticipated by the increasing of k_M and decreasing of v_{max} with increasing loads, the inhibitor is mixed competitive, i.e. $k_{ic} < k_{iu}$. We show the fit for k_M in Figure 7.3 and summarize the values of the parameters in Table 7.1.

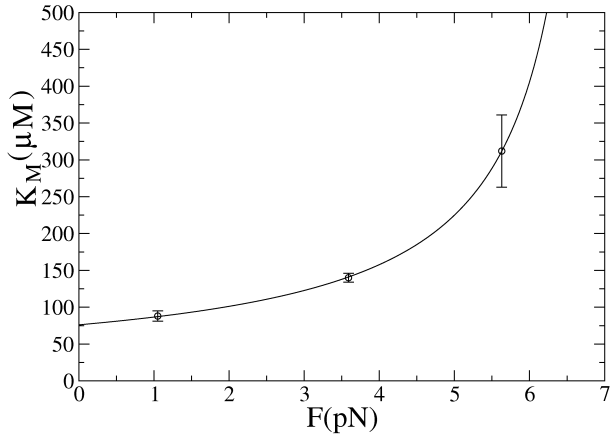

Figure 7.3: k_M versus the load. Points are experimental data and the line corresponds to the fit of the data following eqs(7.9) and (7.7).

At this point we can already write the full expression for the mean velocity as a function of the load and $[ATP]$, which was the main goal of this section,

$$v = v_{max}(i)\frac{s}{s+k_M(i)}. \tag{7.10}$$

We simply use the M-M equation with the variable kinetic parameters that now instead of depending on an inhibitor concentration they depend on a me-

Parameter	Value
$v_{max}(nm/s)$	833.26
$k_M(\mu M)$	76.10
$k_{ic}(\mu M)$	1.15
$k_{iu}(\mu M)$	8.04
F_S (pN)	6.3

Table 7.1: Values of the parameters obtained after the methodology based in mechanical inhibition.

chanical force. We then *plot* this equation for two different ATP concentrations, 5 and $2000\mu M$ (the ones used in the experiment) and see how the agreement is good enough to validate our approach. The curves and the experimental data are shown in Figure 7.4.

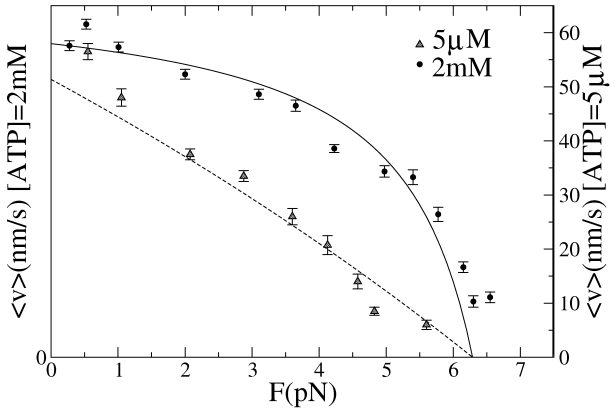

Figure 7.4: Force-velocity curves for $[ATP] = 5, 2000\mu M$. Points are experimental data from Ref.[9] and the line corresponds to the plot of the analytical expression 7.10 obtained in our analysis.

To complete our set of results we focus on two additional aspects. First, it has been measured [36] that using an optical tweezer to assist the motion of kinesin instead of opposing it the velocity does not diverge but saturates not much above $v_{max}(F = 0)$. Within our approach, an assisting load gives $i < 0$, which is not an intuitive value for an inhibitor concentration. The same happens at superstall forces, i.e. when $F > F_S$, also performed in [40]. The limit for high superstall forces and for high assisting forces is $i \to -1$, which means that the effect of inhibition saturates. It seems that we should have added by hand something like $i = 0$ when $f < 0$, so then the velocity would immediately saturate after entering into the assisting regime. However, experimentally it is found that there is some

increasing in the velocity, and our approach is able to qualitatively reproduce this effect. In the next section a quantitative treatment will be applied and it will be seen how, in fact, at zero load there is still a remaining amount of inhibitor that is the responsible for the increase of the velocity at assisting forces. In the context of this approach we restrict ourselves to a theoretical plot of the mean velocity at assisting regimes, as there is no available data in [9]. In the next section we will deal with more complete data in order to compare quantitatively this effect. We show the plot in Figure 7.5. The last feature that we are going to analyze is

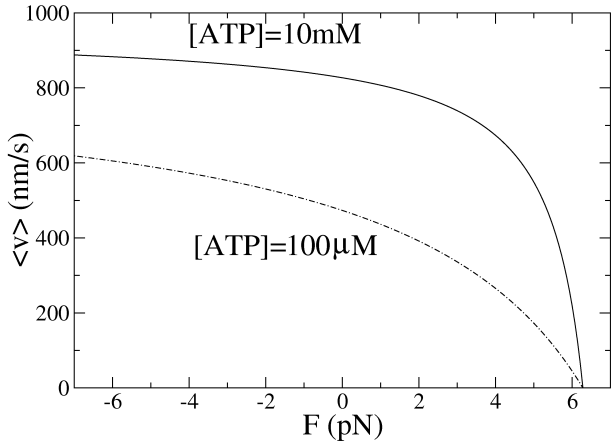

Figure 7.5: Force-velocity curves for opposing and assisting regimes. We can appreciate how the mean velocity saturates at assisting loads.

the randomness parameter, which was defined in eq.(3.7) Interpreting the second moment as a diffusion process we can write

$$r \simeq \frac{2D}{L\langle v \rangle}, \tag{7.11}$$

where $L = 8nm$ is the length of kinesin step. In this relation we see how we only have to fit D in order to obtain a good agreement with the data measured at high ATP concentrations as seen in Figure 7.6. The obtained diffusion constant value is $D \simeq 1350nm^2/s$. It is not very useful to consider $D = k_B T/\lambda$ in this case as we would obtain very high values for the drag coefficient λ and this would be due to reasons previously discussed in the first part of this thesis. What is interesting to see is that for the low $[ATP] = 5\mu M$ case, this approach does not agree with the experimental data (not shown). At high $[ATP]$ and low loads, the randomness is approx. 0.4, which indicates that there are approximately three rate-limiting

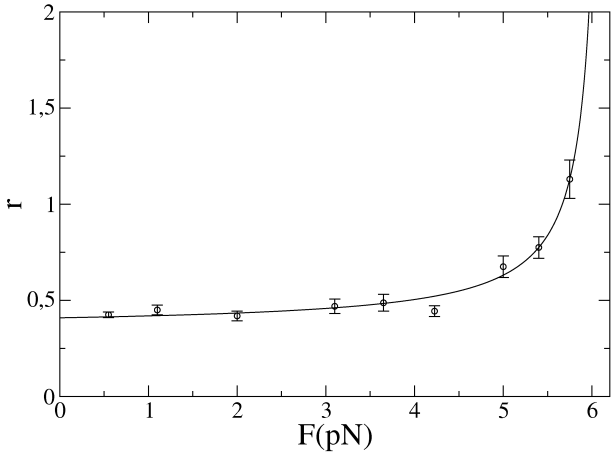

Figure 7.6: **Randomness versus force for** $[ATP] = 2mM$**.** We can notice how the randomness is almost constant until the load approaches the stall force value.

states (maybe diffusive ATP-binding, hydrolysis and phosphate-releasing), while, for high opposing forces and low [ATP], r increases, showing that a single factor becomes the only limiting rate (load and ATP-binding respectively). The r parameter is also related with the mechano-chemical coupling, that is the relation between the full cycle's rate and the physical velocity. As long as the randomness is constant for different loads, the coupling ratio also remains constant. In [9], the value of the coupling ratio was measured as being close to unity, which means that the maximum physical velocity, v_{max}, can be obtained by multiplying the maximum kinetic rate, r_{max} , by the size of the step ($8nm$). However, at high loads, the randomness cannot be considered constant anymore, because of the measured values. Furthermore, r is also interpreted to be inversely proportional to the mean velocity (that decreases with F).

7.3 Discussion

Beyond the simplicity of this approach and its agreement with experimental data, the chemical kinetic scheme proposed here can provide more information concerning kinesin motion. The fact that the load acts as a mixed inhibitor allows us to obtain two quantities that act on different parts of the mechano-chemical cycle. Thus, we can quantify how strong the external force affects the different states of the motor. Specifically, the inverse of k_{ic} quantifies the susceptibility of kinesin

to obtain a new ATP, while $1/k_{iu}$ measures how strong the load acts on ATP hydrolysis and the mechanical power stroke. We see very clearly that is precisely the process of ATP binding what is most affected by the load. In the next section we will interpret this fact as an increase of the entropic barrier that the nucleotide has to surmount in order to reach the binding pocket. This is explained by considering that the cavity is less opened when the load is applied, so the effusion rate in order to pass through the hole is reduced as F increases. What is important now is that we have been able to reproduce the experimental data without drawing a chemical reaction coordinate, so consequently we do not have to deal with the inconvenience of not knowing the isomorphism that transforms the reaction coordinate into the real spatial coordinate that kinesin uses to move along.

We can define again the coupling ratio c in the following way:

$$c \equiv \frac{v_{max}}{L r_{max}}. \tag{7.12}$$

If we suppose that $c = 1$ at $F = 0$ and r_{max} as load-independent, we can interpret, using 7.8, that

$$c = \frac{1}{1 + \frac{i}{k_{iu}}}, \tag{7.13}$$

which would be an evaluation of the load dependence of the coupling ratio. This function is monotonically decreasing and goes to zero when $i \to \infty$. At low loads, however, there is a plateau of an almost constant c while near the stall force c decays very rapidly. Within this interpretation the coupling ratio would almost never be equal to unity but would decrease with increasing loads. It has sense, since after the ATP hydrolysis the trailing head of kinesin is raised in order to reach its next binding site. This process can be strongly affected by the load in such a way that the travelling head cannot reach its target and binds again to its initial microtubule binding site. In such a situation the ATP hydrolysis is performed while the step is not. Thus the coupling ratio, even if maybe decays with the load in a different way that the one we have interpreted here, cannot be equal to unity near the stall force. Moreover, the fact that at superstall forces kinesin steps back while it still continues hydrolyzing ATP indicates that at the stall force regime the coupling ratio must be exactly equal to zero, as ATP hydrolysis is allowed but no net motion is achieved due to the compensation of the

external and the motive forces. This conclusion will be more clear after the developing of the next section, where a more sophisticated approach of this problem is performed.

8

A unified approach

8.1 Introduction

In this section we present a unified phenomenological kinetic framework that describes the load dependence of the different sub–processes contained in the mechano-chemical cycle of a motor protein (either linear or rotatory). It is a double generalization of the formalism shown in the previous section. First, because it can be dealt with a quantitative description of assisting loading regimes and backstepping, and other many features. Secondly, because it is applied to other motors apart from kinesin. This formalism allows us to analyze how the characteristic time of each sub–process is modified due to the presence of an external forcing. Internal, mechanical as well as dwell times are taken into account and joined together in a full-cycle-time where effusion and diffusion rates, viscoelastic friction and overdamped motion are considered. This approach allows the characterization and prediction of the wide variety of force-velocity curves that literature exhibits. We apply our analysis to three real molecular motors for which a complete set of experimental data is available: the bacterial flagellar motor (BFM) [25], conventional kinesin (Kinesin-1) [36] and a RNA polymerase (RNAp) [46]. Moreover, the mechanism of stalling is revised and split into two different concepts that shed light to the understanding of backstepping in Kinesin-1.

Several molecular functions such as directional transport of chemical sub-

stances, active motion, cell division, genetic transcription, etc. are performed by molecular engines. These machines operate as mechanical nanomotors transforming chemical (i.e. nucleotide hydrolysis) or electrochemical potential (ion flux) into mechanical work. Mechanical observables are now experimentally accessible being the mean velocity, linear or angular, the better studied quantity [25, 36, 46, 24, 9, 40, 26]. The behavior of this velocity is evaluated as a function of different and well controlled variables, such as the external load or the concentration of the specific substrate. The obtained force–velocity curves are very useful to analyze biochemical and mechanical properties and are a major criterion for evaluating different theoretical modellings. Several approaches have been proposed such as Kramers rates [44], master equations for chemical steps [45], ratchet-like Langevin equations [47], etc. Kramers–like rates are based in the kinetics to overcome energetic barriers [44, 48, 45]. The reaction coordinate is identified with the direction of motion, or with a projection on this direction, in such a way that when an external force is applied, the barrier increases with the force. In the master equation approach a set of transition probabilities for a set of assumed different chemical steps are proposed. Within this last scheme, mechanical variables such forces and spatial steps are difficult to incorporate and some important assumptions have to be made [45, 43]. On the other hand ratchet–like models are more mechanical but chemical ingredients, such as ATP–hydrolysis, are no so simple to incorporate in this modelling. Nevertheless, it is clear that molecular motors involve chemical and mechanical aspects that cannot be separated and have to be worked together in any modelling.

However, the above mentioned modellings are not the only possible way to study such type of devices. We know that a molecular motor operates in a succession of cycles where each cycle is composed of different subprocesses. Not all of them are necessarily mediated by energetic barriers. There can be entropic barriers [49] or other type of processes that are not directly coupled to displacement of the center of mass of the motor.

In this approach we will focus on the different sub–process that can be relevant in this problem, determining which are dominant and which are less relevant. Our approach has enough generality to be applied to three very different devices: a rotatory motor such as the bacterial flagellar motor (BFM) [25], and two linear motors: a conventional kinesin (Kinesin-1) [36] and a RNA polymerase (RNAp)

[46].

Specifically we postulate that the most relevant quantity is the characteristic time of each subprocess, from which the contribution to the mean velocity can always been obtained. Let t_j be the time (often stochastic) of a subprocess in the motor cycle with a fixed L or $\Delta\theta$ (linear or angular) step displacements per cycle, respectively. Then, if this cycle is composed of the subprocesses $1, 2 \ldots n$, acting in succession, the average total time $\langle t \rangle$ of the cycle can be expressed as

$$\langle t \rangle = \langle t_1 \rangle + \langle t_2 \rangle + \ldots + \langle t_n \rangle, \tag{8.1}$$

and the mean velocity $\langle v \rangle$ or the angular velocity $\langle \omega \rangle$ are,

$$\langle v \rangle = \frac{L}{\langle t \rangle} \qquad \langle \omega \rangle = \frac{\Delta\theta}{\langle t \rangle}. \tag{8.2}$$

Note that these expressions are strictly valid only when the transitions between the subprocesses are irreversible. However, in a protein motor it is reasonable to suppose such an irreversibility, since the chemical-potential differences are considerably bigger than the thermal energy. And even if some backward transitions can be observed experimentally, they don't affect substantially to the mean velocity value. In fact, there is some difference between rotatory motors like F_O or BFM and mechano enzymes like kinesin or RNAp. For the latter type of motors it is quite reasonable to suppose that the products will not meet together inside the pocket and form the product by chance. The probability for this to happen is so small that the irreversibility assumption is well justified, even if this means to use infinite free energies for such a transition. In the rotatory cases, there are mechanical transitions are reversible indeed. But we do take into account such reversibility by using motive forces that instead of being constant they depend on the products and reactants concentration.

From now on we will work with time averages, even though we don't write them explicitly. Since we will assume that both L and $\Delta\theta$ are fixed or known from experimental data, we only have to concern about the subprocess times. The study of fluctuations is a second order improvement not considered in this work in an explicit way, although the effect of temperature is considered in the

process of diffusion. Moreover, without the temperature the free energies that define the motive torque in the rotatory cases would not be justified. This does not mean that higher momenta in the velocity distribution are not important, but a global understanding of the mean value is already lacking, so we will focus on this leaving a more refined description for further work.

We will consider three dominant types of subprocesses, although certainly there are more that may correspond to a second order or more refined description. First, we suppose that there is always a time scale for the motor to perform internal tasks that do not depend either on the external force f_{ext} or the substrate concentration $[S]$. An example of this could be the rate of ADP release in kinesin-1 after ATP binding in the attached head. We call this the *internal time* t_i. The other two subprocesses will be load dependent. On the one hand, the motor needs some time to displace or to rotate in the fluid media. We call it the *mechanical time* t_m which can be evaluated using overdamped dynamics. On the other hand the energetic substrate, i.e. the nucleotides or the ions, employ some time to diffuse and bind the motor. Here diffusion and effusion play an important role, and classical kinetic theory provide theoretical tools to evaluate it. We call this the *waiting time* t_w. All these three characteristic times operate successively in every cycle and are of different nature. We will find the load dependence of these two later times. In particular, the load dependence of the waiting time is the actual core of this work as it allows to describe some crucial questions concerning motor proteins. First, it explains the reason for the increase of dwell times when the load is applied. And secondly, it allows the split of the concept of stall force into two quantities that are different in general. Such difference, as we will see, is the responsible for the existence of a backstepping regime.

Before ending this introduction some comments are in order. Two types of forcing are used in the experiments: conservative and non-conservative. From the three motors that we will analyze in this work, two of them use a conservative force (kinesin and RNAp) and one uses a non-conservative force (BFM). When utilizing optical tweezers (kinesin, RNAp), the applied force is directly a momentum transfer to the bead and, by extension, to the motor. Thus one can obtain the work performed by the motor by simply multiplying the value of the force by the total displacement. In the non-conservative case, the forcing is introduced

through different bead sizes and its corresponding non conservative Stokes friction forces. The substrate that attaches molecular motors is quite different from motor to motor. In BFM is a flux of ions forced by an electrochemical potential, while in kinesin of RNAp are NTP–like nucleotides.

8.2 Theoretical approach

In this subsection we present a detailed analysis of the three main time scales already introduced. Each characteristic time will be treated separately in order to address its specific processes involved.

Mechanical and internal times

Molecular motors move in a viscous media where inertia is suppressed by the friction. As a result, the dynamics is governed by the second Newton's law without the acceleration term. At lowest order, thermal fluctuations are not required to obtain explicit predictions for the motor mean velocity. For an overdamped motor which is able to exert a constant motive force f_m along a single direction, the mean velocity can be written as

$$\langle v \rangle = \frac{1}{\gamma_t}(f_m + f_{ext}) \tag{8.3}$$

where f_{ext} is the external load and γ_t the translational drag coefficient. A negative value of f_{ext} signifies useful work from from the motor. Note that in previous sections we have used both F and f_{ext} in order to describe the load. We think it is useful to think is as a positive quantity when we think it is a load, but when we think it as a external force opposed to motion then it is more natural to think it as a negative quantity. However, from now on we deal with assisting, opposing and backstepping regimes, so we cannot be ambiguous anymore. We will always use f_{ext} and we recall that $f_{ext} < 0$ represents the regime of useful work, while a positive value is for assisting loads. We also have to mention that now we cannot neither be ambiguous with the value of the stall force. As now there will be two different type of stalling we simply write f_m as the motive force, and occasionally we can have $f_m + f_{ext} = 0$, but as this is not the only way to do $\langle v \rangle = 0$ we cannot write f_S instead of f_m. In previous modeling there were only a single

interpretation of the stall force and then the identification $f_m = f_S$ was justified, but in fact this quantity is actually representing the motive force of the motor and not the value at which the motor is stalled. We will see how in kinesin-1 there is a regime where $f_m + f_{ext} < 0$ and motion is still allowed (backwards). The reason, that will be clarified later on, is that the entropic stall force is not reached yet. From eq.(8.3) we can get the expression of the mechanical time,

$$t_m = \frac{\gamma_t L}{f_m + f_{ext}}, \tag{8.4}$$

where the mechanical stall force is found at $f_m + f_{ext} = 0$.

In the case of a rotatory motor (with no conservative forces) we have instead,

$$(\gamma_r + \gamma_{ext})\omega = \tau_m, \tag{8.5}$$

where γ_r is the rotational drag coefficient of the motor, γ_{ext} if the friction of the bead attached to the motor and τ_m the motive torque. The mechanical time is obtained as in eq.(8.4).

From equations (8.3) and (8.5) one can define the maximum physical velocities in the absence of a load,

$$\langle v \rangle_m = \frac{1}{\gamma_t} f_m, \qquad ; \qquad \langle \omega \rangle_m = \frac{1}{\gamma_r} \tau_m. \tag{8.6}$$

It is worth mentioning that the above analysis is obviously incomplete and we need to consider additional types of subprocesses in the cycle. Indeed, the mechanical time alone cannot be responsible for the mean velocity values observed experimentally for linear motors, while for rotatory motors it is better to use a more sophisticated expression such as in Ref. [25]. Let us start with a simple analysis of this problem. First we take that the viscosity of the water is $\eta = 10^{-9} pNs/nm^2$, and the translational drag coefficient is $\gamma_t = 6\pi\eta R$, where R is the radius of the molecule. Using these data we can estimate approximately the maximum velocity expected in kinesin-1 or in RNAp. Silica beads in these cases have typically $R \sim 0.5\mu m$. In kinesin experiments, typical motive forces are of the order of $5pN$ if one consider similar to stall force values, and as a results we expect $\langle v \rangle_{max} \sim 500\mu/s$, which is a value more than 500 times the experimentally measured maximum velocity. For the RNAp, typical forces are

approximately $25pN$. We can then make an estimation of $\langle v \rangle_{max} \sim 2500\mu/s$, a value that is about $5 \cdot 10^5$ times the experimental velocity. From the above calculations it follows that other times scales are involved in the cycle.
The next simple correction to the mechanical time is to assume the existence of an internal time. In fact, every motor needs a time to perform internal jobs that are not necessarily force or substrate-dependent. During this time, internal processes are performed.
For example, in kinesin-1 the rate of phosphate release in the microtubule-attached head or the rate for ADP release in the other head may be candidates for such type of processes. In BFM, the time for the ion to cross the membrane does not necessarily depends on the potential difference between both sides. In general, if there were no such processes, at zero load (or at high assisting forces) and at very high substrate concentrations, the mean velocity would not saturate to a finite value. In this saturating regime, the maximum velocity is approximately proportional to the inverse of these internal times. Then, we denote this time by t_i and we assume it takes a constant value specific of each motor. As a result, the total mean time $\langle t \rangle$ for a cycle is $\langle t \rangle = t_i + t_m$, while the mean velocity (8.2) becomes,

$$\langle v \rangle = \frac{L}{t_i + \frac{\gamma_t L}{f_m + f_{ext}}}. \tag{8.7}$$

In Figure 8.1 we plot force-velocity curves where the influence of the internal time is manifested in reducing the final velocity.

Waiting times: the pocket model approach

Checking the experimental data of any molecular motor it becomes clear that both mechanical and internal times are not enough. We have to consider that there is a certain time used to wait for the substrate which is diffusing in the media. Experimentally, it has been found that the waiting times follow Poisson distribution with, for example, a mean time of about 50ms in the case of highly loaded kinesin [7, 40]. If the substrate concentration is low, these times will increase, while for a very high concentration are reduced, but never this time goes to zero.

After substrate binding, some chemical sub–processes take place. The kinetics

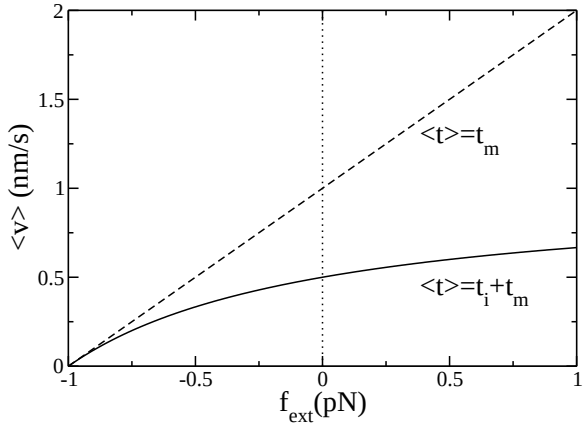

Figure 8.1: Mean velocity $\langle v \rangle$ versus an external force f_{ext}. Dashed line for a process with only mechanical time. Continuous line for a process with mechanical and internal time. For the sake of simplicity, we have chosen $L = 1nm$, $\gamma_t = 1pNs/nm$, $f_m = 1pN$ and $t_i = 1s$.

of these steps is described by the so-called Michaelis-Menten equation, which states that the velocity of reaction involves two different time scales where the substrate binding follows the mass action law.

Moreover it has been observed that this waiting time increases with an opposing load [9]. This is quite a surprising fact. If the load is applied to the motor without affecting the substrate conditions, why does the substrate take longer to reach the motor when the load is applied? Some explanations have been proposed [45, 43] and the most used was to consider that a barrier has to be surmounted by the substrate in order to reach the binding site. Consequently this barrier has to depend on the position and has to be modified by the external force. However, the justification of an energetic wall is not clear, as it does not provide a microscopic explanation. We think that it is more appropriate in this case to assume an entropic barrier as in Ref. [49] , without needing to assume a displacement of the center of mass of the motor associated to such process. Maybe it would be more complete to include energetic or enthalpic terms, but we will see how the entropic contribution is enough to describe the data at least in a first order approach. Essentially, we don't want to incorporate but the minimum necessary ingredients. Basically, an entropic barrier is usually related with effusion-like processes. While the energetic barrier concept is introduced to describe the rate at

which thermal fluctuations help a particle to surmount an energetic obstacle like advancing against an external field, the entropic case is introduced to describe the rates for the same particle to have a specific position and velocity. For example, the rate of escaping through a hole or the rate of entering into a cavity can be understood in terms of entropic barriers, even if the particle inside or outside the cavity has the same enthalpic energy. Consequently, we think that the time that the substrate spends finding and entering into the pocket is a quantity that should be described in terms of entropic walls.

Thus, let's consider that the binding site is a cavity where the substrate has to enter (Fig. 8.2), as it was claimed in [50]. Then, under the influence of an opposing load, the cavity may be strained and thus less accessible to the substrate. This means that the binding process can be interpreted as an effusion process where the load controls the area of the hole to enter the substrate. Then, a different stall force (here entropic) can be defined, as the force that completely closes the pocket and accordingly the waiting time becomes infinite. This concept of entropic stalling is different from the mechanical stall force, where the opposing load equilibrates the motive force of the motor. Our analysis thus predicts that the motor can be stalled by two different mechanisms.

To implement analytically this idea we propose the simple mechanism shown in Figure 8.2.

In order to give an expression for the rate of the substrate entering into the pocket we shall consider a pocket which has a hole of area, $a\delta x$, where a is the width and $\delta x = \delta x(f_{ext})$ is the load dependent aperture of the hole. Then the effusion time for a small diffusing particle to enter into the hole is inversely proportional to the substrate concentration and to the opening area of the cavity, i.e. $\propto \frac{1}{a[S]\delta x}$. Note also that the size of the substrate is comparable with the opening of the pocket, so there is a certain orientation for the molecule to match the cavity (as illustrated in Figure 8.2). This is the effect of final adhesion to the pocket, which is supposed at first approximation to be dependent on the accessible surface but independent on the substrate concentration. Consequently we have to include this effect as a constant contribution $\sim 1/\delta x$. Adding these

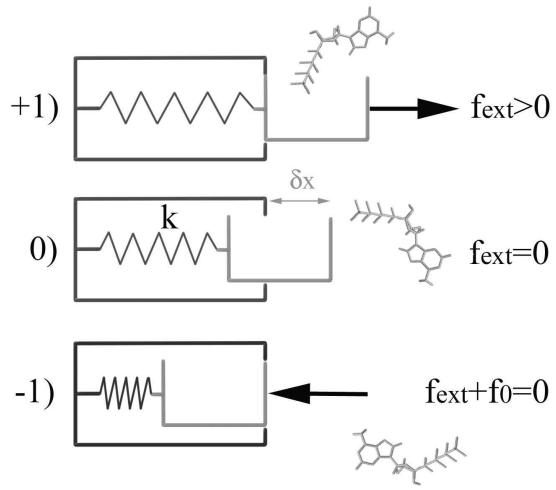

Figure 8.2: Scheme for a simple linear pocket model, given by a box with an opening door that depends on the external load. In 0) we have the pocket without load, and it has a certain natural opening. In +1) we can see the extreme case for an assisting load, where the pocket is totally opened and the substrate, represented here by an ATP molecule, can easily bind the cavity. Finally, in -1) we can see the effect of a large opposing force. For $f_{ext} = -f_0$ the cavity becomes completely closed.

two time scales and grouping the free parameters, the waiting time is ,

$$t_w = \frac{1}{\delta x}(A + \frac{B}{[S]}), \tag{8.8}$$

where A and B are two constants to determine. This is no more than a quite general expression for the mass action law. Notice that the independent term, proportional to A, is substrate shape dependent but $[S]$-independent. To illustrate this idea, we can consider the case of Uracile base in RNAp. For a given pocket, four different substrates can bind it, and all of them have different binding rates. Despite their molar mass and Graham's law effects, the Uracile nucleotide UTP has a very low rate considering that it is a relatively light nucleotide. It has an addition rate about three times slower than CTP, which is very similar in molecular weight. Surely this is due to orientation and steric contributions near the pocket. In the Appendix B1 we justify the explicit form of eq.(8.8) by establishing an equivalence between this waiting time and a mixed inhibition scheme in enzymatic theory. Using 8.8 we arrive to the formalism presented in the previous section, so such an equivalence provides consistency to this form of the waiting

time.

The point now is to guess how this time has to depend on the external force. We can assume, following Fig.8.2, that the pocket has an elastic opening that is stressed when the load is applied. Assuming a linear spring we can propose the dependence,

$$\delta x = \frac{f_0 + f_{ext}}{k}. \tag{8.9}$$

where k is the effective stiffness and f_0 corresponds to the entropic stall force: when $f_{ext} = -f_0$ the hole is closed. For $f_{ext} = 0$ we have the natural opening, and for $f_{ext} > 0$ the hole has more accessible surface.

In Figure 8.3 we show plots of the mean velocity when internal and waiting times are joined. We show force-velocity curves for three different substrate concentrations. One can note that the curvature of the plots strongly depend on the concentration. The reason for the plateau in the high concentration case is that the substrate binding is not rate limiting, as it was experimentally observed [36, 9].

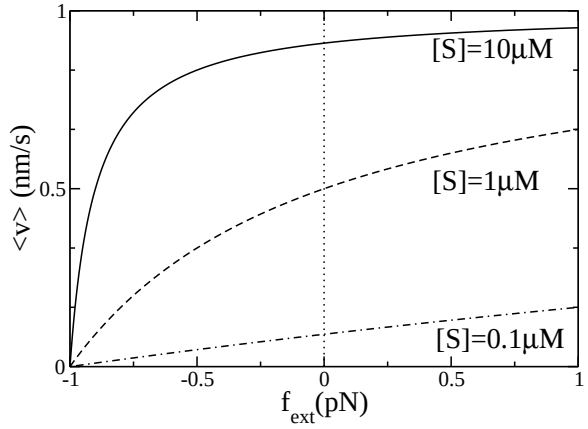

Figure 8.3: Mean velocity versus external force when we have an internal time plus a waiting time, i.e. $\langle t \rangle = t_i + \frac{C}{[S](f_{ext}+f_0)}$. We set $t_i = 1s$, $f_0 = 1pN$ and $C = 1s \cdot pN \cdot \mu M$. Continuous, dashed and dash-dotted lines correspond to $[S] = 10, 1, 0.1\mu M$, respectively.

Although the linear spring pocket model is very useful to illustrate the idea of

the pocket kinetics, it is convenient to introduce a more sophisticated version of the model in order to have more accurate predictions. However, the philosophy remains exactly the same. Instead of a linear spring response it is more realistic to consider a nonlinear response of the pocket that is still linear at low forces and bound at extreme loads. This is achieved by using a sigmoidal function,

$$\delta x = \frac{l_x}{2}[1 + \tanh\,(\frac{2}{kl_x}(f_0 + f_{ext}) - 1)], \tag{8.10}$$

where l_x is the longitudinal size of the pocket. We can see how we recover the linear case for $\tanh x \sim x$. Then, we still can talk of a stiffness of the pocket. The price is the introduction of a new parameter, l_x.

In Figure 8.4 we plot the dependence of δx under an external load. The main difference between the linear and the sigmoidal cases is that in the latter case the pocket never closes completely.

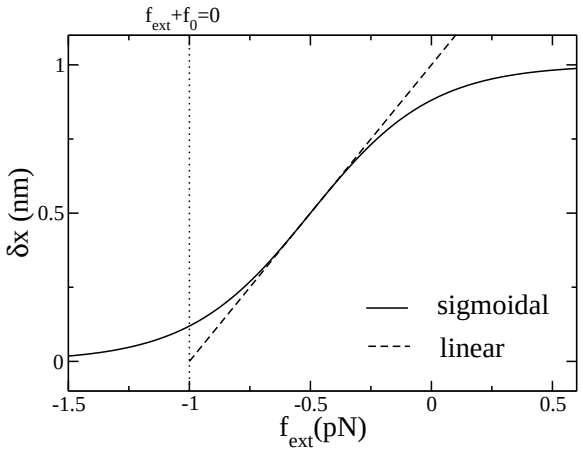

Figure 8.4: Opening of the pocket as a function of the external load. Solid line corresponds to the sigmoidal version, while dashed corresponds to the linear case. All the parameters are set equal to unity.

The generic formula

Once we have all the times involved in a single cycle, we can write down the whole expression (8.1)–(8.2) for the velocity of a linear motor as a function of $[S]$

and f_{ext},

$$\langle v \rangle = \frac{L}{t_i + \frac{\gamma_t L}{f_m + f_{ext}} + \frac{1}{\delta x}\left(A + \frac{B}{[S]}\right)}, \tag{8.11}$$

with δx given by expressions either (8.9) or (8.10). For a rotatory motor we can write the equivalent expression as,

$$\langle \omega \rangle = \frac{\Delta\theta}{t_i + \frac{\Delta\theta(\gamma_r + \gamma_{ext})}{\tau_m} + \frac{1}{\delta x}\left(A + \frac{B}{[S]}\right)}, \tag{8.12}$$

where δx will be considered a constant for the case of BFM analyzed in this work. These last two equations are the main result in this paper. We will start now analyzing the consequences and properties of these formulas.

As we have predicted before, there are two possible values of the external force that can stall the motor, i.e. f_0 and f_m. When f_{ext} equals one of these values with opposite sign, then the motor stalls either entropically or mechanically, respectively. If $f_{ext} + f_0 = 0$, then $t_w \to \infty$ and the velocity vanishes because no substrate can bind the pocket. If $f_{ext} + f_m = 0$, $t_m \to \infty$ and then the motive force cannot drive the motor anymore. This scenario is interesting since the experimental definition of stall force f_S is unique, that is, the force at which the motor stops.

Let's analyze the three possible cases. If $f_m = f_0$, both stall forces are the same. When, $f_m > f_0$, the first limiting factor would be entropic. This means that even if the motor could exert more force, no substrate can bind the pocket and no motion is produced. The last case occurs when $f_m < f_0$. This is the most interesting, because when the motor is mechanically stalled, it still can bind substrate. Moreover if we apply now a load such that $f_{ext} + f_m < 0$ but $f_{ext} + f_0 > 0$, then the motor will tend to move backwards but still consuming the energy of the substrate. To characterize analytically this backstepping we write expression (8.11) as,

$$\langle v \rangle = \frac{L}{t_i + \frac{\gamma_t L}{f_m + f_{ext}} + \frac{A}{\delta x} + \frac{B}{\delta x [S]}} sign[f_m + f_{ext}] \qquad f_0 + f_{ext} > 0, \tag{8.13}$$

where the sign of the resulting balance force is taken into account. With this simple modification, we can see what are the conditions for backstepping to occur,

remarking that for the sigmoidal response of the pocket this condition holds for a broader spectrum of opposing forces. In Figure 8.5 we show plots for the three cases discussed above.

As we can see, the concept of stalling can be split into two different ways of

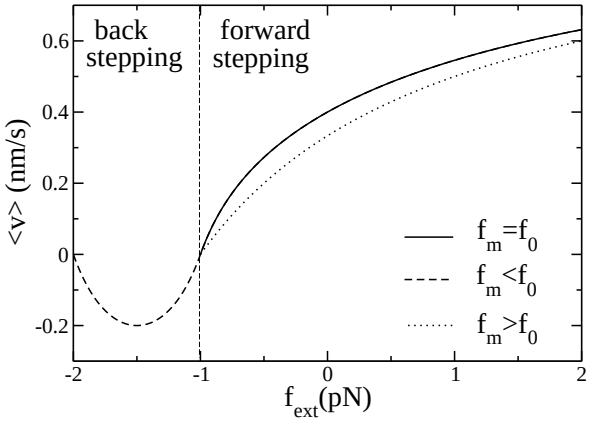

Figure 8.5: Mean velocity versus the external force for a linear response of δx under a load. Now we have internal, mechanical and waiting times. We set all the parameters fixed and equal to unity except f_m and f_0. Continuous line corresponds to a $f_m = f_0 = 1pN$ case. Dashed line corresponds to $f_m = 1$, $f_0 = 2pN$. Dotted line corresponds to $f_m = 2$,$f_0 = 1pN$. Note that all the continuous path holds also for dashed-line values. Both solid and dotted don't have values below $-1pN$. Note the negative velocity section for the dashed-line.

stopping the motor by applying an external force. In Ref.[40] backstepping in kinesin-1 is observed when loaded with very large and negative forces. Despite the reversibility of the motors like the F_O-F_1-Synthase, kinesin-1 does not hydrolyze ATP when walking backwards but it keeps on consuming the energy from the nucleotide. In such a situation, the external mechanical force is greater than the motive force, but the cycle of ATP consumption is not stalled yet. This is the main reason to make such discrimination. We think that the mentioned experiment shows that in kinesin-1 the mechanical stall force is considerably lower than the force required to stop the ATP hydrolysis cycle, i.e. $-f_0$.

8.3 Results

Our aim now is to use the experimental data of velocity versus substrate concentration and load of a particular motor to fit our formula and get the values of the free adjustable parameters. With this information we can guess which features are specific of a particular motor or which ones are common between two or all of them. It is expected that kinesin and RNAp will exhibit a considerable amount of similarities as both are mechanical enzymes powered by nucleotides.

8.3.1 A non-conservative force: the bacterial flagellar motor (BFM)

The bacterial flagellar motor is a rotatory device that performs a torque on an helical flagella to propel the cell. It uses the electrochemical potential across the cytoplasmic membrane to perform the work. This type of engine works with a flux of protons in *Escherichia Coli* and Na^+ ions in alkalophiles and *marine Vibrio* species. Several experiments have been able to track their rotation by different techniques [25, 26] but only very recently [24] discrete steps have been observed. We will focus our attention toward Ref.[25] because they provide a wide and complete set of measurements that can be incorporated in our theoretical framework. In this experiment, a silica bead is attached to the flagellar filament. Then, rotating frequency of this bead is measured through a quadrant photodiode. The applied load is modulated through different sizes of the bead, thus the forcing is simply friction, and then the load is not conservative.
The substrate of this particular motor is the sodium Na^+ ion density gradient, which crosses the cytoplasmic membrane of the cell producing the rotation of the flagellar motor. Across the membrane, there is an electrochemical potential, which is the responsible for the *smf* (Sodium motive force), which we will write like τ_m.

We now proceed to calculate all the values for the different free parameters of the model. First, we need to know which is the step angle $\Delta\theta$ for each crossing ion, if there is a tight coupling between them. It is known [21] that BFM have different and independent torque generating units. The number of the units, depending on the particular device, can be from 5 to 9 in alkalophilic Bacillus, 5 to 8 in

V. alginolyticus[25] and at least 11 in *Escherichia coli*[21]. It is also known that about 1000 Na^+ ions [25] or 1200 protons [24] are required to perform a whole revolution of the motor. Focusing on sodium ions data, we can estimate the angle per ion,

$$\Delta\theta \sim \frac{2\pi}{1000} \sim 0.006 rad/Na^+. \tag{8.14}$$

The chemical free energy due to the concentration difference between both sides of the membrane can be written as

$$\Delta G_{chem} = -k_B T \ln \frac{[Na^+]_{ext}}{[Na^+]_{int}}, \tag{8.15}$$

where $k_B T \simeq 4.1 pNnm$ is the thermal energy, $[Na^+]_{int} = 30mM$ the ion concentration inside the membrane, and $[Na^+]_{ext}$ is the external concentration, which is modulated in the experiment. The concentration gradient between $[Na^+]_{int}$ and $[Na^+]_{ext}$ imposes an electrostatic gradient as well. The free energy for this effect is given by the membrane potential $\Delta\Psi$, which is about $-150mV$. The total free energy is then

$$\Delta G = -k_B T \ln \frac{[Na^+]_{ext}}{[Na^+]_{int}} + \Delta\Psi. \tag{8.16}$$

We choose to use energy units in pN.nm. We have then, $1mV = 0.16 pN.nm/e$ and $\Delta\Psi = -24 pN.nm/e$. We substitute the previous values of the parameters to obtain

$$\Delta G = \left[-10.055 - 4.1 \ln [Na^+]_{ext}\right] pN.nm. \tag{8.17}$$

Now we can write the motive torque τ_m as

$$\tau_m = \frac{-\Delta G}{\Delta\theta}. \tag{8.18}$$

As the value we already have for $\Delta\theta$ is not precise yet, we can obtain another estimation and compare it with the previous one. From the experimental data we know that for different Na^+ concentrations we have values for the torque which can be fitted from the experimental data in Ref. [25],

$$\tau_m \sim C_1 + C_2 \ln [Na^+]_{ext} \tag{8.19}$$

where $C_1 = 1464\,pN.nm$ and $C_2 = 586\,pN.nm$. We can see how these values correspond to different estimations of $\Delta\theta$. As the thermal energy is well known, C_2 is used to give $\Delta\theta = 7{\cdot}10^{-3}$, in a good agreement with our previous estimation. On the other hand, the independent term can be used to give a more precise value for the membrane potential, $\Delta\Psi = -151.2\,mV$, which is agreement with the value given in the Ref.[25].

We can now write down the frequency ν of the motor as a function of the external sodium concentration and of the external torque, which is no more than Eq. (8.12) divided by 2π,

$$\nu = \frac{\Delta\theta/2\pi}{a_0 + \frac{a_1}{[Na^+]^{\lambda}_{ext}} + \frac{\gamma_r \Delta\theta^2}{10.245+4.1\ln[Na^+]_{ext}-\Delta\theta\tau_{ext}}}. \tag{8.20}$$

We recall that in the case of BFM motor we consider δx as a constant. There are some reasons to justify it. First, ions are considerably smaller than nucleotides, and they don't need a specific binding orientation, so a possible small decrease in the cross section of the cavity should not appreciably affect the rate on entrance. Secondly, in this motor the torque is transmitted through the torsion of the connecting axis which is faraway from the cavities, which are not necessarily deformed then. But the main reason is that this non-conservative force is not active when the motor is not rotating, i.e. the bead does not perform a torque: it is resistant to it. Consequently we cannot exactly know whether a conservative force experiment would show that waiting times are appreciably affected by the load. On the one hand a_0 accounts for the sum of internal and for the adhesion time, put together since they do not depend on the load here. Then, $a_0 = t_i + A/\delta x$. On the other hand a_1 modulates the influence of the effusive part of the waiting time, $a_1 = B$. Here λ is the exponent of the law of mass action, which is not necessarily 1 when there is more than one torque generating units. When different active sites are in cooperation the Michaelis-Menten equation is transformed by powering the substrate concentration to a quantity called the Hill exponent λ. In fact, we will use $\lambda = 0.8$ which clearly fits better the frequency-concentration curves as seen in Figure 8.6 for very low ion concentrations. This suggests that the different torque generating units of the motor are in negative cooperation. In this motor we have not assumed that the waiting time depends on the external torque but only on the ion concentration. This is consistent with a picture where the ions don't have

any difficulty to enter into the cavity.

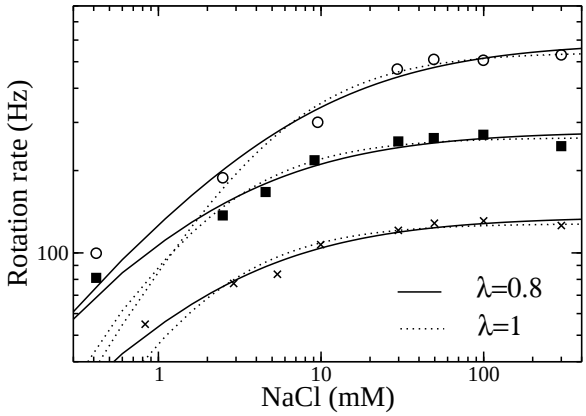

Figure 8.6: Mean rotation rate versus $[Na^+]_{ext}$ concentration. Open circles, filled squares and crosses correspond to beads of diameter 0.60, 0.85 and 1.08 μM respectively. Dotted lines are standard M-M fits. Solid lines correspond to a generalized interpretation of the law mass action, i.e. the rate of a reaction is proportional to $[S]^\lambda$, where if $\lambda = 1$ we recover the classical version. For solid lines we use $\lambda = 0.8$, which is in more agreement with the data at low substrate concentrations.

In Figure 8.7 we plot the frequency-torque curves for the fitted values of Table 8.1. There are three cases which correspond to different ion concentrations. Note that in this case, it is found in the literature plots of the torque versus frequency. We only invert the expression to plot the data as it is presented in the original reference. The overall agreement is reasonably good considering the error that is introduced by the considerable technical difficulties of the experiment.

Parameter	Value
$\Delta\theta$	$7 \cdot 10^{-3} rad$
γ_r	$0.1 pNnms/rad$
a_0	$1.2 \cdot 10^{-6} s$
a_1	$7.5 \cdot 10^{-6} smM^\lambda$
λ	0.8 (dimensionless)

Table 8.1: Values of the parameters for the flagellar motor obtained by fitting Eq. (8.20) to the experimental data of Ref. [25].

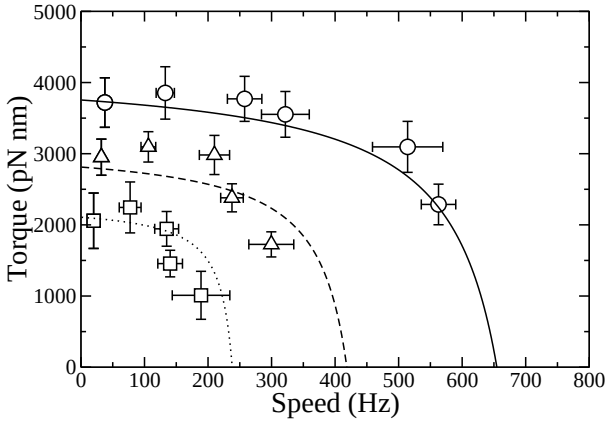

Figure 8.7: Frequency versus the generated torque for the flagellar motor. Hereafter, points are always experimental data and lines are predictions. Circles, triangles and squares correspond to 50,10 and 3mM sodium concentrations respectively. Notice how the stall torque is $[Na^+]_{ext}$ dependent.

8.3.2 A conservative force: kinesin-1 and RNAp

In this section we will simultaneously deal with two examples of molecular motors: the kinesin-1 and the RNAp, whose physical properties can be measured experimentally with optical trapping [36, 46]. These motors have a certain amount of similarities and differences that our approach can discriminate extracting relevant information and interesting conclusions.

Both machines are linear motors walking along unidimensional and polar tracks. They hydrolyze nucleotides in well localized pockets, and most important for our purposes: both motors have waiting times that strongly depend on the load. As the external force is conservative we can also study the case of assisting loads, so we can obtain a wider response spectrum of the motor in the presence of a variety of forcing.

We start using the well known facts: kinesin performs $8nm$ steps and stalls with forces of approximately $\sim 5pN$, while RNAp performs $0.37nm$ steps and stalls with forces of $\sim 25pN$. While kinesin hydrolyzes ATP, RNAp can consume the four types of nucleotides ATP, GTP, CTP and UTP, generally expressed as NTP's. In the experiment for RNAp, NTP concentrations are chosen in such a way that all the nucleotides bind the pocket with same rate. This set of relative

concentrations is called $[NTP]_{eq}$.

First we will focus our attention to kinesin-1, using the experimental data of Refs.[9, 36]. The expression derived in (8.11) can be rewritten in a Michaelis–Menten form (identifying $[S] = [ATP]$),

$$\langle v \rangle = \frac{v_{max}[ATP]}{k_M + [ATP]}, \tag{8.21}$$

where,

$$v_{max} = \frac{L}{\frac{A}{\delta x} + t_i + \frac{\gamma_t L}{f_m + f_{ext}}} \tag{8.22}$$

and

$$k_M = \frac{B}{A + \delta x \left(t_i + \frac{\gamma_t L}{f_m + f_{ext}} \right)}. \tag{8.23}$$

As both k_M and v_{max} are affected by the external load, we can interpret the effect as a mixed inhibition, as reported in Ref.[43]. We provide the proof in the Appendix B2. Now we proceed to fit this expression with the experimental data to get the free parameters. One first interesting result is that γ_t is very small and consequently it implies that the mechanical characteristic time which is much lower than the other times. Thus setting $\gamma_t = 0$, the equation for the velocity is,

$$\langle v \rangle = \frac{L}{t_i + \frac{A'}{1 + \tanh\left(C'(f_0 + f_{ext}) - 1\right)}} \frac{[ATP]}{[ATP] + \frac{B'}{A' + t_i \tanh\left(C'(f_0 + f_{ext}) - 1\right)}}. \tag{8.24}$$

where

$$A' \equiv \frac{2A}{l_x}, \qquad B' \equiv \frac{2B}{l_x}, \qquad C' \equiv \frac{2}{k l_x}, \tag{8.25}$$

and the sigmoidal response of δx has been used. We show in Table 8.2 the values that fit better the experimental data. It is important to remark that we haven't found a constant value for f_0. Specifically, we have found that it depends on ATP concentration in a way that we have approximated as logarithmic. This can be interpreted as the effect of the entropic contribution in the total free energy,

$$\Delta G = \Delta G^0 + k_B T \ln \frac{[ATP]}{[ADP][P_i]}. \tag{8.26}$$

Some additional information can be extracted from the value of C'. If we

Parameter	Kinesin	RNAp
γ_t	$\sim 0pNs/nm$	$\sim 0pNs/nm$
t_i	$0.003s$	$0.034s$
A'	$0.0178s$	$0.016s$
B'	$1.27\mu Ms$	$1.5\mu Ms$
C'	$0.45pN^{-1}$	$0.04pN^{-1}$
f_0	$3.6 + 0.28 \ln [ATP]pN$	$13.53pN$

Table 8.2: Values of the parameters for kinesin and RNAp motors.

consider that l_x is of the order of ATP size, $\sim$ 15Å. Then $k \sim 2/(1.5 \cdot 0.45) \sim 3pN/nm$, which gives an idea of how stiff is the pocket. In Figure 8.8 we can see how our calculations and the experimental data fit together.

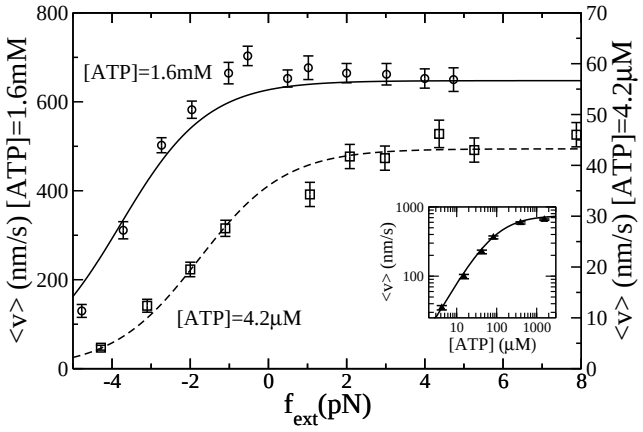

Figure 8.8: Mean velocity versus the external force for the kinesin. Left vertical labels, solid lines and open circles(O) correspond to $[ATP] = 1.6mM$, while right vertical labels, dashed lines and open squares($\Box$) correspond to $[ATP] = 4.2\mu M$. In the inset, we can see the mean velocity versus ATP concentration in the absence of external load. Lines are plots of eq.(8.11) using data from Table 8.2 .

Now we perform a similar analysis to the RNAp motor. Again we obtain that we can neglect the mechanical time. Now $L = 0.37nm$ and $[S] = [NTP]$. In Table 2 we show the best fitted values values of the free parameters which can be compared with the kinesin ones. In Figure 8.9 we can compare our calculations using Eq. (8.11), with the tabulated parameters, versus the experimental results of Ref. [46] for four different NTP concentrations.

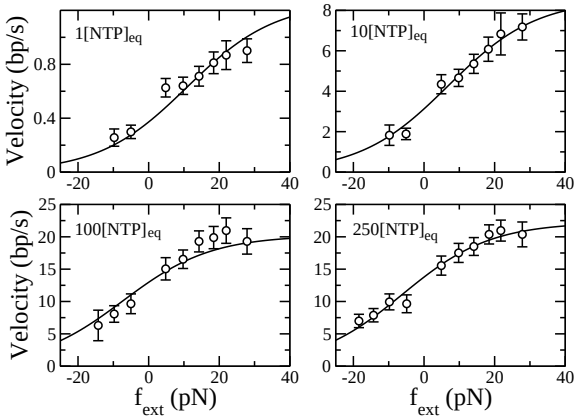

Figure 8.9: Mean velocity, measured in bp/s, versus external force for RNAp. Left-top, right-top, left-bottom and right-bottom correspond to $[NTP] = 1, 10, 100$ and $250[NTP]_{eq}$, respectively. Lines correspond to the theory (8.11) and data of Table 8.2.

8.4 Conclusions and discussion

In BFM, our theory reveals that there is no need for a load-dependent waiting time, as the sodium ions diffuse rapidly into the motor. Maybe extremely low ionic concentrations would require the introduction of such dependence, but it was not needed in the scale of the experiment of Ref.[25]. It is stated in Ref.[51] that every model for BFM must include the soft linkage between the motor and the viscous load. This assumption is based on the compliance of the hook, which is measured in [52]. However, we don't need to use such fact to justify the existence of the plateau region of the motor torque-speed curve. This plateau, which is nothing but a rapid decay of the velocity at high loads, can be explained by considering that the mechanical time slightly increases at low loads while it diverges near the stall torque, and consequently it is not necessary to consider two straight lines to fit the data as in [51]. The concept of knee velocity point discussed in that reference can be understood as the torque value from which the mechanical time begins to dominate over the other processes, but it is not a kind of singular point in the curve.

Moreover, the coupling ratio in the BFM is probably 1, i.e. a single ion is tightly coupled with the rotation, but there is not conclusive evidence for such

an assumption. In Ref. [24] they measure $0.24\,rad$ steps, which correspond to 26 steps per revolution. This is precisely the periodicity of the FliG protein in the structure. However the existence of a smaller periodicity in the steps is not discarded yet. It is estimated that around 1000 ions are needed to complete a revolution, so there is a possibility that an accumulation of several ions is needed to perform a step, but maybe this step can be decomposed in several substeps, each one corresponding to an ion transition. If the numbers above are confirmed, about 40 ions would be needed for a torque generating unit to complete its power-stroke cycle. Our approach allows another way to look at the coupling ratio in BFM. Looking at equation (8.20) we see how the r_{max} is not load dependent, but the total k_M is. This is the case of a competitive inhibitor, which is the case for this motor. Following the interpretation that has done previously in the previous chapter where r_{max} is supposed load independent but v_{max} load dependent in order to obtain an expression for the coupling ratio we can see how if the v_{max} does not depend on the load means that the coupling ratio is constant for any value of the external torque. Then, at least within this interpretation of the coupling ratio, we can explain why this quantity is constant in BFM.

For the BFM we can conclude that our approach is able to deal and fit the experimental data within a reasonable wide range of parameters values. The difficulties of the experiment make a finer approach unavoidable for now. No pocket assumption has been made, so the waiting time is not appreciably affected by the load.

In the case of NTP-driven motors, we can appreciate some differences and similarities between them. First, it is remarkable that the internal time for the RNAp, $t_i = 0.034s$ is an order of magnitude longer than for kinesin, $t_i = 0.003s$. This is consistent with a motor that, apart from transcriptional pauses, which are removed from the data, performs a more sophisticated task every cycle [53]. Concerning the substrate-dependence of the stall force, our model suggests that in RNAp the stall force does not depend on the load, $f_0 = 13.53pN$ while in kinesin it does, $f_0 = 3.6 + 0.28 \ln [ATP]pN$. This dependence was observed in [9] even though more recent measurements [40] suggests that the stall force is [ATP]-independent. However we are trying to fit data where the stall force does

depend on [ATP], even if it is an artefact of the setup. In any case, this is an open question that more refined experiments should clarify. It is interesting to note that in the latter reference the external forces can be up to $-15pN$, which clearly indicates that f_0 should have a stronger value. However the data provided in that reference lacks more realizations to perform a detailed quantitative analysis of the mean velocity in the high-load regime. Additionally, we can see how C' is about ten times greater in the case of kinesin, $C' = 0.45pN^{-1}$ than in the case of RNAp, $C' = 0.04pN^{-1}$. Since both mechanoenzymes bind similar-size nucleotides it is reasonable to suppose that l_x is similar as well in both motors. So then, as the stiffness is inversely proportional to the parameter C', the stiffness of the pocket in RNAp has to be considerably higher than in kinesin (of the order of ten times). This may be the reason why the value of f_0 for RNAp does not seem to depend on the substrate concentration. If the pocket is stiffer, it hardly changes its natural, load-free conformation. It is remarkable as well that A' and B' are very similar in both mechano enzymes ($A' = 0.0178s, B' = 1.27\mu Ms$ for kinesin-1, $A' = 0.016s, B' = 1.5\mu Ms$ for RNAp) which reflects that binding times of the nucleotides do not appreciably differ between them. Mechanical time is negligible in kinesin and RNAp, which means that the power stroke mechanism occurs in a time scale which is much lower than other processes in agreement with the observed step-like trajectories. We expect other $[NTP]$ motors as mysions and dyneins to have this feature as well, since the forces and the frictions involved in their motions imply physical velocities much greater than their corresponding chemical rates.

Concerning the type of inhibition that these mechanoenzymes hold we confirm the result of [43] that establishes the mixed character of kinesin-1. Moreover, RNAp is also mixed. This implies that the maximum velocity depends on f_{ext} and we already know that this can be interpreted as a load dependence of the coupling ratio. In these two motors the coupling ratio would decrease with the load, would vanish when $f_m + f_{ext} = 0$ and would change its sign when $f_m + f_{ext} < 0$.

We thus conclude that the chemical kinetics of kinesin and RNAp is regulated by very similar processes, even though some of them are quantitatively different. Nevertheless, experimental data from both devices can be understood under the same conceptual framework.

Summarizing, in this work we have analyzed the chemical kinetics of three different molecular motors with the intention of providing a general framework to deal with mechano-chemical engines, which can be connected to an expanded inhibition theory as shown in Appendix B2. The three examples we have chosen are an appropriated set because all of them have been accurately measured in single molecule experiments. Even though each individual motor has very specific properties that should be taken into account to provide more refined models, we have shown here a unified approach to quantitatively describe the overall kinetic properties.

Appendix B1: Law of mass action

We show here a derivation for the substrate dependence of the reaction rates given in the law of mass action. We can consider the reaction

$$A + B \xrightarrow{k_1} C \,, \tag{8.27}$$

and write

$$\frac{d[C]}{dt} = \frac{-d[B]}{dt}\frac{-d[A]}{dt} = k_1[A][B]. \tag{8.28}$$

Here k_1 is the reaction constant. We can use a simple scenario to illustrate the internal mechanism of this description. Let's imagine that B is a single enzyme fixed and located at $x = 0$ in a one-dimensional space. On the other hand, A is a set of free diffusing particles that can eventually reach B and bind it. Let's focus from now on the $x > 0$ side. The probability to have a binding event during a time interval Δt is given by the function $p(x, t)$ in the following way:

$$p(0, t + \Delta t) = \int_0^L p(x, t)p(\Delta x \leq x)dx, \tag{8.29}$$

where $[0 : L]$ are the boundaries of the system and $p(\Delta x < x)$ means the probability of A jumping a displacement equal or lower than x. In fact, due to the properties of the thermal noise,

$$p(\Delta x \leq x)dx = \int_x^\infty \frac{1}{\sqrt{2\pi\sigma}} e^{-\frac{x'^2}{2\sigma}} dx'dx, \tag{8.30}$$

where

$$\sigma = \frac{2k_BT\Delta t}{\lambda}. \tag{8.31}$$

Here k_BT is the thermal energy and λ the drag coefficient. We can rewrite the previous probability as

$$p(\Delta x \leq x)dx = \frac{1}{2} erfc(x), \tag{8.32}$$

where we have used the complementary error function, which can be written in this case as

$$erfc(x) = \frac{2}{\sqrt{\pi}} \int_x^\infty e^{-(x/\sqrt{2\sigma})^2} d(\frac{x}{\sqrt{2\sigma}}). \tag{8.33}$$

On the other hand we can write

$$p(x,t) = p(x,0) \tag{8.34}$$

without loss of generality. We can then find and expression for $p(x,0)$. We have in our $x > 0$ system a total of n particles of A, which have a molecular width l_A. Then, we find that

$$\frac{n}{L} l_A \tag{8.35}$$

is the occupation ratio in the system. In order to transform the ratio n/L into concentration we simply use the Avogadro Number N_A,

$$\frac{n}{L} l_A = [A] N_A l_A. \tag{8.36}$$

We find then how the lineal proportionality (exponent=1) of the concentration comes from the hypothesis of a uniform density profile of the reactant. We can rewrite now eq (8.29) for $x \in [-L : L]$ as

$$p(0, \Delta t) = l_A N_A [A] \int_0^L erfc(x)dx. \tag{8.37}$$

Considering that

$$\int_0^\infty erfc(x)dx = \frac{1}{\sqrt{\pi}}, \tag{8.38}$$

we obtain

$$p(0, \Delta t) = l_A N_A [A] \sqrt{\pi}. \tag{8.39}$$

Now to transform this probability into a rate we simply have to consider that

$$r = \frac{p}{\Delta t}. \tag{8.40}$$

So then,

$$r = \frac{l_A n_A [A]}{\sqrt{\pi \Delta t}}. \tag{8.41}$$

Note that we have the ratio $\frac{l_A}{\Delta t}$, which can be interpreted as an approximation of the mean velocity at which particles of A travel in the media. Using Maxwell-Boltzmann distribution we can write

$$\frac{l_A}{\Delta t} \sim \langle v \rangle = \sqrt{\frac{8 k_B T}{m}}, \tag{8.42}$$

where m is the mass of the particle of type A. We can obtain for the rate

$$r \sim \sqrt{\frac{8 k_B T}{m}} \frac{N_A}{\pi} [A]. \tag{8.43}$$

What is interesting is that we have arrived to

$$r \propto \sqrt{k_B T} [A], \tag{8.44}$$

which indicates that reaction rates are proportional to the reactant concentration and to the square root of the thermal energy. It is important to recall that if we would use a reactant A distributed with a non constant density function $\rho_A(x)$ then the law of mass action would be dependent of this profile. For example, ATP nucleotides under a strong electric field may migrate due to their intrinsic charge in a way that the binding probability could not be considered as uniform.

Appendix B2: Connection of the unified approach with inhibition theory

In this appendix it is shown that the formalism presented in this work can be interpreted in the context of an inhibited-enzymatic scheme where the inhibitor concentration depends on the external mechanical load, as reported in Ref.[43].

The load as a competitive inhibitor.

Here we show the equivalence between a load-dependent waiting time that simply follows the law of mass action and the presence of an effective inhibitor. Let's consider the usual M-M scheme

$$E + S \underset{k_{-1}}{\overset{k_1}{\rightleftarrows}} ES \xrightarrow{k_2} E + P \tag{8.45}$$

The average time for this reaction is given by the MM relation

$$t_0 = \frac{[S] + k_M}{k_{max}[S]} \tag{8.46}$$

where k_{max} and k_M are the two classic MM coefficients. If we suppose that the external force only acts now to the free enzyme,

$$\begin{array}{ccccc} E + S & \overset{k_1}{\rightleftarrows} & ES & \xrightarrow{k_2} & E + P \\ {\scriptstyle k_{ic}}\uparrow\downarrow{\scriptstyle I} & & & & \\ EI & & & & \end{array} \tag{8.47}$$

then we have a competitive inhibition, where

$$t = \frac{[S] + k_M(1 + \frac{[I]}{k_{ic}})}{k_{max}[S]}. \tag{8.48}$$

$[I](= i)$ is the inhibitor concentration and k_{ic} the competitive inhibition constant. Then, the time difference Δt between the two cases is

$$\Delta t = t - t_0 = \frac{k_M}{k_{max}k_{ic}}\frac{[I]}{[S]}. \tag{8.49}$$

Recalling that we have the case where the waiting time only follows the simple law mass action

$$t_w = \frac{B}{\delta x[S]}. \tag{8.50}$$

and considering that $\Delta t \sim t_w$, we obtain

$$[I] \propto \frac{1}{\delta x}, \tag{8.51}$$

which for the linear pocket model gives

$$[I] \propto \frac{1}{f_{ext} + f_0}. \tag{8.52}$$

In Ref. [43] it is proposed that

$$[I] \propto \frac{f_{ext}}{f_{ext} + f_0}. \tag{8.53}$$

Consider the case $f_{ext} = 0$. Then, there is a minimum amount of inhibitor

$$[I]_0 \propto \frac{1}{f_0} \tag{8.54}$$

and a variable part which is written as

$$[I] - [I]_0 \propto \frac{f_{ext}}{f_{ext} + f_0}. \tag{8.55}$$

This is the case of BFM, because the load is altering only the k_M parameter. We have shown how the effect of a linear pocket combined with a simple law

mass action for the waiting time is equivalent to have an effective competitive inhibitor concentration. Furthermore, it is interesting to note that this formalism requires that even in the absence of the external force we still have an inhibition effect. This is important concerning assisting loads, as they are able to increase the mean velocity as long as they remove the effect of this remaining inhibitor.

The load as mixed inhibitor.

We now consider the more complete form of the waiting time written in eq. (8.8), i.e.

$$t_w = \frac{A}{\delta x} + \frac{B}{\delta x[S]}. \tag{8.56}$$

Let us take the following scheme of a mixed inhibition catalysis,

$$\begin{array}{ccccc} E + S & \underset{k_{-1}}{\overset{k_1}{\rightleftharpoons}} & ES & \xrightarrow{k_2} & E + P \\ {\scriptstyle k_{ic}}\uparrow\downarrow{\scriptstyle I} & & {\scriptstyle k_{iu}}\uparrow\downarrow{\scriptstyle I} & & \\ EI & & ESI & & \end{array} \tag{8.57}$$

The time expended in a M-M reaction with a mixed inhibitor is

$$t = \frac{1}{[S]k_{max}}([S](1 + \frac{[I]}{k_{iu}}) + k_M(1 + \frac{[I]}{k_{ic}})), \tag{8.58}$$

where k_{iu} is the uncompetitive inhibition constant. Now Δt is

$$\Delta t = \frac{[I]}{k_{max}}(\frac{1}{k_{iu}} + \frac{k_M}{k_{ic}[S]}) \tag{8.59}$$

and if we match $\Delta t \sim t_w$ as before, we obtain

$$\frac{A}{\delta x} + \frac{B}{\delta x[S]} \sim \frac{[I]}{k_{max}}(\frac{1}{k_{iu}} + \frac{k_M}{k_{ic}[S]}). \tag{8.60}$$

We can identify the terms as

$$\frac{A}{\delta x} \sim \frac{[I]}{k_{max}k_{iu}} \tag{8.61}$$

and

$$\frac{B}{\delta x[S]} \sim \frac{[I]k_M}{k_{max}k_{ic}[S]}. \tag{8.62}$$

So again we obtain

$$[I] \propto \delta x. \tag{8.63}$$

Now, in addition, as $[I]$ must be the same in both identifications, we can state that

$$\frac{A}{B} = \frac{k_{ic}}{k_{iu}k_M} \tag{8.64}$$

recalling that $A/B = A'/B'$. This establishes a connection between inhibition formalism and the parameters A and B. Both RNAp and kinesin-1 follow this scheme.

In [43] the relation between $[I]$ and the load was given by hand, being consistent with the extreme cases but with no fundamental reasons justifying the explicit form of the equation. In this latter work we have shown that that expression comes from considering a simple elastic pocket with a linear response to the load. However a sigmoidal type of response is more convenient in order not to have undesirable situations like a pocket with negative or infinite binding surface.

Part III

Deepening into the mechanics of kinesin

So far we have already discussed about many aspects of molecular motors, like energetics, stall forces, mean velocities, etc... But in all those modellings a physical picture of the actual motor mechanism was lacking. In other words, the interactions that we used are highly phenomenological, as we have not explicitly said where they come from.

Specifically, we can clearly discard nuclear and gravitational forces as the sources of energy, which implies that it is the electromagnetic force that drives molecular motors along their paths. But when we reffer to electromagnetic fields we have to be more explicit, as all the chemical reactions are in fact consequences of electromagnetic properties of their components. Then, it is not the same for practical purposes to consider the Coulomb interaction between two point charges than to deal with quantum mechanics to analyze the coupling of several electronic wavefunctions. For example, an ATP molecule is composed of three phosphate subunits each of them being negatively charged. Nevertheless, at physiological conditions the three phosphate groups remain bound with a high activation energetic barrier that prevents the dissociation. One of the accepted explanations for such an attraction (called phosphoanhydride bonds) is resonance stabilization, which indicates that there is much more than Coulomb forces when we approach the scale of orbital clouds.

On the other hand, there is another complication concerning electromagnetic fields. The cytoplasm is full of ions, both positively and negatively charged which converts the media in a plasma, or more specifically in an electrolyte. These ions tend to dump Coulomb forces in an exponential way, which is an effect known as Debye screening or shielding [54]. In addition to the high relative permittivity of water, it seems that the regime of Coulomb interaction as known from more classical physics cannot be applied to scales greater than the molecule size (due to Debye screening) neither to small size components due to quantum effects. However, for lengths of the order of a motor size ($\sim 5nm$) none of the former limits are clearly applicable. At nanometric distances the relevance of quantum orbitals effects concerning molecular motor motion is not absolutely clear. On the other hand, the Debye-Hückel theory is not clearly applicable as well. Such a theory is formulated for continuous media and not for discrete bodies as it is

the case of motor proteins. Moreover, spherically symmetric shielding, dilute solutions and uniform (or even definable) dielectric permittivity are conditions that don't necessarily hold. Moreover the excluded volume that the proteins occupy does not allow shielding to occur inside the protein body.

In this chapter we will try to show how most kinesin features can be explained by considering Coulomb-like interactions between different parts of the motor and the microtubule as well as with ATP or ADP molecules. Even if we can add some Debye shielding, the qualitative picture is not strongly affected. We will see how the whole mechanism of kinesin walking can be a consequence of the electrostatic communications between ATP, kinesin and the protofilaments of the track. After all, they are charged structures and as far as shielding theories are still obscure in such nano-systems we have the intuition that all these charges are there for something more than to be screened. Then, we will first introduce our modelling without considering any shielding and later on we will take this topic into account in order quantify its effects. As far as the consequences of our hypothesis will agree with experiments there will be reasons to take such hypothesis more into account. Actually, we are going to see that kinesin motion can be explained in an easy and elegant way if we consider that Debye shielding is not so strong as it is supposed, at least near the microtubule surface or at distances of the same order than the biomolecules involved.

In the next section we will progressively proceed with the study of kinesin motors with scenarios of increasing complexity. First, we will present a collection of modellings that have their target in explaining kinesin motion using electrostatic interactions. We will see how, on the one hand, these interactions allow us to explain most of the experimental observables. But on the other hand, the existence of ionic screening is deeply rooted in intermolecular forces literature. Such an screening is supposed to strongly restrict the range of electrostatic interactions in electrolyte solutions. This is the reason why in the last chapter of this thesis we will expose our point of view concerning the edges of the applicability of Debye-Hückel theory in protein systems as kinesin-microtubule arrays. In the meantime, and after exposing our electrostatic model, we will introduce an analysis of the interactions between kinesin heavy chains, tubulin heterodimers and the different arrangements of nucleotide components such ATP, ADP or ADP.

This model, based on the hypothesis of a kinesin commutator, sheds light into very recent measurements [55, 56].

9

Mechanics of kinesin step explained by electrostatic interactions

9.1 Introduction

As we have seen in previous sections, kinesin molecular motor is a protein that is able to convert chemical energy from ATP into mechanical work while stepping along microtubules. Until now, how this conversion is produced and how the stepping mechanism acts has been a mystery. Several experiments and theoretical works have been made without satisfactorily answering these essential questions. Even the explanation of the different directionalities that different motors exhibit has not been understood. The reason for this is that the experiments using optical tweezers or fiber-glass rods don't have enough temporal and spatial resolution. Only very recently these resolutions have been improved leading to controversial results about substeps.

In this work we provide clues to understand the role of ATP-hydrolysis, the physical mechanism of the motor and consequently an explanation for its directionality and processivity. Such results are achieved performing calculations on microtubule-kinesin systems, not considering all the details of the structures but trying not to skip the most fundamental properties of the motor. This microscopic but still very phenomenological approach allows us to understand which is the role of every considered element. Mainly, we take into account the electro-

static of the structures and its geometry, showing their relevance to explain the known experimental behaviour. This will an effective model, but in comparison with other works based on ratchet potentials [32, 47, 37] it can be considered as a microscopically physical approach. All the symmetry breaking that we add to the system, like the polarity of tubulin and the stalk, is well justified in the literature. The interactions are no more effective potentials but Coulomb's electrostatic forces complemented with Debye screening terms. And finally, the structure of the motor that we consider is in agreement with the crystalline figures obtained in some crystallographic experiments. The chemical cycle will also be considered, although the relation between chemistry and the electrostatic properties will not be clarified until next chapter. We will see how it is the chemistry that conditions the electrostatic of the systems. This is our main concept: chemistry regulates electrostatics. The rest is Coulomb's physics in the range of kinesin size. There are no global conformational changes, but relatively long-range repulsions and attractions. What kind of forces, if not, can induce such a deterministic motion? Thermal forces are also present and, although smaller than microtubule-kinesin forces, are comparable in magnitude. However, these forces are so uncorrelated that cannot provide mechanical work. It is amazing how, even the most recent literature, we can find concepts like "diffusional search" concerning the travel that the free head performs. Always such a search will prefer to reach the head in the initial site than to travel 16 nm along the protofilament. In addition, there are tubulin sites in the microtubule that are also closer than the target site, like in the two first neighbours in adjacents protofilaments. There is a clear electrostatic polarization along the protofilament and it is a nonsense to consider that the fluctuations, which are not supposed to depend on the electric fields, will drive the head to travel deterministically to the less probable site. Then, the hypothesis of diffusional search will not be considered. There has to be a deterministic mechanism with deterministic forces that drive the motion. Fluctuations only perturb the system and can eventually modify it due to the finiteness of energy differences, but never direct it by themselves.

A lot of experiments have been performed on kinesin. First, minus-directed kinesin were discovered, being the *ncd* the paradigmatic example of this type. The main difference between *wild-type* and *ncd* are the neck linkers and specially

the different orientation of the stalk respect the motor core. Later, a mutant of ncd with a single modification in the neck showed to lose its directionality. These are clues to consider that the key for directionality is located in the neck. Also the processivity is related with this, because minus-ended motors don't seem to be processive at all, and there is evidence that changes in the neck of processive plus-ended motors modify the directionality [8].

In 1999, a proposed model could travel in both directions without changing the microtubule (See Ref.[42]). The ATP was supposed to induce large conformational changes, stretching and contracting a spring that could displace the motor along the track. This model has been recalled and redone several times [57], and we have discussed it with detail in the first part of this thesis. However, there are no evidences for such large conformational changes. The neck linkers are known to be quite rigid and that is why some authors think that only thermal fluctuations drive the movement. We can express the problem of the power stroke in a different way. It is known that the head that hydrolyzes ATP is the one that performs the step. Then, the energy of the hydrolysis is localized in this head, which is not the pivotal one. This is an argument against the global conformational change hypothesis. Normally, for a rotation, the energy is applied in the axis of rotation, i.e. the attached head and not in the rotating. This argument would discard the arm level amplification hypothesis for kinesin, while it may hold for myosins.

We have structured this work following an increasing-difficulty order. The essential ingredients are added successively in a series of generalizations that will drive us until a relatively realistic model.

9.2 Tubulin, protofilaments and microtubules

Here we introduce the structural properties of the components that will be involved in our modelling. Such a description is tightly related with the electrostatic properties from which we will base our proposals.

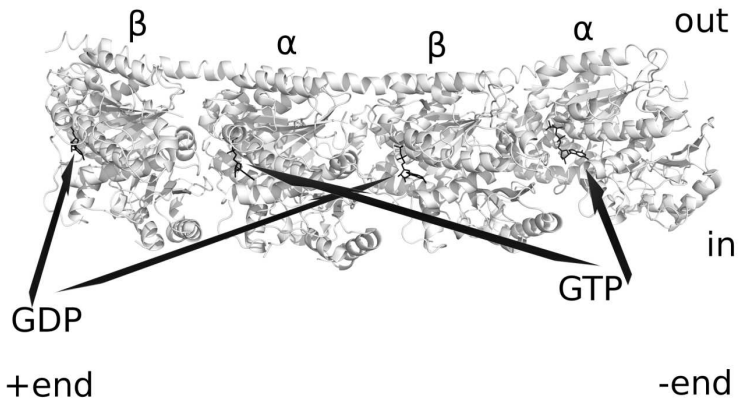

Figure 9.1: Structure of two tubulin heterodimers. Left is plus-end while right is minus-end. The upper side represents the microtubule surface side. We can distinguish the α and β subunits not only by their position with respect to the ends of the microtubule but also because β subunits have a bound GDP while α subunits have bound GTP nucleotides.

The tubulin heterodimer

The dimeric protein called tubulin is the fundamental unit of the microtubules. Its structure can be separated into two subunits, the $\alpha-$ and the $\beta-$subunit, having both very similar structural properties. Every subunit is by itself a globular protein of 50 kDa. This globular part has been crystallized in several occasions showing the structure of Fig. 9.1. However, in each of the subunits there is a C-termini tail that cannot been crystallized due its flexibility. In Fig.9.2 we can see these tails, which have been added by hand [58].

Protofilaments and microtubules

When a collection of tubulin units is arranged in a chain lattice we say that this structure is a protofilament. This new structure has an overall polarity due to the individual polar properties of tubulin. One end will be β or plus-end and the other α or minus-end, in reference to the polymerization rates that each part exhibits at the growing stages of the protofilament. The protofilaments have never

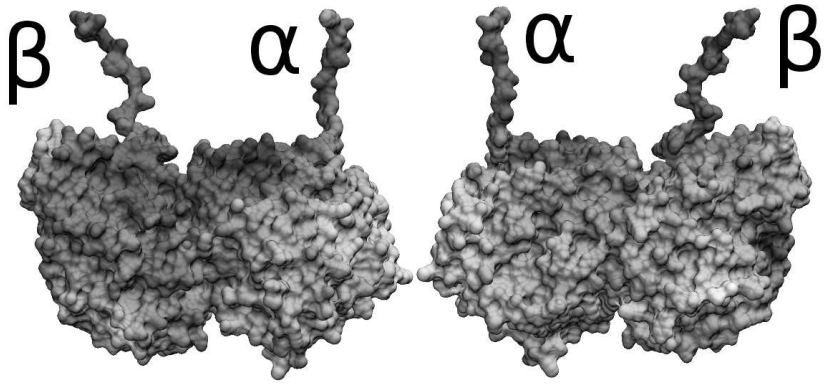

Figure 9.2: Structure of two tubulin heterodimers with their C-termini tails, which are the vertical protuberances. We can see two dimers each one seen from a different side, as it is indicated by the identification of the α and β subunits.

been found alone. They are part of superstructures like microtubules or tubulin-sheets. The microtubules are essentially a collection of protofilaments arranged in a cylindrical way, where the protofilaments can be parallel to the symmetry axis of the cylinder or performing a supertwist around it[41]. The tubulin sheets are flat arrangements of parallel protofilaments that are artificially prepared for experimental purposes. In all cases, no matter how the lattice is organized, kinesin motors seem to run parallel to the protofilaments geometry, although it is not known if the motor uses only one or more rails to advance. In any case, the motor remains *faithfull* to the direction of the protofilaments, at least on average [6].

Microtubule polarity

What has been observed in several experiments is that wild-type kinesins move always towards the plus-end of the microtubules, while the chimeras called ncd walk to the opposite end. In single-molecule experiments with optical traps it has been seen that the probability of performing backward steps is very low if the external load is not high. What it means is that the mechanism of the kinesin has to be *deterministic* even in presence of relatively strong fluctuations. And such a mechanism requires that the microtubule has to exhibit a broken symmetry along the direction of movement. In the literature, one can read that the microtubule is a polar structure, but they always refer to the difference in growing rates at

different ends. In order to have a deterministic motion along the microtubule, there has to be another polarity that can interact with the kinesin motors, even though the polymerization rates difference is a property related with this fact.

In Ref. [58] one can find support for a physical polarity in the microtubule. Although in vacuum the tubulin protein is negatively charged, in the presence of water it becomes polarized, as seen in Fig.9.3. Molecular Dynamics (MD) simulations have been calculated the direction and the approximated magnitude of the polarization vector. This vector is essentially perpendicular to the surface of the microtubule, in according to the well-known negatively charged surface of the structure. However, just below this negative surface, it exists a positive layer that gives to the electric field new and polar properties. The main result of these simulations is that the projection of the polarization vector along the axis parallel to the microtubule is non-zero, which converts the microtubule in a kind of biological ferroelectric material. This is the basic point from where we will build up all of our theory. The results of the calculations of the tubulin dipole

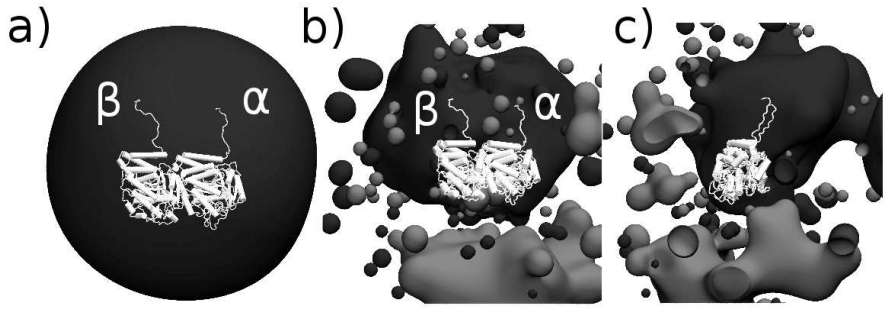

Figure 9.3: a) Tubulin without surrounding water is essentially negative (dark gray). Notice that the $\beta-$subunit is on the left. b) In the presence of water, a polarization appears, with a positively charged zone (light gray). This polarization has a non-zero projection along the direction of motion. c) Seen from the symmetry axis perspective, the polarization has a non-null lateral projection as well.

moment are shown in Table 9.1 and Figure 9.3.

Tubulin models

The $\beta-$model From this MD data we can build a first and very simple model for a single protofilament. We neglect other details of the tubulin keeping only

Magnitude	Value (Debyes)
Total charge:	-54e
Total dipole moment:	4850
x-component:	700
y-component:	4800
z-component:	200

Table 9.1: MD values from [58]. The tubulin properties are calculated for the case of GTP-bound states. The dipole moment unit is the Debye. The x-direction is along the symmetry axis and positive values of x points to the minus-end. The y-direction is radial towards the center of the cylinder and the z-direction is the perpendicular to the other two.

the fact that it is an electric dipole in the direction given in Table 9.1. In Fig.

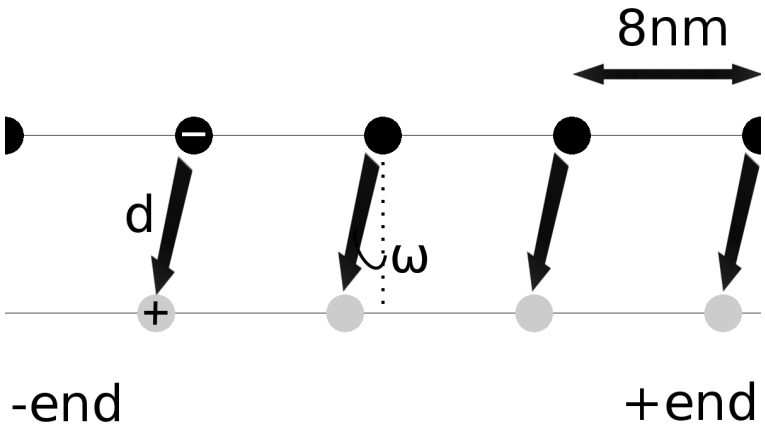

Figure 9.4: $\beta-$model for a protofilament. The polarization of every tubulin dimer allows to differentiate the plus from the minus end. The periodicity of the structures is the same as kinesin's step size $\simeq 8nm$. Notice that charges on the surface (upper row) are negative (dark gray) while inner charges are positive (light gray). The positive charges are located at a distance d from their negative partner and with an angle ω with respect to the vertical direction.

9.4 we can see four tubulin units within the context of this model. We need two parameters, the tilting ω and the dipole distance d. From the values of Table 9.1 we can estimate that $\omega = \arcsin \frac{700}{4850} \sim 8.3^o$. The parameter d can also be estimated as $d \sim 8nm$. A third parameter is needed for the relative values of the charges negative/positive (if one wants to keep the whole dipole global charge as negative). However, this is not strictly necessary now and we assume a dipole

with zero global charge. This model is a coarse-graining of the whole tubulin unit and is not supposed to give extremely fine details. We call this scenario the β-model because in kinesin-decoration experiments like in Ref. [59] it has been shown that the heads of the motor attach essentially to the β subunits.

The $\alpha\beta$ model A more detailed description of the tubulin unit has to take into account the polarization of each subunit separately. In Ref. [60] it is reported that the polarization of the α subunit is smaller, and the direction is slightly different. This fact implies that this subunit is less negative than the β, so the heads don't attach on them with the same frequency as they bind the β-subunits. Consequently, to take this into account we need four parameters, α_α, d_α, and α_β,d_β, for the α and β subunits, respectively. (See Fig. 9.5) The models presented

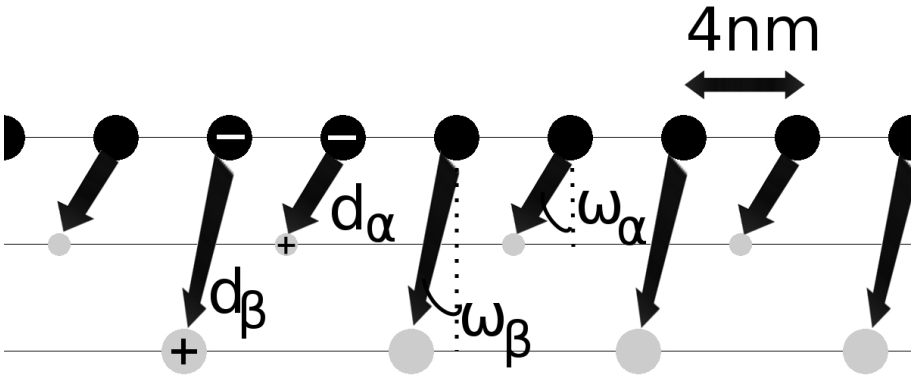

Figure 9.5: $\alpha\beta-$model for a protofilament. This figure is similar to the previous figure, but now we have added the structure of the α subunits, each one with a dipole that has its own length d_α and tilting angle ω_α, while for the β subunits we have d_β and ω_β. Although the periodicity is still $\simeq 8nm$, now we can find a negative surface charge every $\simeq 4nm$.

here are the basis for the modelling of kinesin in next sections. It will be important to realize that tubulin and kinesin act together, and one cannot understand the motion of kinesin without an understanding of mutual MT-kinesin interactions. For us is important to build a detailed model for the track and not only for kinesin, since it is the relation between them what causes the actual motion.

9.3 The ATP hydrolysis

The Adenosine Triphosphate nucleotide (ATP) is an organic molecule that is used in uncountable biochemical processes as energetic supplier. It is composed of an adenine base which is bound to a pentose sugar (called ribose) and three phosphate groups, called P_α, P_β and P_γ. In Fig. 9.6 we can see a pymol representation of this nucleotide.

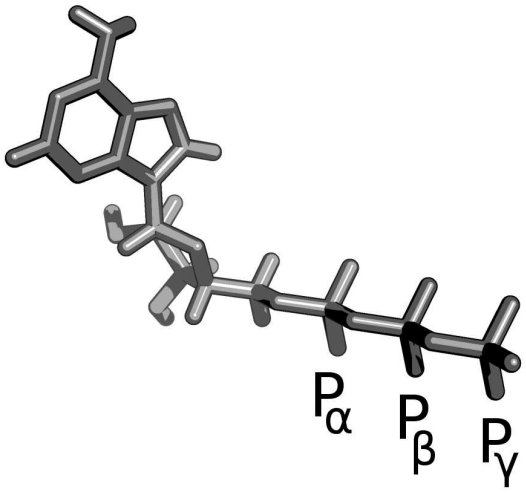

Figure 9.6: Pymol representation of an ATP molecule. We can distinguish the two rings from the adenine, the ribose and the three phosphate groups, indexed by the three first greek letters

In the presence of water, it can hydrolyze following the reaction

$$ATP + H_2O \rightarrow ADP + H_2PO_3. \tag{9.1}$$

This simplified scheme hides one aspect of the maximum importance. When ATP is hydrolyzed, the γ phosphate that breaks its bond with the rest of the nucleotide remains unreleased a certain time. After this time, the phosphate group detaches completely. The presence of the phosphate group is crucial because it can form chemical bonds with other structures. As we will see later, the role of P_i is crucial to understand the interactions of different nucleotide states of kinesin heads with

tubulin. To emphasize this, we should write the following,

$$ATP \rightarrow ADPP_i \rightarrow ADP + P_i. \tag{9.2}$$

Every transition (in the left-to-right direction) has a typical frequency of $250s^{-1}$ (Ref. [61]). Here we don't consider reverse rates. About the energy, it is typically considered that under physiological conditions one ATP can provide $25k_BT = 100pNnm$ of energy. The whole free energy is strictly

$$\Delta G = \Delta G^0 + k_B T \ln \frac{[ATP]}{[ADP][P_i} \tag{9.3}$$

However, as we have already seen in this thesis, the trials to fit the data in theoretical frames (one example is Ref. [43]) suggest that maybe kinesin does not use but the half of the whole value. Or maybe the available energy is not what we expect from eq.(9.3).

Electrostatics of ATP hydrolysis

Until now, one of the biggest misteries about kinesin motion is how the chemical energy of the ATP is translated into mechanical work. We think that in order to clarify this question we have to consider the *electrostatic charges* involved in the reaction, which in absence of Magnesium are

$$ATP^{4-} + OH^{1-} \rightarrow ADP^{3-} + H_2PO_3^{2-}. \tag{9.4}$$

The ATP molecule is strongly negative (-4e) and when it is bound to a kinesin's head, it will modify the electrostatic properties of the head. It has been reported that the ATP binding pocket is positively charged and it attracts the nucleotide by electrostatic attraction (Ref. [62]). On the one hand, we know that when a head is free from ATP it binds strongly to the β subunits in the microtubule (clearly negative, specially the C-termini tails). When it captures an ATP, this interaction becomes unstable and after some time (when P_i releases) the head detaches from the microtubule. On the other hand, we know that the head free from ATP is less negative than with it. In fact, it is very reasonable that the head without ATP will be positively charged, and this would be the reason for the microtubule binding of kinesin heads when they are nucleotide free. After

ATP binding, we suppose that the head *switches the sign of the charge* and then it is repelled from the microtubule's surface. As we can see, the chemical and electrostatic schemes agree mutually in a very appealing way.
While it is true that the ATP hydrolysis involves some charge variations, positive-free ions are able to bind the nucleotides in order to decrease the global charge of ATP and ADP. Specifically, Magnesium ions Mg^{2+} usually bind ATP in such a way that we should write

$$MgATP^{2-} + OH^{1-} \rightarrow MgADP^{1-} + H_2PO_3^{2-}. \tag{9.5}$$

But still we have a charge variation of two electronic charges upon the release of the γ-phosphate group.

ATP binding pocket: the local conformational change

The energy of the hydrolysis has to be used to perform a step. The scenario described until now is not enough. Only with those considerations, the mutual repulsion of the ATP molecule and the microtubule's surface will be enough to take the ATP or the ADP away leaving the head in the same position. What is necessary is that when this repulsion is executed, the ATP molecule will take the head with it dragging the whole motor domain. How can it be possible? In several occasions ([61, 62]) it has been reported that after ATP hydrolysis (sometimes they say after ATP binding, others after phosphate release) a local conformational change in the ATP binding pocket occurs. The fact that this pocket closes and traps the nucleotide inside is essential to understand that an electrical repulsion will make move the whole head away from the microtubule.

Then, what is the role of the ATP hydrolysis? Several times this question has been asked and the most frequent answers talk about uncertain conformational changes that the different chemical states induce. From our new point of view, the only necessary conformational change is the local closing of the ATP binding pocket. If this is the case, the rest of the motion, the so-called global conformational change, is no more than electrostatic repulsion. One can ask about the use of the hydrolysis energy. This energy is used to close the pocket and nothing more. So, surprisingly, the role of the ATP is to take the system motor-microtubule out from the equilibrium closing the ATP binding pockets. The movement of the

power stroke is driven from the electrostatic field of the microtubule.

9.4 Kinesin mechanical 2D model

As we have stated in the previous chapter, the binding and detaching processes of kinesin heads are governed by their chemical, i.e. electrostatic state. As a simplification we will consider that a head with ATP or ADP will have a net charge of $-4e$ and $-3e$, respectively, while without ATP or ADP the net charge will be $+2e$. (We still don't take into account the effects of Mg ions).

The model

The most simple way one can build a model in this frame is considering the kinesin as a rod with a point charge in each of the terminals. We then let this model to interact with a protofilament of the $\beta-$model. Because we deal with only one protofilament it is important to restrict temporarily the problem to 2 dimensions. In Fig. 9.7 we can see the main elements of the movement. Note that the

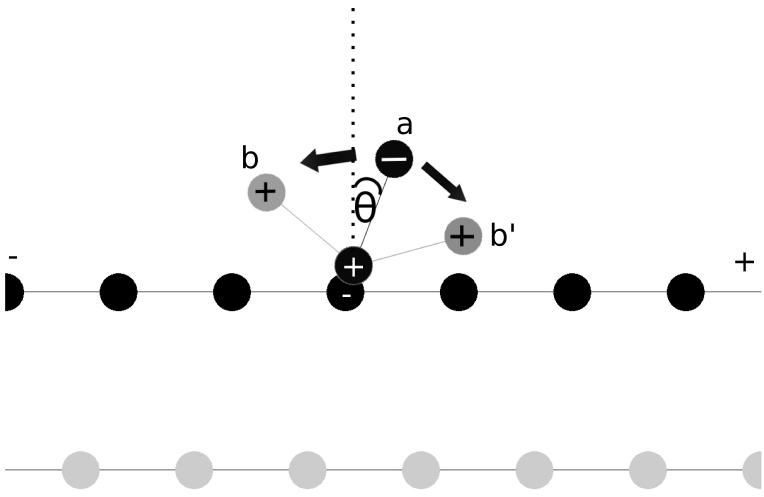

Figure 9.7: Mechanism of the rigid rod model. a) When the free-tethered head is negative, the motor is on its parked state or equilibrium configuration. But when this head suffers ADP release it becomes positive again and will be attracted to the microtubule surface. Now the question is whether the head will fall toward the plus (b) or the minus end (b'), even though the parked state is tilted toward the plus end.

only relevant variable is the angle θ because the rod is rigid. We keep one of the heads positive and then it remains attached to the tubulin. But the other, as it is negative, will rapidly reach the equilibrium value of θ, θ_{eq}. This is the "parked" configuration, in which the motor remains more or less time depending on the ATP concentration. Our hypothesis is that when the attached head receives an ATP, the closed binding pocket configuration of the other head becomes unstable (maybe due to the electrostatic change that the new ATP produces, which increments the radial strain in the rod, although this is an obscure point) and the negative head switches the charge. While the attached head needs a small amount of time to hydrolyze the ATP and eliminate the phosphate group, the free-leading head, now positive, will fall to the surface of the microtubule again. Once this head is on a tubulin site, the other head rises out from the surface looking again for the θ_{eq}. But let's focus our attention into the falling regime now. From this mechanism, two crucial questions appear. First of all, the time for the attached head to perform the hydrolysis and the losing of P_i is in competition with the falling time of the free head to the microtubule. Such a competition can provide interesting clues concerning processivity that we will develop in next chapters. The second question is: after the switch of the free head's charge, does the head goes to the next tubulin unit or falls back to the previous one? This is equivalent to ask: does the motor walks to the plus-end or it just make random displacements. This is the key point for motor directionality.

Parameters and equations of the model For the electrostatic distribution of microtubules we assign negative surface charge $q = -27e$ per tubulin subunit while include a positive charge distribution in the interior leading to dipole moment magnitude of $p = 5000D \simeq 100Cnm$[63], or $d \simeq 4nm$ ($p = qd$). Finally, we use a dipolar tilt with length and angle values equal to $d_\alpha \simeq 2nm$, $\omega_\alpha \simeq 0.07rad$ and $d_\beta \simeq 4nm$, $\omega_\beta \simeq 0.14rad$, for the α and β subunits respectively.

The microtubule-induced kinesin interaction potential is given by

$$V(\vec{r}_i) = \frac{-1}{4\pi\epsilon_0\epsilon_r(1+ka)} \sum_{j=1}^{N} \frac{q_i q_j}{|\vec{r}_i - \vec{r}_j|} e^{k(a-|\vec{r}_i-\vec{r}_j|)}, \tag{9.6}$$

where $\vec{r}_i$ is the position vector labeling the charges on kinesin ($i = 1, 2, 3$), while $\vec{r}_j$ is the location of the N microtubule charges q_j on the α and β subunits. k is

the inverse of the Debye length, which we take around $\sim 3.5nm$, and $a \sim 1nm$ is the excluding volume radius as described in Ref. [64]. A regime with a greater a and lower Debye length l_D is also operative. We considered a single protofilament as we are still in the 2D model, so then $N = 5$, which means that we consider two first neighbour interactions. We have the following overdamped equation of motion for kinesin:

$$\lambda\dot{\theta} = -\frac{1}{L}\frac{dV(\vec{r})}{d\theta} + \xi_\theta(t) \tag{9.7}$$

where λ is the drag coefficient, L the head-to-head distance and $V(\vec{r})$ the total microtubule electrostatic potential of Eq. (9.6) at the Cartesian location $\vec{r}$. The environment is simulated through the thermal forces $\xi_\theta(t)$; for each we have $\langle\xi(t)\rangle = 0$ and $\langle\xi(t)\xi(t')\rangle = 2\lambda k_B T\delta(t-t')$. In order to integrate Eq.(9.7) we need to perform at each instant of time the Cartesian-to-polar transformation $\theta = \theta(\vec{r}, L)$. For the rotation we consider the attached head to coincide with the origin of the coordinate system; the latter is shifted by $8nm$ each time a step is completed. The simple Larmor-like rotation of the protein for $\gamma = \pi$ becomes a more complex rigid body rotation for $\gamma < \pi$.

To analyze such an important aspect as directionality one has to analyze the interaction motor-microtubule in the range $\theta \in (0, \pi)$. Because the rod is, in principle, rigid, only forces that are perpendicular to the rod contribute to the angular velocity $\theta = \frac{d\theta}{dt}$. Calculating the the potential as a function of θ, $V(\theta)$, one obtains that the shape is concave with a minimum in $\theta = \theta_{eq}$. There is no surprise in this. As long as the free head is in the parked state, i.e. negatively charged, the angle θ will remain close to θ_{eq}, slightly disturbed by thermal fluctuations. Now one can ask: which are the values for θ_{eq}? The answer is that it depends on the polarization angle ω. If ω is zero, then the protofilament is a perfectly symmetrical lattice with a potential that will clearly drive the free head to a vertical state, i.e. $\theta_{eq} = \frac{\pi}{2}$. However, we know that ω is not zero, so θ_{eq} will move away from the verticality in the form shown in Fig. 9.8. From this figure, one can see how for positive values of ω, the case we think is the real, the parked position is oriented forward. Does it mean that after converting the charge of the head into positive, the motor will come back to the appropriate position? The answer is, surprisingly, no. As we will see in this model, the value of θ_{eq} does not determine the directionality of the motor. Let's think about it in terms of the potential. If at the parked state the free head is in the minimum of the

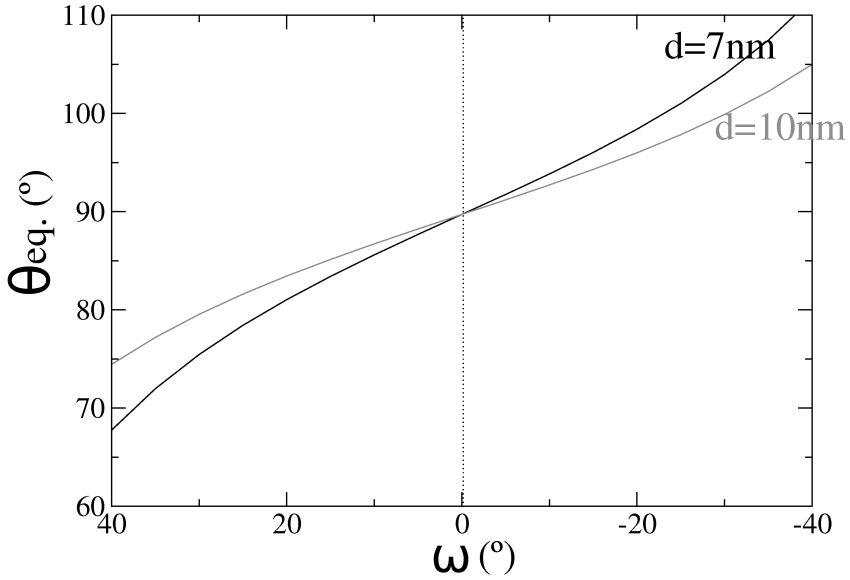

Figure 9.8: θ_{eq} versus ω for two different values of d. We take positive α when the positive charge is closer to the minus-end than the negative, i.e. the case of Ref.[58].

potential's well, when we change the sign of the charge, this minimum will be converted into a maximum and, in general, all the potential will simply switch the concavity leading to a mirror image of the previous potential. Of course the head will fall because it is not stable to remain in the maximum, but the falling side, forward or backward, will be determined only by thermal fluctuations. Then, the probability to go backward or forward is simply the 50%. In Fig. 9.9 we can see the impossibility of deterministic motion in this model. We conclude, then, that

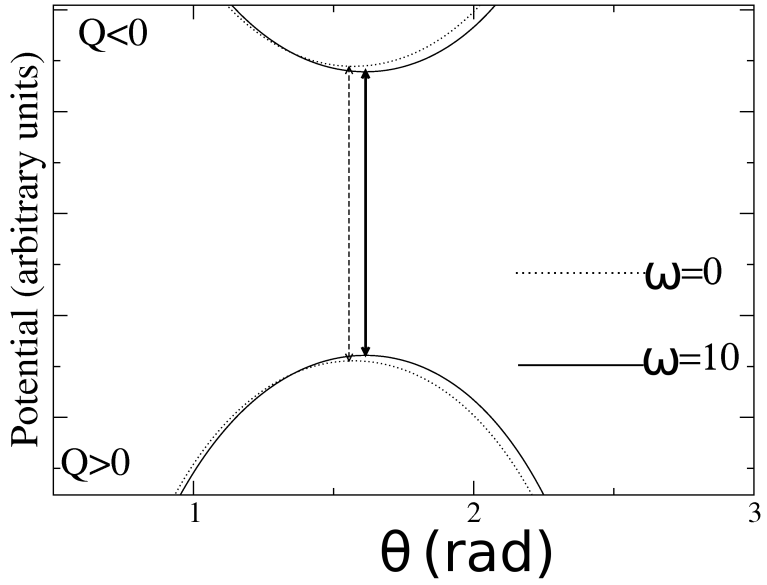

Figure 9.9: Potential for the free head before and after switching the charge for the cases of $\omega = 0^o$ and 10^o. We can see that none of the cases gives a deterministic motion because $\theta_{min} = \theta_{max}$ in both cases. Q is the charge of the free head.

the rigid head model, with no more ingredients, is not enough to produce active motion, although it illustrates the way how chemistry is related with mechanics. What we need to produce directed motion is that the minimum of the potential in the parked state will be shifted to increasing θ respect to the maximum of the convex potential. In such a case, the free head will clearly fall to the next tubulin unit.

Can elasticity give directionality? How can we shift laterally the two potentials, concave and convex? We have seen how using only the θ variable is not possible. However, we can abandon the rigidity of the model to have some freedom in the radial variable as shown in Figure 9.10. This fact can be justified with two explanations. First, it is reasonable to consider that the motor itself has a certain compliance to stretch. Second, it is known from [65] that the attached heads normally bind to the C-termini of the β-tubulin. These C-termini tails are very flexible and can also justify the variation of the effective radius L in the model. This fact opens a second dynamical equation that has to be added to Eq.(9.7),

$$\lambda_r \dot{r} = F_r + \xi(t), \tag{9.8}$$

where F_r is the radial projection of the total force acting on the moving head. In the Fig. 9.10 we can see how when the free head is negative, L is bigger,

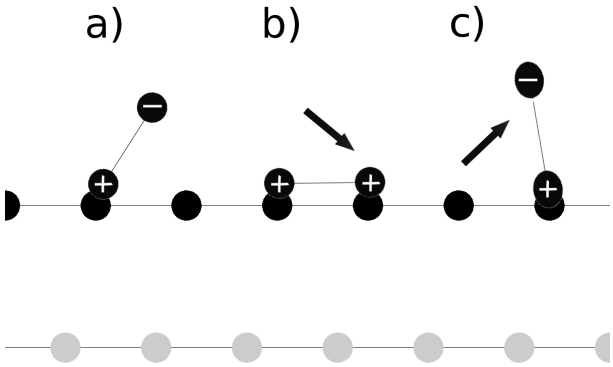

Figure 9.10: Mechanism of the flexible case of the heads model. From a) to b) the free head falls to the microtubule, while from b) to c) the previously attached head raises to reach the next parked state. Notice how while raising occurs (c), there is a stretching in the motor's length, which allows to surmount the symmetry of the rigid case and gives directionality to the motor.

and after charge switching, becomes smaller. A simulation of this system shows that then the motor can perform deterministic steps. What is happening with

the potentials? Are they shifted? The answer is yes. In Fig. 9.11 we can see this effect by observing how θ_{eq} changes with the radius L. When the charge in the free head changes, the motor experiments a contraction that will be traduced in a change of θ_{eq}. It is very interesting how the directionality of the motor depends on the difference in radius between the stretched and contracted state. If θ_{eq} decreases in the contraction, the maximum of the potential will be shifted to the decreasing θ, so the motor will be plus-ended. If it increases, the motor will be minus-ended. Note however that the stretched motor could be more than 10 nm long and stretch so much that the global result will be a decrease of θ_{eq} and the motor will result to be plus-ended.

However, we will see in next sections how directionality is better achieved by other mechanisms. The reason is that this flexibility causes a variation of the γ angle defined by the heads and the neck. It will be clear how this angle has to be very close to 180^o. For this reason, we don't continue considering flexibility as a real way of achieving directionality.

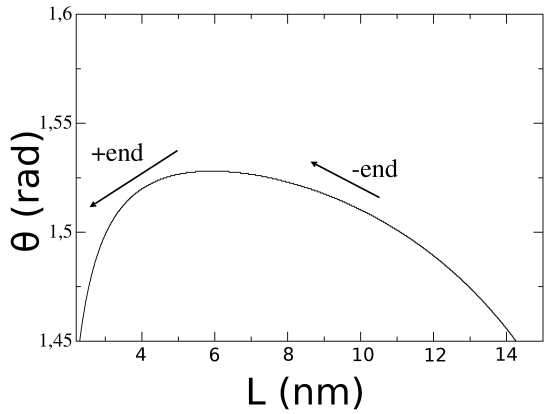

Figure 9.11: $\theta_{eq}(rad)$ as a function of $L(nm)$. Notice that arrows indicate the contraction induced by the switch negative to positive in the free head. Depending on the initial value of L, which is greater when the motor is more elastic and depending on how it shrinks after the change of the charge induced by ADP release, the motor can be plus-directed or minus-ended.

Stepping and sliding We shall comment one experimental fact that has been observed in Ref. [66]. Marking one of the heads of the motor and following the trajectory traced by it, it was observed that the heads don't only perform steps but also they slide along the protofilament. This fact is consistent with two things. First of all, the crystalline structures of the kinesin (Ref. [67]) don't seem to give separations between the heads bigger than 6-6.5 nm, so when the falling head approaches to the new binding site cannot reach it until the attached head detaches from the microtubule. Second, our minimal model predicts this behaviour very well. When the falling head arrives to the microtubule's surface, it has to wait a very small time pointing to the new binding site. After the other head detaches, the positive charged head will slide until its new position. If the motor has enough flexibility, this position can be reached faster.

The problem is that data from [66] has not been contrasted due to the difficulties of measuring single steps without coarse-graining the whole kinesin into a single dot. Moreover, stepping and sliding can overlap and in fact no one how disjunctive are these two regimes.

The central charge model

In this paragraph we continue the philosophy of the previous model but adding a new and important feature that the kinesin motors are shown to have. We will see how the electrostatic interaction with the neck domain will be crucial for directionality purposes.

Kinesin motors have three distinguishable domains, i.e. the tail, the stalk and the motor core. The tail is the domain where the beads or natural organelles are attached to be transported. The stalk is a $\alpha-$coiled-coil structure which lengths from 300 to 900 aminoacids. However, a minimum number of 379 residues is needed in order to have a dimeric kinesin (Ref. [59]). Finally, we have the motor core, where the heads and the ATP binding pockets are. Still there is a small but crucial fourth domain called the neck, which is the connector of the stalk and the motor core. In Fig. 9.12 we illustrate these concepts. As we can see, sometimes the neck and motor core are at the carboxile terminal (ncd) of the stalk and sometimes at the amino terminal (wild-type kinesin). Also we can see that this

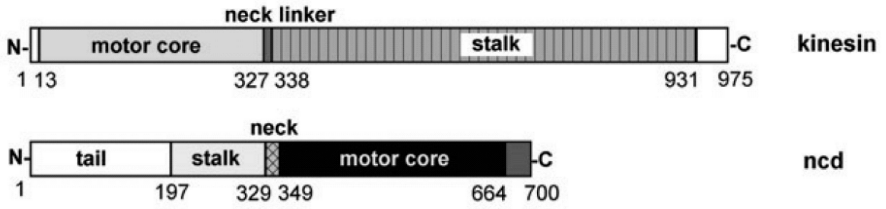

Figure 9.12: Different domains of the motor. Notice how the motor core can be at any of the ends of the stalk, giving very different properties. For the case of kinesin, the motor core is attached to the positive (amino) terminal of the stalk (left), while the ncd motor is bound to the negative (carboxile) terminal (left).

apparently trivial difference makes the motor very distinct, because one is a wild-type kinesin and the other a ncd. Why is this fact so important? The answer is that the stalk structure is a *polar* structure, as all the aminoacids are. The word aminoacid already expresses this polarity, because it makes reference to the two parts of its structure. One is the acid or carboxile part, a group $COOH^-$. The other is an amino group, NH_2^+. It is very clear that this electrical polarity is the essential key for the production of aminoacidic chains. But at the ends of these chains, always an amino or an acid group remains free. In Fig. 9.13 we present a simple scheme of this polarity.

As we saw in Fig. 9.12, the wild-type and ncd (non-claret disjunctional) kinesins have the motor core and the neck at different parts of the stalk domain. It is well known that wild-type kinesins are plus-ended while the ncd is minus-ended. From all the superfamily of kinesin, natural and mutants, we can see that some of them walk in one direction and others in the other. If one tries to correlate the directionality with the position of the stalk at which the motor core and neck are attached, we can arrive to a very promising conclusion. Most of the times, plus-ended kinesins have the neck linker at the amino terminal of the stalk, while minus-ended proteins have it at the carboxile or acid end. And the differences don't finish here. Another property of these motors seems to be correlated in the same way: the processivity. A motor is processive if it is able to perform some consecutive steps without detaching from the microtubules. Of course, no kinesin is infinitely processive, but while wild-type can perform more than twenty steps, the ncd typically performs only one. This property is again correlated with the polarity of the stalk. The minus-ended motor tend to be non-processive while the

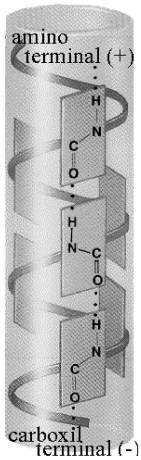

Figure 9.13: Schematic structure of the stalk. The amino terminal indicates a positive charge while the carboxile terminal is negative. This polarity is a direct consequence of the polarity of every single aminoacid. As every aminoacid is a small electric dipole, the stalk has a global dipole moment which is the sum over all the small dipoles.

plus ended are normally processive. It has to be said that not all of the motors hold this correlation, specially in the mutant families. A very special mutant was discovered not to have any directional preference, so it performs steps in both directions, probably decided by fluctuations each time (See Ref. [10]). Additionally, changes in the neck can strongly modify the mean run length [8].

With these experimental facts we will try to understand the relationship between the polarity and directionality (and maybe processivity) using a simple model that is no more than an expansion of the rigid heads model of the previous chapter. We consider again the $\beta-$model for tubulin and a rigid rod for the kinesin. This rod will have a charge in each terminus and one additional charge in the middle of the rod (neck). This latter charge is intended to take into account the terminal properties of the stalk. When the terminal will be the amino, we will put this charge positive (case of the wild-type), while it will be negative if we are in the ncd case. We can see a complete scheme of the model in Fig. 9.14, even with a third dimensional axis that will be considered in short.

This model has again one single and simple equation. In each head we calculate the force of interaction with the microtubule. Because we only deal with tangential

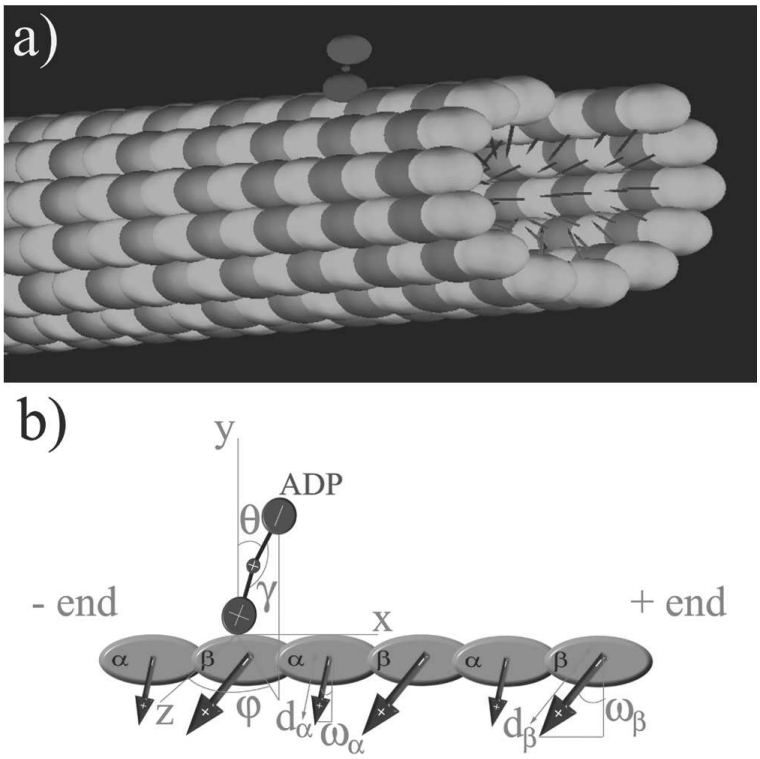

Figure 9.14: a) Microtubule electrostatic model with arrows indicating local dipole moments. The α tubulin subunits (dark gray) have smaller dipole moment that the β units (light gray). b) Electrostatic configuration of kinesin and tubulin made protofilament prior to ATP hydrolysis. Angle θ is polar while φ is azimuthal. The central-neck charge sign depends on the type of molecular protein while the head charges depend on the ATP hydrolysis circle. Dipolar lengths d_α, d_β and dipolar angles ω_α, ω_β are different in α and β subunits respectively.

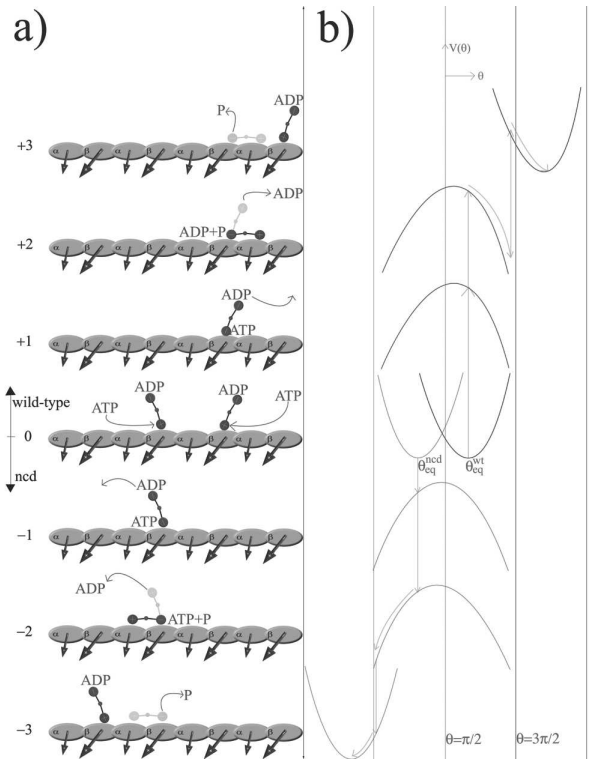

Figure 9.15: Electrostatics driven motor walk: Wild-type kinesin (+ states) and ncd (- states) stepping process (left column) and numerically determined binding protein-microtubule electrostatic potential as a function of local polar angle θ (right column). (0) Before ATP hydrolysis, both kinesin (positive neck) and ncd motors (negative neck) are in parked configuration pointing in opposite directions due to the difference in the central charge. The corresponding equilibrium angles are determined for the minimum potentials. (+1) ATP entry in the kinesin (attached) head pocket, with an accompanying charge change while the ADP at the other (tethered) head becomes unstable. (+2) The reversal and shift of the interaction potential of the previous state leads to falling of the tethered head deterministically towards the plus end. Since the length of the motor is not sufficient for reaching the next tubulin subunit we have (+3) a detachment and rising of the trailing head in such a way that allows the other head to slide to the next binding site. The ncd motor protein cycle proceeds similarly (- states) but the parked state is tilted towards the minus-end. Moreover, the negative-central charge induces a potential shift which is opposite to the plus-ended case. The falling of ncd motors is slower than positive-charged-neck motors, so the probability that the attached heads begins the rising before the tethered heads completes the falling is greater, leading to non-processivity.

forces, the interaction between the different motor's charges can be skipped. We call A to the central charge and B to the free head. Then, we obtain $\vec{F_A}$ and $\vec{F_B}$. Using eq. 4.5 we obtain F_{θ_A} and F_{θ_B}, so

$$\lambda_\theta \dot{\theta} = \frac{F_{\theta_A}}{L/2} + \frac{F_{\theta_B}}{L} + \xi(t). \tag{9.9}$$

As we see, the physics of these models is very simple. It is the complexity of the spatial distribution of the charges the fact that gives such special properties.

It is quite relevant to perform here an analysis of the potential in a similar way to the ones in the previous chapter. In this model, we expect the minimum and the maximum to be shifted only considering the variable θ. In Fig. 9.15 we can see the qualitative differences for both cases.

What is the reason for this shift between the two potentials? To answer this, it is important to notice that while the charge of the free head changes with the nucleotide state, the central charge remains constant all the time. Consequently, the global potential after and before the change are not symmetric because the potential contribution of the central charge is constant (and asymmetric) all the time. The fact that ω is not zero makes that the central charge and the positive charge of the occupied tubulin interact and decide the directionality. Then, we see how the directionality is driven by the polarity of the stalk. A lot of times it has been reported that the neck domain was crucial to decide if the motor was plus or minus-ended. In this section we have confirmed this by showing the qualitative mechanisms involved. In brief, it is the sign of the neck charge what decides the directionality. We have a plus-ended motor for positive necks and minus-ended motors for negative necks.

Fast and slow subprocesses: processivity As long as the central charge is positive, it is intuitive to think that the motor will have more affinity to the microtubule, and as a consequence, more processive. In the opposite case, a negative central charge will produce a repulsion that can difficult this processivity. To shed more light into this, we should separate the step into two stages. Recall that the vertical-tilted configuration is the parked state. Then, in the case of the positive central charge, the falling velocity to the microtubule after the new ATP binding will be clearly higher than in the ncd case. The reason is simply that in

the first case the central charge helps while in the other this neck-charge opposes to the falling movement. Recall also the fact that in such a process the falling of the free head and the hydrolysis and phosphate release of the attached head are in time competition. Then, if the falling time increases, the probability that the attached head detaches before than the free head attaches increases. If this happens, the motor will be completely detached from the microtubule and the processive walking is broken. From Ref.[61] we can estimate the average time for the detaching of the attached head as $\sim 10ms$, although it could be much smaller. We also know from our simulations and from Ref.[40] that the typical falling times for ncd are big, normally the double of the wild-type case. However they give times of the order of $50\mu s$, much smaller than 1ms. In any case, in the case of ncd, this time should be comparable with the detaching time of the attached head and that's why the probability of perform a consecutive step is low. However, falling times are much smaller in the wild-type case, and then the probability of detaching decreases although it is not zero. To make accurate predictions of these probabilities it is necessary to be in a very precise scale of the physical parameters like the relative permittivity or the drag force. On the other hand, the rising times for the head to reach the parked state are much longer in the wild-type kinesin than in the ncd. But this difficulty is not a problem for processivity because the attached head will remain attaches and without ATP a time which is always big compared with the rising times.
In Fig. 9.16 we see high experimental temporal resolution recording of some kinesin steps [40]. In the case of the forward (up) steps, we see an small initial displacement of 1-2nm with a very small waiting time after it. This would correspond to the falling process, while the second displacement would correspond to the rising. It is interesting to notice how the motor slows down at the end of the rising, in agreement with our simulations. From this figure we can see that $\sim 1-2nm$ are from the falling while $7-6nm$ are from the rising. This would correspond to a $\theta_{eq} \sim 135$, which make us to think that maybe the tubulin has more polarization than what is measured in Ref.[58]

The rigid γ model

In this subsection we sophisticate the previous model by considering that the motor is no more a rod but an arm with an angle γ (See. Fig.9.14).

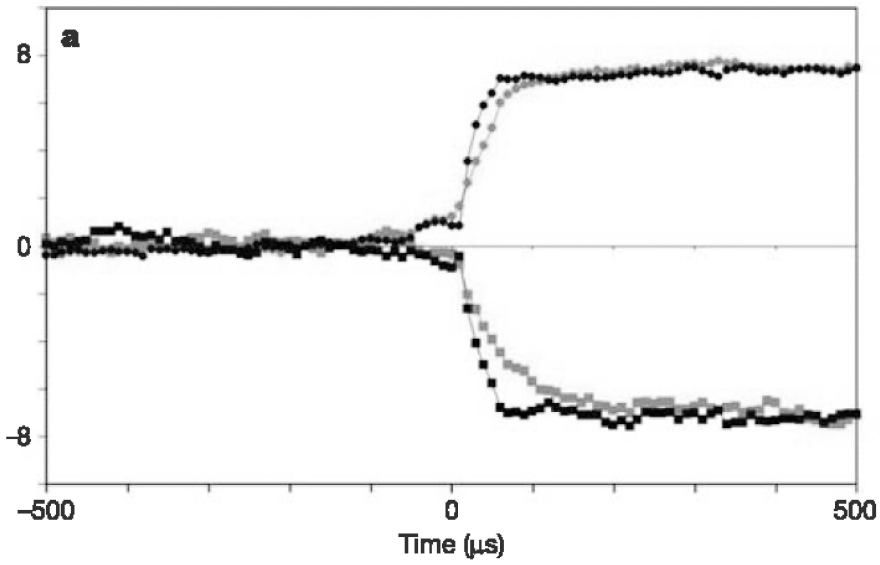

Figure 9.16: High temporal resolution recording of some wild-type kinesin averaged trajectories for single step-events[40]. Notice the two phases in every step. Upper trajectories correspond to loaded forward motion, while lower trajectories correspond to a backstepping regime.

The central charge will be in the vertex because the angle is located in the center of the motor. What is the motivation for this angle? Several crystallizations made on the structure indicate that tracing a straight line from head to head, the neck does not fall in this line, but slightly away. The quantitative estimations of this angle can belong to $(120, 175)$ although its flexibility should motivate us to consider γ as an elastic variable. For the purposes of this section let us consider the angle as constant and see how it modifies the stepping properties.
A very important remark concerning this model is that the restriction to 2 dimensions drives us to consider that γ and $360 - \gamma$ are different motors, although they would correspond to 2 opposite orientations of the same motor in 3D.

This generalization does not increase the number of dynamical equations. The only difference respect Eq.4.8 is that we have to make the following substitution

$$\theta_A \Rightarrow \theta_B + \frac{\gamma}{2} + 90 \tag{9.10}$$

and then we have again a single variable θ giving

$$\lambda_\theta \dot{\theta} = \frac{F_{\theta_B B + \frac{\gamma}{2} + 90}}{L/2} + \frac{F_{\theta_B}}{L} + \xi(t). \tag{9.11}$$

After what has been said until now, it is very clear which is the relevant variable for the step. Undoubtedly, $\Delta\theta$, i.e. the shift between the maximum and the minimum in the potentials. Let us show in Fig. 9.17 the evolution of $\Delta\theta$ as a function of γ. We define $\Delta\theta$ as $\theta_{max} - \theta_{min}$, so a plus-directed motor needs $\Delta\theta < 0$. Values of $\gamma > 180^o$ give steps more robust to fluctuations and external forces. However, in Fig.9.18 we see how for $176.5^o < \gamma < 180^o$ we also have plus-ended motion. The figures are for $\omega = 10^o$. Greater values of this parameter reduces the value for γ_{min}.

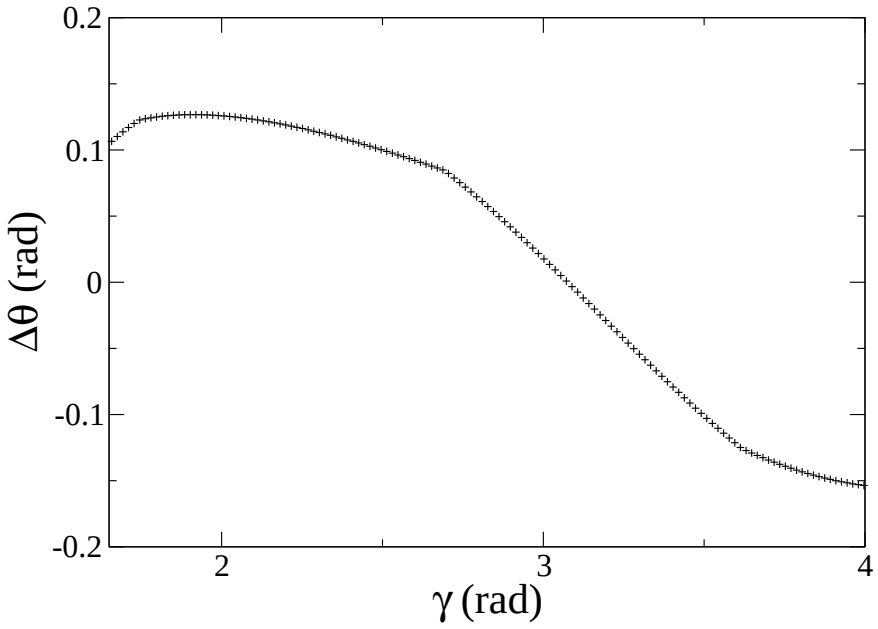

Figure 9.17: Plot of $\Delta\theta$ as a function of γ for $\omega = 10^o$.

The external load F In almost all the experiments that have been done with kinesins, the external force is a standard variable that is used to evaluate how

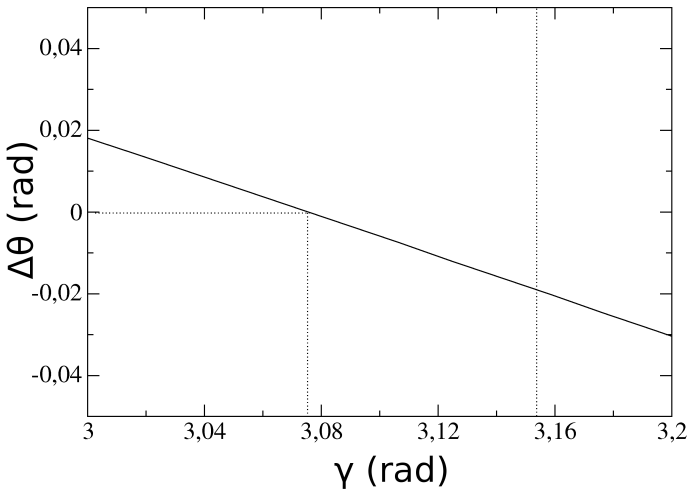

Figure 9.18: Magnification of Fig.9.17. We see how the critical γ to have directed motion is $\sim 3.07 rad$. This value corresponds to $\Delta\theta = 0$, where there is no directionality.

the motor behaves under its influence. Optical traps and fiber-glass devices have measured that wild-type kinesin can still walk until they are pulling forces of the order of $5pN$. In our models, one has to put this force only in the central charge because it is the place where the stalk begins and the load is supposed to be applied to the stalk. However, if one pulls these motor-models with loads bigger than 0.1pN, the motor reverses its direction. The stepping back mechanism has been recently discovered in Ref. [40], so our models are not in contradiction with it. But the magnitude of the stall force that we have is ridiculous compared with the experimental. What is wrong then? Maybe the parameter values are far from being realistic?

Parameters for an experimental scale The principal reason to question the values of the parameters used until now is that the motors are not able to pull with the experimental forces. The simulations in Ref.[58] are made in some very specific conditions in which the results can depend dramatically. Although we think that the tubulin is indeed dipolar, maybe the values of polarization are different from the ones reported in [63, 58]. From Fig.9.16 we estimated that the

θ_{eq} should be approximately 135^o, which makes us think that α should be close to this value. Such a value of α implies a reduction of d. In order to interpret the positive-negative pairs of charge as dipoles, it is important that

$$d < \frac{l_0}{2\sin\alpha}. \tag{9.12}$$

If this does not hold, the positive charge associated to a tubulin site would be closer to the tubulin site below and the concept of polarity would change. Then, we reduce to $d \sim 4nm$. With these new values, we are able to pull with loads up to 5pN, which is much more realistic. The source of this power is essentially the interaction of the central charge with the positive charges below the negative surface, so then a modification of the neck charge also helps to enter into a scale closer to the experimental.

9.5 The kinesin 3D model

From protofilaments to microtubules

The work that has been done in the previous chapters is no more than the preparation for a three-dimensional system where the kinesin works in reality. The first generalization one has to make is to take into account a set of protofilaments instead of a single one. We are not going to consider a full microtubule because the electrostatic forces decrease their strength as $\frac{1}{r}e^{-kr}$ and it is a nonsense to consider long-range interactions. What we will do is to consider the neighbourhood where the kinesin can be affected by electrostatic potentials. This system will consist in one protofilament in which the motor walks and the two first neighbours. Later we will show why it is not necessary to consider the interactions beyond the first neighbour. In any case, new concepts like the shift between protofilaments will appear. Others, like the curvature of the microtubule, have not been considered to be relevant.

The main difference between an electrostatic system in 2D and 3D is that we have to consider the lateral electric fields. To take this into account, we have to expand the microtubule lattice in a lateral coordinate. It is well know that while the axial periodicity of the tubulin is 8nm, the lateral is about 5-6nm. In Fig.

9.19 we show this schematically. Then, a crucial new question appears. If the

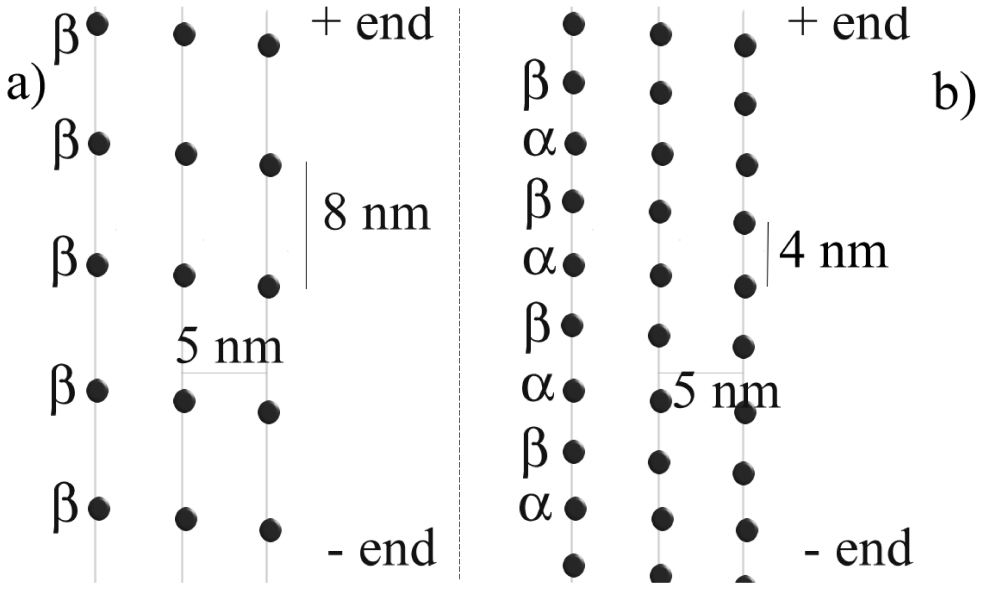

Figure 9.19: Scheme of the microtubule lattice showing the two different modellings. In a) we see the scheme for the β model, whereas in b) we have the scheme for the $\alpha\beta$ model.

characteristic distance along a protofilament is bigger than the lateral distance, won't be the lateral electric field stronger than the axial? One can see that the motor will rise when the free head is negative, but after the charge switching, will not fall to the adjacent protofilament? The answer is that, with the $\beta-$model of tubulin, yes. If we coarse-grain the full charge of the tubulin single points separated by 8nm, the lateral forces will dominate and the motor can no be faithfull to a single protofilament (in fact, it cannot even perform steps). This is the reason why we have to abandon the $\beta-$model of tubulin and concentrate in a more realistic one, the $\alpha\beta-$model. If one makes this, the resulting lattice is the one shown in Fig.9.19 (b).

In this new case we see how now the axial characteristic distance is of 4nm while the lateral distance remains above 5 nm. In fact, there is no surprise. The fidelity that kinesin show to protofilaments is so clear that is not difficult to accept that along this protofilaments the electric field is stronger than in other directions.

In Ref.[6] it is reported that kinesin walks parallel to the protofilaments not

only in the standard microtubule lattice, but also in other variants where the protofilaments are not parallel to the symmetry axis of the microtubule. These different lattices show different shifts between protofilaments, from 0.9 nm (in the standard lattice) up to 6 nm. This fact shows that the shift is a factor that does not affect the fidelity to a single protofilament. Moreover, we believe that the shift favours this fidelity because it increases the distance between to lateral tubulin sites and consequently reduces the strength of the lateral electric field in the rising or parked configuration.

In Ref.[59] it is reported that decorating tubulin sheets with kinesins, most of them attach parallel to the protofilaments, i.e. with both heads in the same protofilament. The same experiment reveals that heads always attach to the β-subunits of tubulin, although other references state that both α and β subunits have the same net charge ($\sim -25e$). One possible explanation for these evidences could be that the polarization of the $\alpha-$subunit is smaller, as it has been reported in Ref.[60]. In the context of our tubulin models, it would mean that d_α and α_α are smaller than d_β and α_β, respectively. These values will decrease significantly the negativity of the effective $\alpha-$subunit and then the reason of why the heads don't attach them becomes clear.

As we have already mentioned, the tubulin also exhibits a certain lateral polarization, i.e. perpendicular to the protofilaments and to the radius of the microtubule. We think that this fact is not relevant for the directionality, although it maybe explains some experimental facts. For example, in Ref. [59] the decorated tubulin sheets showed that the attached motor head had more probability to be shifted to the left (if the plus end is up). This would be explained by a 3D model of tubulin where the lateral polarization would be considered. Furthermore, in Refs [36, 7] asymmetric lateral properties were reported in the response to a lateral external load and in the dwell times, respectively. Maybe the lateral polarization has the key for the explanation of these properties.

Which value of γ shall we use in the 3D model? As we saw in previous sections, only angles greater than $\sim 173^o$ where effective to produce directed motion. However, two important restrictions have to be made. First, recall than in 3D γ

is always smaller or equal to 180^o because of the localization of the stalk and the external force that is transmitted through it. (See Ref.[67]). Then, we only have a valid domain of $\gamma \in (175, 180)^o$. On the other hand, one has to consider that the directionality is decided in the parked state. In this situation, the negativity of the free head strains the motor away from microtubule's surface. This allows us to consider that $\gamma = 180^o$ is the best choice. We will take this angle for the whole movement although we suppose that in other phases of the step its value can change. However, these supposed changes are not relevant. Any flexibility in the raising or in the falling will produce a step in the same direction because only the parked state decides if the step has to be produced to the plus or the minus end. Consequently, we take the most simple assumption: that the angle γ is always 180^o and that the neck does not permit significant compliance. These assumptions also simplify very much the numerical simulations.

As we are now considering a 3D system, we have to add an equation of motion to our simulations, so now the microtubule-induced kinesin interaction potential is given by

$$V(\vec{r}_i) = \frac{-1}{4\pi\epsilon_0\epsilon_r(1+ka)} \sum_{j=1}^{N} \frac{q_i q_j}{|\vec{r}_i - \vec{r}_j|} e^{k(a-|\vec{r}_i-\vec{r}_j|)}, \tag{9.13}$$

where $\vec{r}_i$ is the position vector labeling the charges on kinesin ($i = 1, 2, 3$), while $\vec{r}_j$ is the location of the N microtubule charges q_j on the α and β subunits. k is again the inverse of the Debye length, which we take around $\sim 3.5nm$, and $a \sim 1nm$ is the excluding volume radius as described in Ref. [64]. A regime with a greater a and lower Debye length l_D is also operative. We considered a flat microtubule with five protofilaments; due to the rapid decay of the force out from protein volumes, we include in total the $N = 10$ closest tubulin charges to kinesin, 5 from the surface and the other corresponding 5 partners below. For the simplest case when neck and head charges are aligned we have $\gamma = \pi$ and the protein reduces to a triply charged rigid rod. As a result the polar angle θ and the azimuthal angle ϕ are sufficient for describing the motor rotation, leading to the following overdamped equations of motion for kinesin:

$$\lambda\dot{\theta} = -\frac{1}{L}\frac{dV(\vec{r})}{d\theta} + \xi_\theta(t) \tag{9.14}$$

and

$$\lambda\dot{\phi} = -\frac{1}{L}\frac{dV(\vec{r})}{d\phi} + \xi_{\phi}(t) \tag{9.15}$$

where λ is the drag coefficient, L the head-to-head distance and $V(\vec{r})$ the total microtubule electrostatic potential of Eq. (9.13) at the Cartesian location $\vec{r}$. The environment is simulated through the thermal forces $\xi_{\theta}(t)$ and ξ_{ϕ}. For each we have $\langle\xi(t)\rangle = 0$ and $\langle\xi(t)\xi(t')\rangle = 2\lambda k_B T\delta(t-t')$. In order to integrate Eqns. (9.14, 9.15) we need to perform at each instant of time the Cartesian-to-polar transformation $\theta = \theta(\vec{r}, L)$. For the rotation we consider the attached head to coincide with the origin of the coordinate system; the latter is shifted by $8nm$ each time a step is completed. The simple Larmor-like rotation of the protein for $\gamma = \pi$ becomes a more complex rigid body rotation for $\gamma < \pi$.

9.6 Summary

What is the physical mechanism of the kinesin, then? We have seen how there are a lot of geometrical and physical properties in the system microtubule-motor and we have analyzed them step by step. In this paragraph, we can summarize the keys of the mechanism. First, it is clear that the microtubule has a broken symmetry along the axis of motion. This fact allows directional transport, although the specific direction is determined by the aminoacidic polarity of the stalk or other electrostatic properties of the neck. Considering $\gamma \sim 180^o$ we consider the 3D motor walking in a similar fashion than the central charge model. The reason is that the electric field along the axis of symmetry is stronger than in lateral directions. Differences in left-right lateral electric fields due to the shift between protofilaments and to lateral tubulin polarization can induce asymmetric steps, but don't modify directionality.

For some years, a long discussion about the stepping way of kinesin was produced. The main candidates were the inchworm mechanism, the symmetric hand-over-hand and the asymmetric hand-over-hand. Ref.[7] seemed to clarify that the last choice was the correct, although here we can make some comments about it. In our calculations, the mechanism of the kinesin results to be hand-over-hand but neither symmetric nor asymmetric because the motor rises vertically, i.e. without any rotation with respect to the axis defined by the vector which is perpendicular to the MT surface. However, in reality the stalk will disturb a perfectly vertical

rising and will force the motor to slightly turn left or right to allow the stalk to rotate and be oriented back, i.e. pulling the cargo. One can think then of the alternation left-right in such a rotation. We call B to a clockwise rotation and C to the counter-clockwise rotation. A perfectly asymmetric mechanism predict the pattern BCBCBC... while the symmetric one predicts BBBBBB... or CCCCCC... Most probably, it is the torsional stiffness of the stalk the responsible of the asymmetric stepping. After one step, the elastic restoring force will help the next step to be rotated by the opposite side. However, in Ref. [68] this stiffness is reported to be very low, so several things can be said about it. First of all, this stiffness may be reduced with decreasing lengths in the stalk, in such a way that this left-right compensation would be more significant for short stalks. If the stalk is long enough, kinesins don't seem to limp, and then one cannot suppose that the motion is strictly asymmetric. For example, one could observe the pattern BBBCCCBBBCCC... if the stiffness is so low that until three turns the elastic force is not significant. On the other hand, the thermal fluctuations would disorder any regular pattern. We conclude that for long stalks, the mechanism could be a mixture between symmetric and asymmetric hand-over-hand, although globally, the number of left and right events may be equal. For short stalks, the asymmetric hand-over-hand would dominate, but not necessarily in a regular way like BCBCBC... Once that the torsion spring is relaxed, the new event is probably decided by chance, so we could have BCCBCBBCCBBCBC... Of course, the shift between the microtubules and the lateral polarization of the tubulin could make this patterns more regular. For example, it is reasonable to suppose that if the stalk is relaxed, the preferential side will be the one with the lateral tubulin site shifted forward. In the case of the standard microtubule lattice, the shift is about 1nm in the left protofilament and -1nm in the right. Most probably, in the absence of torsional forces, the kinesin would prefer to turn to the left because is the lowest potential way.

In Figs. 9.20 and 9.21 we show our simulations for the 3D mechanism from different views. In Fig. 9.22 we have plot the three-dimensional potentials.

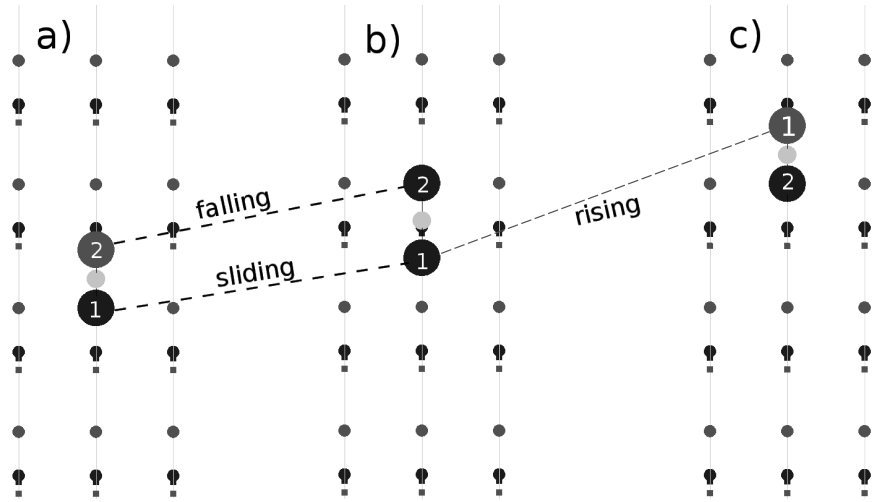

Figure 9.20: 3D aerial sight of plus-ended kinesin simulations. The motor is in a) Parked state with head 2 tethered and negative, and head 1 attached and positive. In b) head 2 (positive) starts to fall, and in c) the attached head 1 detaches and becomes negative, performing the power stroke. The transition from a) to b) shows explicitly the sliding of head 1 to its next tubulin binding site.

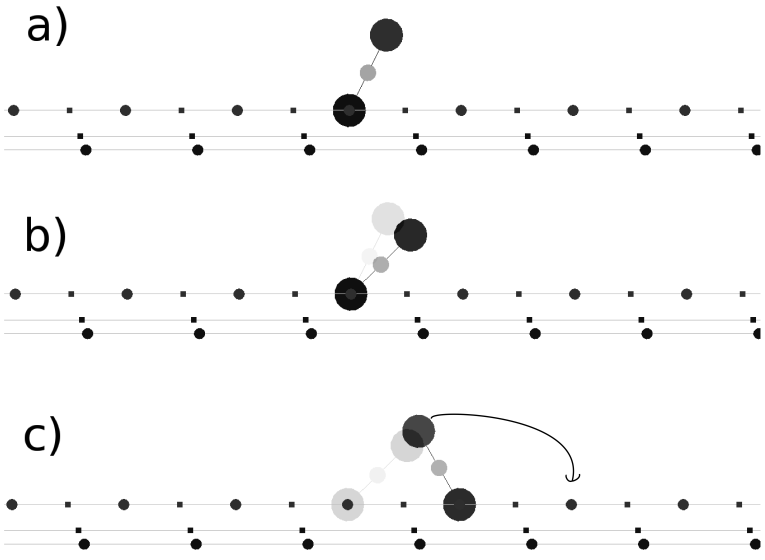

Figure 9.21: As in the previous figure, we show the three stages of the step from a lateral sight. In a) we see the parked state. In b) the falling regime with the parked state shown with transparency. State c) is for the rising regime, with a transparent representation of the previous state.

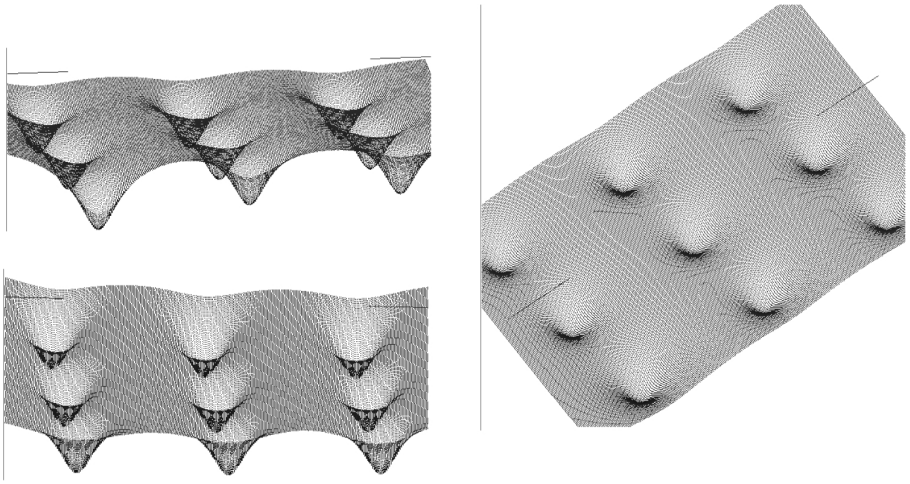

Figure 9.22: 3D microtubule potentials in the case of the $\alpha-$model of tubulin. These images illustrate the existence of binding sites arranged as in Figure 9.5

9.7 Mechano-chemical considerations

In kinesin motors, chemistry and mechanics are mutually connected in such a way that it is difficult to understand one without the other. In the previous chapters we have paid more attention to the physical part, maybe the most unknown until now. Now we will connect these mechanisms with the chemical paths that are involved in kinesin's cycle. As we explained in several chapters of this thesis, the essential chemistry of the kinesin is governed by ATP hydrolysis. Despite the simplicity of such a reaction, it is important to remark the different conditions in which every chemical state can act and the rates that depend on them.

Chemical pathways In Ref. [61] we can see an excellent chemical scheme that we reproduce also in Fig.9.23. We can see how in the absence of ATP, the head attaches strongly to the microtubule. However, when an ATP attaches the head, this head is still strongly bound to the microtubule. It is interesting to say that in myosin motors, when the ATP attaches, the head unbinds immediately from the tubulin. Of course, it is the negative charge of the ATP the responsible of detaching, but in the case of kinesin-tubulin systems, the way is more complex. From the Fig.9.23 we can see that after ATP binding, there is a cascade of rapid reactions that drives the system to unbind the head. First, there is a conforma-

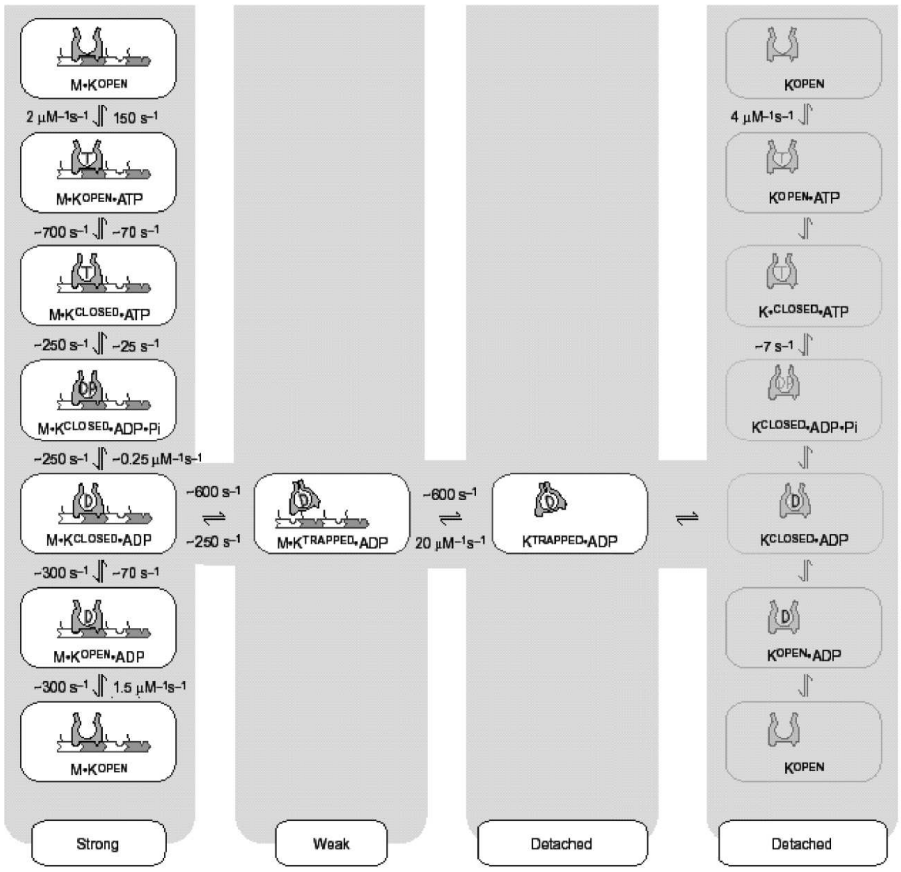

Figure 9.23: Chemical pathways of kinesin. Figure extracted from Ref.[61]

tional change that is supposed to close the ATP binding pocket. After this, the hydrolysis of ATP is produced. The energy to close the binding pocket should be taken from the ATP hydrolysis, so maybe the closing process and the hydrolysis run parallel. Later, the γ-phosphate group from ATP is released from the head, marking the crucial moment of microtubule detaching. In this moment, the binding pocket is supposed to close even stronger. If we consider the rates of the process we have that after ATP binding there are five rapid reactions with rates 700, 250, 250, 600 and 600 s^{-1} respectively, while the inverse reactions are clearly less probable. In next chapter we will provide a detailed explanation for this.

Rates In the already mentioned Fig.[61], there are 30 rates to be given, but only five are measured experimentally and 13 are estimations based on simulations. What does this mean is that any proposed model where the chemical and physical times are in competition is necessary speculative. More precise data about these rates is required. Specially in the fast cascade of microtubule detaching and in the detached states. For example, the rate at which the ADP is released from a detached head is thought to be fundamental in our workframe. However, there are more pathways to consider the full chemical cycle. Specifically, one of the most important aspects is to consider the rates in one head as a function of the chemical state of the other head. The scheme in Fig.9.23 is admirable, but it does not consider yet the mutual influence between the two heads. For example, we think that the ADP in the free head is strongly attached until an ATP attaches to the other head. In our opinion, the ADP has to unbind the binding pocket just to begin the step, and not after as other models propose (Ref.[69, 61]). Only ADP release before the step can convert the head's charge into positive and then to be attracted by the microtubule.

Physical and chemical velocities There are two different types of velocities in kinesin: physical and chemical. Looking at a position-time trajectory as the one in Ref. [9] we will rapidly notice that there are two very different slopes in the graph. One of these slopes is zero on average because it corresponds to the waiting time in the parked state and consequently the motor only experiments fluctuating displacements with zero mean. The other slope seems to be infinite and corresponds to the physical step. Although it is not infinite indeed, the time of the step is very small compared with the typical dwell times at low ATP con-

centration (which is the case in the plotted trajectories because the authors want to show the steps clearly). Only very recent techniques can show trajectories with greater (microsecond) resolution, see Refs. [70, 40]. While the physical velocity is about 10000nm/s, the global or chemical velocity never reaches the 1000nm/s. Furthermore, an [ATP] reduction or F increase implies the reduction of the global velocity but it has not been shown the same in the case of the physical velocity. Intuitively, we can speculate that under an external force, the physical velocity will decrease until the direction is reversed at superstall loads. However, under [ATP] reduction, the physical velocity is probably the same.

The difference in time scales is the reason why the kinetic models, like Ref.[43] have been successful fitting the experimental data. Furthermore, mechanical details rely on a temporal an spatial scale that are not easily accessible yet.

Mechanical substeps In Refs. [70, 40] the authors have studied the possibility of having substeps, i.e. to observe a tiny dwell time at some intermediate point of the step. Ref. [70] reports that there is one substep at $x \simeq 4$ nm when they pull with a $F = 3pN$. Ref.[40] reports that there are not substeps longer than 30μs under pulling loads of about $F = 5pN$. Several things can be said about this. First, that in the experiment where the authors find substeps the optical laser is focused diagonally. The optical trapping techniques may be affecting the system when studying a protein that behaves electrostatically. The laser beam produces an intense electric field that could modify the polar properties of the motor and the tubulin. Second, in the reference where the authors state that they don't find substeps, they show a figure (shown here as Fig.9.16) where there are indeed two well separated processes forward step.
What is clear about substeps in the context of our model is that there are two different physical regimes in one step: the falling and the rising (and we suppose the sliding regime as overlapped into these two). The consecutivity in time between them depend on the coordination of ATP hydrolysis in one head and ADP release in the other. We have also reported that these two processes have different rates and that this can be related with processivity. In fact, a clearer definition of substep has to be done. One can say that a substep is a step divided by a certain dwell time between the main step. In this sense, when the experimental

resolution will be high enough, they will find this waiting time (maybe Ref.[70] is already an good example of this, although maybe they have found an artifact). However, if what is wanted is to see that there are two different subprocesses in the step, then one has to be sure that there are indeed. The considerations made in the central charge model are a clear evidence of this.

Processivity Substep and processivity concepts are indeed very related. If there is no substep, processivity cannot be achieved. After ATP binding in the attached head there is a competition between this head trying to detach from tubulin (process A) and the other head releasing ADP and falling to the next tubulin (process B). What can happen in a competition? That any of the processes win or that they equal... If process A is slower than B, the full motor detaches from microtubule and the motor loses the processivity. If A is faster, then, there will be a time between ADP falling and process B where both heads will be attached to the microtubule. This time will be interpreted as a substep. In the case of a processive motor without substep, the difference in time between the two process has to be zero, or at least smaller than the temporal resolution of the experiment. Fig. 9.24 illustrates what has been said in this paragraph.

Trajectories In this last section we would like to show different perspectives of the trajectories traced by our 3D model. First of all, in Fig.9.24 we see the properties of two steps with micrometer resolution. The continuous line has a substep that is longer. Normally, in processive motors we will expect small substeps. Recall that the longer the substep, the less the probability of losing the processivity. The falling and rising regimes are differentiated, and also a very fast process of sliding. This corresponds to the moment at which the attached head detaches and allows the other to travel until the next binding site. Furthermore, in Fig.9.25 we plot a step in a millisecond scale, just to see how our model predicts the measured behaviour.

However, these trajectories, obtained with the polarization values from [63], do not seem to agree quantitatively with the averaged μs trajectories shown in Fig.9.16, where it seems to be an intermediate state located at a $\sim 15\%$ of the step displacement. If the first part of the curve corresponds to the falling regime and the second part to the rising regime, then the values of our parameters should be tuned in order to agree with this asymmetry between falling and rising, which

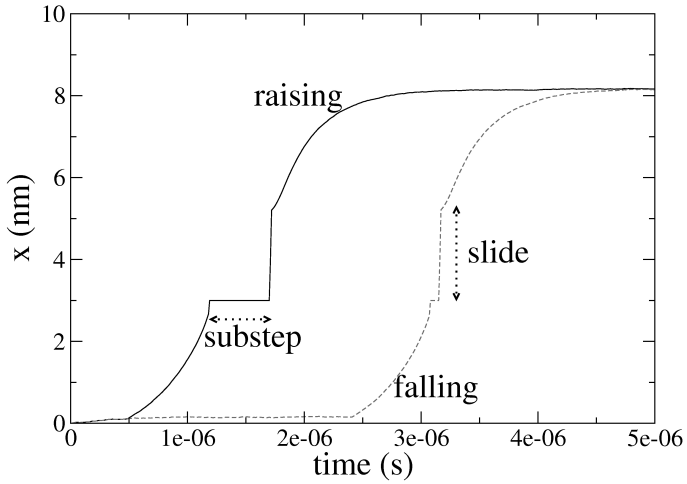

Figure 9.24: Details of two different steps. We follow the position of the central charge. The one with dashed line has a shorter substep. Note the microscale time of the processes.

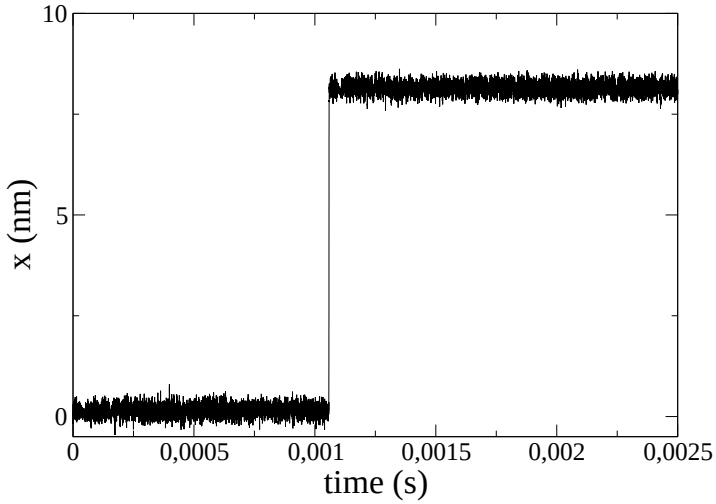

Figure 9.25: Trajectory of the central charge with millisecond resolution

is tightly related with θ_{eq}, the angle of the motor at the parking state. There are two main quantities that modify the angle of the parked state. First, it is better to increase the polarization angle until $\omega \simeq 20^o$, but strongest angles don't affect very much the output. It is the increasing of the neck charge what makes the difference. In order to reach a strongly tilted parked state we need to change the neck charge to $4e$. Then, we can obtain trajectories more similar to the experimental data shown in Fig.9.16. We show in Fig.9.26 an example. We can see how the falling regime produces only a small fraction of the step. After such displacement, an arbitrary (i.e. not known) time (we use 10^{-4} s) is waited until the rising of the attached head begins. Then, we can see how there is a complex rising curve that covers most of the 8 nm-step.

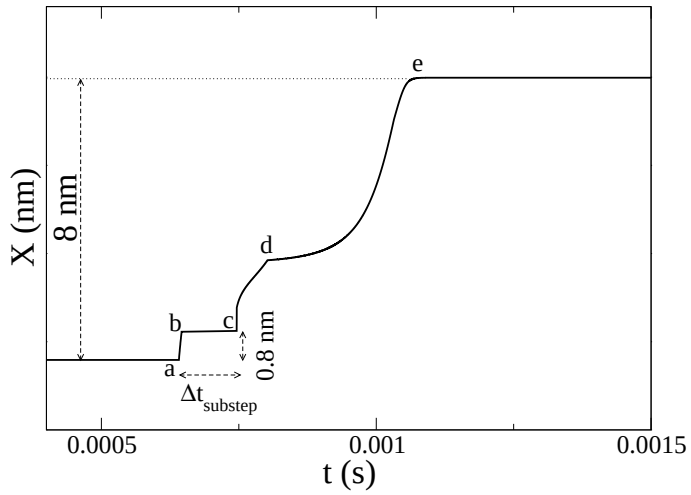

Figure 9.26: Simulated deterministic trajectory of a step for a neck charge of 4e and a polarization angle $\omega = 20^o$. a) The step begins with the falling regime, which drives a displacement of about 1 nm. The time between b) and c) is added by hand (10^{-4} s), since it is not known how long does the motor waits with both heads attached to the MT. After c), the rising begins until e), where the step is completed. In d) we see a singular point which is an artifact of the simulation. At every point, there is a criterion for which neighboring charges interact with the charges of the motor. At this point d), the neighboring sites change and the interactions are slightly modified, not affecting the qualitative behaviour. Such a singularity would be avoided by considering Debye screening, which is not included here.

9.8 Conclusions

In this section we have developed the idea that the kinesin acts as an electrostatic motor and showed how the results are in good agreement with the experimental features, even the most recent ones. To achieve a global understanding of its physical mechanisms, we have built a series of models of increasing complexity.
The main external input of this work comes from the numerical simulations made with the tubulin structure [63, 58]. The calculated polarization vector showed an axial asymmetry along the axis of the microtubule, fact that motivated us to perform these new calculations.
In the first part of this work, we presented two 2D models for tubulin. The first, the $\beta-model$, allowed us to deal with the majority of the motor models presented here, although at the end the $\alpha\beta$ model was required to have an axial electric field that should be stronger than the lateral one.

We have taken into account the electrostatics of the ATP molecule and showed that the charges involved in its hydrolysis are enough to justify microtubule's binding and detaching. Later, we introduced our most simple models for the kinesin motors. We saw how the switching charges in the head allow an stepping behaviour. A simple rigid dimer with charges at the ends was not enough to produce directed motion, but some elasticity in the effective radius of the motor allowed the system to step. We also saw how the specific changes in length determined the directionality of the motor. Only with this very reduced scheme we reproduce some principal features of kinesin.
The next qualitative jump in the way to a realistic model was to take into account the polarity of the stalk, leading to a central charge that depended on the aminoacidic polarity of the α-coiled coil. This charge results to be the essential factor for the directionality, because of its interaction with the positive region under the microtubule's surface. We showed by changing only the sign of this charge that the direction of motion is reversed, in agreement with the experimental results in real motors. Later, a discussion about the elasticity and the geometry defined by the $\gamma-$angle is made, arriving to the conclusion that this angle has to be near to 180 when the motor is on the parked position. The neck linkers shouldn't be so flexible because then the power of the central charge cannot be

easily transmitted to the free head.
Finally, a 3D dimensional model is presented with a high similarity to the central charge model. We justified the fidelity to protofilaments with electric field arguments and typical distances of the microtubule lattice.

As a general conclusion, we can say that the electric polarity of the tubulin protein allows the directed motion, while the polarity of the stalk or other electrostatic properties of the neck give the specific directionality. The role of ATP is not to induce global conformational changes but local ones, changing the sign of the head's charge and allowing the repelled ADP to bring the motor with it. Of course, some further improvements are needed, like to explain the high value of the stall force, maybe due to higher polarization in tubulin.
After a long time of many models, diverse speculation and frequently controversial experiments, we think that this work gives a general understanding of many of the crucial keys in kinesin motion. It also gives a new perspective to deal with other motors that may share similar properties. There is no surprise in our conclusions. At the molecular scale, the electrostatic forces are of the crucial importance, specially if the structures involved are known to be highly charged. The succession of attractions and repulsions, the combination of switching and constant potentials, the opening and closing of the binding pockets and the electrostatic structure of the microtubule have provided us the clue of how the chemical energy is converted into mechanical work in kinesin-1. The most relevant results of this section are published in [71].

10

An analysis of the nucleotide-dependent conformations of kinesin

10.1 Introduction

In order to understand how kinesin walks along microtubules it is essential to clarify how each of the heavy chain domains interact with tubulin heterodimers depending on the nucleotide state of the enzyme. Very recently [55, 56] new sets of experiments have been performed with kinesin-1 in order to shed some light to this interaction. Even though these references don't exactly agree between each other concerning the relative position of the tethered head with respect to the attached heavy domain, they both give some pieces to complete the ATP-head-tubulin puzzle. Our previous work on the electrostatic interactions on kinesin-microtubule systems [71] dealt with medium range forces that are based on Coulomb potentials and Debye screening effects. However, the nucleotide-dependent charge of each head was not modelled. The so called question of how the chemical energy is converted into mechanical work was reduced to the question of how the chemical hydrolysis manages to carry with itself the head domain when repelled from the microtubule. Furthermore, even though the role of the γ-phosphate group was known to be crucial in the process of head detaching [61], it was not clear how P_i could have such a regulating task. In this section we will give some new insight on the mechano-chemical energy conversion clarifying how the role of the phosphate

group is essential to the whole cycle.

In Ref.[56] some stationary situations between the head domains and the microtubule have been characterized with the FRET (Fluorescence Resonance Electron Transfer) technique. The main scenarios can be summarized as follows: in the presence of no nucleotide, both heads of the dimer are mainly attached to the microtubule. If we add AMP-PNP, a non-hydrolyzable analogue of ATP, we can see a similar situation, i.e. both heads are attached, but the distributions are less broad, i.e. the bindings are more tight. If we prepare a system where only ADP is available, then there are two mainly stable configurations: the heads that are attached to tubulin have no nucleotide in the pocket, while heads that are tethered but relatively faraway from the microtubule have ADP in their pockets. Furthermore, if we add P_i in a quantity that $[P_i]/[ADP] \sim 5 \cdot 10^4$ we can still see how the motor is mainly attached with a single head but a two-bound-state appears with a relatively small frequency.

Given this experimental information we will try now to complete our previous analysis of kinesin motion by modelling the interaction between four objects: a tubulin dimer (T), a kinesin's head (H) domain, an ADP and a P_i (P) group. Our main goal will be to describe the experimentally observed states of $T-H$ as a function of the state of ADP and P. We will introduce effective interactions between these four elements sheding some light into the question of how the stored energy in ATP is able to produce the necessary head detachment. In fact, it will be shown that the role of the phosphate P_i is pivotal in understanding the whole mechano-chemical cycle of kinesin. Specifically, it is the ability of P_i (which is negatively charged) of confining itself near also negatively charged structures like the ADP or the tubulin dimer at small distances what allows ATP energy storing, delayed head detachment and other phenomena that we will see on next sections. On the other hand, the other main assumption is based on the catalytic activities of the enzyme.

It is commonly accepted that an enzyme is able to lower the activation barrier of the ATP allowing the hydrolysis to occur with a huge increase in rate. We will incorporate this effect in our modelling in a more detailed way. Specifically,

we consider that the activation barrier, given by a gaussian potential term, is transferred from the ADP-P interaction to the interaction between the ADP and the head domain. In other words, when the ATP binds the pocket, the phosphate group and the ADP will not be confined anymore and thus they will repell to each other, while the confinement is transferred to the head, so the ADP is trapped into the head. In other words, the activation barrier of the ATP molecule is converted into a closing of the pocket. Additionally, we will consider that such a barrier transference produces the opposite effect on the other-tethered head, which causes the opening of the pocket and the subsequent ADP release.

First we will model the interactions between the four objects of the system. Then we will show the results, beginning by the simulation of the situations that have been performed in [56] and finally extrapolating the model to an ATP hydrolysis, which is a situation that is not trivial to measure in an experiment.

10.2 Modelling the interactions

In this section we will introduce analytical expression for effective potentials and subsequent forces between the six pairs formed by T, H, ADP and P. Most of them are essentially Coulomb potentials with a screening exponential correction due to the ionic environment. However, there are other interactions that, even though we have tried to write them in the most simple form, there are no available standard descriptions of them, as far as we know. The main goal is to describe the phenomenology involved in nucleotide-dependent kinesin-MT interactions, but some of the specific quantities presented here, even if they are reasonable, are introduced without experimental support. Specifically, it is the confinement effect of ADP into H, P into ADP and P into T what is not included in the Coulomb-Debye terms, so then we will make use of gaussian terms in order to model confinement barriers and wells.

Tubulin-Head (T-H) interaction

The interaction of a tubulin dimer with a kinesin's head is modelled by considering that the tubulin T is simply a charge Q_t with an excluding volume radius R_t. It interacts electrostatically with the head, with is also modelled as a charge Q_h

with radius R_h. We know from [63, 58] that a tubulin subunit can have about -27 electronic charges, but we will use $-35e$ as in [72]. For the kinesin head we will use $Q_h = 0.5$. The reason to consider the head as an effective positively charged structure is to be able to explain the affinity of free heads for the microtubule. The specific value of $+1/2e$ is based on the fact that we want a $MgADP$, which has $-e$, to be able to invert the sign of the head. So, if we choose these values, a head with $MgADP$ (we will omit the Mg for simplicity) will have charge $-1/2e$ and with ATP the total charge will be $-3/2e$.

The Coulomb interaction with a screening correction can be written as

$$V(r_{ij}) = \frac{kQ_iQj}{\epsilon_r r} e^{-r_{ij}/\lambda_D}, \tag{10.1}$$

where $k \simeq 230pNnm^2/e^2$, $\epsilon_r \simeq 80$ and $\lambda_D \sim 1nm$ are $1/(4\pi\epsilon_0)$, the relative permittivity and the Debye length, respectively (all in $[nm - pN - s]$ units system). The only missing ingredient is a contact repulsion in order not to allow H to penetrate T. This repulsion is incorporated through a Van der Waals term inversely proportional to x_h^{12}. We write x_h for the position of the head, which is bound between the interval $[0, L]$ and $L = 8nm$. We fix the position of the tubulin at $x_t = 0$ and we suppose its motion is negligible compared to the motion of the head. Then, we can write for the whole potential

$$V_{[t,h]}(x_h) = \frac{kQ_tQ_h}{\epsilon_r} e^{-x_h/\lambda_D} \left(\frac{1}{x_h} - \frac{(R_t + R_h)^{11}}{12x_h^{12}}\right). \tag{10.2}$$

This potential accomplishes the fact that the head has significant affinity for the microtubule when free from any nucleotide. We can see the plot of the potential in Figure 10.1.

Tubulin-ADP (T-ADP) interaction

The ADP molecule is again a charged object but now with charge $Q_{adp} = -1e$ and radius R_{adp}. Except from these two differences, the $T - ADP$ potential is the same as the $T - H$ potential. But now the ADP, being negative, will be repelled away from the microtubule and only thermal noise will be able to force

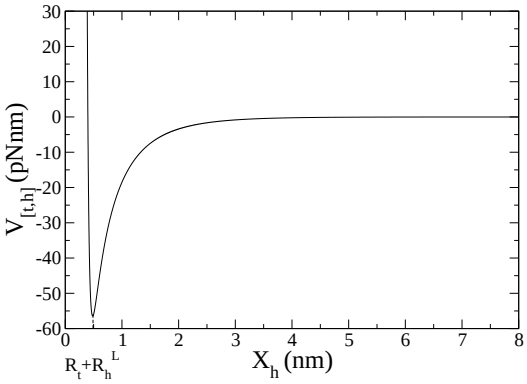

Figure 10.1: Potential between the head and the tubulin along a one-dimensional coordinate system. We can see how the head is mainly attracted to the microtubule due to its positive charge, even though it cannot penetrate it beyond $R_t + R_h$. In this potential, Debye screening predominates at long distances, while Van der Waals repulsion dominates at short distances.

an approach. The ADP particle, as all of them except the tubulin, can swim along the one-dimensional path between $x_{adp} = 0$ and $x_{adp} = L$. At $x_{adp} = L$ there is a reflecting barrier, for the ADP as well as for P and H. In the P and ADP cases, such a barrier is a way of introducing the concentration of these molecules. Specifically, the closest the barrier to the microtubule, the greatest the effective concentration. The existence of a reflecting barrier for H is simply a way of consider the tethering of the head by the rest of kinesin structure. Since in this model we are not considering dimeric-structural properties, we don't want the head to diffuse more than $\sim 8nm$ away from the microtubule. Thus we can write

$$V_{[t,adp]}(x_{adp}) = \frac{kQ_tQ_{adp}}{\epsilon_r} e^{-x_{adp}/\lambda_D} \left(\frac{1}{x_{adp}} + \frac{(R_t + R_{adp})^{11}}{12x_{adp}^{12}}\right). \tag{10.3}$$

With such a potential, as it can be seen in Figure 10.2, only thermal fluctuations allow the ADP to explore the vicinity of tubulin.

Tubulin-Phosphate (T-P) interaction

We know that when two charges are sufficiently closed, other effects apart from the Coulomb interaction appear. In fact, all the chemical types of bonding are

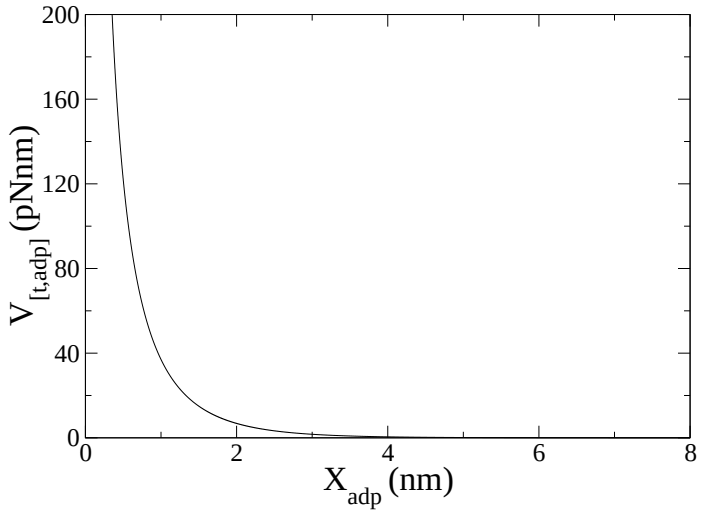

Figure 10.2: Interaction potential between the ADP molecule and the microtubule along the coordinate that defines the position of ADP, x_{adp}. Such an interaction is always repulsive, but the existence of a reflecting barrier at $x_{adp} = L$, due to a finite ADP concentration, allows the ADP to approach the tubulin helped by thermal fluctuations.

based on this highly nontrivial electrodynamics. The structure of the effective potential between the microtubule and the phosphate group is more subtle than the T-ADP potential. At medium and long distances, we can consider the same Coulomb-Debye potential as in the two previous cases. However, when P will explore, due to thermal noise, the region close to the tubulin, it will be able to bind it due to a well in the potential. With such a profile, the phosphate can eventually bind the microtubule in a higher energy configuration for a reasonably long time. We model this confinement effect through the addition of a gaussian potential to the Coulomb-Debye profile. The gaussian is centered at $x_p = R_p$, has a height $E_{[t,p]}$ and a standard deviation σ such that $\frac{1}{2\sigma} = A_{[t,p]}$. We can write the potential as

$$V_{[t,p]}(x_p) = \frac{kQ_tQ_p}{\epsilon_r x_p} e^{-x_p/\lambda_D} - E_{[t,p]} e^{-A_{[t,p]}(x_p - R_p)^2}. \tag{10.4}$$

This potential, plotted in Figure 10.3, even though is partially phenomenological, achieves the interesting property that allows the P_i confinement. Such a confinement is an hypothesis that is part of our model, but it allows to understand the stability of the AMP-PNP states of kinesin when attached to the microtubule and also prevents the ATP to be repelled from the microtubule before the hydrolysis process. Furthermore, the appearance of a relatively low-frequent state of two-bound-heads kinesin in ADP solution with high $[P]$ can also be explained with the confinement of P in T. However, such an hypothesis implies the fact that every tubulin site (at high $[P]$) may be occupied by a phosphate group. This phenomenon could be tested experimentally by labelling phosphates with isotopic techniques, and maybe it is this effect what determines the preference of kinesin to walk above the beta subunits of the protofilament. What is necessary then is that the binding of a new ATP in the attached head could be able to expel the phosphate that could be confined in the same tubulin site.

Head-Phosphate (H-P) interaction

We will simply consider that the phosphate group does not interact with the head. At first sight, it may seems counter-intuitive, but it's perfectly reasonable. Nevertheless, there is a strong connection between the head and P, but this

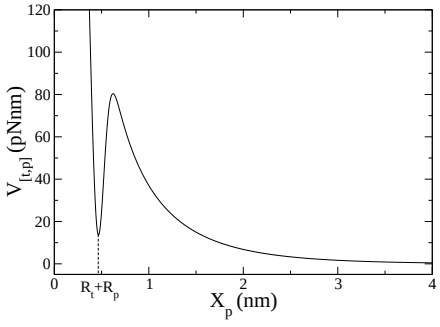

Figure 10.3: Potential between the phosphate P_i and the microtubule, T, as a function of P's position, x_p. We can notice how this potential is very similar to $V_{[t,adp]}$ except at very short distances $(R_t + R_p)$, where a confinement phenomenon appears. Our hypothesis is that the phosphate group is able to strongly bind the microtubule. This hypothesis can explain the affinity of AMP-PNP state of kinesin to the microtubule, and also the appearance of a low but finite frequency state of kinesin with two heads bound in the presence of free ADP and a big concentration of P [56]. But such an hypothesis suggests that every tubulin site, at high $[P]$, may be occupied by a phosphate group.

connection has the ADP molecule as mediator. Thus we write

$$V_{[h,p]} = 0 \qquad F_{[h,p]} = 0. \tag{10.5}$$

Head-ADP (H-ADP) and Phosphate-ADP (P-ADP) interactions: enzymatic barrier transfer and coordination between the two heads

The interactions of ADP with H and P constitute the main core of the model concerning enzymatic activity. It is known that enzymes are able to reduce the height of the activation barrier of the substrate facilitating the formation of the product. As we are modelling the interaction between ADP and P we need to consider such an effect. But there are evidences [61] that kinesin not only lowers the ATP activation barrier but also is able to close the nucleotide pocket upon ATP hydrolysis. Thus it is reasonable to suppose that the activation barrier is transferred from the $ADP \cdot P$ complex to the $ADP \cdot H$ system. We model this

barrier term as,

$$E_A = E_\Gamma e^{-E_\Gamma (r-R_\Gamma)^2}, \tag{10.6}$$

where the distance r can be either $r_{[h,adp]}$ or $r_{[p,adp]}$, depending on whether the enzyme is in a state $\Gamma = 1$ or $\Gamma = 0$. In fact, the $\Gamma = 0$ state corresponds to the ATP molecule in a stable conformation and the nucleotide pocket in an opened configuration, while $\Gamma = 1$ corresponds to an unstable ATP and a confined $H - ADP$ state (the ADP trapped into the closed pocket). We can write

$$\begin{aligned} V_{[h,adp]}(r_{[h,adp]}) = \Gamma E_\Gamma e^{-a_\Gamma (r_{[h,adp]}-R_\Gamma)^2} + \\ + \frac{kQ_hQ_{adp}}{\epsilon_r} e^{-r_{[h,adp]}/\lambda_D} \left(\frac{1}{r_{[h,adp]}} - \frac{(R_h+R_{adp})^{11}}{12 r_{[h,adp]}^{12}}\right) \end{aligned} \tag{10.7}$$

and

$$V_{[p,adp]}(r_{[p,adp]}) = (1-\Gamma) E_\Gamma e^{-A_\Gamma (r_{[p,adp]}-R_\Gamma)^2} + \frac{kQ_pQ_{adp} r_{[p,adp]}}{\epsilon_r} e^{-r_{[p,adp]}/\lambda_D}, \tag{10.8}$$

where we have added to each case the Coulomb-Debye contribution, with short-range repulsion in the $H - ADP$ case.

In this context, the activity of the enzyme is to change the value of Γ, which we will consider as an instantaneous switch between $\Gamma \in [0, \Gamma_{max}]$. We will discuss later which value of Γ_{max} is more appropriate in order to agree with experimental data. Furthermore, the Γ parameter is involved in the coordination between the two heads of kinesin. What is accepted is that ATP binding at the attached head promotes ADP release on the tethered head, but it is not known how both heads communicate, even though some mechanisms are proposed. First, a mechanical strain model in which ATP binding on the attached head induces a strain in the other head, but such a mechanism is ruled out since ATP gating is also observed with unpolymerized tubulin [55]. On the other hand, extra electrostatic repulsion due to the presence of ATP in the attached may help to ADP release [73] but it is not clear yet how this interaction can be channeled along $8nm$ without being completely screened. We will consider here the following assumption: let Γ_1, Γ_2 be the states in heads 1 and 2, respectively. Then, the states must always hold $\Gamma_1 + \Gamma_2 = 2 - \Gamma_{max}$, which implies that if one of the heads changes its state the other head changes it automatically. Such an entanglement, which could be

due to quantum effects, allows the two-head coordination, which is necessary for a processive hand-over-hand motion. The role of Γ is quite similar to the commutators of brushed DC electric motors.

In Figure 10.4 we can see plots of $V_{[p,adp]}$ and $V_{[h,adp]}$, at both $\Gamma = 0$ (solid line) and $\Gamma = \Gamma_{max}$ (dashed line). We can explicitly see the transfer of the activation barrier from $V_{[p,adp]}$ to $V_{[h,adp]}$ when $\Gamma : 0 \rightarrow \Gamma_{max}$ and from $V_{[h,adp]}$ to $V_{[p,adp]}$ when $\Gamma : \Gamma_{max} \rightarrow 0$. In our model we are considering that the height of the protection barrier is $\sim 150pNnm$, but as it represents the activation barrier of an ATP molecule it should be much higher. We are considering here a lower value for the sake of simplicity, as it does not significantly change the scenario in a qualitative way. However, a more realistic situation would require a much higher barrier, in order to obtain an approximately one-week-stable ATP [41].The mechanism of the barrier transfer is the following: When the ATP enters into the kinesin pocket, which in fact means that the ADP enters into the pocket and what is more important, the phosphate group is confined in the microtubule, the barrier is transferred to the interaction between the head and the ADP. Then, the repulsion between P and ADP without a high protection barrier helps the ADP expulsion away from the microtubule, but as now the head is confined with ADP, both ADP and H are expelled from the microtubule surface, which is the rising process of the trailing head described in [71]. When this head reaches the parked state and an ATP binds the attached head and it changes it barrier-Γ state, the tethered head changes its Γ-state as well in the reverse order and then ADP is easily released from the pocket, which causes the head to be attracted again by the microtubule, but this time to the next tubulin site. It is in Ref. [71] where the role of the neck in producing directional motion is discussed, while here we are focusing on how the substeps of the whole cycle are sequenced as the nucleotide states changes in each of the heads.

Furthermore, this approach allows us to model the experimental situation where we substitute ATP by the non-hydrolyzable analogue AMP-PNP. We will consider that the AMP-PNP simply does not activate the switch in Γ values, so we will see how the head domain remains stably bound to the microtubule thanks to the confinement of the phosphate, which in AMP-PNP is supposed to be able to bind the microtubule as in the ATP case. Numerical details and parameters of the model are shown in Table 10.1.

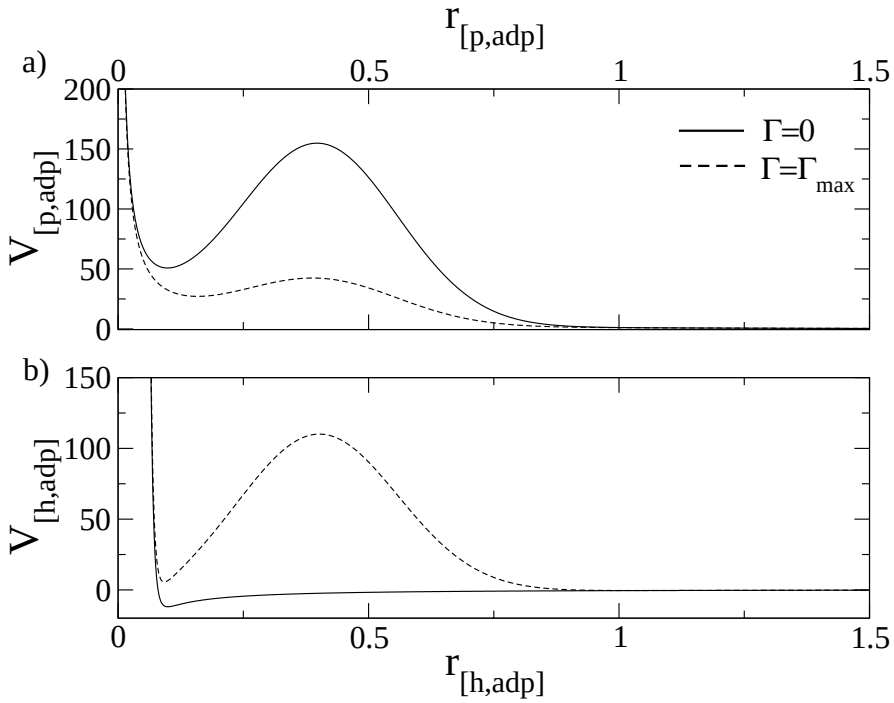

Figure 10.4: Interaction potentials of ADP with P (upper figure) and with H (lower figure). Each potential is plotted for $\Gamma = 0$ (solid line) and $\Gamma = \Gamma_{max}$ (dashed line). a) $V_{[p,adp]}$ versus $r_{[p,adp]}$, which is the distance between P and ADP. We can see how P and ADP can be confined at close distances ($\leq 0.25nm$) at a energy of $\sim 50pNnm$, which is the enthalpic value for the ATP hydrolysis. When they are mutually confined at this state we can say we have an ATP molecule. We can see, nevertheless, that when $\Gamma = \Gamma_{max}$, which here is 0.75, the protection barrier is strongly reduced, allowing a fast hydrolysis inside the enzymatic cavity. b) $V[h, adp]$ versus $r_{[h,adp]}$. When $\Gamma = 0$ the head and the ADP are electrostatically attracted, and ADP can bind the catalytic pocket, even though the average time of residence inside this cavity is low, specially if the head is bound to the microtubule. However, when $\Gamma = \Gamma_{max}$ the protection barrier is transferred from $V_{[p,adp]}$ to $V_{[h,adp]}$, and then, after ATP hydrolysis the ADP remains inside the pocket until Γ returns to a zero value promoting ADP release.

Parameter	Value	Units
ϵ_r	80	dimensionless
λ_D	1	nm
k	230	$pNnm^2/e^2$
$Q_p = Q_{adp}$	-1	e
Q_t	-35	e
Q_h	$-1/2$	e
L	8	nm
k_BT	4.1	$pNnm$
Δt	$\lambda_p 10^{-7}$	s
R_p^{stokes}	0.05	nm
R_{adp}^{stokes}	0.20	nm
R_h^{stokes}	2.00	nm
R_t	0.10	nm
R_{adp}	0.10	nm
R_H^L	0.40	nm
R_H^R	0.00	nm
R_p	0.45	nm
R_Γ	0.40	nm
$A_{[t,p]}$	100	nm^{-2}
A_Γ	20	nm^{-2}
$E_{[t,p]}$	125	$pNnm$
E_Γ	150	$pNnm$

Table 10.1: Paremeters of the model with their values and units

10.3 Numerical results and discussion

We perform Langevin simulations in one dimension with a gaussian white noise of intensity $k_BT = 4.1pNn$ where the drag coefficients follow the Stokes relation $\lambda = 6\pi R\eta$ where η is the viscosity of the medium, which we approximate to be equal to the viscosity of the water, $\eta_{H_2O} = 10^{-9}pNs/nm^2$. Here R is the Stokes radius, also called Van der Waal radius, and it is different for each of the four objects. Specifically, we consider that it is infinite (very large compared with the rest) for the microtubule, while $R_p^{stokes} = 0.05nm$, $R_{adp}^{stokes} = 0.2nm$ and $R_h^{stokes} = 2nm$. The equations are the following,

$$\lambda_p \dot{x}_p = F_{[total,p]} + \xi_p(t), \tag{10.9}$$

$$\lambda_{adp} \dot{x}_{adp} = F_{[total,adp]} + \xi_{adp}(t) \tag{10.10}$$

and

$$\lambda_h \dot{x}_h = F_{[total,h]} + \xi_h(t), \tag{10.11}$$

where

$$F_{[total,p]} = F_{[t,p]} - F_{[p,h]} - F_{[p,adp]}, \tag{10.12}$$

$$F_{[total,adp]} = F_{[t,adp]} + F_{[adp,h]} + F_{[p,adp]}, \tag{10.13}$$

and

$$F_{[total,h]} = F_{[t,h]} - F_{[adp,h]} + F_{[p,h]}, \tag{10.14}$$

are the forces associated to the potentials by $F_i = -dV_i/dx_i$. Furthermore, we fix $x_t = 0$.

The experimental cases

Now we will use the potentials described above to emulate the situations measured in Ref.[56]. First, we will simulate only kinesin with tubulin. Later, we will "add" AMP-PNP and then we will study the system with ADP and finally with ADP + P.

Kinesin with no nucleotide and AMP-PNP solution In order to reproduce the case where kinesin has no available nucleotide neither P_i, we will fix

the tubulin at $x = 0$ and allow the head to move along $x_h \in [0, L]$ interacting with V_{th}. This case is quite simple, since the positively charged head likes to be near the negatively charged microtubule. When we add AMP-PNP, a non-hydrolyzable analogue of ATP, it is observed that both heads of kinesin stably bind the microtubule. In the context of our approach this means that each head has an AMP-PNP attached with a phosphate group confined in the microtubule. Furthermore, as the AMP-PNP is not able to activate a switch in the Γ-state of the enzyme, the head remains attached to the tubulin. This case is quite interesting, since it is supposed to be a frozen image of what happens exactly after ATP binding, but without destabilizing the system towards a power-stroke cycle.

Thus these two cases, with no nucleotide and with AMP-PNP added, are quite similar and experiments confirm it. We show in Figure 10.5 two trajectories of the head, one (a) with no nucleotide and the other (b) with AMP-PNP added. In both cases the head remains bound to the microtubule, but in the presence of AMP-PNP and due to P confinement, the distribution in the latter case is wider, as it is experimentally found in [56]. There is relatively small portion of the x_h trajectory in the nucleotide-free case where the head is unbound from the microtubule, which corresponds to the experimentally observed one head bound state that appears with low frequency in the FRET setup of [56].

ADP In the case where we add ADP to the motor-microtubule solution we can distinguish two situations, depending whether the head is in a Γ-state or in the other. If $\Gamma = 0$, the head will not be able to trap an ADP in its interior and then it will collapse to the microtubule, while the ADP will mainly remain away from the heavy chain domain. Thus the situation can be summarized as ADP diffusing in the media and an empty head attached to the microtubule, as in the case where we add no ADP at all. However, if the head changes to a Γ_{max} state, it will have the ability to trap an ADP, so then the head and the ADP will diffuse together away from the microtubule. Such a diffusion is biased by the repulsion of the whole ADP-H system, which is negatively charged. Additionally, if we are supposing that the Γ-states of both heads in each dimer are entangled in such a way that in each head the state has to be different, we obtain a scenario where one head is nucleotide-free and attached to the microtubule while the

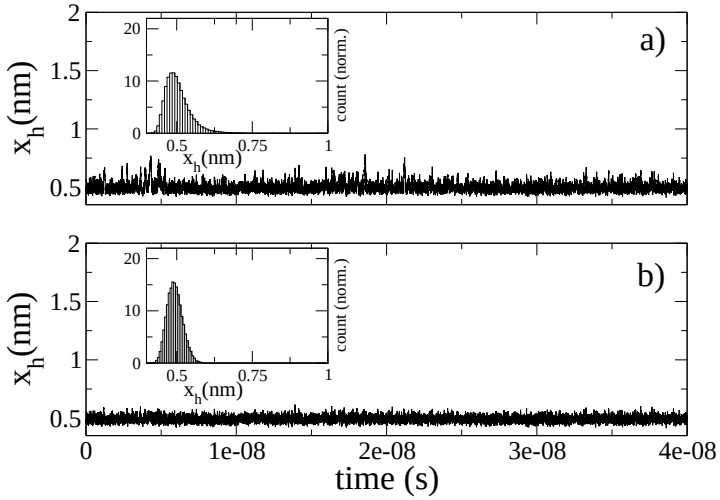

Figure 10.5: Trajectories and normalized histograms for x_h with no nucleotide (a) and with AMP-PNP added (b). We simulate the trajectories along $\sim 5 \cdot 10^{-8} s$, which is enough for the histograms to be smooth. In b), the initial conditions are taken with the AMP-PNP already bound to the T-H system. We can see how in the nucleotide-free case the distributions are broader, pointing to the fact that the head is not restricted by the confinement of a phosphate group in the microtubule, as is the situation in b). With AMP-PNP added, we can observe transitions from AMP-PNP bound and AMP-PNP free, but a high concentration of the non-hydrolyzable ATP analogue ($1mM$ in [56]) ensures that the head will mostly in the state we show in the figure.

other head is occupied by an ADP molecule and repelled by the tubulin electric field. Eventually, the ADP can overcome the protecting barrier and produce the collapse of the tethered head towards the microtubule again, and even though it is not the most probable situation, the FRET distributions observed in [56] that a two-bound-head state is also plausible (with low frequency). If the tethered head prefers to bind an ADP instead of being nucleotide-free we can guess that there is an electrostatic interaction (attraction) between the head and the ADP that makes the energy level of the HADP complex lower than the two elements alone. In Figure 10.6 we show our results for this case.

ADP+P When adding P_i to the ADP solution the state where one head is bound and the other is tethered changes to a state where kinesin can have one or both heads attached, showing bimodal diagrams from FRET experiments [56]. In the context of our model the explanation is straightforward. When we add phosphate groups to the system, (and the experiments add a $[P] = 10mM$ for $[ADP] = 200nM$), the tubulin sites may be mostly occupied by P. Kinesins are with one attached head and with another head unbound from tubulin. However, and because $\Gamma_{max} < 1$, there is still some affinity of ADP for the phosphate, i.e. if we use $\Gamma_{max} = 0.75$ there is still a 1/4 fraction of the activation barrier that prevents ADP·P binding (and confines them if the barrier is surmounted). Then, the ADP-tethered-head fluctuates and eventually the ADP interacts with the microtubule-confined P. This results in a relatively short lived state where the head is bound to the microtubule via the chain T-P-ADP-H. In [56], the peaks of the bimodal distribution show that the peak corresponding to a one-head-bound state doubles the counting number of the two-heads-bound peak. This indicates that the two-heads-bound state is not so shortlived in comparison with the one-head-bound state. On the one hand the former case is magnified by adding a big concentration of P, but on the other hand this suggests that the tethered head is quite close to a tubulin binding site when kinesin is on its parked state. This corresponds to a strongly tilted parked state, as it seems to indicate the results in [40] following the interpretation of [71]. Under this interpretation, the interaction of tubulin dipole moments with the neck and with the tethered head charges produces a tilted parked state. The more tilted the dipole moment and the greatest

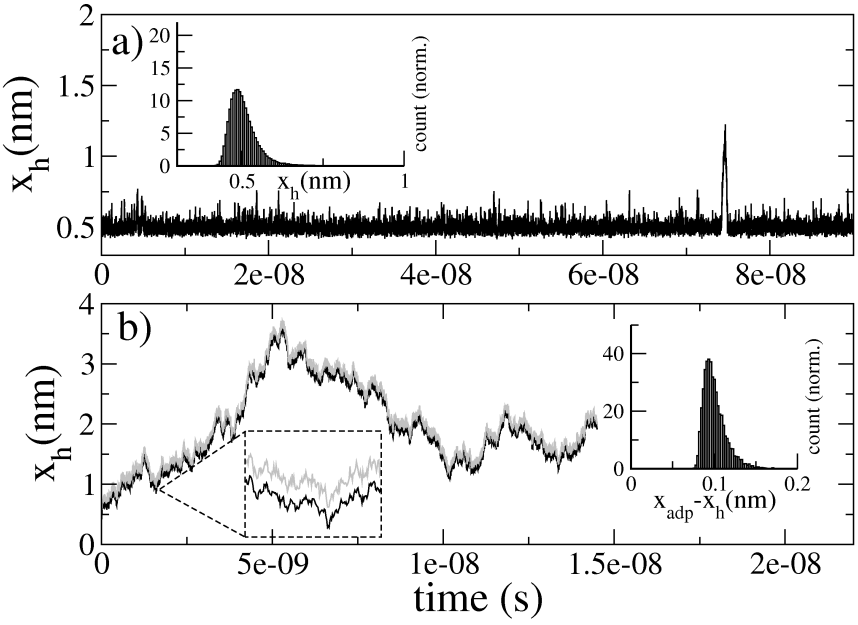

Figure 10.6: Two trajectories of the head (a) and the head and ADP (b) versus time for $\Gamma = 0$ (a) and $\Gamma = 0.75$ (b). a) This case, where $\Gamma = 0$, is quite similar to the nucleotide-free solution, as the head is almost permanently collapsed to the microtubule. The normalized distribution is also very similar to the one observed in 10.5a). In b) we have $\Gamma = \Gamma_{max}$, so then the head (black trajectory) is no more bound to the microtubule (located at $x = 0$). In grey we explicitly plot the trajectory for the ADP in order to illustrate how is the mutual confinement of ADP and H what allows the head expulsion from the tubulin site. The left inset shows a magnification of these two trajectories. The right inset shows the distribution of $x_{adp} - x_h$, which is peaked at $0.1nm$. The distributions shows no finite frequencies for distances bigger than 1 because there are no ADP release transitions during the simulation.

the charge of the neck linker the more tilted the parked state. From the μs resolution trajectories measured in [40] we can estimate that the tethered head is less than $2nm$ away from its target site. Then, in our simulations we have forbidden the head to diffuse beyond $x \sim 1.5nm$. Furthermore, we have located the H-ADP complex confined in the T-P complex as initial conditions and we have let the dynamics evolve for several runs. With this methodology we are able to quickly see a good approximation of the frequencies in the two possible states. It is interesting how the appearing of the bimodal distribution due to the presence of a high concentration of P reveals the close distance between the tethered head and the microtubule, giving more support to our electrostatic model presented in [71].

We show in 10.7 the plots of three consecutive runs, all of them with confined-state initial conditions, for the position of the head. In the inset we show the normalized distribution of this position where two well distinguished peaks are observed with relative frequencies in good agreement with the data presented in [56]. We can notice how we have restricted H's motion into $x_h \in [0, 1.5]nm$ in order to emulate the strongly tilted parked state of kinesin suggested by [71, 55] among other works.

ATP hydrolysis scenario

Finally, we should discuss the case where we add ATP and hydrolysis occurs. Such a situation is not stationary as the others but dynamic, as it implies kinesin stepping. In fact, whenever we have a realistic solution, i.e. ATP with ADP and P, we can observe all the previous features in a sequential way. First, when kinesin is in its parked state, the dimer has one head bound to the microtubule with no nucleotide while the other is tethered through the neck linker with an ADP bound. This is equivalent to the situation where we added only ADP. Later, when an ATP binds the attached-trailing head, the phosphate binds the microtubule, as in the AMP-PNP case. The difference is that AMP-PNP binds the tubulin with a long life time while ATP promotes the activation barrier transfer and it becomes hydrolyzed. But for a small time the AMP-PNP and the ATP scenarios are equivalent. After ATP hydrolysis kinesin returns to the parked state.

In our simulations we start with initial conditions where P from ATP is al-

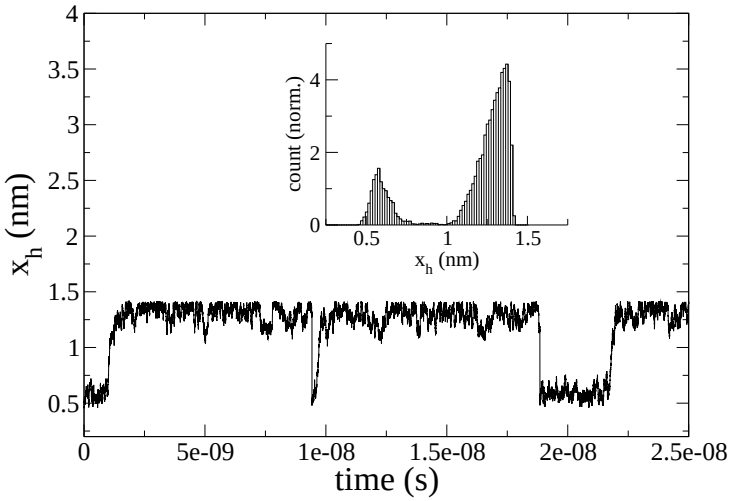

Figure 10.7: Three different and consecutive runs for the trajectory of the head with $\Gamma = 0.75$. The initial conditions locate the head confined due to the weak P-ADP interactions at high values of Γ. The bimodal distribution in the inset illustrates the existence of two metastable states, one where kinesin has one head bound and other where the dimer has its two heavy chains attached to the microtubule.

ready confined in the microtubule. Then, we must impose a condition where the enzyme performs its barrier transfer activity. We impose that $\Gamma : 0 \rightarrow \Gamma_{max}$ when $x_p < R_p$ and $r_{[p,adp]} > 0.1nm$. Then we observe how ATP hydrolysis is produced and after some time the head and the ADP, bound together, leave the microtubule. This time is crucial concerning processivity, as the slowest this process it is the higher the processivity of the motor. As it is discussed in Ref. [71], the ATP binding on the attached head promotes ADP release on the other head, which causes the collapse of this head to the next tubulin site. This falling process has to be faster than the detachment of the trailing head to ensure that at least one head is always bound to the filament. Otherwise the motor would detach from the structure and the processivity would be lost. Then, the time for the attached head from ATP binding to head detachment in comparison with the time from ATP binding to the leading head collapse is essential to achieve a processive coordination between the heads. Next we will analyze an ATP hydrolysis process and then we will characterize this crucial time.

In Figure 10.8 we can see the simulation performed for an ATP hydrolysis. First of all, we set the initial conditions with the ATP already bound to the tubulin site, since the time for the nucleotide to reach the P-confinement barrier in T is too long to for a simulation with a time integration step of $10^{-16}s$. Then the Γ-state switch occurs when $x_p < R_p$ and $r_{[p,adp]}$ is smaller than $0.1nm$. After this switch (which promotes the complementary Γ-state in the other head), the head detachment with the bound ADP occurs when a characteristic time (the necessary delay for the processivity) has passed. Then the head and the ADP leave the microtubule and travels due to diffusion and to the repulsion between the ADP·H complex and the negative microtubule surface. In the simulation, when the head passes through a position of $\sim 3.5nm$, we artificially switch the Γ-state (it is not necessary to wait more for a qualitative analysis). Then, the ADP is not strongly confined in the head anymore and this head starts an erratic trajectory to the microtubule again. Here we do not distinguish between different tubulin units because the directionality is given by the neck [71]. We can notice how the time left between the ATP binding and the head detachment is quite small, of the order of $1ns$. However, the time from the next Γ-switch until the arrival of the head to the microtubule is several times bigger. Under these circumstances,

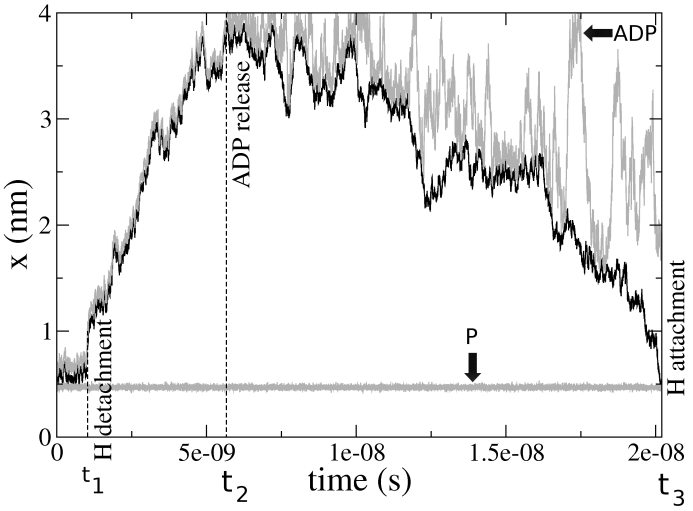

Figure 10.8: Trajectories for a whole mechano-chemical cycle in kinesin. The grey trajectory stabilized at $x \simeq 0.5nm$ corresponds to the position of the phosphate group P. The other grey trajectory corresponds to the ADP, while the black trajectory is the plot of the head trajectory. The initial conditions are located at $x_h = 0.5, x_p = 0.46, x_{adp} = 0.56nm$, which correspond to an ATP which has already bound the attached head. In $t_1 \simeq 0s$ the Γ-state switches from 0 to $\Gamma_{max}(= 0.75)$. In $t \simeq 10^{-9}s$ the head detaches from the microtubule. The ADP and the head leave together the microtubule until the Γ-state of the head comes back to 0 due to a eventual ATP binding on the other head, which is not simulated here but given by hand (at $t_2 \simeq 5.7 \cdot 10^{-9}s$, which should be much greater in a realistic situation). At $t_3 \simeq 2 \cdot 10^{-8}s$ the head has come back to the microtubule while the ADP remains away from the filament, diluted in the bulk.

the motor would not be processive. What could make the initial time bigger in order to achieve processivity? If Γ_{max} is smaller than the value in the Figure 10.8 (0.75), the time for head detaching increases. If we set $\Gamma_{max} = 0.65$, the detaching time is about $\sim 2ns$, and $\Gamma_{max} = 0.55$ produces a time of $\sim 4ns$, but then the hydrolysis process is not so efficient and undesirable events where P, H and ADP leave the microtubule are found with some probability. The reason for this is related with the value of E_Γ, which has the unrealistic value of 150 pN when in fact a more appropriated value should be much bigger. The problem is that very big values make the simulations very slow, as the potentials include huge forces. However, with higher values of E_Γ, the time delay would reach values that allow to explain processivity.

10.4 Conclusions

The confinement effects between the interactions of P, ADP, kinesin head and microtubule are responsible for the coordination of the mechano-chemical cycle. Specifically, the ADP and P are able to bind in a stable way, the phosphate group is able to become confined in the microtubule and the ADP is able to be confined into the head. These confinements, added to the electrostatic and steric interactions already discussed in our previous work [71] allow to have a broad description of the whole mechanism. If in the previous work we discussed how the electrostatic changes in the head allow the hand-over-hand motion with a directionality given by the neck, now we have discussed how the nucleotide states are related with the affinity of the heads with the tubulin. We have given phenomenological expressions for the potential interactions between the four elements which are located in a one dimensional system for the sake of simplicity. Even though this is a strong simplification, the results that we obtained are in agreement with very recent results and allow to give some hints on the mechanisms that underlie the interaction between kinesin heavy chain and tubulin heterodimers.

Specifically, there are two major points that constitute the essence of our approach. On the one hand, the ability of the phosphate group to bind the microtubule plays a pivotal role in the understanding of the affinity of AMP-PNP bound heads for the microtubule and also gives a clue of how the phosphate re-

lease is related with head detachment. It was previously accepted that P_i release promoted head detachment [61], but it was not clear from what did it detach. We understand the such a release means that P unbinds the ADP·H complex so this complex can leave the vicinity of the tubulin binding site. On the other hand, the hypothesis of the Γ commutator represents an assumption that is strongly phenomenological. The true nature of such interaction should be discerned experimentally.

Part IV

Summary of results and perspectives

Throughout this thesis we have developed three blocks of analysis. The first was based on ratchet models, which allowed to introduce energetic aspects and mechanical deformations. In the second block we developed a formalism which is shown to be useful for introducing mechanical forces into enzymatic reactions. Finally, the third block was devoted to have a deeper understanding of kinesin-microtubule motion from the point of view of electrostatics. Thus, we have analyzed physical and chemical aspects of some molecular motors focusing on mechanical, chemical and electrostatic details. In this small chapter we briefly list and summarize the most relevant aspects of the thesis from a critical and retrospective point of view.

11

Results

11.1 Ratchet-based models

In the first chapter, after the introduction, we begin with a ratchet-based approach to the kinetic properties of kinesin-1, also called the conventional kinesin. Under the experimental data of Ref.[9] we propose a simple model that is already an expansion of the model of Ref.[32]. The main idea is to use a tilted ratchet potential and simulate the trajectory of a brownian particle that is subject to this potential. The idea is to be able to reproduce the trajectories and most of all the mean velocity and randomness as a function of the two main control variables, the ATP concentration and the external load. Furthermore, the fact that there is a tight coupling between kinesin steps and ATP hydrolysis, at least at low load regimes, allows to couple the energetics with the mechanics in a very simple way. Considering a one-dimensional motion, kinesin advances 8 nm per ATP consumed. The step distance, given by the periodicity of the arrangement of tubulin dimers, is fixed, and the energy of an ATP molecule is also fixed, although there is some controversy if has to depend on [ATP]. But constant or variable, the potential that models the interaction between the microtubule and kinesin captures a 8 nm displacement every time the energy difference is ΔG_{ATP}.

With such a simple scheme we obtain reasonably good analytical expressions for the mean velocity and for the randomness. The trajectories obtained from

numerical simulations agree with the experimental. In fact, they agree *too much*. While experimental limitations for temporal resolution don't allow to discriminate discrete steps for high ATP concentrations, the simulations should do it as one can choose an arbitrary small step integration time. However, the model consider that at high [ATP] the potential is a single tilted-straight line, so no stepping occurs. We work in the limit where trajectories at high ATP concentrations and low loads are not step-like. This assumption is the main virtue and at the same time the most remarkable defect. The reason is that we work with an effective friction that makes a coarse-grain of the rapid steps that in fact are discrete. This allows to simple calculations that remarkably agree with experimental data. Furthermore, such a useful friction parameter does not has a realistic value.

When ATP concentration is lowered and the load is increased, discrete steps are experimentally discriminated, and our model captures this feature thanks to the addition of [ATP]-dependent barriers to the potential. Relating Kramers rates with Michaelis-Menten chemical kinetics we are able to give an expression for the [ATP]-dependence of the barrier. However, in our model we don't introduce a load-dependence on this barrier, but we simply introduce the external force as an external field that acts on the whole potential. With such scenario we are able to fit all the experimental data for the mean velocity within a reasonable confidence. The results for the randomness are not so good, since it is systematically underestimated.

After the physical analysis of kinesin motion, which was published in Ref.[37], we turned our attention to a model which could include a degree of freedom for the conformational changes that the motor undergoes. Specifically, the model is an inchworm machine that is able to work even without fluctuations. In order to do this, we based our work on a previous model ([42]) which was a two elastic-coupled-particles system where the spring changed periodically its elastic properties. The dimer, defined by the two particles and the spring, was under the influence of a ratchet potential. Then, the energy was introduced by flashing the rest length of the spring between a value L and $2L$. We changed the input of the energy by adding stretching forces between the particles, allowing the rest length to be constant. In short, the dimer initiates a stretching process until

its elongation doubles the rest length and then the system is left to be relaxed. With such a modification, our model presents significant improvements on the inchworm model literature. First of all, we implement a gaussian white noise in the modelling. Strictly speaking, the model can work without fluctuations, but the range of the parameters for an operating regime becomes too narrow. Thus thermal noise makes the choice of the parameters much more flexible. Moreover, the way of adding the energy to the system allows to control how much energy are we introducing. Even if in the previous modelling this could also be done, but was not done, the amount of energy depended linearly on the stiffness in such a way that high stiffness implied huge energy inputs. In our work, the energy does not have this kind of dependences, so we can be concerned with actual values for the energy of ATP. We find that a 8 nm displacement produced with a single ATP hydrolysis does not allow to exhibit a current reversal regime that is considered in Ref.[42] unless a lever arm mechanism is introduced in order to amplify a small conformational change to reach a long elongation in the dimer. Thus our model restricts, due to energetic considerations, the motion to the direct-forward mechanism, postponing the explanation for directionality of motors to another model.

There are more relevant results in our inchworm model to be considered. First, we introduce the process of nucleotide-fuel binding through a probability of catching the fuel molecule. Not only we can control how much energy we are adding but we can also control the concentration of the energetic substrate. This is very important since experimental measurements use the substrate concentration as their main control variable. Thus, through a probability that is considered when the motor is not experiencing a stretching-relaxing cycle, we can simulate a substrate dependence. But maybe the most relevant contribution of the work is the loaded conditions that we simulate on the model. By adding an external field against the dimer motion, we can see how the velocity is decreased with increasing loads until we see the stalling regime at which the motor does not walk on average.

The addition of the load in the model not only permits the evaluation of force-velocity curves but to analyze the response of the efficiency and the coupling ratio. As far as we know, the concept of global efficiency for a global trajectory

is introduced. While the more canonical efficiency, which holds for a single step, evaluates the ratio between the useful work and the energy input, the fact that a percentage of the steps are not produced even when substrate is consumed makes this efficiency poorly defined. It is more convenient to multiply the canonical efficiency by the coupling ratio. This is a major point, because the canonical efficiency includes the external force only in the useful work. But now, in the global efficiency, we have a load-dependent coupling ratio which gives to the efficiency a more complex load dependence. Classically, in an overdamped motor, the local (canonical) efficiency rises to one at the stalling regime, since there is no motion and no dissipation. But it is the case that our inchworm model, as kinesin and other motor do, presents a dropping coupling ratio at stalling loads, Then, even though the canonical efficiency rises, the global efficiency drops to zero. Thus, the maximum efficiency is reached at medium loads, as in macroscopic-inertial motors. We have to add that inhibition theory, as it is explained in the chemical-kinetic chapter, allows to give analytical expressions for all the variables of the system and for all the control variables dependence. We find that while kinesin is a mixed-competitive motor (in the sense that the load performs a mixed-competitive inhibition on the protein), our inchworm model is a mixed-uncompetitive motor. This means that the load affects the motor stronger when the dimer is on its stretching-relaxing cycle.

Summarizing, our inchworm model introduces significant improvements on previous inchworm modelling. For some time, the inchworm mechanism was a candidate for kinesin actual mechanism motion. However, today is discarded, see Ref.[7]. However, it is not discarded that other molecular motors and probably future artificial nano-devices can be based on this mechanism. The main results of this work are published in Ref.[57].

Finally, our ratchet-based model chapter finishes with a preliminary study of rotatory devices inspired from inchworm mechanisms. The idea is to generalize the stretching-relaxing cycles of the dimer model to circular arrays of particles connected by springs. The introduction of rotatory devices is inspired on the existence of nano-machines like the Bacterial Flagellar Motor or the F_O-F_1 ATP synthase. For us, the modelling of such machines is a challenge. Furthermore, the

available experiments are not so directly reproducible like in kinesin measurements. Rotatory devices are harder to measure. First, it is not easy to force the motor to a conservative external force, so normally non conservative loads are applied, like variable size beads or attached actin filaments. Secondly, and most important, is that there is no experimental evidence for a tight coupling between fuel consumption and step performance on the ion powered motors. In a BFM, about 1000 ions cross the membrane per revolution, but measurements show only 26 steps per revolution with no clues for a tight stechiometry. Furthermore, we can distinguish between motors with a single torque-generating-unit (active site) and motors with several units. To consider the 8 to 10 torque generating units of a Bacterial Flagellar Motor is a desirable target to model, but we have stayed at the case with a single torque generating unit.

We have modelled 10 particles coupled by springs and subject to a ratchet potential that is non-zero only at the active site. Otherwise, at every step all the particles should surmount an energetic barrier and the mechanism would be not neither realistic nor possible. What we do is to stretch the spring, as in the inchworm case, which is closer to the torque generating site, which belongs to the stator. Then, the whole rotor performs a displacement of an angle step. What we find is that the proposed mechanism is extremely inefficient, with maximum efficiencies of about ~ 0.005. This indicates that further work is needed in other to find more efficient mechanisms, but we have to admit that the coupling ratio of real rotatory motors is not experimentally known. Moreover, the inchworm approach to rotatory machines have to consider two main handicaps. First, many rotatory devices are reversible, i.e. inverting the flow of the ions the mechanism is reversed. In our modelling, the energy flow cannot be reversed. Secondly, many rotatory motors are based on ion interactions with the stator, not on elastic deformations. When considering elastic stretchings one has to consider that soft couplings are not efficient, and maybe the available energy is not enough to stretch very stiff springs. Summarizing, the last section of this chapter is an extension of the inchworm model to rotatory systems and a first trial to apply the inchworm mechanism to understand some rotatory devices. However, some caution has to be taken when thinking of ion powered machines. We think a good rotatory candidate to be explained by this mechanism can be the F_1 part of the

ATP synthase, since it has a well defined stechiometry, it has only three units and deformations play a role in the communication between the three nucleotide sites [5].

11.2 Chemical kinetic models

Briefly speaking, we can say that the chemical kinetic chapter constitutes the part with better agreement with experimental data and with lower degree of controversial hypothesis. While the first chapter uses standard and well accepted tools of analysis, the quality of its predictions is not very high and the theoretical models are not easy to be applicable to real molecular motors. On the other hand, the last chapter, based on electrostatic interactions and (probably quantum) confinements, is focused in a very particular molecular motor, kinesin-1, and we are able to understand many experimental features that are explicitly measured. However, the hypothesis that we used are controversial, since for most part of the scientific community the screening effects forbid electrostatic interactions on the range we are using them (we will expand this topic later). Moreover, the commutation and confinement hypothesis that we formulate in the last work of this thesis are pending to be measured in order to be discarded or accepted. However, the second chemical-kinetic chapter is based on a well established and accepted classical inhibition theory, which is an expansion of Michaelis-Menten formalism. Additionally, the hypothesis that we use are quite reasonable and have found good acceptance when presented in public. But what is most important, the agreement of our predictions with experimental data is not only qualitatively good but quantitatively accurate. We have been able to apply our formalism to different experiments on kinesin, to Bacterial Flagellar Motor and to RNA polymerase with a significant success in all cases.

In this chemical-kinetic chapter, we review the formalism of classical inhibition theory as we consider it is of capital importance to understand our work. In addition, we have calculated the free energies associated with the canonical examples. These energies could be used for further work on the analysis of efficiencies in molecular motors.

The first of the two main blocks of this chapter is aimed to introduce a mechanical force in the kinesin chemical kinetics using classical inhibition formalism. One can think this is useless since there is already a way of introduce the force in the chemical reactions. The already known method consists on modifying the kinetic rates with Kramers coefficients. However, when coupling the reaction coordinate with the longitudinal dimension of kinesin's motion, we have to introduce some longitudinal quantities that represents intermediate states of the cycle. And, as far as we know, these states are not observed in the motor trajectories at least for temporal resolutions lower than 30μs. And there is another and more severe problem with such formalism. As it modifies the equilibrium state between the reactants and the products, at the stalling regime, the Kramers coefficient are such that they compensate the driving free energy leading to a chemical equilibrium. In other words, the chemical potential vanishes at stalling conditions. The point is that this is not true, at least for kinesin, because even at stalling conditions, and even at backstepping regimes, ATP is still being hydrolyzed and as far as we know chemically inverted events are not measured (if detectable). Thus the previous formalism, which is still common to be found in recent literature and which for ion powered rotatory devices may be adequate, is not ideal for dealing with mechano enzymes.

We have developed a formalism that is able to introduce the mechanical force in a chemical reaction without affecting the equilibrium rates between ATP and its products. Instead, we use inhibition theory to inject the force as a lateral influence. In other words, we consider the mechanical force to be a inhibitor (or activator for assisting loads, but we will say inhibitor only for the sake of simplicity) of the reaction. At first sight, it may seem that with inhibitors we are also altering the equilibrium between the reactants and the products, but we are not. The critical point is to see that the rate of hydrolysis, k_2 in Scheme 6.56, has not a reversing partner, i.e. k_{-2}. Thus by adding inhibitor we are not promoting a reversible stalled state but a stalling regime where the motor cannot progress on its reaction. Furthermore, by using mixed inhibitors we are able to split the influence of the force on the two different chemical states (or more if we consider a more detailed reaction). In a classical michaelian scheme, we can consider that

the external force acts on the motor in a different way when it has an ATP bound or when it is nucleotide-free.

The main point of this work is to relate the inhibitor concentration, for which there was already a developed theory, and the mechanical force. What we have done is to *guess* a relation by examining the conditions that such a relation must hold, i.e. that for no inhibitor there is no force and that for an infinite inhibitor concentration we have a stalling force. In the following chapter, deeper reasons come to justify the explicit form of the inhibitor-force relationship. The important fact in the current work is that such a simple relation allows to apply in a straightforward way classical inhibition theory and obtaining excellent results when predicting experimental kinesin data. The inhibition theory, added to our I-F relationship, provides analytical-nonlinear expressions for the mean velocity as a function of the substrate concentration and the external force.

Furthermore, as kinesin shows to be a mixed motor, we are able to give a quantitative measure of how the mechanical force affects the different chemical states. Specifically, the two inhibition constants, k_{ic} and k_{iu} are given for the kinesin motor showing that $k_{ic} < k_{iu}$, i.e. it is a competitive-mixed motor. This allows to explain the fact that kinesin trajectories are modified in two different ways by the force. First, the jumping events, the 8 nm displacements, even though they seem instantaneous in a ms-resolution plot, they have a finite slope that is decreased in the presence of an opposing force. However, this effect is not so strong as the other consequence of the presence of the load. Waiting, or dwell times are strongly increased when the motor is loaded, and this is again due to a mechanical force, even if the binding rate it is usually considered a purely chemical-diffusive process (a physical interpretation of this fact is given in the following chapter). The fact that the two inhibition constants are different reflects these two types of influence of the force on kinesin motion.

Another important aspect of this work is that it presents a formalism and a methodology in order to characterize a motor. We have applied exactly the same methodology to the inchworm device obtaining an excellent agreement with the simulation data. Thus such a formalism is useful for characterize the kinetics of

a motor, no matter if it is a real protein or a theoretical machine. But the main goal is to apply this formalism to other real molecular motors as long as there is a complete set of measurements available. This is exactly the point of the next chapter. Following the idea that a general formalism can be given for every simple motor exhibiting michaelian behaviour under substrate concentration variations, we have developed a unified framework that is not only successful when tested with three different molecular motors, but also provides hints for a better understanding of the processes by which the mechanical force affect chemical rates.

The unified approach presented in the last section of the chemical kinetic chapter is based on the idea that the total average time of each mechano-chemical cycle can be expressed as the sum of the characteristic times of the different subprocesses that compose the whole step. Specifically, we split the total cycle time into the internal, waiting and mechanical time. With a characterized cycle time, we can characterize the mean velocity if we consider a tight coupling between mechanical and chemical events. The internal time is a variable that includes all the processes that are not dependent on the load or the substrate concentration. The mechanical time is simply calculated with overdamped dynamics. Normally, it is a fast process that even though is load-dependent, such a dependence is weak in comparison with the load dependence of the waiting time. This latter time is characterized by an effusion process of the fuel molecule to the binding site. In fact, the main point of this work is to explain the load dependence of the dwell times by considering that the external force increases or decreases the opening of the binding pocket when this force is assisting or opposing, respectively.

As a first approximation, we consider an harmonic load response of the pocket, but a sigmoidal, more sophisticated response, fits better the experimental data. When applied to three different molecular motors, kinesin-1, BFM and RNAp, the unified approach is in appealing agreement with the experiments. However, the main result of this approach is the splitting of the concept of stall force. As far as we know, the stall force has been defined as the force that stops the motor, but a distinction of whether the motor is mechanically or chemically stalled was lacking. With our approach, we can distinguish between these two types of stalling, mechanical and chemical. The mechanical stall force is that force that applied to

the motor compensates the motive force of the motor and then there is no mechanical bias to drive the motion. The chemical force, less intuitive, consists in closing the fuel pocket in a way that the nucleotides cannot be hydrolyzed. Then, even if the motive force is still greater than the external force, if the load completely closes the pocket the motor cannot perform further steps. At this point, we can distinguish between a motor where the mechanical stall force is greater than its chemical stall force and a motor where the chemical force is greater. In the first case, once we arrive to the mechanical stalling there is no more directed motion. However, in the latter case, we first arrive to a mechanical stalling when the pocket is not fully closed yet. Then, nucleotides still can be hydrolyzed. This window, between the mechanical and chemical stall forces, allow the existence of kinesin backstepping, where the mechanical cycle is inverted while the chemical keeps going forward.

As our approach is generic for all individual molecular motors, we can establish some quantitative comparisons between different types of motor. For example, the internal time in BFM is of the order of μs, while kinesin-1 has internal time of the order of ms and RNAp needs ~ 0.02s for its internal work. Such a parameter can give an idea of the complexity of the motor tasks. It is interesting that from the hypothesis of an elastic, load dependent pocket, we can have an idea of the relative stiffness of this pocket. For example, the pocket in RNAp seems to be ten times greater than kinesin's. This is consistent with the fact that a mechanical stalling of RNAp needs about 15 pN while kinesin needs ~ 5 pN. Moreover, the kinetic parameters of the pocket, modelled by a modified law of mass action, provide an interesting result: both kinesin-1 and RNAp have almost identical properties concerning nucleotide binding at free-load conditions.

11.3 Mechanics of kinesin

This part is probably the most far-reaching but also the most controversial part of this thesis. It first consists in analyzing the mechanics of the kinesin step by considering electrostatic interactions between the tubulin heterodimers and the motor protein. Later, there is an analysis of the interactions between kinesin heads and tubulin for different nucleotide states. In molecular biophysics there

is an explosion of experiments with optical traps, AFM and other devices that are able to measure single molecule techniques. However, it is beyond the current technology to deepen into the actual details of each molecular machine. Focusing on kinesin, optical tweezers allow to measure kinetics or directionality, while very recently, FRET has been able to measure nucleotide dependent conformations in an indirect way. But all these techniques don't allow yet a direct observation of the interactions that occur between tubulin and the different domains of the motor. However, there are many experimental facts with a lack of theoretical explanation. For example, some kinesin types walk toward the plus-end of the microtubule while other types have the opposite directionality. In addition, some kinesins are more processive than others. These and other topics have been without serious explanations, as far as we know. Perhaps there is a need for more experimental data, but we show in our work how there are many pieces that can be matched together in a quite simple and reasonable way.

The work is mainly based on the MD simulations of Ref.[63, 58], which show that is plausible to assignate an electric dipole moment to each tubulin unit. Such a dipole has a non-zero projection along the axis of kinesin motion. This result is a very interesting clue, since it represents a *physical* property that produces polarity in the track. Literature already distinguished the plus-end and minus-end of the microtubule in terms of polymerization rates, but a more specific polar property was lacking. Thus we took advantage of this result in order to model a microtubule as a periodic array of electric dipoles. Later, if an electric property defines the polarity of the track, this polarity has to be read by the motor by means of electrostatic interactions. The problem is that there is not very much specific information on the electrostatic properties of kinesin. In fact, electrostatics in proteins is known to be a major topic with very active research but with no clear and general results. We will discuss this topic more extensively later. Consequently, in order to advance with a model for microtubule-kinesin motion, some electrostatic assumptions on kinesin were made. We already know that ATP itself has negative charges, and this was taken into account. Additionally, kinesin heads were supposed to be positively charged when free from nucleotide, since they bind the microtubule surface, which is known to be highly negative. The strong point of the hypothesis is to consider that the head's charge changes sign

upon ATP binding. Thus the head and the microtubule are repelled. In addition to this assumption, another hypothesis is made concerning the neck linker. Under the light of some experiments [8, 10], we understand that the neck gives the directionality to the motor, and even a single mutation on it can produce directionless motors. Thus the neck *reads* the polarity of the track, so then we suppose that the neck interacts electrostatically with tubulin dipole moments. The most simple assumption was to consider the neck as a point charge, while the two heads of kinesin were two ATP-dependent charges. All three charges are supposed to be connected by a rigid rod. In brief, when considering this rod interacting with the array of microtubule charges, a directed motion is observed. Such motion is coupled in a way that an ATP hydrolysis produces a single step. This represents an actual *mechanical* model for kinesin, where "realistic" interactions are considered.

There are many relevant results of our electrostatic model for kinesin. First, it utilizes MD realistic simulation data in order to incorporate a physical polarity to the track, which interacts with a kinesin dimer in order to achieve directed stepping motion as it is measured on experiments. The energy input is given as the change of sign charge of the attaching head. In addition, it is very remarkable that such model gives a tilted parked state with the leading head pointing to the sense of motion, the plus end for a kinesin-1. This is in accordance with [55]. However, and this is a major point, such a tilting is not the responsible of directed motion. With no neck, the motor still exhibits a tilted parked state and no directionality is observed. The actual directionality comes from the interaction between the neck and the tubulin dipole moment, so *if the neck charge has a positive sign, the motor is plus-ended, while a negative neck produces a minus-ended kinesin.* This is in agreement with experimental data in the sense that motors with the amino-end of the stalk bound to the motor domain are plus-ended while C-term necks produce minus-end motion. Probably there are more electrostatic contributions to the neck than those coming from the polarity of the stalk, but the scheme proposed here is simple and agrees notably with experimental data.

Furthemore, the combination of electrostatic interactions with chemical rates provide clues for understanding processivity and why it seems to be related with directionality. In fact, plus-ended motor seem to be more processive than minus-

ended, and in addition this processivity seems to be enhanced when adding positive charges to the neck [8]. Our explanation lies on the competition of kinesin falling with trailing head detaching. When the trailing head binds an ATP, there is a time until this head detaches. While this occurs, the leading head releases its bound ADP and collapses to the microtubule. In order to achieve processivity, the motor has to be in a two-heads-bound state for at least some microseconds. If not, the whole protein would detach. Then, the falling process has to be faster than the initiation of the rising. This is tightly related with the charge of the neck, since a positive neck produces a fast collapse while a negative neck slows this falling. Then, as the charge of the neck is more negative (so the motor is minus-ended) the falling is slower and the chances for processivity are strongly lowered. While it is true in the context of this model that we don't have an explanation for the delay between ATP binding and trailing head detaching (and ADP release in the leading head), we know it has to exist and we also can explain how it competes with the mechanical falling in order to achieve processivity.

The second section of this chapter is the last work of this thesis and it tries to understand the interactions between the different nucleotide states of kinesin heads and the tubulin heterodimers, as such interactions are indirectly measured with FRET in recent experiments [56]. Our work is able to reproduce all the different states that the experiment performs: When kinesin-1 is nucleotide-free, it binds the microtubule with two heads. When ATP-PNP, a non-hydrolyzable ATP analogue, is added, kinesin still binds tubulin with both heads in a more tight way. However, if we only add ADP, the motor protein seems to bind the microtubule only with a single head while the other remains detached. Finally, if a huge concentration of phosphate groups is added to the ADP solution, some transitions between two-heads and one-head bound states can be detected. Our work is able to reproduce these stationary states and also the ATP state, which is dynamical and more difficult to access experimentally at this level of description.

Two main hypothesis are needed. First, that the γ-phosphate group of the ATP is able to be confined by ADP (this is not the hypothesis, but a well known ATP synthesis description) and *also by tubulin*. This latter confinement property is a key point to understand the different kinesin-MT states during the mechano-

chemical cycle. Specifically, when an ATP binds the attached head, the enzymatic activity is supposed to be manifest by a barrier transfer process, i.e. the enzyme is thought to transfer the confinement barrier of the ADP-P complex to its own interaction with ADP. Then, upon ATP binding, the ADP detaches from the phosphate group and becomes confined to the kinesin head. In other words, the head pocket becomes closed trapping the ADP inside, which was a necessary ingredient for our previous modelling in order to achieve a mechanical rising. On the other hand, the phosphate group becomes confined by the tubulin site. When ATP is bound, P is supposed to be already bound by the microtubule, while the ADP part is still not fixed to the kinesin pocket. However, upon the barrier transference, the phosphate is released from the ADP and this ADP is repelled by the microtubule bringing the head with it. This mechanism is in accordance with our previous model in the sense that now we have an explanation for the delay between ATP binding and head detaching.

The second hypothesis is as necessary as speculative. It consists to suppose that when the enzyme in one of the heads produces the barrier transference from ADP-P to the head-ADP interaction, in the other head, the other enzyme is coupled in a way that it switches its barrier state to the opposite state. We can think the heads as having two complementary states that mutually commutate. And even though we don't know how such interaction can be produced, it is clear that there is a communication between the heads, so our hypothesis makes sense.

With these hypothesis, we propose half-phenomenological potentials to model all the interactions between the heads, ADP, P and the tubulin unit and we obtain results in a good agreement with experimental data. If we let the heads in a nucleotide-free state, they bind the tubulin sites. If we simulate an AMP-PNP solution by considering an ATP which cannot induce barrier transference to the enzyme, then the heads also bind the microtubule in a more tight way than in the previous case. Even though the output is similar in both cases (they both bind tubulin), the reasons for such a binding are different. While in the first case a positively charged kinesin head is attracted to a negative tubulin molecule, when AMP-PNP is considered, the tubulin repels the head, which now has a global negative charge due to the presence of the ADP domain of ATP. However, the

phosphate group becomes confined in the tubulin heterodimer and this phosphate, on the one hand, has the ADP confined, while on the other hand the ADP is slightly attracted to the head.

When only ADP is added, one has to remind that each head is in a different enzymatic state (barrier-Γ state). Then, while one of them will confine an ADP, the other will not, so while the latter will bind the microtubule (free-nucleotide case), the other head will remain away from the microtubule with a trapped ADP in its interior. This leads to the tilted parked state described before. However, the addition of a high phosphate concentration produces transition between the tilted parked state and a two-heads-bound state. This is a non-expected experimental result that we are able to reproduce since we the phosphates are bound to the binding sites and these phosphates have a certain ability to confine an ADP (with a low confinement barrier, since the ADP head has transferred the high barrier to the ADP-head interaction). Then, due to thermal fluctuations, the leading head can explore the tubulin site where the phosphate is and form a metastable state where tubulin strongly confines phosphate, the phosphate weakly confines ADP and ADP is strongly confined to the head. Such a chain of confinements produce a transient bound state that we observe in our simulations.

This last section is in a good agreement with the experiments, but it is supported on strong hypothesis that have no direct experimental support. It is known that enzymes are able to lower the activation barrier of ADP-P, but there is no evidence, as far as we know, of a transference of this barrier. But what is true is that such a transference is an effective way to consider that upon ATP hydrolysis, the nucleotide pocket becomes closed trapping the ADP in its interior. And all these phenomena are well accepted in the literature. In other words, we have expressed with a very specific hypothesis well accepted assumptions in order to perform quantitative calculations. The other hypothesis, the Γ-state commutation, is again well supported by experiments even though the actual commutating mechanisms remain unknown. In addition, our model also needs that phosphate groups are confined by the microtubule, which can be tested in an experiment. If this is correct, under high P concentrations, ATP binding needs not only to reach the nucleotide pocket, but the phosphate group of the ATP has to expel

the phosphate that can be already confined in the current tubulin site.

12

Perspectives

Even though this thesis can be improved and expanded in all of its sections and aspects, we would like to remark two interesting directions that would be worth exploring them with more detail. First, the introduction of the load in chemical kinetics coupled systems should be of a reasonable interest. For example, tetrameric kinesins involved in mitosis can be thought as to kinesin-1 coupled to each other, i.e. the motive force of one is the external force of the other. This is interesting, since these forces would not be constant anymore, and mostly because the success in reproducing experimental data of our approach could be expanded by trying to couple both systems. If an opposing/assisting force were inhibitors/activators that we introduced to the system by hand, now each motor has to produce these kinetic factors in order to alter the motion of the other. Moreover, there is an example of capital importance that should be the target of such an study: the F_O-F_1 ATP synthase, which mechanically couples two rotatory systems through a shaft that is able to accumulate torsion. A complete understanding of the chemical kinetics of this system would condense all the difficulties, i.e. mechanical coupling of chemical systems, load-dependent kinetics of reversible motors, *even if they are mechanoenzymes as the* F_1, and a good model for reversible rotatory motion for different number of structural units. In short, a model for this motor would complete the formalism that we have introduced here.

The second aspect that would be interesting to develop, even more for the per-

spective of a physicist work, is based on electrostatic effects in protein systems. In fact, this is a very active and difficult field, so we should specify a specific direction to follow. Our ideas are motivated by the following problem: kinesin data can be explained by considering Coulomb electrostatic interactions between the heads, the neck linker and the tubulin dipole moment. However, Debye-Hückel theory states that such electrostatic interactions must be screened in the presence of an ionic environment [64]. Calculations using this theory for physiological conditions provide a value of the Debye length slightly smaller than 1 nm. This quantity means that beyond its value the strength of the interactions has been strongly disminished. Thus, if we are considering in our kinesin model some interactions that reach distances which are greater, i.e. more than 5 nm, such a model is not according with Debye theory at least in the physiological regime that is usually accepted. Given the problem, we have two choices. First, to abandon our model arguing that no electrostatic force can travel such a distance between kinesin and tubulin. Second, we can think that, even though screening is undoubtedly a strong effect in electrolytes, the theory may not hold for protein systems as the one we have been studied. Actually, there are many reasons to suppose that electrostatic shielding deserves a better understanding and it is not prudent to refuse models that, even though they contradict the 1 nm screening, it agrees with many experimental features.

In Ref. [64] we can find a detailed review on electrostatic in biological systems. Nevertheless, there are many approximations that may not be strictly correct in all cases. Debye theory, first of all, is a continuous theory, i.e. it considers a density of ions surrounding an object which is bigger than the ions. However, at physiological conditions this hypothesis may not be well justified. In fact, one can easily calculate that in the volume of about $100nm^2$, the number of ions that can be found is by no means big enough to make a continuous approximation. Then, the nature of the screening, when considered discrete, may alter the results of Debye theory. Later on, the canonical shielding calculations are considered under spherical symmetry, and again this is not the case of proteins. Given a charged object, if we allow ions to explore all the available spherical surface, we can place a maximum amount of ions. For example, if we had a charged object with a charge of 10e and radius R and we allow ions of charges +1e and -1e and radius

$r \lesssim R$ to freely move and surround the object, then some counterions, about 10 of them, will surround the first object forming a 10-side regular polygon. The point is that these counterions do repel from each other and then they try to be as separated as possible. Now imagine we only allow half of the spherical surface to be available to ions. Then, the 10 counterions will try to shield the big object, but they cannot be so spread as before. Now the interactions between ions produce an increase of the energy that in fact makes the screening less effective. Now we could reduce even more the available surface and the screening would be less and less strong. As far as we've been looking for asymmetric Debye theories we have not found concluding results, so we think it would be worth to analyze the implications of asymmetry in screening problems.

Another important aspect is volume exclusion. When Debye theory is considered in a system where ions occupy a certain volume, it can be shown that the Debye length has an exponential effect beyond the volume size. In other words, if no ions can penetrate the object, inside this object cannot be an effective shielding. This is very important when working with proteins, since the interior of their bodies are usually hydrophobic, thus no unstructured water and even less free ions can penetrate the peptide. Only with this qualitative and reasonable consideration one should not take Debye theory in a fully strict way when considering electrostatic interactions inside the protein body. For example, it is more or less accepted that kinesin takes advantage of the flexible C-termini of tubulin heterodimers, which are highly charged with negative sign. Thus it is supposed that a considerable amount of positive ions will surround these structures in order to reduce the overall energy. However, when a kinesin head attaches a tubulin site, it is not so straightforward to consider that these ions remain there and are not expelled by the hydrophobic presence of kinesin. This is a highly complex scenario, even for supercomputing capabilities, so we have to try with more simple schemes to gain some understanding. It is crucial to know that, without screening ions, the charges in the molecules are so high that the interactions between them would be incredibly greater than the measured forces. Then, we are not trying to say there is no screening at all, but simply to give reasons to think why probably the screening effects are not so strict under some circumstances.

Furthermore, there are even more complications that a complete theory should include. It consists in the dielectric properties and discontinuities that are found in protein media. Water is known to has a relative permittivity of $\epsilon_r \simeq 80$, while the interior of proteins, if definable [74], can be characterized by a dielectric constant of $\epsilon_r \sim 4$. As far as we know, there is no clear theories for proteins with low permittivity that are in contact, establishing paths of connection where there is no water or ions. Debye theory is considered for an homogeneous ϵ_r everywhere. Again, this is a strong hypothesis that is not faithfull to the real conditions. In our simulations, we have also considered an homogeneous permittivity, and we have also included a Debye screening of length ~ 3 nm, obtaining that the model still can work. But to consider that the path between the interior of tubulin to the interior of kinesin is electrostatically homogeneous with a continuous density of ions in the middle is an abuse of a nice theory such the Debye-Hückel formalism, which is applicable for many situations in physics and chemistry. The problem is too complicated to have strong opinions about it. But our electrostatic model is a hint for thinking that electrostatic interactions within a range of ~ 10 nm can play important roles in producing global conformational changes.

Part V

Resumen[1]

[1]We include this summary written in spanish because of the current legislation of the University of Barcelona

13

Resumen de la tesis

Un motor molecular es una proteína o un complejo de estas en el que una energía química, almacenada en forma de ATP o a través de un potencial de membrana, se transforma en trabajo mecánico, que se aprovecha para producir un transporte lineal, mover una hélice, introducir material genético dentro de la célula, etc. De hecho, las funciones asociadas a los motores moleculares son innumerables, en el sentido en que toda nuestra actividad motora está basada en en la motricidad de dichas proteínas y que buena parte de la actividad metabólica requiere movimientos mecánicos para llevarse a cabo. Por ejemplo, orgánulos y vesículas deben ser transportadas en la célula a través del complejo citoesqueleto. En este caso, kinesinas, dineínas y miosinas se encargan de caminar sobre filamentos de tubulina y actina para transportar dichos objetos. En el caso de células especialmente alargadas como las del sistema nervioso, la necesidad del transporte activo se hace patente. La difusión, si bien es útil para la accesibilidad general de varias sustancias como el ATP o algunos iones, no es suficientemente rápida y direccional como para ser un mecanismo útil en muchos casos. Tampoco hay que olvidar que incluso mecanismos exclusivamente químicos en apariencia como es la síntesis del ATP en la F_O-F_1 ATP sintetasa están mediados por un forzamiento mecánico que aporta la energía necesaria para dicha síntesis. En definitiva, la acción enzimática que producen las proteínas está íntimamente ligada con cambios conformacionales que producen fuerzas mecánicas que se han revelado importantes para su función catalítica. Si bien hace unas décadas las fuerzas generadas por una proteína indi-

vidual no se podían medir, las nuevas técnicas nanométricas como AFM, pinzas ópticas o FRET han hecho posible la medición en el rango de los pN (10^{-12}N), lo cual ha abierto todo un campo de investigación en el que la mecánica y la química se presentan íntimamente ligadas. De hecho, una de las vertientes más interesantes desde el punto de vista físico consiste en entender por qué las velocidades de reacción química dependen de las fuerzas mecánicas que se aplican a la enzima. La introducción de fuerzas en esquemas de cinética química se ha convertido en un ingrediente esencial, pues la mayoría de los motores moleculares funcionan en regímenes forzados.

En este breve capítulo se resumen las ideas principales de esta tesis así como sus resultados más relevantes. Todo el trabajo está dividido en tres secciones bien diferenciadas aunque con evidentes solapamientos que son ineludibles cuando se ataca a un mismo problema una y otra vez. El problema en sí es tratar de entender los mecanismos del funcionamiento de algunos motores moleculares, aunque la kinesina-1 es claramente el ejemplo paradigmático del que se tienen más datos experimentales y por lo tanto el objeto de estudio más detallado en nuestros análisis. El primer capítulo está basado en modelos tipo ratchet, es decir, modelos en los cuales el potencial de interacción del motor con el filamento viene dado a mano por un perfil diente de sierra que ya incluye la periodicidad del sistema así como su polaridad. A veces, hasta incluye el aporte de energía [37] aunque a veces dicha energía se introduce a través de alguna deformación [57]. En el segundo capítulo nuestro análisis se basa en una aproximación desde el punto de vista de la cinemática química, es decir, partiendo de esquemas cinéticos de reacción tipo Michaelis-Menten para luego poder ampliarlos e incluir en ellos una fuerza mecánica de forma apropiada. Finalmente, en el tercer capítulo se intenta un análisis más detallado sobre el funcionamiento específico de la kinesina-1 caminando por un microtúbulo. Se aborda el problema primero desde una perspectiva electrostática para poder explicar fenómenos como la direccionalidad o la procesividad para luego pasar a un análisis de potenciales químicos implicados en los diferentes estados del motor dependiendo de su estado enzimático.

13.1 Modelos basados en potenciales ratchet

En el primer capítulo, tras la introducción, empezamos nuestro estudio con una aproximación basada en ratchets y que tiene como objetivo reproducir los resultados experimentales de la Ref.[9] sobre la kinesina-1, también llamada kinesina convencional. El modelo que proponemos es ya una ampliación del modelo presentado en la Ref.[32]. La idea principal consiste en usar un potencial ratchet inclinado y simular la trayectoria de una partícula browniana sujeta a ese potencial. El objetivo es reproducir las trayectorias experimentales así como la velocidad media y el coeficiente de aleatoriedad (randomness) que se extrae de ellas. Además, tales magnitudes dependen de dos variables control principales: la concentración de ATP, [ATP], y la fuerza externa, F. El ingrediente principal que permite relacionar la química con la mecánica proviene del hecho experimental según el cual la hidrólisis de una molécula individual de ATP en la kinesina está relacionada con la realización de un paso mecánico. Al cociente entre el número de pasos efectuados y el número de ATP hidrolizados se le llama el cociente de acoplamiento, que es aproximadamente 1 para forzamientos suaves. Para fuerzas externas cercanas al régimen de fuerza máxima, al cual el motor se para, no está claro si dicho cociente se mantiene en la unidad o bien decrece. En realidad, no es descartable que se haga prácticamente cero.

En nuestro modelo consideramos un movimiento unidimensional, motivado por la fidelidad que la kinesina profesa a los protofilamentos del microtúbulo [6]. Además, sabemos que cada paso de la kinesina mide 8 nm, que es precisamente la periodicidad estructural del microtúbulo. En cambio, no está tan claro si la cantidad de energía disponible por ATP es conocida con precisión. Para dicha energía hay varias contribuciones: la entálpica, la entrópica (que es insignificante) y finalmente la debida a las concentraciones relativas entre reactantes y productos, lo cual completa la energía de Gibbs. No obstante, hay cierta controversia en si la energía que saca un motor individual de una molécula individual se puede precisar a través de términos que están basados en termodinámica de equilibrio y que requieren un número de moléculas grande para tener sentido. Nosotros, en cualquier caso, trabajamos aquí con la hipótesis de que sabemos la energía disponible a través del valor de la fuerza máxima, que es $\sim$ 6pN y el del tamaño

del paso, $\simeq 8$ nm. Entonces podemos estimar la energía que usa la kinesina en unos ~ 50 pNnm, que ya es la mitad de lo que normalmente se supone que es el valor estándar. En realidad, este valor puede significar que la kinesina alcanza una eficiencia del 50% o bien que la energía disponible no está bien calculada. Para medirla, haría falta observar transiciones químicamente inversas en el motor, sobre lo cual se ha trabajado [75] pero se está lejos de obtener números fiables. En cualquier caso, una vez que tenemos un valor para la energía que el motor usa por cada paso, podemos construir un potencial periódico que acople el cambio de energía ΔG_{ATP} con una variable espacial del tamaño del paso, L.

Con este esquema sencillo, es decir, con un potencial que es una recta inclinada cuya pendiente está determinada por el acoplamiento mecánico-energético, podemos fácilmente resolver de forma analítica expresiones para la velocidad media y el randomness en función de la fuerza externa. También podemos utilizar una dinámica de Langevin con ruido blanco gaussiano para simular una partícula browniana (el motor) sujeta al potencial (el filamento) y observar las trayectorias resultantes. Lo que se obtiene se parece a lo que se ve experimentalmente. De hecho, se parece *demasiado*. El motivo es sencillo: la precisión temporal en los experimentos no permite resolver pasos discretos en la kinesina a concentraciones de ATP saturantes, de forma que lo que se mide como trayectoria es una función claramente rectilínea con algunas fluctaciones debidas al ruido térmico. Eso es precisamente lo que se obtiene con nuestro modelo sencillo. Mientras que el experimento no resuelve pasos discretos, el modelo no tiene en cuenta que existe en realidad un tiempo de espera entre esos pasos. Esto es solo una primera aproximación, pero que ya permite unos cálculos interesantes y que no quedan muy lejos de los resultados experimentales. Además, este caso permite entender una de las hipótesis esenciales del modelo. Se trata de considerar que hay una fricción efectiva a condiciones de [ATP] saturante y fuerza externa nula. Es decir, que aun cuando en realidad la pendiente de la trayectoria experimental la determina en gran parte el tiempo de espera en cada paso, nosotros consideramos que no hay pasos y que una fricción, que evidentemente será superior a la real, es la encargada de producir esa pendiente. Así, en la fricción, introducimos los tiempos de espera que hay en condiciones no forzadas.

Cuando la concentración de ATP se reduce y/o la fuerza externa se incrementa, las trayectorias experimentales permiten discriminar pasos discretos. Eso obliga a nuestro modelo a introducir unas barreras de forma periódica que aumentan con la concentración en una forma que se deduce del siguiente argumento: al tener una barrera podemos asociar una frecuencia de paso usando la teoría de Kramers, lo cual introduce cuantitativamente la altura de la barrera de activación. Por otra parte, la teoría cinético-química de Michaelis-Menten permite relacionar la velocidad de reacción con la concentración de sustrato, ATP en este caso. Así, podemos llegar, a través de una identificación razonable entre las dos velocidades de reacción, a una dependencia de la barrera de activación con [ATP]. Todo esto nos permite, por una parte, obtener trayectorias con pasos discretos, cuyos tiempos de espera aumentan al disminuir [ATP]. Por la otra, nos permite comparar la dependencia de la velocidad media y el índice de aleatoriedad con la fuerza externa y con la concentración del sustrato. Mientras que para los datos de la velocidad media obtenemos un ajuste aceptable, los resultados para el coeficiente de aleatoriedad no son tan optimistas. En la figura 13.1 mostramos algunos detalles del modelo y sus principales resultados.

Estos resultados fueron publicados en [37] y suponen un primer avance en nuestro análisis. A pesar de que obtiene unos resultados, sobretodo en lo que a la velocidad media se refiere, que llegan a un buen compromiso con los valores experimentales, hay algunas críticas que se pueden hacer sobre él. De hecho, la hipótesis de la fricción efectiva, si bien es uno de los pilares del modelo y por tanto una de las herramientas que permite unas derivaciones analíticas, falsea en realidad la fricción real y enmascara la existencia de una velocidad global mecano-química por una parte y otra velocidad mecánica que es mucho más rapida y que desvela el verdadero coeficiente de fricción. Por otra parte, hay una larga controversia en si la fuerza máxima depende de la concentración de ATP o no. Aunque nuestro modelo, suponiendo un factor dependiente de la concentración en la energía disponible, reproduce aproximadamente los datos experimentales, luego dichos datos han sido puestos en entredicho e incluso refutados por nuevas medidas más precisas [40].

Tras un modelo en el que la introducción de la energía viene dada a mano, es

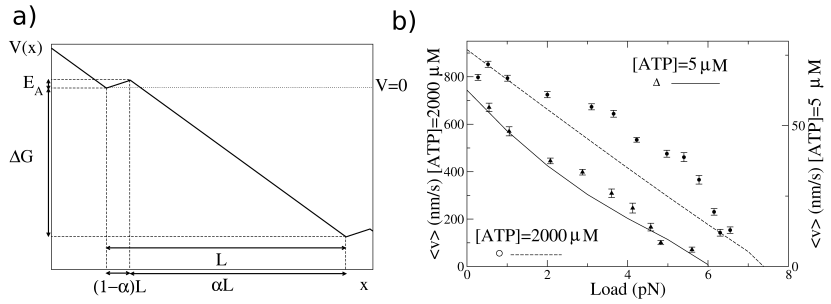

Figure 13.1: **Análisis de la dinámica de la kinesina a través de un potencial ratchet inclinado [37].** a) Esquema del potencial utilizado en el modelo, en el que se puede apreciar el acoplamiento mecánico-químico que hay entre el desplazamiento de L y el desnivel energético ΔG. Nótese también la barrera de activación del altura E_A que es la encargada de modular las diferentes concentraciones de ATP. Finalmente, α es el coeficiente de asimetría. b) Gráfica de velocidad-fuerza para dos concentraciones de ATP distintas, $[ATP] = 2\mu M$ y $[ATP] = 2mM$. Los puntos son datos experimentales [9], donde los triángulos representan los valores para el caso de concentración baja. Las líneas corresponden a las predicciones teóricas del modelo, las cuales están en un acuerdo cualitativo con los valores del experimento.

decir, sin suponer que existe un cambio conformacional, nos centramos en otro modelo que sí que incluye una deformación, aunque mantiene la interacción con el potencial ratchet, que ahora ya no está inclinado. De nuevo, nuestro modelo supone una ampliación de otro ya existente [42]. En este caso, no tenemos una partícula browniana sino dos, que están acopladas por un potencial armónico a través de un muelle que tiene longitud natural L, que a su vez coincide con el periodo del potencial de forma que en equilibrio las dos partículas reposan en mínimos consecutivos. En la modelización previa, la deformación se introducía a través de un cambio periódico en las propiedades elásticas del muelle. Concretamente, la longitud natural del muelle pasaba a ser $2L$ y tras otro periodo de tiempo volvía a ser L, lo cual además suponía una adición energética en dos tiempos. De esta forma, el sistema siempre tendía hacia un estado de equilibrio que había sido desplazado a mano. En cambio, nuestra forma de introducir la deformación se basa en la aparición de una fuerza de estiramiento que finaliza cuando el dímero ha alcanzado una longitud $2L$. Entonces el sistema relaja una sola vez y la energía ha sido dada también una sola vez, aunque de forma no instantánea, como el otro modelo, sino continua. Como consecuencia de estas diferencias, en el

modelo anterior la energía aportada depende linealmente de la constante de elasticidad del muelle mientras que en nuestra versión esta dependencia no aparece. Esto tiene implicaciones a la hora de poner límites a las cantidades de energía aceptables en un motor molecular. En Ref.[42], una constante elástica alta produce un cambio de sentido en el movimiento, pero como vemos en los cálculos eso implica un aporte de energía que no es aceptable en el rango experimental a menos que consideremos una ampliación de la deformación en un modelo de compás o de *lever arm*.

De forma estricta, el modelo funciona sin la ayuda de flucutaciones térmicas, es decir, se trata de un mecanismo puramente newtoniano. No obstante, la adición de ruido blanco gaussiano, lo que también representa un avance significativo en este tipo de modelos de gusano o *inchworm*, mejora notablemente la efectividad del mecanismo. Como, por otra parte, no consideramos más que energías dentro del rango experimental para la kinesina y el ATP (aunque este modelo es puramente teórico y de hecho el modelo de gusano no se corresponde al verdadero mecanismo de ese motor [7]), el único régimen que obtenemos es el directo, es decir, aquel en el que el dímero se mueve solo en la dirección favorable marcada por el potencial ratchet (aquel sentido cuyo movimiento encuentra pendientes negativas más suaves). Así pues, el mecanismo de la direccionalidad creemos que difícilmente puede ser explicado en el contexto de este modelo.

Hay más innovaciones en nuestro modelo que son relevantes. Primero, introducimos un mecanismo aleatorio en el proceso de los ciclos químicos a través de una probablidad de iniciar ese ciclo. De esta forma, las trayectorias que obtenemos muestran una distribución aleatoria de tiempos de espera que permite emular las distintas concentraciones de substrato a partir de esa probabilidad. Esto es importante en tanto que dicha concentración suele ser la variable control más utilizada experimentalmente. Además, el saber cuánta energía se está añadiendo al sistema nos permitirá cálculos de eficiencia y del cociente de acoplamientos, dos magnitudes importantes que además no son independientes. Por otra parte, una de los aspectos más relevantes a mencionar es el hecho de que evaluamos la respuesta del motor en condiciones forzadas, lo que permite obtener las deseadas curvas velocidad-fuerza así como permite el estudio de otras cantidades, como la

eficiencia, en función de dicha fuerza.

En relación a la eficiencia y al cociente de acoplamiento, definido para el modelo anterior, se introduce el concepto de eficiencia global en contraposición al de eficiencia convencional. Esta última se define en un motor molecular como el trabajo obtenido, es decir, el producto de la fuerza externa con el tamaño del paso, dividido por la energía aportada por la molécula. Cuando uno utiliza esta definición se encuentra con el resultado de que la eficiencia crece linealmente desde 0 (a fuerza externa 0, pues no se extrae trabajo) hasta 1 en el régimen de fuerza máxima, pues no hay movimiento global y tampoco disipación. Pero esta situación es incompleta si no se tiene en cuenta que existen eventos químicos (hidrólisis de ATP) que no producen un paso, es decir, eventos futiles. Estas moléculas no aprovechadas deben entrar en el cómputo de la energía suministrada para tener un buen cómputo de la eficiencia. Por tanto, basta con multiplicarle el cociente de acoplamiento a la cantidad anterior para lograr una evaluación de la trayectoria global, que es válida no para un paso sino para una trayectoria entera. De esta forma, la eficiencia encuentra otra dependencia con la fuerza, a través del cociente acoplamiento, que depende de esta de forma no trivial. Así, incrementando la fuerza externa y tras pasar por una valor máximo, la eficiencia vuelve a caer hasta hacerse cero en el valor de fuerza máxima, pues en este el motor gasta energía sin producir ningún trabajo útil. El valor máximo de esta eficiencia se encuentra alrededor de la mitad del valor de la fuerza máxima, como es el caso en los motores macroscópicos.

A todo esto cabe añadir que usando teoría de inhibición, como se explica en el capítulo cinético-químico que resumiremos más adelante, se pueden encontrar expresiones analíticas para la velocidad media en función de las variables control así como para el cociente de acoplamiento, lo cual permite contrastar los resultados de las simulaciones con los obtenidos con dicha teoría. Este contraste resulta ser satisfactorio en tanto que las simulaciones y la teoría están en perfecto acuerdo, lo cual no es tan relevante como un acuerdo con valores experimentales, inexistentes en este caso. Encontramos que, en contraposición a la kinesina, que como se verá es un motor mixto competitivo, el modelo inchworm que desarrollamos es un motor mixto no competitivo, lo cual significa que la fuerza actúa sobre el

dímero de forma más severa cuando este experimenta su ciclo de estiramiento-relajación que cuando simplemente sufre las fluctuaciones térmicas.

En resumen, nuestro modelo supone un avance significativo respecto a anteriores modelizaciones tipo inchworm. De todas formas, y auque dicho mecanismo fue durante cierto tiempo un candidato serio, incluso con soporte experimental, a ser el mecanismo real de la kinesina-1, hoy en día se sabe que es otro mecanismo el más adecuado para la descripción de ese motor. De todas formas, no es descartable que se encuentren otros motores que sí usen este tipo de desplazamiento, o bien que nano-máquinas artificiales se construyan inspirándose en él. Estos resultados fueron publicados en [57]. En la figura 13.2 mostramos detalles del modelo y algunos de sus resultados.

Finalmente, el capítulo de modelos basados en potenciales ratchet acaba con un estudio preliminar de motores rotatorios inspirados en el mecanismo inchworm del modelo anterior. La idea es generalizar los ciclos de estiramiento y relajación que se vieron antes en un dímero a una serie de partículas conectadas cíclicamente por medio de muelles elásticos. La introducción de los motores rotatorios en este contexto viene motivada por la existencia de máquinas biológicas como el BFM (Bacterial Flagellar Motor), responsable del movimiento de los flagelos en bacterias, o la ATP sintetasa, que gracias al gradiente electroquímico que guarda la membrana de la mitocondria, se produce una rotación mecánica que induce la síntesis del ATP. De hecho, la modelización de máquinas rotatorias es todavía un reto, pues son mucho más complejas que la ya nada simple kinesina. Además, los experimentos disponibles en este tipos de motores no proporcionan un conjunto de datos tan completo como en el caso de la kinesina. Por una parte, el forzamiento que se les hace no proviene de una fuerza conservativa, como es el caso del láser en la trampa óptica, sino que se utiliza el implante de estructuras con diferentes fricciones para poder medir momentos de fuerza distintos, como fragmentos de actina de longitud variable o micropartículas de silicona de tamaño también variable. Esto hace el análisis un poco diferente de los casos en los que una fuerza conservativa se aplica en el experimento.

También hay un aspecto en los motores rotatorios, en particular en los que

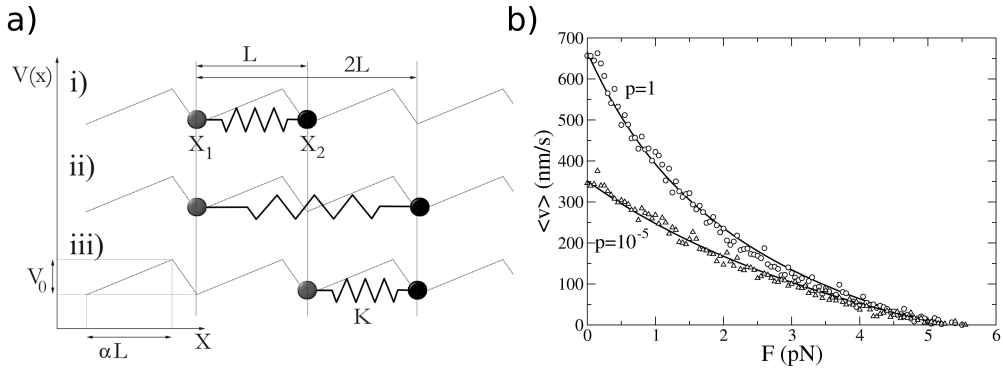

Figure 13.2: **Detalles del modelo inchworm [57].** a) Esquema del modelo, en el cual podemos ver cómo un dímero sufre un ciclo conformacional basado en una fase de estiramiento y otra de relajación en las que la interacción con un potencial ratchet produce un movimiento determinista hacia la derecha. L es el periodo del potencial y también la longitud de equilibrio del muelle. V_0 es la altura de la barrera del potencial y α es el factor de asimetría. En i) tenemos al dímero relajado. En ii) el dímero experimenta un estiramiento hasta alcanzar una longitud total $2L$. Justo en ese instante la fuerza de estiramiento desaparece y comienza la relajación que conduce al estado de equilibrio mostrada en iii) y que completa el ciclo. b) Curvas velocidad-fuerza en la que los puntos corresponden a valores que provienen de simulaciones y las líneas a cálculos teóricos. Los círculos corresponden a simulaciones donde la probabilidad de captar un ATP es $p = 1$, lo cual emula una situación de ATP saturante. Los triángulos indican un valor de $p = 10^{-5}$, lo cual corresponde a una concentración de ATP considerablemente más baja.

son movidos por flujo iónico, que dificulta el acoplamiento entre cantidades cinemáticas como la velocidad angular y las químicas como el flujo de protones. En un BFM, por ejemplo, alrededor de 1000 iones cruzan la membrana por una revolución completa del motor. No obstante, los experimentos [24] muestran solamente 26 pasos discretos por vuelta, lo cual no proporciona información suficiente para establecer una estequiometría estricta. De hecho, es probable que tal estequiometría no exista, de modo que un paso de rotación pueda ser debido al paso de un número variable de iones. También hay que tener en cuenta que mientras que algunos motores rotatorios como la parte F_O de la ATP sintasa tienen solamente una unidad generadora de momento de fuerza, otros motores como el BFM tienen un número variable de estas. En concreto, pueden tener de 8 a 10 unidades, lo cual tampoco corresponde a las periodicidades estructurales observadas en ese motor que es de 26 unidades. Lo que sí está en acuerdo es este número de unidades con el número de pasos por vuelta. De todas formas, en este análisis preliminar nos limitamos a modelizar un caso con una sola unidad activa o generadora de momento de fuerza.

Proponemos un modelo con 10 partículas acopladas por muelles lineales, sometidas a un potencial que es nulo en todas partes excepto en el entorno de la zona generadora de momento de fuerza. Allí hay dos periodos no nulos de potencial ratchet que permiten la aplicación de un mecanismo parecido al del modelo anterior. De hecho, el modelo podría probablemente mejorar su eficiencia si se consideraran tres periodos no nulos, pero debido a que el mecanismo con dos ya funciona preferimos en un principio tratar este caso más simple. La idea es muy parecida a la del modelo anterior, ya que el estiramiento, introducido a través de una fuerza como la del modelo inchworm, se produce solo entre las dos partículas (consecutivas) que están más cerca de la unidad activa. La diferencia respecto al otro caso es que esta vez el estiramiento es más costoso porque supone la fuerza de oposición del resto de energías elásticas de los otros muelles. Así pues, resulta mucho más costoso energéticamente completar el ciclo si los muelles tienen una constante elástica elevada. Si dicha constante es baja, entonces el acoplamiento entre las partículas es pobre y cuesta mucho hacer girar a todo el sistema. En resumen, el mecanismo inchworm para máquinas rotatorias con muchas unidades no es sencillo como el caso del dímero.

El ciclo mecánico acopla un desplazamiento angular por cada evento producido por la unidad activa. De todas formas, el cociente de acoplamiento resulta ser siempre bajo lo cual quiere decir que una significativa proporción de los ciclos no resultan en ningún trabajo útil. Aunque probatinas hechas con un modelo de 3 partículas acopladas sugieren que el modelo inchworm puede ser relevante, los resultados con muchas unidades estructurales no son excesivamente optimistas. De hecho, utilizar modelos de gusano para máquinas rotatorias supone afrontar dos obstáculos importantes. Primeramente, la mayoría de las máquinas rotatorias son reversibles, incluso las que, como el F_1 de la ATP sintetasa, no están animadas por un flujo de iones. Esto es un problema porque no está claro cómo se puede invertir el flujo de energía introducido en el estiramiento para poder obtener una reversibilidad. Si en vez de usar una fuerza de estiramiento fuera esta de compresión, todavía estaríamos añadiendo energía al sistema, no extrayéndola. En segundo lugar, la mayoría de los motores rotatorios, estando movidos por potenciales de membrana, basan sus interacciones en repulsiones y atracciones con dominios situados en el estátor, que es donde se sitúan las unidades generadoras de momento de fuerza. Por lo que sabemos, en esas máquinas no hay deformaciones elásticas apreciables, sino que fuerzas electrostáticas pueden mover a toda una corona rígida sin necesidad de deformarla. Lo que sí es cierto es que el F_1 de la ATP sintetasa sí parece experimentar transiciones elásticas que implican la síntesis/hidrólisis del ATP [5], con lo cual es probable que un modelo inchworm pueda ser útil de cara a modelizar este motor, siempre y cuando pueda conseguirse una forma de invertir el flujo de energía. En resumen, este último estudio representa una extrapolación del mecanismo inchworm a otro tipo de máquinas, en este caso rotatorias, así como la evaluación preliminar de la conveniencia de usar este tipo de modelos o no en algunos ejemplos biológicos. En la figura 13.3 mostramos algunos detalles del modelo propuesto así como algunos resultados obtenidos.

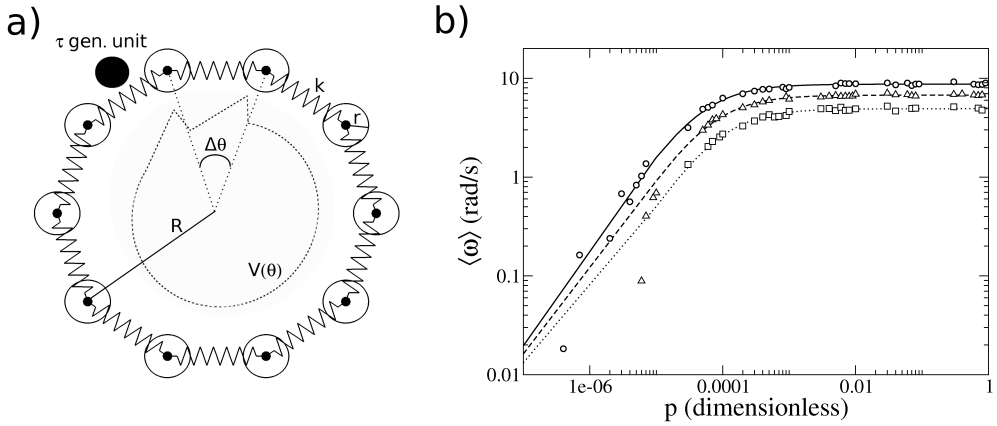

Figure 13.3: **Análisis de modelos inchworm aplicados a sistemas rotatorios [57].** a) Esquema de un sistema rotatorio con una sola unidad generadora de momento de fuerza, la cual se muestra como un círculo negro en el margen superior izquierdo. Este modelo en concreto tiene 10 unidades estructurales conectadas entre sí por muelles lineales de constante k. El potencial al que dichas unidades se ven sometidas está representado con línea punteada en el interior de la figura. Podemos ver cómo la única zona de potencial no constante es la que está junto a la unidad generadora de momento de fuerza. b) Curvas velocidad-probabilidad para tres valores diferentes del forzamiento externo. Los puntos son datos de la simulación mientras que las líneas son ajustes michaelianos. p es la probabilidad, como en el modelo inchworm, de iniciar un ciclo mecánico.

13.2 Modelos de cinética enzimática

El segundo bloque de la tesis, dedicado a la cinética química, consituye el conjunto de aportaciones originales que mejor se ajusta a los datos experimentales a la vez que las hipótesis implicadas no implican una controversia que dificulte su aceptación. Mientras que en el primer capítulo, dedicado a los modelos ratchet, se usan herramientas ampliamente aceptadas, la calidad de las predicciones, en el caso de modelos que no son solo de interés teórico, no es muy alta. Por otro lado, el último capítulo, que resumiremos en breve, está basado en interacciones electrostáticas y confinamientos (probablemente cuánticos), cosa que implica un grado de controversia e incertidumbre en lo que se refiere a la confirmación de tales hipótesis por la vía experimental. Especialmente en relación a las interacciones electrostáticas en medios nanométricos, los rangos de interacción que suponemos chocan de frente con la teoría reinante, de Debye-Hückel, según la cual dichas interacciones son apantalladas en rangos mucho menores que los que nosotros utilizamos. Lo que se quiere resaltar aquí es que el segundo capítulo, el basado en cinética química, es el que más aceptación ha tenido, por utilizar herramientas bien aceptadas así como por reproducir mangnitudes más ligadas a la tecnología actual, que en motores moleculares está muy focalizada en medir propiedades cinéticas. Además, la calidad de las predicciones es cuantitativamente alta, no solo para diferentes experimentos con kinesina-1, sino también con otros motores como el BFM o la RNAp.

En la primera parte de este capítulo se repasa la teoría clásica de inhibición para luego aplicarla a sistemas motores donde intervienen fuerzas mecánicas. Se pone énfasis en los ejemplos canónicos, en concreto el de la inhibición mixta, que servirá luego para describir a motores reales como la kinesina o teóricos como el inchworm. También se calculan energías libres asociadas a cada proceso como herramienta para una posible ampliación de la teoría basada en la modificación de estas energías por parte de las fuerzas mecánicas.

En la siguiente sección se presenta cómo a partir de la teoría clásica de inhibición se puede introducir la fuerza mecánica que actúa en la kinesina (debido a la trampa óptica) a través de un inhibidor al que se le asigna una concentración

efectiva que está relacionada con el valor concreto de la diferencia entre la fuerza y la fuerza máxima (stall force). En un principio, se puede pensar que el formalismo que introducimos es superfluo en tanto que ya existe un método que sirve para inyectar una fuerza en una reacción química. Dicho método consiste en la modificación de los coeficientes cinéticos de la reacción a través de términos exponenciales de Kramers para desviar el equilibrio químico entre los dos estados de la reacción. No obstante, para hacer eso es necesario identificar la coordenada de reacción química con la dimensión longitudinal del desplazamiento del motor y además es necesario definir unas longitudes características que permitan modular la influencia de la fuerza y convertir las fuerzas en energías, necesario para completar el término de Kramers. A esta aproximación se le pueden criticar principalmente dos cosas. La primera es que la introducción de las distancias de modulación suponen estados intermediarios del motor a lo largo del ciclo. En concreto, la Ref.[45] predice unos estados intermedios que luego, al menos para tiempos inferiores a 30μs [40] no se observan en las trayectorias. La segunda crítica, más importante que la otra, consiste en que la aproximación con términos de Kramer modifica el equilibrio químico de forma que para el valor de la fuerza máxima, la situación de equilibrio es alcanzada. Se suele partir de una función de potencial químico a la que se añade el trabajo de la fuerza externa. Cuando el motor llega a pararse, el potencial químico total se anula, lo cual quiere decir, desde el punto de vista químico, que la reacción se produce tantas veces en un sentido como en el otro. Este esquema es totalmente válido para un motor como el BFM o el F_O de la ATP sintetasa. No obstante, en una kinesina, cuando el motor está en el régimen de fuerza máxima, aunque no se mueva, el ATP sigue hidrolizándose. En cualquier caso, es inadmisible el aceptar que se producen tantas síntesis de ATP como hidrólisis. De forma que, aunque mecánicamente el motor ya está parado, el potencial químico dista de haberse anulado. Tanto es así, que transiciones químicas inversas en la kinesina ni siquiera han sido observadas de forma evidente, aunque hay tentativas para estimar los bajísimos coeficientes cinéticos inversos de dicha reacción [75]. Por lo tanto, creemos que es necesario introducir otro formalismo que por una parte no necesite de un desplazamiento del centro de masas para poder efectuar transiciones químicas como también poder tener una forma de modular la velocidad de reacción sin por ello desviar el equilibrio químico entre el ATP, ADP y P_i.

Para ello desarrollamos un formalismo que en vez del alterar los coeficientes de equilibrio entre ATP y sus productos, use una influencia lateral a la reacción a través de la teoría de inhibición, que si bien altera el ritmo global de la reacción, no presupone que en condiciones cercanas a la fuerza máxima el ritmo de la reacción inversa se vuelve tan fuerte como el de la reacción directa. En realidad, ni siquiera nos hace falta suponer el último paso de la reacción de forma reversible, sino que podemos seguir trabajando en la aproximación (típica en cinética de Michaelis-Menten) de que el último paso de la reacción es irreversible, lo cual está mucho más de acuerdo con los experimentos. En concreto, lo que hacemos es considerar una fuerza mecánica como un inhibidor, o activador si la fuerza asiste al movimiento en vez de oponerse, pero para simplificar nos referiremos al caso en el que la fuerza se opone al movimiento, aunque luego apliquemos la teoría en todo su rango experimental, que incluye los dos regímenes. De hecho, un inhibidor no tiene por qué ser una sustancia química sino cualquier otro factor que altere los ritmos globales de las reacciones. Lo que sí es cierto es que la teoría clásica de inhibición se centra en el caso de inhibidores químicos, para los cuales hay definida una concentración. Por eso uno de los objetivos de nuestra teoría es poder definir una concentración de inhibidor efectiva a partir de una fuerza mecánica. En este primer trabajo lo que hacemos no es deducir esta relación de otros principios sino adivinarla y ensayarla. En primer lugar, la adivinación no tiene más misterio que la de elegir la funcionalidad más sencilla que cumpla los requisitos imprescindibles que tiene que cumplir la relación fuerza-inhibidor. En primer lugar, si la fuerza es nula, la concentración del inhibidor debe serlo también. En segundo lugar, si la fuerza llega al valor de la fuerza máxima, el inhibidor debe hacerse infinito. Una vez que se escoge la expresión más sencilla que cumple estas dos condiciones se ensaya usando los valores experimentales a través de una aplicación directa de la teoría de inhibición y se ve que la concordancia con dichos valores es satisfactoria, lo cual implica que no es necesario, de momento, buscar expresiones más complicadas. Veremos más adelante cómo puede deducirse la expresión dada a partir de otras hipótesis microscópicas, pero no es este el propósito de este bloque. En resumen, tenemos una función sencilla (aunque no lineal) de la relación inhibidor fuerza que nos permite una expresión analítica para la velocidad media en función de la fuerza externa y de la concentración de ATP. Además, contrastado con los

experimentos, el nivel de concordancia es realmente bueno.

Adicionalmente, como la kinesina resulta ser un motor mixto (en el sentido en que la fuerza actúa en ella como un inhibidor mixto), podemos dar, a través de las constantes de inhibición, que son dos, una medida cuantitativa de cómo la fuerza mecánica afecta los diferentes estados químicos. En concreto, las dos constantes de inhibición, k_{ic} y k_{iu}, se deducen de los datos experimentales demostrando que se trata de un inhibidor mixto competitivo, ya que $k_{ic} < k_{iu}$. Esto permite explicar el hecho de que las trayectorias en la kinesina se ven afectadas de dos formas distintas por la fuerza. En primer lugar, los saltos que corresponden a los desplazamientos de 8nm, aunque parecen instantáneos en una escala de milisegundos, tienen en realidad una pendiente finita que decrece cuando la fuerza aumenta. No obstante, este efecto es menos importante que el hecho de que la fuerza externa aumenta enormemente el tiempo de espera entre dos enventos consecutivos. Este hecho, que no deja de ser curioso en tanto que un factor mecánico afecte a un tiempo de espera que parece puramente basado en la efusión (en la probabilidad de que un ATP entre en la cavidad de la enzima), es el que predomina a la hora de ver cómo la velocidad global decrece cuando la fuerza externa crece. Estos dos efectos desiguales se reflejan en la desigualdad de las dos constantes de inhibición. En la figura 13.4 se muestra el esquema del modelo de este bloque así como algunos de sus resultados principales, los cuales están publicados en [43].

Otro aspecto importante de este trabajo es que presenta un formalismo y una metodología para las cuales la aplicación a la kinesina es solo un ejemplo particular. Esta aproximación permite caracterizar otros motores, incluso teóricos como se vio en el modelo inchworm lineal o el rotatorio. No obstante, lo interesante de verdad es contrastar en qué medida la aplicación de esta teoría a otros motores reales sigue siendo válida. Ese es exactamente el objetivo de la siguiente sección. Con la idea de que cada motor individual que presente un comportamiento michaeliano ante modificaciones de la cantidad de substrato pueda explicarse usando teoría de inhibición, hemos desarrollado un modelo unificado que se demuestra útil en los tres motores moleculares en los que ha sido ensayado, a saber, en la kinesina-1 (con datos experimentales nuevos, diferentes a los del

trabajo anterior), en el BFM y la RNA polimerasa. Como veremos, además del buen acuerdo entre teoría y datos experimentales, este nuevo formalismo nos permitirá entender con más profundidad la forma en que las fuerzan alteran los procesos químicos.

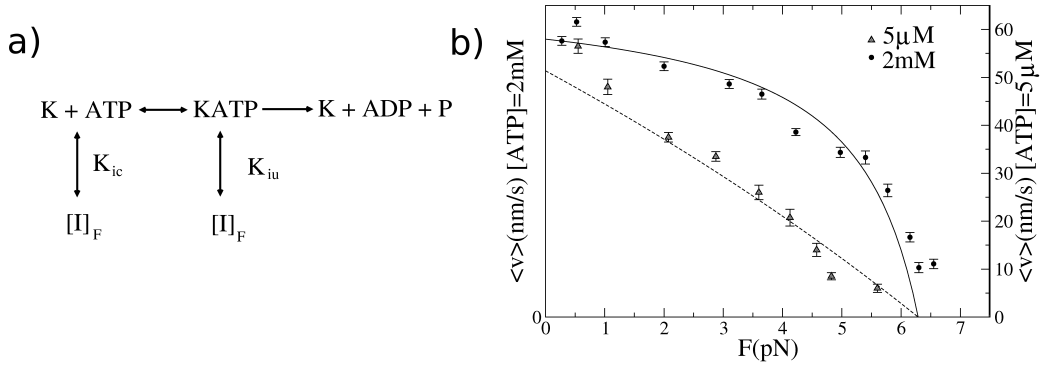

Figure 13.4: **Teoría de inhibición aplicada al forzamiento de la kinesina-1 [43].** a) Esquema de inhibición sobre la reacción enzimática que la kinesina-1 produce sobre el ATP. La concentración efectiva de inhibidor, $[I]_F$ se obtiene de la fuerza externa, F. b) Curvas velocidad fuerza en las que la información experimental es la misma que en la figura 13.1. Las líneas son predicciones teóricas que están en buen acuerdo con los valores experimentales.

El formalismo unificado para motores individuales, lo que constituye el bloque final del capítulo cinético-químico, está basado en la idea de que el tiempo promedio de cada ciclo mecánico-químico puede ser expresado a través de la suma de tiempos característicos de cada subproceso involucrado en dicho ciclo. Lo que hacemos es separar el tiempo total en la suma de tres sub-tiempos: el tiempo interno, el de espera y el mecánico. Una vez que estos tiempos están bien estimados, ya podemos obtener una expresión para la cinética, pues normalmente los motores moleculares con los que tratamos tienen un tamaño de paso fijo y conocido, con lo cual todo el interés cinético se esconde en el conocimiento de cómo las fuerzas mecánicas afectan a cada subtiempo. Definimos al tiempo interno como la suma de los tiempos de aquellos procesos que no dependen de ninguna de las dos principales variables control, que son la concentración del substrato y la fuerza externa. El tiempo de espera es el tiempo que tarda el motor entre dos eventos mecánicos (dos pasos), y aunque es bien sabido que este tiempo es aleatorio, también es cierto que de cara a analizar la cinética global promediada nos

basta con caracterizar el tiempo promedio de la distribución de tiempos que se observa en realidad. Finalmente, el tiempo mecánico consiste el tiempo que tarda el motor en realizar el paso mecánico, y se estima de forma sencilla utilizando una dinámica sobreamortiguada a través de las fuerzas y el coeficiente de fricción asociado.

Mientras que el tiempo externo es simplemente una constante a ajustar a partir de los datos y que el tiempo mecánico proviene de un cálculo sencillo en el que la acción de la fuerza es totalmente lineal, el tiempo de espera se revela menos trivial y en realidad es donde se esconde buena parte de la fenomenología que aquí estudiaremos. De hecho, cuando se aumenta la fuerza externa, el tiempo de espera crece razonablemente, lo cual no deja de ser sorprendente. Si el ATP, o los substratos pertinentes en cada caso, se aproximan por difusión a la zona del bolsillo catalítico, ¿cómo es que tal proceso se ve tan afectado por la acción de una fuerza? Esta pregunta motiva la principal hipótesis de este trabajo, que consiste en suponer que dicho bolsillo tiene una apertura que se ve afectada por la fuerza. De esta forma, si consideramos al proceso de captura del substrato como un proceso de efusión, el ritmo de paso de la partícula a través del agujero que define la entrada a la cavidad enzimática depende de la superficie de ese agujero. De esta forma, si la fuerza externa, cuando se opone al movimiento, reduce dicha superficie, entonces el substrato necesita más tiempo para poder pasar a la cavidad y por tanto el tiempo aumenta. Si en cambio la fuerza asiste al movimiento, la cavidad se abre aún más de lo que lo está cuando no hay fuerza, lo que explica que el ritmo de la reacción aumente cuando esta fuerza se aplica. Esta es una hipótesis que nos llevará a resultados muy relevantes pero que, según creemos, no está demostrada experimentalmente.

Como primera aproximación, un primer modelo sencillo para la respuesta de la cavidad a la presencia de la fuerza externa es suponer que la apertura del bolsillo está modulada por un potencial armónico. Esto, como se ve en los apéndices de la sección, permite demostrar la expresión que se utilizó en el estudio anterior. No obstante, podemos ver que una expresión más sofisticada es más apropiada para describir al motor en un rango de fuerzas más amplio, pues los experimentos más recientes exploran no solo un espectro de fuerzas asistentes al movimiento

más ancho [46], sino que también se explora el régimen de fuerzas opuestas al movimiento que son mucho mayores que la fuerza máxima [40], lo cual llevó al descubrimiento de la existencia de un régimen en el que la kinesina realiza una inversión del ciclo mecánico que sin embargo no supone la inversión del ciclo químico. Para un modelo de potencial armónico de bolsillo, pues, es necesario acotar los casos extremos. Por ejemplo, es preciso que el modelo no adquiera aberturas negativas para la cavidad, como tampoco aberturas infinitas para fuerzas asistentes demasiado grandes. Lo que hacemos es conservar el comportamiento de respuesta armónica lineal cerca de fuerzas de módulo pequeño o moderado mientras que suavizamos la respuesta para fuerzas extremas de forma que existe una saturación que implica que existe un máximo de apertura así como un mínimo, que es cero. Esto lo conseguimos a través de una función sigmoidal que recupera el caso armónico simple para deformaciones pequeñas.

El modelo se aplica a los tres motores ya mencionados con un acuerdo excelente en los casos de la kinesina-1 y la RNAp, que son mecanoenzimas, mientras que el acuerdo con los datos para el BFM es solamente notable, lo cual no es poco si se tiene en cuenta que los experimentos son más difíciles y se presentan con mucha menos precisión. En cualquier caso creemos que la conclusión es que nuestro formalismo se revela muy útil para caracterizar cualquier motor individual, especialmente si se trata de mecano-enzimas. No obstante, una restricción del modelo es que tal y como está presentado aquí solamente sirve para predecir resultados en un régimen de irreversibilidad química, aunque admite la reversibilidad mecánica. Un motor como el F_1 de la ATP sintetasa requeriría una modelización mucho más compleja.

Más allá del acuerdo con los resultados experimentales, cabe destacar que este trabajo aporta un resultado teórico muy relevante. Se trata de la necesidad de separar el concepto de fuerza máxima (stall force) en dos elementos bien diferenciados. Esta separación, inédita según creemos, permite explicar un fenómeno tan curioso como la inversión mecánica, pero no química, de la kinesina. Hasta ahora, el concepto de fuerza máxima había sido unívoco: era el valor de la fuerza externa al cual la velocidad promedio del motor se hacía nula. Pero en vista de que ahora sabemos que la fuerza afecta al comportamiento del motor de dos formas

distintas, ¿qué clase de inmovilización es la que para al motor? Hay dos opciones. Una es que la fuerza motriz del motor se iguala en módulo a la fuerza externa y por lo tanto se llega a un equilibrio mecánico que impide al motor avanzar más. La otra opción, menos evidente, es que la fuerza externa cierra completamente la cavidad de modo que el acceso del substrato al motor queda vedado. Según esto, aunque la fuerza motriz siga siendo mayor que la fuerza externa, el motor se parará. En el caso de la kinesina es interesante discernir a qué tipo de límite se llega primero a medida que la fuerza externa aumenta. Si se llega primero al límite de fuerza máxima química (aquella que ya cierra la cavidad), entonces el motor ya no se moverá más porque el tiempo de espera se volverá infinito. En cambio, si se llega primero al valor de fuerza máxima mecánica, la fuerza motriz se ve igualada por la externa pero el acceso del ATP a la cavidad sigue estando permito, lo cual posibilita que el ciclo químico siga avanzando. Si estiramos con una fuerza externa muy grande (régimen de superstall force), la fuerza externa desvía el equilibrio mecánico de forma que el paso mecánico puede darse hacia atrás, como en realidad se observa, mientras que el ciclo químico sigue yendo hacia adelante e incluso en el límite en el que la irreversibilidad química siendo siendo una aproximación muy buena. Ahora bien, si uno sigue aumentando la fuerza externa, se llegará eventualmente a un valor para el que el bolsillo quedará cerrado del todo y por tanto la velocidad media, que había empezado a crecer en el dominio negativo, vuelve a cambiar de rumbo hasta hacerse cero de nuevo. Estos resultados permiten entender los resultados obtenidos en [40] a la vez que predicen una anulación final de la velocidad que no puede discernirse con claridad en los datos experimentales debido a la dificultad para explorar esos regímenes. En la figura 13.5 mostramos algunos detalles y resultados de este estudio, que está por publicar.

13.3 Modelos electrostáticos para la kinesina-1

Este capítulo es el que probablemente contiene resultados más interesantes pero a la vez el más controvertido de la tesis. Está dividido en dos bloques principales, aunque asimétricos, pues al primero se le concede mucho más peso que al segundo. Así, por una parte presentamos un análisis de la mecánica de la ki-

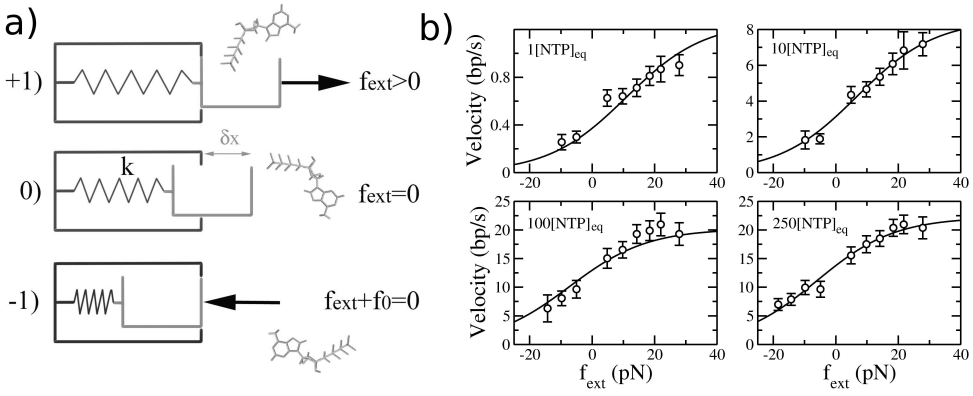

Figure 13.5: **Modelo unificado para caracterizar las curvas velocidad-fuerza** a) Esquema de la hipótesis de un tiempo de espera que está modulado por la apertura de la cavidad enzimática, que a su vez depende de la fuerza externa. En 0) observamos la cavidad con su apertura natural, no forzada. Si la fuerza externa asiste al movimiento abrimos más la cavidad (+1) mientras que si la fuerza se opone al movimiento la cavidad se cierra (-1) aumentando así el tiempo de espera. b) Curvas velocidad fuerza para la RNAp. Los puntos experimentales provienen de [46], mientras que las curvas son las predicciones del modelo. Vemos cómo el ajuste es satisfactorio a todas las $[NTP]_{eq}$, que son las concentraciones relativas de ATP, UTP, CTP y GTP a las que los ritmos de reacción no forzados se igualan para las cuatro bases.

nesina considerando algunas interacciones electrostáticas entre el microtúbulo y el motor. Por la otra, analizamos las interacciones entre la cabeza de la kinesina con el microtúbulo en función de los diferentes estados que aquella tiene respecto al substrato, lo que viene a completar algunas lagunas de la primera parte. El motivo de adentrarnos de forma más profunda en los mecanismos que subyace el paso de la kinesina es principalmente la existencia de múltiples evidencias experimentales aparentemente inconexas pero que cobran sentido en el contexto de nuestros modelos. Por otra parte, constituye un modelo verdaderamente físico en el sentido en que la mayoría de los modelos para dicho motor, aunque muchos con elementos mecánicos, usan fuerzas fenomenológicas sin especificar el posible origen y naturaleza de estas. Nosotros, aunque no abordamos el problema en su por otra parte inmensa complejidad, sí que apuntamos a algunos datos sobre propiedades electrostáticas que permiten entender buena parte de la fenomenología conocida. El problema de adentrarse en detalles que requieren una precision temporal y espacial (esta última en un sentido dinámico) que están más allá o justo en el límite experimental es que el grado de especulación aumenta, por mucho que las hipótesis intenten ser mínimas y razonables. Además, nuestra utilización de interacciones electrostáticas en un rango algo superior al que la teoría de Debye-Hückel estricta permite, no nos ha ayudado mucho de cara a la difusión y aceptación de este trabajo. No obstante, tenemos motivos de peso para dudar de la aplicación a la ligera de la teoría del apantallamiento iónico en condiciones como las que nos ocupa, algunas de las cuales se han hecho explícitas en esta tesis. Por otra parte, nuestro modelo reproduce numerosas propiedades experimentales que, al menos por lo que nos consta, otros modelos más aceptados y no siempre más conservadores no reproducen. Entre los numerosos resultados de nuestro trabajo, podríamos destacar el de cómo la interacción de la carga del cuello de la kinesina con el momento dipolar de la tubulina proporciona una direccionalidad al movimiento que sin carga el motor no puede tener, por mucho que el estado de espera sea inclinado con respecto a la dirección del protofilamento. Además, el cambio de signo en la carga del cuello produce un cambio de sentido en dicho movimiento, lo cual está en gran acuerdo con el hecho de que la direccionalidad se ve totalmente afectada ante un cambio puntual en el cuello [10].

El primer bloque de este capítulo está basado principalmente en unas simula-

ciones de dinámica molecular destinadas a estudiar las propiedades electrostáticas de la tubulina en solución acuosa [63, 58]. El resultado principal de estas referencias es que la tubulina tiene un momento dipolar permanente que se desarrolla en presencia de los iones del medio y el agua, pues es un monopolo negativo en el vacío. Lo más importante es que estas tubulinas, una vez polimerizadas en un microtúbulo, conservan ese momento dipolar y lo tienen orientado en una forma tal que la proyección del dipolo sobre el eje del movimiento de la kinesina es no nulo. De este modo, la superficie del microtúbulo resulta ser negativa, pero con una capa subyacente positiva que además le da carácter dipolar a toda la estructura. Estos datos suponen una rotura de simetría espacial en el filamento que nos permite pensar un modelo que la tenga en cuenta para poder explicar el movimiento del motor. Cierto es que hasta entonces ya se sabía que los dos extremos del filamento son distinguibles, pero esta propiedad estaba basada en términos de frecuencias de polimerización (el extremo positivo es el que polimeriza más deprisa). Y probablemente, ambos fenómenos estén bien relacionados, pero si bien usando velocidades de polimerización no tenemos forma de plantear un modelo válido, una estructura con propiedades ferroeléctricas abre mucho margen de posibilidades.

Como utilizamos una propiedad electrostática del microtúbulo para modelizar la kinesina, es necesario establecer unas hipótesis sobre las propiedades electrostáticas de esta. Por simplificadoras que parezcan, aportan sentido a muchos fenómenos importantes. Sabemos que la molécula de ATP también lleva asociadas cargas eléctricas. En concreto, un ATP tiene cuatro cargas electrónicas negativas, aunque normalmente se considera que tiene solo dos, puesto que suele ir acompañada de un ión de magnesio. Por otra parte, a la superficie de una tubulina se le asocian de 27 [63] a 35 [72] cargas negativas, lo cual significa que incluso considerando la alta permitividad relativa del agua las fuerzas entre un ATP y la tubulina pueden ser descomunales, mucho mayores que las fuerzas máximas producidas por la kinesina. Es cierto que los iones del medio apantallarán en parte esas fuerzas, pero tampoco parece razonable suponer que ninguna de esas fuerzas son relevantes en el problema que tratamos. El ATP se introduce en una de las cavidades catalíticas del motor, como ya hemos comentado antes, lo cual significa que en cada cabeza, cada vez que se produce un cambio de estado de nucleótido,

se produce un significativo cambio electrostático. Además, como una cabeza de kinesina que está libre de nucleótido tiene tendencia a permanecer ligada a la superficie del microtúbulo, suponemos que la carga global de la cabeza es ligeramente positiva, lo justo para que en presencia del nucleótido el signo global del complejo cabeza-ATP o cabeza-ADP se vuelva negativo. Esto nos permite tener una cabeza en el motor que es afín o no al microtúbulo dependiendo de si no tiene un nucleótido adherido o si sí lo tiene, respectivamente. Finalmente, una tercera carga es añadida al motor justo en la posición del cuello (neck linker). Esta carga es lo que confiere la direccionalidad y su signo al motor. En definitiva, suponemos al motor como una barra rígida con una carga central (el cuello) que es fija y una carga variable (depende del estado del nucleótido) en cada extremo, lo que emula a la cabeza.

La introducción de la carga del cuello enel modelo está motivada por varios hechos. Primero, se sabe que mutaciones puntuales en los pocos aminoácidos que representan ese dominio producen cambios radicales en la procesividad [8] así como en la pérdida de direccionalidad [10]. Esto apoya la tesis de que el cuello, aunque pequeño y relativamente distante del microtúbulo, *lee* las propiedades de este para poder decidir el sentido del movimiento e incluso condicionar su procesividad, que es una medida del número de pasos consecutivos que puede dar el motor sin desengancharse del microtúbulo. El otro motivo por el cual se introduce una propiedad electrostática en el cuello y de hecho, la razón que nos lleva a elegir el signo de la carga que consideramos está basada en la polaridad del tallo del motor (stalk), que es el dominio filamentoso que une las cabezas con la carga que el motor transporta. Este tallo tiene una polaridad eléctrica bien definida en tanto que son dos cadenas aminoacídicas. El hecho es que el tallo puede estar conectado al cuello a través de su terminal amino, que es positivo o de su terminal carboxil, que es negativo. Y parece ser [76] que mientras las primeras producen kinesinas que se mueven hacia el extremo + (plus-end) del microtúbulo, las otras caminan en sentido inverso. Es cierto que otras propiedades electrostáticas cercanas al cuello y que no dependan de la polaridad del tallo pueden afectar a la direccionalidad, pero nosotros solamente consideramos una carga puntual que resume de forma efectiva, *a grosso modo*, las propiedades electrostáticas del cuello.

Cuando simulamos el modelo, incluso sin tener en cuenta la carga del cuello, obtenemos un resultado remarcable: la posición de mínima energía, lo que se suele llamar el *parked state*, adquiere una inclinación respecto la vertical definida por la superficie del microtúbulo. Este estado se da cuando una cabeza, la trasera, es positiva (sin nucleótido) y está adherida a una tubulina, mientras que la otra cabeza, que es negativa (tiene un ADP atrapado) y a la que llamamos cabeza delantera, no está en posición exactamente vertical sino inclinada, lo que es natural por otra parte debido a la polarización de la tubulina. A menudo en la literatura [55, 56] se trata el problema de la inclinación del estado de espera sin dejar claro que dicha inclinación no define una direccionalidad. Es cierto que a primera vista, el hecho de que la cabeza delantera ocupe una posición de espera más cerca de su objetivo que del lugar de donde proviene (la tubulina anterior en la que estaba adherida en el estado de espera anterior) parece que vaya a favorecer la caída de esta cabeza hacia "delante". Pero eso no es cierto. Nuestras simulaciones demuestran que a pesar de la inclinación del motor, una vez que cambiamos la carga de la cabeza delantera, lo cual equivale a la expulsión del ADP, la caída de la carga ocurre tantas veces hacia un lado como hacia al otro. Es este hecho lo que hace tan importante la introducción de la carga en el cuello, la cual por una parte acentúa la inclinación del estado del espera (o la invierte si la carga del cuello es negativa) y además decide *de forma determinista* el sentido del movimiento del motor, por mucho que las fluctuaciones térmicas le induzcan transiciones inversas de forma esporádica.

Se puede también establecer una relación entre la procesividad de la kinesina y nuestro modelo, aunque a falta de saber datos reales sobre algunos coeficientes cinéticos necesarios no hemos podido realizar cuantificaciones sobre ello. Pero la idea cualitativa es por sí sola suficientemente clara. Un motor como la kinesina, para ser procesivo, es decir, para poder efectuar varios pasos consecutivos sin separarse del microtúbulo, debe tener las dos cabezas adheridas simultáneamente al microtúbulo por un intervalo de tiempo determinado, por pequeño que este sea (y de hecho se ha podido acotar que este es al menos inferior a 30μs [40]). Ahora bien, para que esto pueda ser posible, el proceso de colapso de la cabeza delantera hacia el microtúbulo debe ser más rápido que la ascensión y liberamiento de la cabeza trasera. Cuando el motor está en su estado de reposo, aparcado,

un ATP se adhiere eventualmente a la cabeza trasera. Esto activa dos procesos en paralelo. Por una parte, y de forma totalmente misteriosa a día de hoy, esto activa la expulsión del ADP atrapado en la cabeza delantera. Se ha especulado con que la trasmisión de esta información viaja debido a deformaciones elásticas, pero esta hipótesis no está demostrada e incluso hay algunas razones para pensar que no es así [55]. Más adelante nosotros nos veremos obligados a suponer que existe un conmutador entre las cabezas, la naturaleza del cual no es conocida. Quizá algún efecto de transferencia electrónica pueda estar implicado, o bien exista algún mecanismo de canalización electrostática, sobre la cual hemos trabajado de forma preliminar [73] sin obtener todavía resultados conclusivos. Por otra parte, el otro proceso que activa la llegada del ATP a la cabeza trasera provoca la hidrólisis del nucleótido, obteniendo un grupo P_i que al desprenderse de la cavidad se produce el desprendimiento de esta cabeza del microtúbulo, de forma que esta inicia la ascensión hasta la posición inclinada del nuevo estado de reposo. La clave para comprender la procesividad está en que el primer proceso debe completarse antes de que la cabeza trasera inicie su disociación de la tubulina. En la última sección de esta tesis damos una explicación plausible al retraso del segundo paso.

En nuestro modelo, cuando el cuello tiene una carga positiva, el motor, además de estar direccionado hacia el límite de rápida polimerización (+end), se muestra muy favorable a ser procesivo porque el proceso de caída de la cabeza delantera es muy rápido, ya que el cuello y la cabeza se ven atraídos por el microtúbulo. En cambio, motores con el cuello negativo, experimentan un proceso de caída lento, lo cual propicia la desunión del motor que supone la pérdida de procesividad. Así pues, la relación de las fases de nuestro ciclo mecánico con la interacción del cuello-tubulina es crucial para determinar la procesividad de un motor. No obstante, sin datos fiables de qué tiempos caracterizan los procesos de expulsión de ADP y de desunión de la cabeza trasera una vez que el ATP se ha unido a ella no podemos establecer cuantitativamente unos valores para el recorrido promedio (mean run length), que es la magnitud que mide la procesividad y de la que hay disponible una buena cantidad de datos experimentales. Cabe mencionar que, además, hay evidencia experimental de que este recorrido medio se ve severamente afectado por modificaciones puntuales en las propiedades del cuello [8], lo

cual ratifica más la importancia de este aspecto en nuestro modelo. En la figura 13.6 mostramos algunos detalles del modelo tal y como fue publicado en [71].

El segundo bloque de este capítulo es el último trabajo de esta tesis. Está basado en la modelización de las interacciones entre cuatro elementos clave para el funcionamiento de la kinesina: la cabeza del motor, el tubulina, el ADP y el P_i. A la luz de recientes medidas [56] obtenidas con FRET intentamos reproducir los estados estacionarios entre la kinesina y el microtúbulo para cuatro situaciones diferentes. La primera consiste en una solución sin nucleótido, en la cual ambas cabezas, la delantera y la trasera, se adhieren al filamento. En la segunda situación se añade AMP-PNP, que es una molécula análoga al ATP pero con la peculiaridad de que no es hidrolizable por la kinesina, lo cual permite observar de una forma congelada el estado de la cabeza justo después de la captación del ATP. El resultado es, como ya se sabía de otros experimentos de decoración de microtúbulos [59], que las dos cabezas se adhieren al microtúbulo. La diferencia respecto al caso anterior es que con AMP-PNP parece haber un enlace más rígido. La tercera situación consiste en preparar una kinesina en una solución de ADP. En este caso se observa el estado de reposo, con una cabeza adherida (sin nucleótido) al filamento y la otra disociada pero con un ADP en su interior. El cuarto caso es una variante del tercero, en la que se añade al ADP una gran concentración de P_i. Esto promueve que haya transiciones de la cabeza delantera entre el estado de reposo y un estado en el que está adherida al microtúbulo, siendo este estado menos frecuente que el otro.

Nuestro trabajo permite reproducir todos estos resultados y da un paso más allá, pues también permite reproducir el estado dinámico correspondiente a la adición de ATP. Para ello, dos hipótesis principales son necesarias, ambas razonable en relación a lo que ya se conoce de las enzimas en general y la kinesina en particular. Lo que se acepta de las enzimas es que son capaces de reducir enormemente la barrera de activación que protege la energía almacenada en el sustrato. De la kinesina se sabe que además es capaz de cerrar su cavidad catalítica atrapando el ADP resultante en su interior. Además, se acepta que entre las dos enzimas, una por cabeza, existe una trasmisión de información muy efectiva que posibilita el movimiento coordinado del motor. Estos tres aspectos son los que

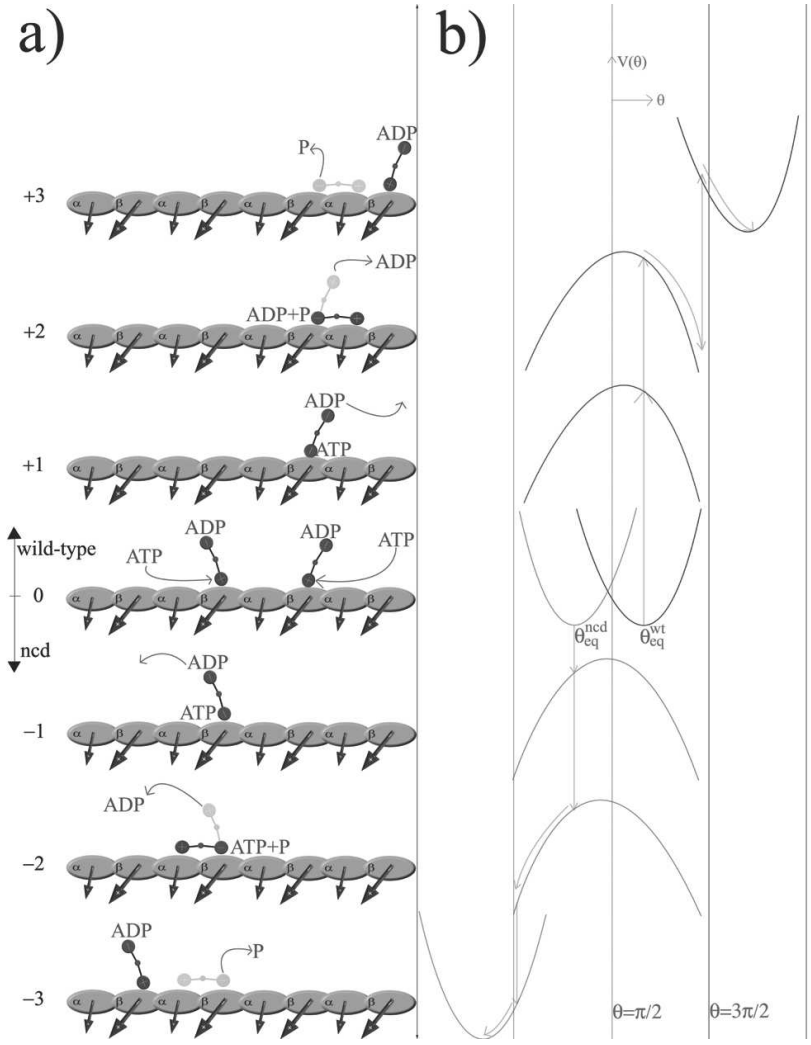

Figure 13.6: **Modelo electrostático de la kinesina [71].** a) Esquema del modelo en cuatro fases distintas para el caso de una kinesina convencional (wild-type) y otra ncd. Partiendo del caso 0) ambas están en su estado aparcado, inclinadas según sus respectivas direccionalidades. En ambas, un ATP llega a la cabeza unida al microtúbulo y desestabiliza dicho estado. En +1) y -1) el ADP en la cabeza libre sale de la cavidad enzimática dejando a la cabeza libre con carga global positiva, lo cual propicia la caída de esta cabeza al microtúbulo. En +2) y -2) vemos la direccionalidad de cada una de las caídas, que vienen dadas por la interacción de un cuello positiva o negativamente cargado, según tengamos la kinesina convencional o una ncd, respectivamente. Finalmente, en +3) la cabeza trasera se desune del microtúbulo y asciende a un nuevo estado aparcado que completa el ciclo. En -3) dibujamos una situación similar (y simétrica) aunque es poco probable que el ascenso de la cabeza trasera se produzca después de la caída de la cabeza libre. En el motor ncd, tal caída es probablemente muy lenta debida a la repulsión cuello-microtúbulo y eso reduce drásticamente la procesividad del motor. b) Respecto a todos los casos de a) hay asociados unos potenciales que ilustran las inestabilizaciones que produce el ATP así como la direccionalidad de cada motor, evidente al ver que la contribución del potencial cuello-microtúbulo desplaza lateralmente los puntos de derivada nula que hay antes y después de la desestabilización.

explicitaremos cuantitativamente en forma de hipótesis en el modelo. Además, incluimos otra hipótesis adicional que creemos necesaria para poder explicar la fenomenología observada en [56] y que en cualquier caso es verificable experimentalmente de forma directa o bien a través de lo que esta predice.

Para comenzar con esta última hipótesis, podemos decir que el grupo P_i resultante de la hidrólisis del ATP (o necesario para su síntesis) parece tener una cierta afinidad química por el microtúbulo, hecho del que no tenemos noticia experimental. No obstante, sabemos que tanto el microtúbulo (en su superficie) como el grupo P_i son electrostáticamente negativos. Entonces, dicha afinidad solo puede deberse a que ambos pueden confinarse mutuamente como también lo hace P_i con el ADP a la hora de formar un ATP, siendo el ADP negativo también. Esta suposición, aunque pueda parecer sorprendente al principio, es necesaria para entender cómo la kinesina actúa con el microtúbulo.

A continuación, podemos formalizar el resto de hipótesis de la siguiente forma. Supondremos que la actividad enzimática es capaz de eliminar parcialmente la barrera de activación entre el ADP y P_i, pero que en vez de ser una simple eliminación, esta barrera se transfiere a la interacción entre el ADP y la propia cabeza, lo cual permite explicitar el fenómeno catalítico y el del encierro del ATP en el bolsillo. La transferencia de esta barrera le hace pasar a la cabeza de un estado A a un estado B. La última hipótesis, la de coordinación entre cabezas, consiste en suponer que cuando una cabeza realiza la transición $A \rightarrow B$, la otra cabeza realiza la opuesta, $B \rightarrow A$. Este tipo de trasmisión, que no es más que una conmutación, muy típica en los motores macroscópicos, posibilita que la cabeza delantera pueda desprender el ADP que lleva dentro y activar así el ciclo mecánico descrito en el trabajo anterior.

Con todas estas hipótesis, elaboramos potenciales de interacción basados en las cargas que cada elemento posee (según el trabajo anterior y otras estimaciones en [63, 58, 72], en un apantallamiento moderado debido a los iones del medio y en barreras de confinamiento que sirven para incorporar las hipótesis anteriores. La barrera que confina a la tubulina con el P_i es fija, mientras que la que confina a ADP-P_i y ADP-cabeza dependen de su estado de conmutación, al que llamamos

estado Γ. Sin suponer aquí la tubulina como un dipolo ni tener en cuenta más que una dimensión de movimiento por razones de simplicidad, simulamos los cuatro elementos con una dinámica sobreamortiguada en la que incorporamos fluctuaciones térmicas a través de un ruido blanco gaussiano.

Si simulamos el sistema con solo la cabeza y la tubulina vemos cómo la atracción electrostática hace que ambos elementos queden atrapados mutuamente. Si añadimos AMP-PNP, que modelizamos como un estado confinado de ADP-P_i con una barrera que no permite la conmutación del estado Γ (lo que implica que la hidrólisis no puede ocurrir), vemos cómo el grupo P_i se confina en el microtúbulo mientras que el ADP queda ligeramente atrapado en la cabeza. El complejo cabeza-ADP se ve globalmente repelido por el microtúbulo, ya que la suma de sus cargas es negativa, pero la barrera de confinamiento entre ellos no es suficientemente alta como para que la repulsión del ADP pueda llevarse a la cabeza consigo. De todas formas, el ADP está fuertemente confinado al grupo fostato, el cual está atrapado en la tubulina. Como vemos, aunque el resultado experimental es muy parecido al del caso sin nucleótido, la situación es ahora bastante más compleja. Esta diferencia se aprecia en un enlace más rígido en este caso (con AMP-PNP), lo cual nuestro modelo también reproduce claramente.

Los dos casos restantes se explican de forma más compleja, y se necesita tener en cuenta nuestro trabajo anterior para poder completar el razonamiento. Cuando se introduce ADP en el sistema, las fluctuaciones térmicas harán que moléculas de ADP entren eventualmente en los dos bolsillos de la kinesina. No obstante, uno de ellos tendrá un estado Γ que permitirá confinarlo fuertemente mientras que el otro no podrá retenerlo. En consecuencia, la primera cabeza, unida al ADP, se verá repelida del microtúbulo, mientras que la otra, sin ADP, quedará atrapada por este. Sabiendo que esto define el estado de reposo de la kinesina es de esperar que la cabeza con ADP quede fuertemente inclinada hacia el +end del microtúbulo, pero sin poder caer al microtúbulo de forma estable debido a la interacción de esta cabeza y el cuello con el potencial que marcan los dipolos de la tubulina. Esto explica el bloqueo al que se alude en [55] por el cual la cabeza delantera no puede colapsar hasta que un ATP no se adhiera a la cabeza trasera. En nuestra simulación, si tenemos una cabeza en un estado Γ u otro

obtendremos que la cabeza quedará unida al microtúbulo sin ADP o bien vemos cómo se forma el complejo ADP-cabeza y cómo este se aleja del microtúbulo. Todo esto nos prepara para entender el cuarto estado estacionario experimental, en el cual se añade a este escenario una gran cantidad de grupos P_i. Bajo el marco de nuestro modelo, esto aumenta mucho las posibilidades de que los grupos fosfato acaben ocupando una buena parte de las tubulinas, quedando confinadas en ellas. Así pues, tenemos una cabeza con ADP cerca del microtúbulo pero con un mínimo de equilibrio fuera de él. Tenemos en la tubulina cercana un grupo fosfato confinado. Si tenemos ahora en cuenta que el ADP y el grupo P_i tienen una barrera de confinamiento mutua que debido al estado Γ es baja *pero no nula* (la conmutación no transfiere la barrera inicial más que parcialmente), entendemos cómo el grupo fosfato en la tubulina y el ADP del bolsillo enzimático pueden formar un complejo metaestable, que es lo que se observa tanto en los experimentos como en nuestro modelo. Para mayor apoyo experimental, es interesante ver cómo en [75] se observa en la cabeza delantera de la kinesina que hay una cierta facilidad de que grupos fosfato se adhieran de forma metaestable al ADP atrapado.

Finalmente, podemos observar todo el ciclo dinámico que consiste en tener una cabeza libre de nucleótido atrapada en el microtúbulo. Entonces un ATP, que es un complejo ADP-P fuertemente confinado, tras un tiempo que computacionalmente es casi inalcanzable en nuestro modelo (y por eso preparamos la condición inicial que sabemos que eventualmente acabará pasando), llega a la tubulina de forma que el fosfato se confina en el microtúbulo. Entonces, tras un cierto tiempo, la cabeza efectúa su actividad enzimática transfiriendo parte de la barrera entre ADP-P_i al complejo ADP-cabeza. Obtenemos entonces que el complejo cabeza-ADP se ve repelido por el microtúbulo, aunque aún confinado a través de una barrera entre ADP y P_i que ahora es más débil. Este tiempo, durante el cual en la cabeza remota ya se ha debido iniciar el colapso que asegura la procesividad, es de competición entre un ADP que se ve repelido por el microtúbulo pero atrapado por el grupo fosfato. Finalmente, de produce el desligamiento y el ADP se aleja del microtúbulo llevándose al ADP consigo hacia la posición del estado de reposo. Esta discusión completa de forma notablemente los huecos que el modelo electrostático anterior dejaba y supone una aproximación altamente fenomenológica

pero con un nivel de predicción que queda bien patente al ver cómo los resultados concuerdan con los experimentos. En la figura 13.7 podemos ver algunos de los resultados más notables de este modelo.

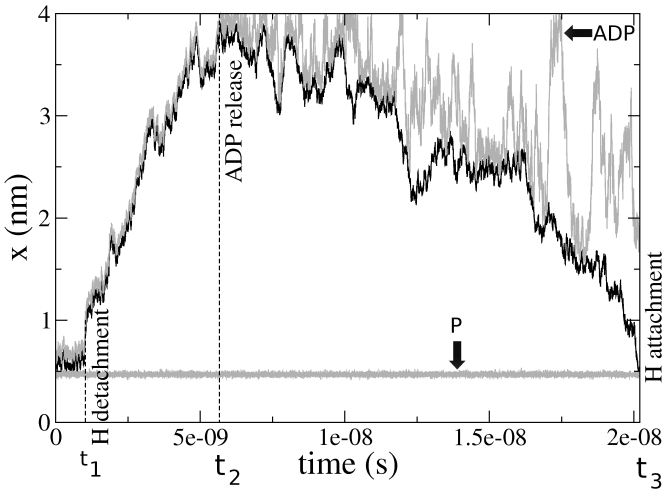

Figure 13.7: **Proceso de hidrólisis en la cabeza de una kinesina-1.** Resultados de la simulación de un proceso de hidrólisis. Vemos cómo la cabeza, inicialmente afín al microtúbulo, se desune (t_1) del filamento llevándose al ADP resultante consigo. Es crucial el hecho de que $t_1 > 0$, ya que es esta diferencia entre t_1 y $t = 0$ lo que permite al motor ser procesivo. En t_2 tenemos el proceso de unión de un ATP en la otra cabeza, la cual no simulamos aquí explicitamente. Entonces el ADP sale de la cavidad enzimática y la cabeza vuelve a ser afín por el microtúbulo, al cual cae tras un cierto tiempo que dura hasta t_3.

13.4 Publicaciones y preprints

- A. Ciudad and J. M. Sancho. External mechanical force as an inhibition process in kinesin's motion. *Biochem. J.* **390**, 345–349 (2005).

- A. Ciudad, A. M. Lacasta and J. M. Sancho. Physical analysis of a processive molecular motor: the conventional kinesin. *Phys. Rev. E* **72** 031918 (2005). Selected for the Virtual Journal of Biological Physics Research, October 1, (2005).

- A. Ciudad, J. M. Sancho and A. M. Lacasta. Dynamics of an inchworm nano-walker. *Physica A* **371**, 25–28 (2006).

- A. Ciudad, J. M. Sancho and G. Tsironis. Kinesin as an electrostatic machine. *J. Biol. Phys.* **32**, 455–463 (2006).

- A. Ciudad and J. M. Sancho. A unified phenomenological approach to force-velocity curves in molecular motors (2008). Preprint. Submitted to *J. Chem. Phys.*

- A. Ciudad. An analysis of the nucleotide-dependent conformations of kinesin-1. (2008). Preprint in preparation.

Bibliography

[1] Kron, S. J. & Spudich, J. A. Fluorescent actin filaments move on myosin fixed to a glass surface. *Proc. Natl. Acad. Sci. USA* **83**, 6272–6276 (1986).

[2] Funatsu, T. Y., Tokunaga, M., Saito, K. & Yanagida, T. Imaging of single fluorescent molecules and individual atp turnovers by single myosin molecules in aqueous solution. *Nature* **374**, 555–559 (1995).

[3] Svoboda, K., Schmidt, C. F., Schnapp, B. J. & Block, S. M. Direct observation of kinesin stepping by optical trapping interferometry. *Nature* **365**, 721–727 (1993).

[4] Rigler, R. & Vogel, H. (eds.) *Single Molecules and Nanotechnology* (Springer; 1 edition, 2007).

[5] Schliwa, M. (ed.) *Molecular Motors* (Wiley-Vch, 2003).

[6] Ray, S., Meyhöfer, E., Milligan, R. A. & Howard, J. Kinesin follows the microtubule's protofilament axis. *J. Cell. Biol.* **121**, 1083–93 (1993).

[7] Asbury, C. L., Fehr, A. N. & Block, S. M. Kinesin moves by an asymmetric hand-over-hand mechanism. *Science* **302**, 2130–2134 (2003).

[8] Thorn, K. S., Ubersax, J. A. & Vale, R. D. Engineering the processive run length of the kinesin motor. *J.C.B.* **151**, 1093–1100 (2000).

[9] Visscher, K., Schnitzer, M. J. & Block, S. M. Single kinesin molecules studied with a molecular force clamp. *Nature* **400**, 184–189 (1999).

[10] Endow, S. A. & Higuchi, H. A mutant of the motor protein kinesin that moves in both directions on microtubules. *Nature* **406**, 913–916 (2000).

[11] King, S. M. Aaa domains and organization of the dynein motor unit. *J. Cell Sci.* **113**, 2521–2526 (2000).

[12] Wang, S. Z. & Adler, R. Chromokinesin: a dna binding, kinesin-like nuclear protein. *J. Cell Biol.* **128**, 761–768 (1995).

[13] Raya, A. *et al.* Notch activity acts as asensor for extracellular calcium during vertebrate left-rightdetermination. *Nature* **427**, 121–128 (2004).

[14] Bray, D. *Cell movements: from molecules to motility* (Garland Publishing, 2001).

[15] Walker, M. L. *et al.* Two-headed binding of a processive myosin to f-actin. *Nature* **405**, 804–807 (2000).

[16] Hameroff, S. R. & Penrose, R. Orchestrated reduction of quantum coherence in brain microtubules: A model for consciousness? In Hameroff, S. R., Kaszniak, A. & Scott, A. (eds.) *Toward a Science of Consciousness - The First Tucson Discussions and Debates* (Cambridge, MA: MIT Press, 1996).

[17] http://chemistry.gsu.edu/glactone/index.shtml.

[18] Yazaki, K., Yoshida, T., Wakiyama, M. & Miura, K. Polysomes of eukaryotic cells observed by electron microscopy. *J. Elec. Microsc.* **49**, 663–668 (2000).

[19] Berry, R. M. & Armitage, J. P. The bacterial flagella motor. *Adv. Microb. Physiol.* **41**, 291–337 (1999).

[20] Murphy, G. E., Leadbetter, J. R. & Jensen, G. J. In situ structure of the complete treponema primitia flagellar motor. *Nature* **442**, 1062–1064 (2006).

[21] Reid, S. W. *et al.* The maximum number of torque generating units in the flagellar motor of *Escherichia coli* is at least 11. *Proc. Natl. Acad. Sci. USA.* **103**, 8066–8071 (2006).

[22] Ryu, W. S., Berry, R. M. & Berg, H. C. Torque generating units of the flagellar motor of *Escherichia coli* have a high duty ratio. *Nature* **403**, 444–447 (2000).

[23] Zhou, J., Lloyd, S. A. & Blair, D. F. Electrostatic interactions between rotor and stator in the bacterial flagellar motor. *Proc. Natl. Acad. Sci. USA* **95**, 6436–6441 (1998).

[24] Sowa, Y. A. *et al.* Direct observation of steps in rotation of the bacterial flagellar motor. *Nature* **437** (2005).

[25] Sowa, Y., Hotta, H., Homma, M. & Ishijima, A. Torque–speed relationship of the na^+-driven flagellar motor of vibrio alginolyticus. *J. Mol. Biol.* **327**, 1043–1051 (2003).

[26] Berg, H. C. & Turner, L. Torque generated by the flagellar motor of escherichia coli. *Biophys. J.* **65**, 2201–2216 (1993).

[27] Turner, L., Ryu, W. S. & Berg, H. C. Real-time imaging of fluorescent flagellar filaments. *J. Bacteriol.* **182**, 2793–2801 (2000).

[28] Oster, G., Wang, H. & Grabe, M. How f_o-atpase generates rotary torque. *Phil. Trans. R. Soc. Lond. B* **355**, 523–528 (2000).

[29] Brown, R. A brief account of microscopical observations made in the months of june, july and august, 1827, on the particles contained in the pollen of plants; and on the general existence of active molecules in organic and inorganic bodies. *Phil. Mag.* **4**, 161–173 (1828).

[30] Einstein, A. über die von der molekularkinetischen theorie der wärme geforderte bewegung von in ruhenden flüssigkeiten suspendierten teilchen. *Ann. Phys.* **17** (1905).

[31] Gardiner, C. W. *Handbook of Stochastic Methods* (Springer, 1983).

[32] Bier, M. Processive motor protein as an overdamped brownian stepper. *Phys. Rev. Lett.* **91** (2003).

[33] Kojima, H., Muto, E., Higuchi, H. & Yanagida, T. Mechanics of single kinesin molecules measured by optical trapping nanometry. *Biophys. J.* **73**, 2012–2022 (1997).

[34] Coppin, C. M., Finer, J. T., Spudich, J. A. & Vale, R. D. Detection of sub-8-nm movements of kinesin by high-resolution optical-trap microscopy. *Proc. Natl. Acad. Sci. USA* **93**, 1913–1917 (1996).

[35] Schnitzer, M. J. & Block, S. M. Kinesin hydrolyses one atp per 8-nm step. *Nature* **388**, 386–390 (1997).

[36] Block, S. M., Asbury, C. L., Shaevitz, J. W. & Lang, M. J. Probing the kinesin reaction cycle with a 2d optical force clamp. *PNAS* **100**, 2351–2356 (2003).

[37] Ciudad, A., Lacasta, A. M. & Sancho, J. M. Physical analysis of a processive molecular motor: the conventional kinesin. *Phys. Rev. E* **72**, 031918 (2005).

[38] Lindner, B. & Schimansky-Geier, L. Noise-induced transport with low randomness. *Phys. Rev. Lett.* **89** (2002).

[39] Reimann, P. *et al.* Giant acceleration of free diffusion by use of tilted periodic potentials. *Phys. Rev. Lett.* **87** (2001).

[40] Carter, N. J. & Cross, R. A. Mechanics of the kinesin step. *Nature* **435**, 308–312 (2005).

[41] Howard, J. *Mechanics of Motor Proteins and the Cytoskeleton* (Sinauer, 2001).

[42] Stratopoulos, G. N., Dialynas, T. E. & Tsironis, G. P. Directional newtonian motion and reversals of molecular motors. *Phys. Lett. A* **252**, 151–156 (1999).

[43] Ciudad, A. & Sancho, J. M. External mechanical force as an inhibition process in kinesin's motion. *Biochem. J.* **390**, 345–349 (2006).

[44] Bustamante, C., Chemla, Y. R., Forde, N. R. & Izhaky, D. Mechanical processes in biochemistry. *Annu. Rev. Biochem.* **73**, 705–748 (2004).

[45] Fisher, M. E. & Kolomeisky, A. B. Simple mechanochemistry describes the dynamics of kinesin molecules. *P.N.A.S* **98**, 7748–7753 (2001).

[46] Abbondanzieri, E. A., Greenleaf, W. J., Shaevitz, J. W., Landick, R. & Block, S. M. Direct observation of base-pair stepping by rna polymerase. *Nature* **438**, 460–465 (2005).

[47] Jülicher, F., Ajdari, A. & Prost, J. Modeling molecular motors. *Rev. Mod. Phys.* **69**, 1269–1281 (1997).

[48] Skau, K. I., Hoyle, R. B. & Turnery, M. S. A kinetic model describing the processivity of myosin-v. *Biophys. J.* **91**, 2475–2489 (2006).

[49] Grigoriev, I. V., Makhnovskii, Y. A., Berezhkovskiia, A. M. & Zitserman, V. Y. Kinetics of escape through a small hole. *J. Chem. Phys.* **116**, 9574–9577 (2002).

[50] Naber, N. *et al.* Closing of the nucleotide pocket of kinesin-family motors upon binding to microtubules. *Science* **300**, 798–801 (2003).

[51] Xing, J., Bai, F., Berry, R. & Oster, G. Torque-speed relationship of the bacterial flagellar motor. *Proc. Natl. Acad. Sci. USA.* **103**, 1260–1265 (2006).

[52] Block, S. M., Blair, D. F. & Berg, H. C. Compliance of bacterial flagella measured with optical tweezers. *Nature* **338**, 514–518 (1989).

[53] Wang, H. Y., Elston, T., Mogilner, A. & Oster, G. Force generation in rna polymerase. *Biophys. J.* **74**, 1186–1202 (1998).

[54] Israelachvili, J. N. *Intermolecular and Surface Forces, Second Edition: With Applications to Colloidal and Biological Systems* (Academic Press; 2nd edition, 1992).

[55] Alonso, M. C. *et al.* An atp gate controls tubulin binding by the tethered head of kinesin-1. *Science* **316**, 120–123 (2007).

[56] Mori, T., Vale, R. D. & Tomishige, M. How kinesin waits between steps. *Nature* (2007).

[57] Ciudad, A., Sancho, J. M. & Lacasta, A. M. Dynamics of an inchworm nano-walker. *Physica A* **371**, 25–28 (2006).

[58] Tuszynski, J. A., Luchko, T., Carpenter, E. J. & Crawford, E. Electrostatic properties of tubulin and their consequences for microtubules. *J.Comput.Theor .Nanosci.* **1** (2005).

[59] Thormählen, M. *et al.* Interaction of monomeric and dimeric kinesin with microtubules. *J. Mol. Biol.* **275**, 795–809 (1998).

[60] Mershin, A., Kolomenski, A. A., Schuessler, H. A. & Nanopoulos, D. V. Tubulin dipole moment, dielectric constant and quantum behavior: computer simulations, experimental results and suggestions. *ACT-03-01 CTP-TAMU-01-03* .

[61] Cross, R. A. The kinetic mechanism of kinesin. *TRENDS in Biochemical Sciences* **29**, 301–309 (2004).

[62] Song, Y. H. *et al.* Structure of a fast kinesin: implications for atpase mechanism and interactions with microtubules. *The EMBO journal* **20**, 6213–6255 (2001).

[63] Tuszynski, J. *et al.* Molecular dynamics simulations of tubulin structure and calculations of electrostatic properties of microtubules. *Mathematical and Computer Modelling* **41**, 1055–1070 (2005).

[64] Levin, Y. Electrostatic correlations: from plasma to biology. *Rep. Prog. Phys.* **65**, 1577–1632 (2002).

[65] Skiniotis, G. *et al.* Modulation of kinesin binding by the c-termini of tubulin. *The EMBO journal* **23**, 989 (2004).

[66] Sosa, H., Peterman, E. J. G., Moerner, W. & Goldstein, L. Adp-induced rocking of the kinesin motor domain revealed by single-molecule fluorescence polarization microscopy. *Nature Structural Biology* **8**, 540–544 (2001).

[67] Kozielski, F. *et al.* The crystal structure of dimeric kinesin and implications for microtubule-dependent motility. *Cell* **91**, 985–994 (1997).

[68] Hunt, A. J. & Howard, J. Kinesin swivels to permit microtubule movement in any direction. *Proc. Natl. Acad. Sci. USA* **90**, 11653–11657 (1993).

[69] Kasprzak, A. A. & Hajdo, L. Directionality of kinesin motors. *Acta Biochimica Polonica* **49**, 813–821 (2002).

[70] Nishiyama, M., Muto, E., Inoue, Y., Yanagida, T. & Higuchi, H. Substeps within the 8-nm step of the atpase cycle of single kinesin molecules. *Nature Cell Biology* **3**, 425–428 (2001).

[71] Ciudad, A., Sancho, J. & Tsironis, G. Kinesin as an electrostatic machine. *J. Biol. Phys.* **32**, 455–463 (2006).

[72] Hyeon, C. & Onuchic, J. N. Mechanical control of the directional stepping dynamics of the kinesin motor. *Proc. Natl. Acad. Sci. USA* **104**, 17382–17387 (2007).

[73] Tsironis, G. P., Ciudad, A. & Sancho, J. M. "insertar titulo". *Unpublished* (2007).

[74] Daune, M. *Molecular biophysics. Structures in motion.* (Oxford University Press, 2004). Translated by W. J. Duffin.

[75] Hackney, D. D. The tethered motor domain of a kinesin-microtubule complex catalyzes reversible synthesis of bound atp. *Proc. Nat. Acad. Sci. USA* **102**, 18338–18343 (2005).

[76] Sharyn, A. & Endow, A. Determinants of kinesin motor polarity. *Science* **2001**, 1200–1202 (1998).